

Technische Universität München
Lehrstuhl für Ernährungsmedizin

Inflammatory, metabolic, and vascular changes upon high-fat diet feeding and
n-3 LCPUFA supplementation in mice

Stefanie Worsch

Vollständiger Abdruck der von der Fakultät Wissenschaftszentrum Weihenstephan
für Ernährung, Landnutzung und Umwelt der Technischen Universität München zur
Erlangung des akademischen Grades eines

Doktors der Naturwissenschaften

genehmigten Dissertation.

Vorsitzender: Prof. Dr. Martin Klingenspor

Prüfer der Dissertation:

1. Prof. Dr. Johann J. Hauner
2. Prof. Dr. Hannelore Daniel

Die Dissertation wurde am 24.10.2017 bei der Technischen Universität München
eingereicht und durch die Fakultät Wissenschaftszentrum Weihenstephan für
Ernährung, Landnutzung und Umwelt am 05.03.2018 angenommen.

Table of contents

Zusammenfassung.....	4
Summary.....	8
1 Introduction.....	11
1.1 High-fat diet-induced obesity.....	11
1.1.1 Obesity and its complications.....	11
1.1.2 Diet-induced obesity mouse model.....	11
1.2 Adipose tissue depots and their functions.....	12
1.3 Long-chain polyunsaturated fatty acids.....	14
1.3.1 Classification and conversion.....	14
1.3.2 Mechanism of action.....	16
1.4 Obesity and inflammation.....	17
1.5 Obesity and the vessel system.....	18
1.5.1 The vessel system.....	18
1.5.2 Vascular permeability.....	20
1.5.3 Obesity and endothelial dysfunction.....	21
1.6 Fatty acids and metabolism.....	21
1.6.1 Lipid homeostasis.....	21
1.6.2 Diet-induced thermogenesis.....	24
1.7 Preliminary results of mouse feeding studies that used differential HFDs.....	25
1.7.1 Previous findings regarding the impact of n-3 LCPUFA-enriched HFD.....	25
1.7.2 Previous findings regarding the impact of methyl-donor supplemented HFD.....	26
2 Aim of the thesis.....	28
3 Methods.....	29
3.1 Study designs.....	29
3.1.1 Feeding trial analysing the impact of n-3 LCPUFA and/or n-3/n-6 PUFA ratio on DIO.....	29
3.1.2 Feeding trial analysing the impact of methyl-donor supplementation on DIO.....	30
3.2 Diets.....	31
3.3 Fat intake.....	36
3.4 RNA and protein isolation.....	36
3.5 Primer design and primer testing.....	37
3.6 Agarose gel electrophoresis.....	38
3.7 Gene expression analysis.....	38
3.8 SDS-PAGE and Western blot.....	38
3.9 Chemical analysis.....	39
3.10 Para-formaldehyde fixed and paraffin-embedded tissue sections.....	39
3.11 Immunohistochemical stainings and morphometry.....	40
3.12 ELISA.....	41
3.13 Statistical measurements.....	41
3.14 Buffer recipes.....	42
3.14.1 Protein isolation and SDS-PAGE.....	42

3.14.2	Western blot.....	43
3.14.3	Agarose gel electrophoresis.....	43
3.14.4	TAG analysis.....	43
4	Results.....	44
4.1	Changes in inflammatory status upon HF and HF/n-3 (48 kJ% fat).....	44
4.1.1	Inflammatory status of MAT and EAT.....	44
4.1.1.1	T and B cells.....	44
4.1.1.2	Macrophages.....	46
4.1.2	Inflammatory status of iBAT.....	54
4.1.3	Inflammatory status of spleen, plasma and liver.....	58
4.2	Gene expression analysis indicating inflammatory and vascular changes in small intestine upon HF and HF/n-3 (48 kJ% fat).....	61
4.2.1	Small intestine and inflammation.....	61
4.2.2	Summary of the findings regarding inflammatory status.....	63
4.2.3	Small intestine, vasculature and NO biology.....	66
4.2.4	Small intestine, endothelial permeability and serum albumin level.....	68
4.3	Changes in fatty acid uptake and metabolism upon HFDs.....	71
4.3.1	Changes in fatty acid oxidation in small intestine upon HF and HF/n-3 (48 kJ% fat).....	72
4.3.2	Fatty acid metabolism in liver.....	73
4.3.2.1	Impact of HF and HF/n-3 (48 kJ% fat) on hepatic lipid metabolism.....	73
4.3.2.2	Impact of HF ^A and HFMS (60 kJ% fat) on hepatic lipid metabolism.....	77
4.3.2.2.1	Impact of HF ^A and HFMS (60 kJ% fat) on hepatic <i>de novo</i> lipogenesis.....	77
4.3.2.2.2	Comparison of data on hepatic lipid metabolism generated by analysing the material of feeding studies that used differential HFDs.....	79
4.3.3	Impact of HF and HF/n-3 (48 kJ% fat) on iBAT.....	80
4.3.3.1	iBAT mass, lipid droplets and lipid metabolism.....	80
4.3.3.2	Thermogenic capacity of iBAT.....	86
4.3.3.3	Thermogenic activation and whitening of iBAT.....	88
4.3.4	Summary of results obtained from the analysis of lipid metabolism.....	94
4.4	Association between food / fat intake or fat quality and obesity or inflammatory status.....	98
5	Discussion.....	101
5.1	Differential effects of HFDs on inflammation.....	102
5.1.1	Moderate and tissue-specific inflammatory changes in adipose tissues upon HF.....	102
5.1.2	Immunosuppressive effects of HF/n-3.....	103
5.1.3	Immunoenhancing effects of HF/n-3.....	105
5.1.4	Inflammatory changes in the small intestine upon HFDs.....	106
5.2	Differential effects of HFDs on genes and proteins involved in vascular function in USI.....	107
5.2.1	Regulation of NO bioavailability upon HFDs in USI.....	108
5.2.2	RT-qPCR analyses of proteins involved in the regulation of intestinal barrier integrity..	108
5.3	Differential effects of HFDs on obesity.....	110
5.3.1	Impact of HFDs on lipid metabolism in small intestine and liver.....	110

5.3.2	Impact of HFDs on iBAT energy metabolism - increased thermogenic and oxidative potential in iBAT upon HF/n-3.....	113
5.3.3	Induction of a TAG / FFA cycle in iBAT upon HF/n-3.....	115
5.3.4	Balanced energy metabolism in iBAT upon HF/n-3.....	117
5.3.5	Pathways induced in iBAT upon HF/n-3.....	118
5.4	Conclusion and perspectives.....	119
6	Appendix.....	122
7	References.....	129
8	Abbreviations.....	147
9	Materials.....	153
9.1	Primers.....	153
9.2	Antibodies.....	156
9.3	Consumables.....	157
9.4	Chemicals.....	159
9.5	Kits.....	161
9.6	Machines.....	161
9.7	Software.....	163
10	List of figures.....	164
11	List of tables.....	166
12	Acknowledgements.....	168
13	Curriculum Vitae.....	170

Zusammenfassung

Die Zahl der Menschen mit Adipositas und Stoffwechselerkrankungen wie Diabetes Typ 2 steigt weiterhin an. Zudem können die damit einhergehende Hyperlipidämie, Hyperinsulinämie und Hyperglykämie zur Beeinträchtigung des kardiovaskulären Systems führen und das potentielle Zusammenspiel zwischen dem Darm, dem angrenzenden mesenterialen Fettgewebe (mesenteric adipose tissue - MAT) und der Leber kann entzündliche, metabolische und vaskuläre Veränderungen in mehreren Geweben begünstigen. Es konnte bereits durch Tierversuche gezeigt werden, dass Lipopolysaccharide (LPS) die mit Adipositas einhergehenden Entzündungsprozesse einleiten können. Die mittels Fütterung von Hochfettdiäten (HFD) hervorgerufene Störung der Darmbarriere kann nämlich ihre Translokation ins Darmgewebe und in den Blutkreislauf erhöhen. Aufgrund der gegenläufigen Effekte von Fettsäuren können die bei Studien der ernährungsbedingten Adipositas (diet-induced obesity - DIO) beobachteten Phänotypen jedoch von der Zusammensetzung der Diät abhängen. Es konnte ein signifikanter Zusammenhang zwischen dem n-6 zu n-3 Verhältnis von mehrfach ungesättigten Fettsäuren (polyunsaturated fatty acids - PUFA), das in der Ernährung der westlichen Industrieländern im Laufe der Zeit stetig erhöht wurde, und zunehmender Adipositas festgestellt werden. Dieser Zusammenhang wurde zuvor bereits für gesättigte Fettsäuren (saturated fatty acids - SFA) beobachtet. Im Gegensatz dazu konnte mit Hilfe von Tier- und *in-vitro* Studien gezeigt werden, dass langkettige, mehrfach ungesättigte Fettsäuren (long-chain polyunsaturated fatty acids - LCPUFA) des Typs n-3 und/oder ihre Metaboliten Adipositas und Entzündungen entgegenwirken und zur Stärkung der vaskulären Integrität beitragen können. Da es noch keine standardisierte und definierte HFD für das Versuchsmodell der DIO in Mäusen gibt, lassen sich die bei Studien der DIO beobachteten Phänotypen bisher nur schwer vergleichen oder sind sogar kontrovers. Mit dem Ziel, besser kontrollierte Studien mit erhöhter Vergleichbarkeit zu erhalten, war deshalb der Einsatz einer Diät mit klar definierter Zusammensetzung (Experimentalfutter) und ein wohldefiniertes Studiendesign im hohen Maße wünschenswert. Somit wurde an der Technischen Universität München (TUM) am Lehrstuhl für Ernährungsmedizin (Prof. Dr. Hauner; Dr. Bernhard Bader) ein Mausmodell für DIO etabliert. Zur Entwicklung von Adipositas wurde eine 12 Wochen dauernde Fütterungsstudie mit C57BL/6J Mäusen durchgeführt, wobei die Mäuse unter spezifisch pathogenfreien (SPF) Bedingungen gehalten wurden und eine definierte auf Soja- und Palmöl basierende Diät (48 kJ% Fett) verwendet wurde. Im Vergleich zur Kontrolldiät C (13 kJ% Fett), zeichneten sich die beiden isokalorischen HFD, HF und die mit n-3 LCPUFA ergänzte HFD (HF/n-3), durch ihren hohen Fettgehalt (48 kJ% Fett) aus. Für HF/n-3 wurden SFA und einfach ungesättigte Fettsäuren (monounsaturated fatty acids - MUFA) teilweise durch die n-3 LCPUFA Eicosapentaensäure (eicosapentaenoic acid - EPA) und Docosahexaensäure (docosahexaenoic acid - DHA) ersetzt. Darüber hinaus wiesen die Diäten ein unausgewogenes (C, 9.85:1; HF, 13.5:1) oder ein

ausgewogenes (HF/n-3, 1:0.84) n-6/n-3 PUFA Verhältnis auf. Bereits veröffentlichte Ergebnisse dieser Mausstudie offenbarten eine Adipositas entgegenwirkende Wirkung für HF/n-3, obwohl die HF/n-3 Mäuse mehr Energie aufgenommen und zugleich weniger Energie ausgeschieden haben als die HF Mäuse. HF/n-3 erwies sich zudem als entzündungsfördernd wie auch entzündungshemmend und das interskapuläre braune Fettgewebe (interscapular brown adipose tissue - iBAT) der mit HF/n-3 gefütterten Tiere zeigte einen signifikant erhöhten mRNA Gehalt des Uncoupling Protein 1 (UCP1).

Diese Ergebnisse und vorläufige Genexpressionsdaten bildeten die Grundlage für die vorliegende Dissertation, in der untersucht wurde, ob

(1) die Immunzellinfiltration und die Entzündungsprozesse innerhalb der viszeralen weißen Fettdepots [(visceral white adipose tissues - VATs; MAT und epididymales Fettgewebe (epididymal adipose tissue - EAT))] und des iBAT durch die HFD unterschiedlich beeinflusst werden,

(2) n-3 LCPUFA die durch HF im oberen Abschnitt des Dünndarms (upper small intestine - USI) induzierte/n endotheliale Zellaktivierung und/oder potentielle Änderungen in der endothelialen Barrierefunktion abschwächen können, und

(3) die Adipositas entgegenwirkende Wirkung der HF/n-3 auf den erhöhten Energieverbrauch mittels postprandialer Thermogenese zurückzuführen ist.

Um stärker auf die bisher beobachteten und/oder postulierten Wirkungen von Langzeitfütterungen auf Mäuse einzugehen, wurden RT-qPCR und immunhistochemische Analysen durchgeführt um das Entzündungspotential der HF und HF/n-3 in unterschiedlichen Geweben zu beleuchten. Des Weiteren wurden Stoffwechsel- und Signalwege mit Hilfe von RT-qPCR und Proteinexpressionsanalysen untersucht. Aus den Daten dieser Experimente und anschließender Korrelationsanalysen lassen sich die folgenden Aussagen dieser Dissertation ableiten:

(a) Es zeigten sich unterschiedliche Auswirkungen der HFD auf die VATs, wobei die HF die größten Effekte im EAT erzielte [z.B. signifikante Erhöhung des Makrophagen Markers F4/80 und der Stickoxid Synthase 2 (nitric oxide synthase 2 - NOS2)] und zudem waren nach der Fütterung von HF einige Entzündungsmarker im USI signifikant erhöht [z.B. CD86].

(b) Bei den mit HF/n-3 gefütterten Mäusen konnte man interessanterweise entzündungshemmende aber auch entzündungsfördernde Wirkungen in den Fettgeweben und der Milz feststellen. Die nach Fütterung von HF/n-3 festgestellte signifikant erhöhte Anzahl von eher entzündungshemmenden Makrophagen (M2) in den Fettgeweben begünstigt vermutlich physiologische Umbauprozesse in den VATs und die Thermogenese im iBAT.

(c) Im USI der mit HF gefütterten Mäusen, jedoch nicht bei den mit HF/n-3 gefütterten Mäusen, wurden bei Proteinen, die bestimmte Prozesse regulieren, nämlich die Bioverfügbarkeit von Stickoxid [Caveolin 1 (CAV1) und Arginase 2 (ARG2)] und den transzellulären Transport [Plasmalemma vesicle-associated protein (PLVAP)], eine signifikant erhöhte mRNA Expression festgestellt. Dies lässt darauf

schließen, dass die HF/n-3 vermutlich zur Stärkung der vaskulären Integrität beiträgt. Zudem war im Dünndarm der mit HF/n-3 gefütterten Mäuse die Genexpression von Enzymen mit antioxidativer Wirkung [z.B. Superoxid Dismutase 1 (SOD1) und Katalase (CAT)] signifikant erhöht.

Um die Adipositas entgegenwirkende Wirkung der HF/n-3 näher zu charakterisieren, wurde der Fettstoffwechsel des Dünndarms, der Leber und des iBAT untersucht. Darüber hinaus wurde mittels vergleichender Analysen von Expressionsdaten die Auswirkung der Fettqualität und des Fettgehalts auf den Stoffwechsel der Leber ermittelt. Zwei unterschiedliche Fütterungsstudien mit Mäusen wurden dafür herangezogen [Studie 1: zuvor beschriebene Fütterungsstudie mit einer auf Soja- und Palmöl basierenden Diät; Studie 2: Fütterungsstudie mit einer auf Sojaöl und Rindertalg basierenden Diät, die am Lehrstuhl für Ernährungsphysiologie der TUM durchgeführt wurde]. Bei beiden Studien lassen die Gen- und Proteinexpressionsanalysen von Schlüsselenzymen der Lipogenese, wie die Acetyl-CoA Carboxylasen (ACC1 und ACC2), nach der Langzeitfütterung mit HFD auf eine verringerte hepatische *de novo* Lipogenese schließen. Die posttranslationale Regulation mittels AMP-aktivierter Proteinkinase α (AMPK α) scheint dabei keine Rolle zu spielen, obwohl die Ergebnisse auf unterschiedliche Mechanismen hindeuten. Bei den HF/n-3 gefütterten Mäusen lassen die Ergebnisse dieser Dissertation auch einen Zusammenhang zwischen dem geringeren Gehalt an Triacylglycerol (TAG) in der Leber, der beobachteten Adipositas entgegenwirkenden Wirkung und der erhöhten Verbrennung von Fettsäuren vermuten. Im iBAT beeinflussen die n-3 LCPUFA oder ihrer Stoffwechselprodukte transkriptionelle Regulationswege und AMPK α , und der Fibroblasten-Wachstumsfaktor 21 (fibroblast growth factor 21 - FGF21) könnte als Vermittler ihrer metabolischen Wirkung fungieren. Des Weiteren legen Expressionsdaten und anschließende Korrelationsanalysen die Vermutung nahe, dass die HF/n-3 im Dünndarm und in der Leber weniger energieeffiziente Stoffwechselwege, wie zum Beispiel die peroxisomale β -Oxidation aktivieren. Sie erhöhen zudem den ATP-Verbrauch, indem sie im iBAT einen zyklischen Prozess [TAG / freie Fettsäuren (free fatty acids - FFA)] in Gang setzen. Dazu kommt noch das erhöhte thermogenetische und oxidative Potential von iBAT, das bei den mit HF/n-3 gefütterten Mäusen festgestellt wurde.

Insgesamt ermöglichen die auf Expressionsdaten basierenden Ergebnisse dieser Dissertation einen neuen und interessanten Einblick in potentielle Mechanismen, die der Adipositas entgegenwirkenden und entzündungshemmenden Wirkung von n-3 LCPUFA zugrunde liegen können. Zum besseren Verständnis der physiologischen Relevanz dieser Ergebnisse und der daraus gezogenen potentiellen Schlussfolgerungen müssen jedoch noch physiologische und metabolische Analysen durchgeführt werden. In dieser Dissertation konnte die Vermutung, dass die HF/n-3 die negativen Auswirkungen der HF auf die Darmbarriere und auf die endotheliale Permeabilität beheben kann, nur unzureichend belegt werden, da die verwendete, auf Pflanzenöl basierende HF (48 kJ% Fett) anscheinend zu moderat war, um eine Entzündungsreaktion hervorzurufen und somit nach einer

Langzeitfütterung die Darmbarriere zu beeinträchtigen. Andere veröffentlichte Studien verwendeten hingegen HFD mit höheren Fettgehalt. Zudem sind für dieses Forschungsgebiet noch einige offene Fragen zu klären, unter anderem die kontroversen Daten und die unterschiedlichen Phänotypen, die bei Untersuchungen der durch chronische Hochfettfütterung hervorgerufenen Störung der Darmbarriere erhalten bzw. beobachtet wurden. Mögliche Parameter, die in diesem Zusammenhang eine Rolle spielen könnten, wären die Fütterungsdauer - kurzzeitige, intensive Fütterung versus Langzeitfütterung - und Anpassungsprozesse oder andere Faktoren wie der Hygienestatus der Tierhaltung - SPF Tierhaus versus konventionelle Tierhaltung - da Unterschiede in der Darmflora der Mäuse zur Veränderung des Phänotyps beitragen können.

Summary

Obesity and metabolic disorders like type 2 diabetes continue to rise in humans. Moreover, associated dyslipidaemia, hyperinsulinemia and hyperglycemia can contribute to irregularities in the cardiovascular system and a potential crosstalk between the intestine, the adjacent mesenteric fat (MAT) and the liver might promote inflammatory, metabolic and vascular changes within different tissues. Data from mouse studies have shown that inflammation, which is associated with obesity, can be caused by lipopolysaccharides (LPS), whose entry into the intestinal tissue and blood circulation was found to be increased upon high-fat diet (HFD)-induced disruption of the intestinal barrier. However, given the opposing effects of fatty acids, diet composition might influence the observed diet-induced obesity (DIO)-phenotypes. Besides saturated fatty acids (SFA), the n-6/n-3 polyunsaturated fatty acids (PUFA) ratio, which has steadily increased in Western diets, significantly correlates with increasing obesity, whereas animal and *in-vitro* studies reported that n-3 LCPUFA and/or their metabolites have anti-obesogenic and anti-inflammatory potential and enhance vascular integrity. Since there exists no standardised defined HFD for modelling DIO in mice, the observed DIO-phenotypes are sometimes difficult to compare or controversial across studies. Thus, it was highly desirable to start using a well-defined diet composition and study design to achieve better controlled studies and greater comparability between studies. Therefore, a DIO mouse model was established at the Technical University of Munich (TUM), Chair of Nutritional Medicine (Prof. Dr. Hauner; Dr. Bernhard Bader), using male C57BL/6J mice, which were housed under specific-pathogen-free (SPF) conditions and fed defined soybean / palm oil-based diets for 12 weeks to induce obesity. Compared to the control diet C (13 kJ% fat), both isocaloric HFDs, HF and the n-3 LCPUFA-enriched HFD (HF/n-3), were characterised by high-fat content (48 kJ% fat). For HF/n-3, SFA and monounsaturated fatty acids (MUFA) were partially substituted by n-3 LCPUFA eicosapentaenoic acid (EPA) and docosahexaenoic acid (DHA). Moreover, the diets had an unbalanced (C, 9.85:1; HF, 13.5:1) or a balanced (HF/n-3, 1:0.84) n-6/n-3 PUFA ratio. Previous published data from this mouse study revealed that HF/n-3 has an anti-obesogenic effect, although HF/n-3 mice ingested more and excreted less energy than HF animals. In addition, HF/n-3 exerted pro- and anti-inflammatory effects and significantly increased uncoupling protein 1 (UCP1) mRNA levels in interscapular brown adipose tissue (iBAT). These data and preliminary gene expression data established the basis for the present thesis, the overall aim of which was to examine whether

- (1) HFDs have differential effects on the immune cell infiltration and inflammation of visceral white adipose tissue (VAT) depots [MAT and epididymal adipose tissue (EAT)] and iBAT,
- (2) n-3 LCPUFA alleviate HF-induced endothelial cell activation and/or potential changes in endothelial barrier function in the upper small intestine (USI), and

(3) the anti-obesogenic effect of HF/n-3 can be due to increased energy expenditure by diet-induced thermogenesis.

To explore the previously observed and/or postulated effects of long-term feeding in mice, RT-qPCR and immunohistochemistry were applied to analyse the inflammatory potential of the HF and HF/n-3 on different tissues, and additional RT-qPCR and protein expression analyses were performed to examine metabolic and signalling pathways. Data from these experiments and subsequent correlation analyses revealed the following main findings of this thesis:

(a) Differential effects were observed for VATs upon HFDs, whereby for HF the highest impact was observed analysing EAT [e.g., significant upregulation of macrophage marker F4/80 and nitric oxide synthase 2 (NOS2)] and inflammatory markers were found to be significantly increased in USI [e.g., CD86] upon HF.

(b) For the HF/n-3 mice, interestingly, both immunosuppressive and -enhancing effects were found in adipose tissues and the spleen. The significantly increased number of rather anti-inflammatory M2 adipose tissue macrophages observed upon HF/n-3 was associated with healthy adipose tissue remodelling in VATs and thermogenesis in iBAT.

(c) In USI, for HF but not for HF/n-3 mice, significantly increased mRNA expression levels were found for proteins regulating nitric oxide bioavailability [caveolin 1 (CAV1) and arginase 2 (ARG2)] and the transcellular pathway [plasmalemma vesicle-associated protein (PLVAP)]. This suggests a favourable impact of HF/n-3 on vascular integrity. In addition, gene expression levels of enzymes acting as antioxidants [e.g., superoxide dismutase 1 (SOD1) and catalase (CAT)] were significantly upregulated in the small intestine of HF/n-3 mice.

To further characterise the anti-obesogenic effect of n-3 LCPUFA, fatty acid metabolism was examined in the small intestine, liver and iBAT. Moreover, the impact of fat quality and quantity on hepatic metabolism was examined by comparative analyses of expression data from two different mouse feeding studies [study 1: feeding study described above using a soybean / palm oil-based diet; study 2: feeding study performed at the TUM-Chair of Nutrition Physiology using a soybean oil / beef tallow-based HFD (60 kJ% fat)]. For both studies gene and protein expression analyses of key lipogenic enzymes, such as acetyl-CoA carboxylases (ACC1 and ACC2), indicated diminished hepatic *de novo* lipogenesis (DNL) upon long-term HFD feeding without posttranslational regulation via AMP-activated protein kinase α (AMPK α), although the mechanisms seem to differ. Data from this thesis suggest that the reduced hepatic triacylglycerol (TAG) content and the anti-obesogenic effect observed upon HF/n-3 were rather related to enhanced combustion of fatty acids, whereby n-3 LCPUFA or their metabolic products target transcriptional regulatory pathways and AMPK α , and fibroblast growth factor 21 (FGF21) might mediate their metabolic effects in iBAT. Furthermore, expression data and subsequent correlation analyses suggest that HF/n-3 activated less efficient

pathways for energy production, such as peroxisomal β -oxidation, in the small intestine and the liver, and increased ATP consumption upon the induction of a TAG / free fatty acid (FFA) cycle in the iBAT, which showed increased thermogenic and oxidative potential in HF/n-3 mice.

Altogether, the findings of this thesis based on expression data give new and interesting insights into potential underlying mechanisms of the anti-obesogenic and anti-inflammatory impact of n-3 LCPUFA. However, for a better understanding of the physiological relevance of these findings and potential conclusions, additional physiological and metabolic analyses should be performed. The postulated counteractive impact of HF/n-3 on adverse effects induced by HF on the intestinal barrier and endothelial permeability were difficult to study, since the fed plant oil-based HF (48 kJ% fat) was too moderate to induce an inflammatory response to disturb the intestinal barrier upon chronic HF feeding compared to other published studies that applied HFDs with much higher fat content. In addition, there are still open questions to be answered in the research field to explain controversial data and different phenotypes with regard to intestinal barrier disruption upon chronic HFD feeding. Possible parameters to consider in this context are feeding duration - acute versus long-term feeding - and adaption processes or other factors like the hygiene status of the animal facilities - SPF animal facility versus conventional animal housing - since differences in the intestinal microbiota of the mice might change the phenotype.

1 Introduction

1.1 High-fat diet-induced obesity

1.1.1 Obesity and its complications

Worldwide obesity has more than doubled since 1980. In 2014, more than 1.9 billion adults, 18 years and older, were overweight, having a body mass index (BMI) above 25 kg/m², and over 600 million of these adults were obese (BMI > 30 kg/m²; WHO 2015). The proportion of overweight adults in Germany remained stable but on a high level, whereas the prevalence of obesity continued to rise, especially among young adults (Mensink 2013). It is well established that obesity can increase the risk of all major metabolic disorders, especially diabetes, cardiovascular disease, hypertension, and fatty liver disease. The constellation of other diseases, which often coexist with obesity and include hypertension, dyslipidaemia and insulin resistance, has been labelled the metabolic syndrome (MetS; Eckel 2005). It was postulated, that the perivascular adipose tissue might hold the key to link obesity with the development of MetS and diabetes as a result of an adverse influence upon the vasculature (Yudkin 2005).

Moreover, hyperglycemia, a characteristic feature of type 1 and type 2 diabetes, plays a pivotal role in diabetes and is associated with microvascular complications. However, dyslipidemia, hyperinsulinemia, and adipose tissue-derived factors play a more dominant role by the occurrence and progression of macrovascular disease (Bakker 2009). Macrovascular abnormalities include myocardial infarction and cerebrovascular disease. They are associated with the damage in arteries, whereby endothelial dysfunction favors atherosclerotic diseases. Microvascular abnormalities affect small blood vessels, and include diabetic retinopathy, nephropathy and neuropathy (Bakker 2009, Cade 2008). Albuminuria is the most important early clinical risk factor for diabetic nephropathy, which is caused by hemodynamic changes and by the impairment of the glomerular filtration barrier (Dronavalli 2008).

1.1.2 Diet-induced obesity mouse model

Besides genetic models of obesity, such as ob/ob or db/db mice, rodent models of diet-induced obesity (DIO) through the administration of high-fat diet (HFD), are frequently applied to study obesity and symptoms of metabolic syndrome like dyslipidemia and adipose tissue inflammation (Kennedy 2010, Buettner 2007). In general, diets containing more than 30 % of total energy as fat lead to the development of obesity. Therefore, the best approach to induce obesity in animals is to use semi-purified HFDs containing animal fats at 40 % of energy, with a low amount of n-3 fatty acids and of plant oils rich in n-6 and n-9 fatty acids (Buettner 2007). Fat is a very energy dense

macronutrient and high-fat feeding is positively correlated with an increase in body fat mass. Initially, this is likely to be caused by overconsumption due to weaker satiety signals from fat than from carbohydrates and proteins but may be transient and substituted by other mechanisms like lowered physical activity or a decrease in basal metabolic rate (Hariri 2010, West 1998). There exists no standardised HFD for modelling HFD-induced obesity. Either animal fat (lard, beef tallow, fish oil) or plant oils are used, with fat contents ranging from 20 % to more than 60 % of energy, but mixtures are also possible (Buettner 2007). Apart from fat quantity (de Wit 2011) and type of fat (Buettner 2006), feeding duration (acute vs. chronic treatment; Newberry 2008, Yoshioka 2008), age and gender (Lemonnier 1972), macronutrient composition (Hao 2012) and genetic background (Svenson 2007) determine the observed phenotypes. The n-6/n-3 fatty acid ratio is also considered important. Its value is increased in Western diets (Simopoulos 2011). Due to this high variability, diet composition and study design have to be characterised for comparison with other studies of HFD-induced obesity.

1.2 Adipose tissue depots and their functions

The adipose tissue comprises besides adipocytes, non-fat cells such as immune cells, preadipocytes and fibroblasts, in addition to connective tissue matrix, vascular and neural tissues (Ibrahim 2010). It is classically divided into two types, with origins in different precursor cells. The first one is the white adipose tissue (WAT), a highly complex tissue well known by its ability to store energy in the form of triacylglycerols (TAG). The other one is called brown adipose tissue (BAT). It shares with WAT the capacity to synthesise and store lipids but it is specialised in oxidising lipids to dissipate chemical energy in form of heat, in a process called adaptive thermogenesis (Cannon 2004). White adipocytes usually contain a single giant (unilocular) lipid droplet, which occupies most of the cytoplasm, while brown adipocytes, rich in mitochondria, are filled with a number of smaller (multilocular) lipid droplets (Reddy 2014). A third type of adipocyte, named “beige” or “brite”, was described more recently in rodents as an inducible cell type in WAT depots (Wu 2012a). Beige adipocytes are most abundant in the inguinal WAT (Vitali 2012). However, it is still a matter of debate whether mature white adipocytes undergo transdifferentiation into brown adipocytes (Cinti 2009) or if precursors, which are already present in the tissue, differentiate into mature brown adipocytes (Wu 2012a). Moreover, WAT can be further differentiated into subcutaneous - dorsolumbar, inguinal and gluteal - and visceral - epididymal, mesenteric, perirenal and retroperitoneal - WAT (SCAT and VAT) depots (Cinti 2005a). Perivascular adipose tissue is present around almost all blood vessels, particularly conduit arteries (Yudkin 2005) and brown adipocytes can be found interspersed in many of the

aforementioned depots. The most prominent brown fat depot in mice is the interscapular brown adipose tissue (iBAT; Cinti 2005a, Figure 1).

During weight gain, different fat depots enlarge via hyperplasia, hypertrophy, or both (Tchoukalova 2010), whereby the visceral fat mass changes principally through adjustments in adipocyte size, rather than number (DiGirolamo 1998). The principal function of adipose tissue is to store and release fat in response to energy balance needs, but it also has immune, endocrine, regenerative, mechanical, and thermal functions, with differences among fat depots (Tchkonia 2013). The adipose tissue as an endocrine organ synthesises and secretes more than 100 factors (Hauner 2005). Generally, the adipokines can influence energy metabolism as well as neuroendocrine and immune functions (Tilg 2006). Once inflamed, the dysregulated adipose tissue shifts from storing to releasing fatty acids (Faty 2012) and the fatty acid overflow into “ectopic” sites can lead to lipotoxicity and insulin resistance (Yki-Jarvinen 2002). Ectopic lipid deposition affects different tissues, such as the liver, which shows impaired insulin signalling (Kumashiro 2011). This in turn leads to increased glucose output and the pancreas, which tries to counteract the hyperglycemia, induces hyperinsulinemia (Kahn 2006). Besides its influence on the development of non-alcoholic fatty liver disease (NAFLD; Angulo 2007), the VAT is also associated with the pathophysiology of inflammatory intestinal and mesenteric diseases, e.g., Crohn’s Disease (Schäffler 2005). The role of mesenteric adipose tissue (MAT) in obesity-related pathologies might be caused by impaired gut barrier function (Li 2008). MAT is attached to the abdominal back wall and the small intestine (Cinti 2005a) and it releases free fatty acids (FFA) into the portal circulation, which goes directly into the liver (Matsuzawa 1995). Furthermore, another study shows its critical role in the development of insulin resistance (Catalano 2010). However, active BAT is associated with the protection against obesity and associated metabolic alterations, whereby its beneficial effect could involve the release of endocrine factors (Villarroya 2013a).

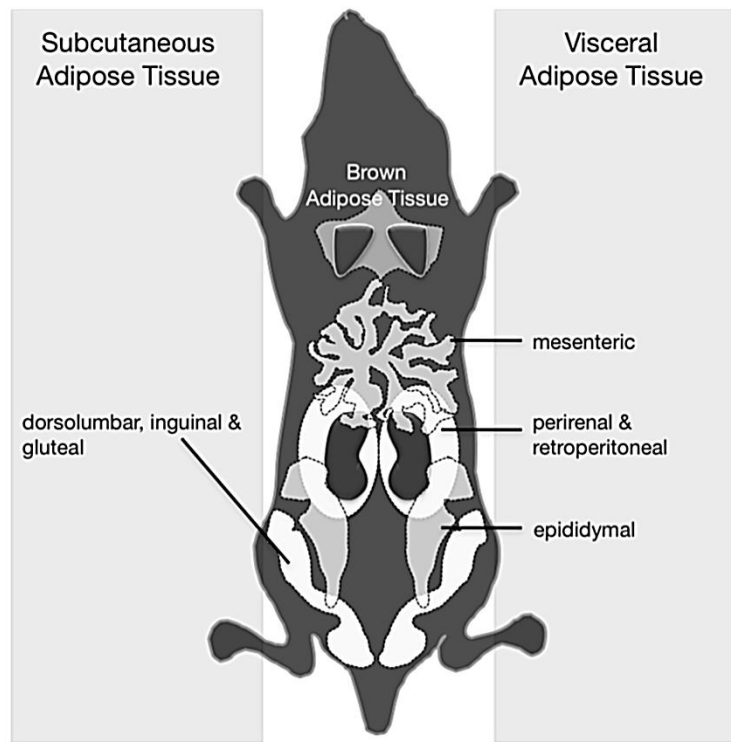


Figure 1. Selected adipose tissue depots in the mouse. Adipose tissue depots can be classically divided into white adipose tissue (d) and brown adipose tissue (BAT). The BAT shown here is the interscapular depot (iBAT) in the neck region of the animal. WAT can be further divided into subcutaneous (SCAT) and visceral white adipose tissue (VAT) depots. The SCAT is shown here with dorsolumbar, inguinal and gluteal fat depots. The VAT depots include the intra-abdominal mesenteric adipose tissue (MAT) attached to the abdominal back wall and the small intestine, the perirenal and retroperitoneal fat depots surrounding the kidneys and the epididymal adipose tissue (EAT) attached to the epididymis of male mice. Adapted from Cinti 2005a

1.3 Long-chain polyunsaturated fatty acids

1.3.1 Classification and conversion

Fatty acids are carboxylic acids that are characterised by variable carbon chain lengths and the number of carbon double bonds. Besides the classes of saturated and monounsaturated fatty acids (SFA and MUFA) there are the polyunsaturated fatty acids (PUFA), which are distinguished by two or more double bonds in their carbon chain skeleton. The position of the double bond is depicted by n or ω . The $n-6$ PUFA possess a double bond at the sixth carbon while the $n-3$ PUFA possess the double bond at the third carbon counted from the methyl end (Poudyal 2011). Generally, SFA have been associated with the appearance of obesity and insulin resistance, whereas MUFA and long-chain polyunsaturated fatty acids (LCPUFA) are considered beneficial (Nettleton 2014).

Complex series of desaturation and elongation reactions can transform linoleic acid (LA, 18:2n-6) and α -linolenic acid (ALA, 18:3n-3) to their higher unsaturated derivatives: arachidonic acid (AA, 20:4n-6) from LA, eicosapentaenoic acid (EPA, 20:5n-3) and docosahexaenoic acid (DHA, 22:6n-3) from ALA, but with very low conversion rates (Goyens 2005). Limited retro-conversion of DHA to EPA by peroxisomal β -oxidation is also possible (Poudyal 2011). LA and ALA are abundant in plant oils, whereas EPA and DHA are mainly found in fatty fish enriched from feeding on marine microbes (Russo 2009). Moreover, AA and EPA are precursors of different classes of pro-inflammatory or anti-inflammatory eicosanoids (Figure 2), which are also involved in vasoregulation, platelet activation and the regulation of permeability or chemotaxis (Schmitz 2008).

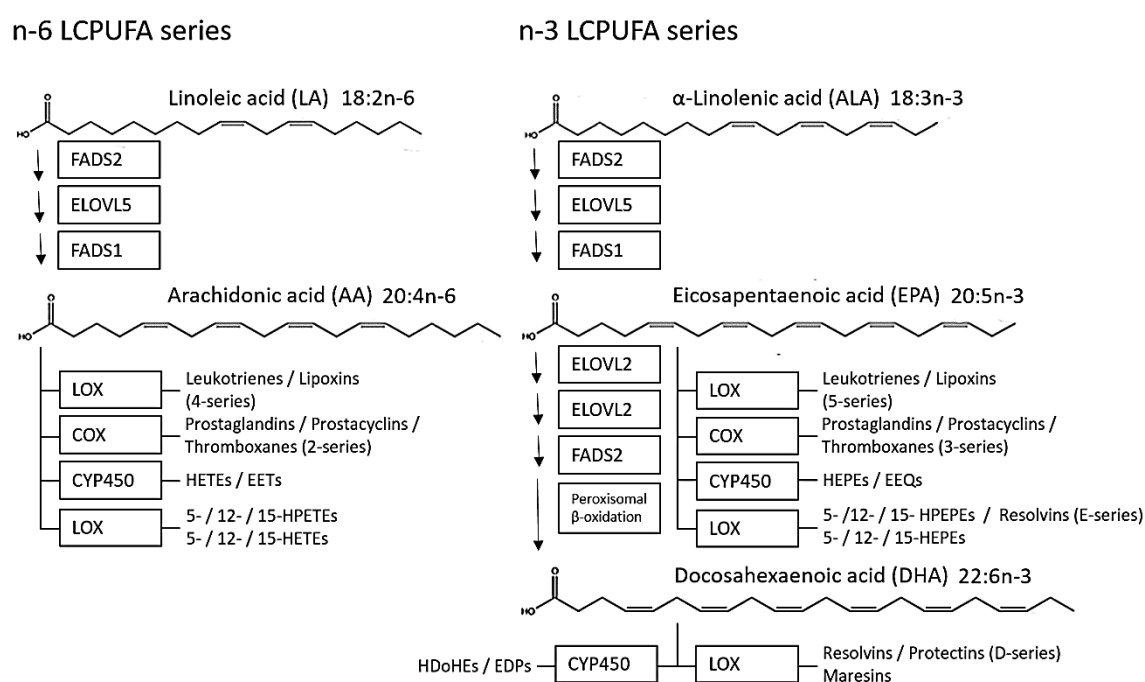


Figure 2. Lipid mediators generated from long-chain polyunsaturated fatty acids (LCPUFA). LCPUFA can be divided into two groups depending on the position of the double bond, depicted by n or ω . The n-6 PUFA possess a double bond at the sixth carbon while the n-3 PUFA possess the double bond at the third carbon counted from the methyl end. Linoleic acid (LA, 18:2n-6) and α -linolenic acid (ALA, 18:3n-3) are essential fatty acids and are precursors for arachidonic acid (AA, 20:4n-6) and eicosapentaenoic acid (EPA, 20:5n-3), respectively, but also for enzymatically generated lipid mediators. These lipid mediators often possess contrary actions depending on the molecule of origin. They are involved in the modulation of inflammation, vasoregulation, platelet activation and in the regulation of permeability or chemotaxis. Moreover, EPA can be further elongated and desaturated into docosahexaenoic acid (DHA, 20:6n-3) and it serves as precursor to certain anti-inflammatory and pro-resolution lipid mediators. Enzymes are framed. COX, cyclooxygenase; CYP450, cytochrome P450; EDP, epoxydocosapentaenoic acid; EEQ, epoxyeicosatetraenoic acid; EET, epoxyeicosatrienoic acid; ELOVL, elongation of very long-chain fatty acids protein (elongase); FADS, fatty acid desaturase; HDoHE, hydroxydocosahexaenoic acid; HEPE, hydroxyeicosapentaenoic acid; HETE, hydroxyeicosatetraenoic acid; HPEPE, hydroperoxyeicosapentaenoic acid; HPETE, hydroperoxyeicosatetraenoic acid; LOX, lipoxygenase. Adapted from Poudyal 2011 and Russell 2012

1.3.2 Mechanism of action

Both n-6 LCPUFA and n-3 LCPUFA are precursors of signalling molecules with opposing effects, which modulate membrane microdomain composition, receptor signalling and gene expression (Schmitz 2008). EPA and DHA are vital for cellular function, whereas DHA is high abundant in membrane phospholipids of the retina and the brain (Singh 2005). Moreover, LCPUFA derived from diet or endogenous synthesis can be incorporated into membrane phospholipids and they can be released again by phospholipase A2 or phospholipase C for eicosanoid synthesis (Figure 2). During this process also diacylglycerol (DAG) is released. An increase in n-3 LCPUFA in membrane phospholipids reduces the availability of AA for eicosanoid production, and EPA and DHA also decrease the liberation of AA from phospholipids (Shikano 1994). Besides that, the LCPUFA content of biological membranes significantly influences their physical properties. It increases membrane fluidity and alters protein function and trafficking, and vesicle budding and fusion (Spector 1985, Stulnig 2001). Furthermore, LCPUFA influence gene expression indirectly via changes in membrane composition, alterations in second messenger concentrations (Calder 1998), and the activation of membrane receptors (Oh 2010) by inducing cell signalling processes (Sampath 2005). The transcription factor activity is regulated either by this LCPUFA-mediated signalling or by direct activation with LCPUFA as transcription factor ligands, but also nuclear abundance of transcription factors can be regulated (Jump 2008). LCPUFA and their metabolites can directly bind the transcription factors peroxisome proliferator activated receptors (PPAR α , β/δ , γ 1 and γ 2), hepatic nuclear factor 4 α (HNF-4 α), retinoic acid X receptor (RXR), and liver X receptor α (LXR α). However, sterol regulatory element binding protein 1 (SREBP1), nuclear factor κ B (NF κ B), carbohydrate regulatory element binding protein (ChREBP), max-like factor X (MLX), CCAAT / enhancer binding protein (C/EBP β), and hypoxia-inducible factor 1 (HIF1 α) are regulated independently of ligand binding (Jump 2008, Schmitz 2008, Sampath 2005).

N-3 LCPUFA exert numerous beneficial effects on health, including improvements in lipid metabolism and the prevention of obesity and diabetes. However, data in humans are scarce and not clear (Buckley 2009). Only few studies in obese humans demonstrate a reduction of adiposity after n-3 LCPUFA supplementation, which might depend possibly in part on the dietary macronutrient composition (Hao 2012). In animals, the majority of literature indicates anti-obesity effects. As found in mice, the anti-obesity effect could reflect in part the inhibition of fat cell proliferation (Ruzickova 2004), while the metabolic effects could depend on increased lipid catabolism in the small intestine (van Schothorst 2009) and the liver (Dossi 2014). In WAT, n-3 LCPUFA can increase mitochondrial oxidative capacity (Flachs 2005). Moreover, increased uncoupling protein 1 (UCP1)-mediated adaptive thermogenesis in BAT might also play a role in the anti-obesity effect of n-3 LCPUFA

(Ohinata 1998, Oudart 1997), whereby some reports also say that every PUFA is capable to induce thermogenesis to the same extent (Sadurskis 1995, Cannon 2004).

LCPUFA are also important mediators of inflammation, whereby n-6 LCPUFA and n-3 LCPUFA have potent pro- and anti-inflammatory effects, respectively. Furthermore, n-3 LCPUFA affect several functions of immune cells. They can decrease leukocyte chemotaxis and inflammatory cytokine production (Calder 2013) or increase phagocytosis (Gorjão 2006) and induce the anti-inflammatory M2 polarization in macrophages (Titos 2011). The anti-inflammatory effects of n-3 PUFA (Todoric 2006) depend in large on the formation of their active metabolites, which originate from either targeted enzymatic synthesis, as in case of resolvins and protectins (Serhan 2008) or from non-enzymatic oxidation reactions (Musiek 2008). They can act as ligands for surface receptors, namely the lipid sensor G protein-coupled receptor 120 (GPR120; Oh 2010) or might interact with transcription factors like PPAR γ and NF κ B.

In addition to a classic lipid-lowering action, n-3 LCPUFA can regulate blood pressure and enhance vascular integrity and compliance. Beside that, they can protect vascular endothelial cells by decreasing oxidative stress, halting atherosclerotic events, and preventing vascular inflammatory and adhesion cascades. The enhanced generation and bioavailability of endothelium-derived relaxing factor nitric oxide (NO), through upregulation and activation of endothelial nitric oxide synthase (NOS3) by n-3 LCPUFA, might explain the improved vascular endothelial function (Balakumar 2012). However, the cardio-protective effect of n-3 LCPUFA seems to depend on their dosage (Lavie 2009). Moreover, the effect of n-3 LCPUFA on vascular integrity might involve the regulation of tight junctions (Jiang 1998).

1.4 Obesity and inflammation

Obesity is associated with a chronic low-grade inflammatory state (Hotamisligil 2006). Thus, the enlarged adipocytes, the decreased blood flow (Frayn 2003) and the hypoxic condition (Trayhurn 2013) favour pro-inflammatory conditions (Rausch 2008), which can in turn induce insulin resistance (Olefsky 2010). Moreover, metabolites of fatty acids and glucose (DAG, ceramide, reactive oxygen species (ROS), etc.) and the induction of endoplasmic reticulum (ER) stress contribute to inflammation by activation of serine kinases (Brose 2002, Ozcan 2004). On the one hand, the expansion of the fat depots in obesity is accompanied by the infiltration of immune cells, including macrophages (Weisberg 2003), T cells (Kintscher 2008, Nishimura 2009), B cells (Winer 2011), natural killer T cells (Wu 2012b) and neutrophils (Elgazar-Carmon 2008). On the other hand, the numbers of regulatory T lymphocytes (Feuerer 2009) and eosinophils (Wu 2011) seem to be reduced compared with lean mice. Furthermore, in obesity, increased fatty acid release from either viable or dying

adipocytes may attract macrophages into adipose tissue (Suganami 2007, Kosteli 2010) with the help of monocyte chemoattractant protein-1 (MCP1; Yu 2006) or osteopontin (OPN; Nomiya 2007). Besides that, the macrophages may shift their phenotype from the anti-inflammatory M2 towards the pro-inflammatory M1 phenotype (Lumeng 2007) and form crown-like structures (CLS). M1 and M2 macrophages are merely regarded as two extremes of a continuum of functional stages (Mosser 2008), which can be further subdivided according to their function. For instance, M2a designation defines those macrophages stimulated by interleukin (IL)4 / IL13, M2b refers to macrophages activated by stimuli such as apoptotic cells in concert with lipopolysaccharide (LPS) and M2c relates to polarization in response to IL10, transforming growth factor (TGF) β , or glucocorticoids (Martinez 2008). However, macrophage activation seems to be plastic and fully reversible. They are involved in inflammation and resolution (Porcheray 2005).

In addition to adipose tissue, the liver shows increased numbers of macrophages during obesity, which can promote obesity-induced hepatic steatosis (Obstfeld 2010). In obesity-related diseases, toll-like receptor and inflammasome pathways have been suggested to drive low-grade inflammation. They are triggered by SFA and elevated glucose level (Masters 2011), and mediated by the transcription factor NF κ B (Baker 2011). Furthermore, LPS absorbed by the intestine might promote systemic low-grade inflammation (Cani 2008). On the whole, it seems that inflammation induced by DIO affects adipose tissue, liver and intestine (Li 2008).

1.5 Obesity and the vessel system

1.5.1 The vessel system

The endothelium, a monolayer of endothelial cells, constitutes the inner cellular lining of the blood vessels and the lymphatic system, and forms collectively with pericytes, smooth muscle cells and the basal membrane the blood vascular wall. Moreover, the vascular tree is subdivided into macrovasculature, composed of arteries and veins, and microvasculature, which consists of arterioles, capillaries and venules (Figure 3). These different vessel types differ in their diameter, the thickness of the glycocalyx lining the surface of endothelial cells, and in their function. Furthermore, the macrovasculature is responsible for the rapid transport of blood and the microvessels regulate local blood perfusion and conduct blood-tissue exchange. The arterioles control the local blood flow and blood-tissue exchange takes place in capillaries and postcapillary venules, whereas the capillaries are major sites of fluid passage and postcapillary venules are the primary location for leukocyte diapedesis and plasma protein leakage (Yuan 2010). The lymphatic system in turn plays a role in the maintenance of tissue fluid pressure homeostasis, the immune response and the intestinal absorption and transport of dietary lipids (Jurisic 2009). Besides its barrier function, the endothelium

is a predominant player in the control of blood fluidity, platelet aggregation and vascular tone, and it takes part in the regulation of immunology, inflammation and angiogenesis.

A structural heterogeneity is observed in endothelial cells, which accounts for their different basal permeability properties. Thus, the differences in intercellular junctions lead to the classification of continuous, fenestrated and discontinuous / sinusoidal endothelium (Figure 3). Continuous endothelium is found in most arteries, veins and capillaries of the brain, skin, lung, heart and muscle. Fenestrated endothelium is identified by the presence of transcellular 50- to 60-nm-wide pores, which are sealed by a 5- to 6-nm-thick diaphragm and is observed in tissues with an elevated transendothelial transport or an increased filtration role, such as endocrine and exocrine glands, gastrointestinal tract, choroid plexus, kidney glomeruli and subpopulations of renal tubules. Finally, the discontinuous endothelium, found predominantly in sinusoidal vascular beds in the liver, is associated with a poorly structured basal membrane and is characterised by the presence of large 100- to 200-nm-wide fenestrations without diaphragm (Félétou 2011, Sarin 2010).

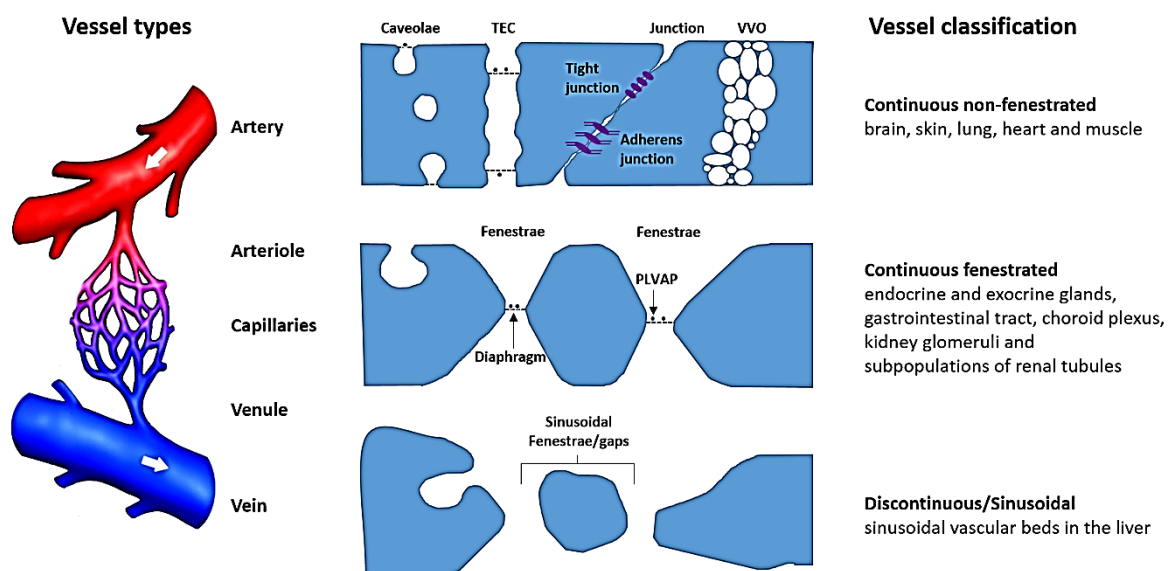


Figure 3. The vessel system. The vascular tree is subdivided into macrovasculature, composed of arteries and veins, and microvasculature, which consists of arterioles, capillaries and venules. These different vessel types differ in their diameter, the thickness of the glycocalyx lining the surface of endothelial cells, and in their function. A structural heterogeneity is observed in endothelial cells, which accounts for their different basal permeability properties. The differences in intercellular junctions led to the classification of continuous, fenestrated and discontinuous / sinusoidal endothelium. PLVAP, plasmalemma vesicle-associated protein; TEC, transendothelial channel; VVO, vesiculo-vacuolar organelle. Adapted from Atkins 2011 and Sarin 2010

1.5.2 Vascular permeability

Hence, like the epithelial lining of several organs (e.g., small intestine) the vascular endothelium acts as a barrier but, at the same time, it behaves as a permeable filter. Macromolecules, fluids and cells can pass the endothelium either through (transcellular) or between cells (paracellular). The vascular permeability is defined by the combination of these pathways, whereas the latter is a major contributor to the inflammation-induced permeability (Komarova 2010). Moreover, vascular hyperpermeability, which can be subdivided into acute or chronic (Dvorak 2010), provides the access of leukocytes to the inflamed tissue and can be accompanied by fluid accumulation in the interstitium. Besides that, normal basal vascular permeability is regulated by sphingosine-1-phosphate and cyclic adenosine monophosphate (cAMP) signalling (Belvitch 2012, Roberts 2014), and angiopoietin-1 binding to its receptor endothelial-specific receptor tyrosine kinase (TEK) is barrier protective (Augustin 2009).

The kind and mass of plasma solvents and solutes crossing the vascular wall depends on size, shape and charge of the extravasating molecule, pressure and concentration gradients, hemodynamic forces (blood flow, vascular area available for exchange), lymphatic drainage, and the intrinsic permeability of the vascular wall. Moreover, the intrinsic permeability is defined by the thickness of the negatively charged glycocalyx that serves as a size- and charge-selective filter, the nature of the endothelium (continuous, fenestrated or discontinuous), and the pathway (transcellular or paracellular) the molecule takes (Yuan 2010).

The transcellular transport involves receptor-dependent or -independent mechanisms (fluid phase transcytosis), and is mediated by endothelial caveolae, vesiculo-vacuolar organelles (VVO), transendothelial channels (TEC) and fenestrae (Figure 3). The paracellular pathway is defined by the intercellular junctions (Figure 3), the adherens junctions (AJ; cadherins (CDH) and platelet-endothelial cell adhesion molecule (CD31)) and the tight junctions (TJ; claudins, occludin (OCLN), junctional adhesion molecules), whereby AJ mainly govern the permeability of endothelial cells and TJ proteins the permeability of epithelial cells (Harris 2010, Suzuki 2013). Moreover, gap junctions, mainly found in larger vessels, not significantly contribute to endothelial barrier function, but they are involved in the transport of small metabolites, second messengers and ions, and mediate cell-to-cell communication (Brisset 2009).

The stability of the CDH5-catenin-cytoskeleton complex is essential for the maintenance of junction integrity. The actomyosin contractility is increased by phosphorylation of myosin regulatory light chain and AJ disassembly is induced by phosphorylation of AJ proteins. Besides that, physical forces (e.g., shear stress) or biological factors (e.g., inflammatory mediators) cause changes in endothelial permeability by altering the expression of cell-cell junction proteins or cell-matrix adhesion molecules over the long-term or by inducing conformational reorganisation of the junction or focal

adhesion complexes when stimulated by acute inflammatory agents. A variety of intracellular signalling molecules are involved in these changes. In general, the canonical pathway, which leads to increased permeability, includes the elevation of intracellular calcium and the activation of protein kinase C, myosin light-chain kinase, Src family kinases, and the small GTPase RhoA (Yuan 2010, Geraldes 2010, Rigor 2013, Hu 2008, Amado-Azevedo 2014).

1.5.3 Obesity and endothelial dysfunction

The development of the obese condition can have profound impacts on integrated vascular function, whereby dyslipidemia, glucose intolerance, insulin insensitivity, hypertension, pro-thrombotic and pro-inflammatory environments play an important role in the pathophysiology of obesity (Stapleton 2008). During obesity-associated chronic inflammation, the vasculature undergoes functional and structural changes, a phenomenon termed endothelial cell activation. These changes include impaired perfusion and increased vascular permeability as well as proadhesive, antigen-presenting and procoagulant activities (Félétou 2011, Aird 2007). However, activated endothelial cells also exhibit a reduction in glycocalyx thickness and an increased rate of apoptosis. Under normal conditions, endothelial cells become activated according to environmental needs, however, endothelial dysfunction, a term that encompasses multiple potential defects of the endothelial cells, contributes to various pathological states. Endothelial dysfunction is thought to be a key event in the development of atherosclerosis, a macrovascular complication associated with obesity, but endothelial dysfunction also takes place in microvessels (microvascular rarefaction and hyperpermeability). Endothelial dysfunction is characterised by reduced NO availability secondary to an enhanced oxidative stress production and subsequent impaired vasodilatory response. It is also associated with endothelial hyperpermeability that clinically manifests as edema, an abnormal fluid accumulation in the interstitium (Granger 2010, Yuan 2010).

1.6 Fatty acids and metabolism

1.6.1 Lipid homeostasis

Lipid homeostasis (Figure 4) depends on a well-orchestrated balance between fatty acid synthesis, lipid oxidation, and lipid storage. It is also tightly intertwined with carbohydrate and protein metabolism (Rui 2014). The small intestine is the primary site for the absorption of fatty acids, glucose, amino acids and other nutrients. Moreover, in the intestine parts of the nutrients are oxidised for energy generation but most of the nutrients are released. On the one hand, amino acids and glucose enter the portal vein through the mucosal vasculature and then reach the liver (Rui

2014), on the other hand, TAG, packaged as soluble chylomicrons and very low-density lipoprotein (VLDL), is transported through lymph vessels and enters the blood circulation through the thoracic duct (Yáñez 2011). Reaching the tissue, lipoprotein lipase (LPL) hydrolyzes the TAG of chylomicrons and VLDL to form FFA, which are subsequently taken up by the fatty acid translocase CD36 (Goldberg 2009). In this process angiopoietin-like 4 (ANGPTL4) is an extracellular inhibitor of LPL (Lafferty 2013). Within the cell, e.g., hepatocyte, the fatty acids released from adipose tissue or absorbed from food digestion in the intestine are oxidised to generate energy or are esterified with glycerol-3-phosphate to generate TAG, which are stored in lipid droplets or are secreted into the circulation as VLDL particles. Fatty acids are also incorporated into phospholipids that are an essential component of cell membranes and the surface layer of lipid droplets or VLDL (Rui 2014). Fatty acid β -oxidation can occur in both mitochondria and peroxisomes, whereby peroxisomal and mitochondrial β -oxidation essentially differs in substrate specificities, for example, peroxisomes can also handle very long-chain and branched-chain fatty acids (Violante 2013). Moreover, fatty acids also undergo ω -oxidation forming dicarboxylic acids, which are further oxidised in peroxisomes (Wanders 2011). Endproducts of peroxisomal β -oxidation (medium-chain fatty acids) can be converted to acylcarnitines and are further oxidised to acetyl-CoA in mitochondria (Violante 2013). Beside that, glucose is taken up by glucose transporters (GLUT). Within the cell, glucose is converted into pyruvate by glycolysis or is stored as glycogen. Acetyl-CoA, a common intermediate of glucose and fatty acid oxidation, enters either the citric acid cycle for complete oxidation, producing reducing equivalents that fuel mitochondrial respiration, or it is utilized for lipogenesis (Rui 2014). Two separate genes, acetyl-CoA carboxylases ACC1 and ACC2, encode the two major isoforms of ACC. They are involved in different pathways. The malonyl-CoA synthesised by ACC1 is used in fatty acid synthesis, whereas the malonyl-CoA synthesised by ACC2 is involved in the control of FFA oxidation (Abu-Elheiga 2001). Carnitine palmitoyltransferase 1 (CPT1), which controls the rate limiting step of mitochondrial β -oxidation, is known to be regulated allosterically by malonyl-CoA. Thereby, malonyl-CoA that is generated by ACC2 causes an inhibition of CPT1 and leads to reduced fatty acid import into mitochondria. Malonyl-CoA levels are mainly controlled by AMP-activated protein kinase (AMPK)-induced phosphorylation of ACC. AMPK as a central regulator of cellular energy homeostasis activates catabolic processes and represses many anabolic processes (Hardie 2011).

For storage, the fatty acids have to be esterified with glycerol-3-phosphate, which can be formed from glucose via glycolytic pathway; from glycerol, which is converted to glycerol-3-phosphate by glycerol kinase (GK); and from precursors other than glucose and glycerol (such as pyruvate, lactate and amino acids) by glyceroneogenesis. During glyceroneogenesis, phosphoenolpyruvate is formed via the mitochondrial dicarboxylic shuttle and subsequently glycerol-3-phosphate is produced by a partial reversion of glycolysis (Festuccia 2003). Finally, lipid storage is regulated by TAG synthesis and

lipolysis, whereby proteins involved in lipolysis are highly controlled by phosphorylation or co-regulatory proteins (Nielsen 2014).

Furthermore, PPAR α is the master regulator of fatty acid β -oxidation and peroxisome proliferative activated receptor, gamma, coactivator 1 (PGC1) is capable of driving virtually all aspects of mitochondrial biogenesis. PGC1 increases the number of mitochondria, thereby elevating mitochondrial respiratory capacity and it activates genes that encode proteins of the respiratory chain and proteins involved in fatty acid oxidation (Scarpulla 2012). Moreover, in BAT, FFA are the substrate for thermogenesis and they are also involved in the regulation of UCP1 (Rial 1983).

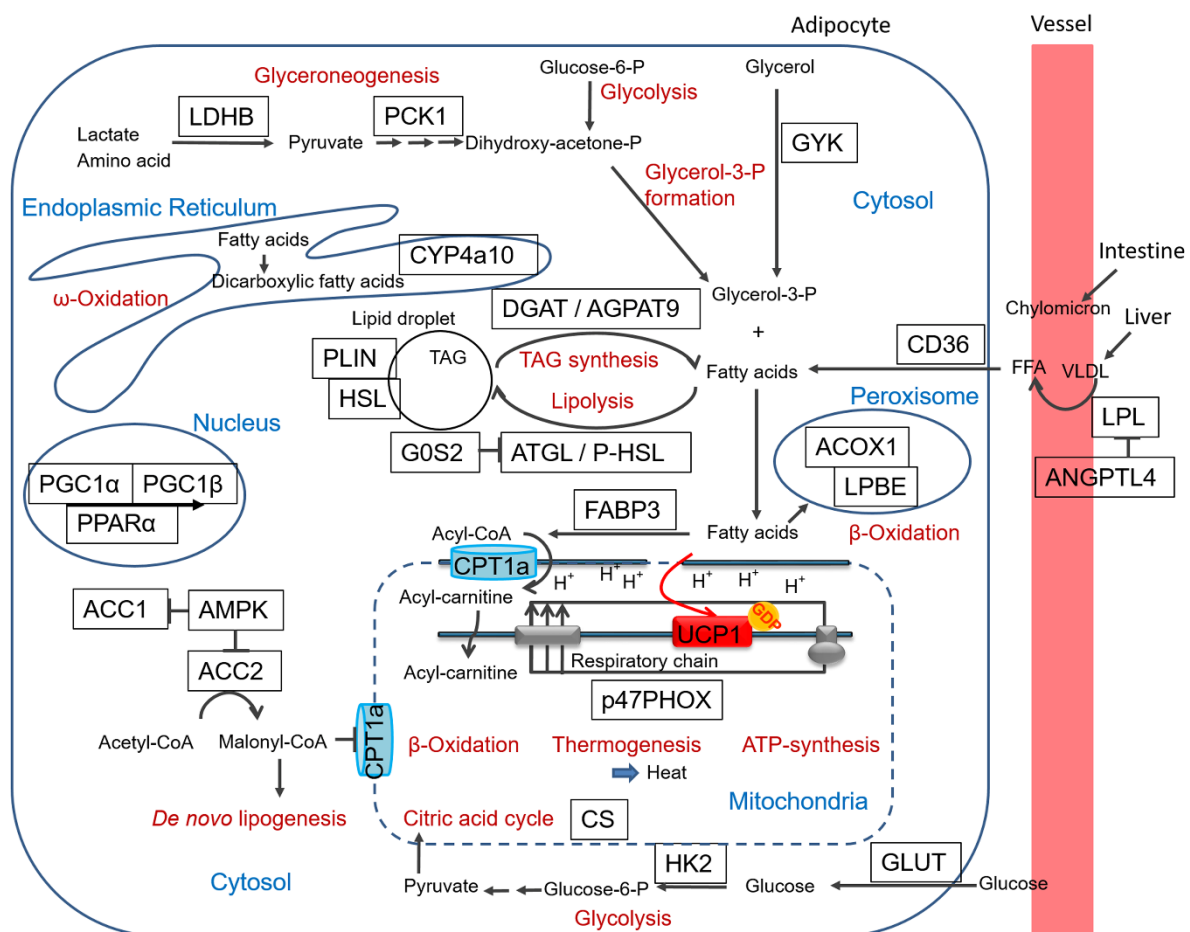


Figure 4. Lipid homeostasis in BAT. Enlisted are pathways and their enzymes involved in fatty acid and glucose uptake and metabolism. Cellular compartments are marked in blue writing and metabolic pathways in red writing. Proteins involved in the pathways are highlighted by boxes. ACC, acetyl-CoA carboxylase; ACOX1, acyl-CoA oxidase 1; AGPAT9, 1-acylglycerol-3-phosphate O-acyltransferase 9; AMPK, AMP-activated protein kinase; ANGPTL4, angiopoietin-like 4; ATGL, adipose triglyceride lipase; ATP, adenosine triphosphate; CD36, fatty acid translocase; CPT1a, carnitine palmitoyltransferase 1a; CS, citrate synthase; CYP4a10, cytochrome P450, family 4, subfamily a, polypeptide 10; DGAT, diglyceride acyltransferase; FABP3, fatty acid binding protein 3; FFA, free fatty acids; GOS2, G0/G1 switch 2; GDP, guanosine diphosphate; GLUT, glucose transporter; GYK, glycerol kinase; H⁺, proton; HK2, hexokinase 2; HSL, hormone sensitive lipase; LDHB, lactate dehydrogenase; LPBE, enoyl-Coenzyme A hydratase; LPL, Lipoprotein lipase; P, phosphate or

phospho; p47PHOX, neutrophil cytosolic factor 1; PCK1, phosphoenolpyruvate carboxykinase 1; PGC1 α/β , peroxisome proliferative activated receptor, gamma, coactivator 1 α/β ; PLIN, perilipin; PPAR α , peroxisome proliferator activated receptor α ; TAG, triacylglycerol; UCP1, uncoupling protein 1; VLDL, very low-density lipoprotein.

1.6.2 Diet-induced thermogenesis

BAT has been recognised as the main site of nonshivering thermogenesis in mammals, and there are indications that it is also the site of the process called diet-induced thermogenesis (DIT). Compared to cold-induced thermogenesis, DIT is triggered by specific food compounds. PUFA, as well as other dietary components, induce thermogenesis, inter alia, impinging on UCP1 expression / activity (Sadurskis 1995, Oudart 1997). It must be kept in mind that DIT, in absolute terms, not only includes the heat production in iBAT (facultative DIT), but also the energy cost due to absorption, digestion and storage of nutrients (obligatory DIT; Oudart 1997). Thermogenic processes occur via a unique biochemical property of the mitochondria in brown adipocytes, wherein the brown adipocyte-specific protein UCP1 physiologically uncouples the respiratory chain by interacting with the respiratory chain and dissipating chemical energy as heat (Figure 4). In this context, the activation of the sympathetic nervous system by cold or overfeeding induces the thermogenic activity of BAT via distinct cellular processes. They include the rapid activation of the existing UCP1 and transcriptional induction of the genes that encode UCP1, components of the enzymatic machinery responsible for oxidising metabolic substrates, and components of the cellular machinery, which are responsible for the active uptake of lipids and glucose from the circulation to sustain oxidation and thermogenesis. Thermogenic capacity is also enlarged by increasing the total number of brown adipocytes, its degree of differentiation and its mitochondrial density. In addition, the vascular supply must be considered (Cannon 2004). Thermogenic capacity can also be increased by PPAR γ agonists (Sell 2004), whereby FFA are the substrate for thermogenesis, but they are also involved in the regulation of UCP1 (Rial 1983).

Activation and recruitment of BAT by various physiological and pharmacological stimuli (Villarroya 2013b) give rise to consistent reduction of body fatness (Rothwell 1979, Feldmann 2009). Thus, impaired thermogenesis by BAT might be one of the causes of obesity, at least in small rodents. Moreover, recent studies have indicated regulatory roles of BAT for insulin sensitivity, glucose homeostasis, and lipoprotein metabolism (Stanford 2013, Bartelt 2011), suggesting that BAT may also improve metabolic syndrome. Besides that, an imaging study in humans has revealed that adults possess BAT depots that are metabolically active and thus make BAT a target for obesity management (Ouellet 2012). Finally, the induction of browning might be a novel method of increasing whole body energy expenditure and combating obesity (Harms 2013).

1.7 Preliminary results of mouse feeding studies that used differential HFDs

Two mouse feeding studies were performed at the TUM-Chair of Nutritional Medicine (Prof. Dr. Hauner) and the TUM-Chair of Nutrition Physiology (Prof. Dr. Daniel), respectively. The corresponding studies examined the improvement of overall health status in DIO mice upon different substitution / supplementation of HFDs (Ludwig 2013, Dahlhoff 2014). However, the mouse studies not only differed in the kind of substitution / supplementation analysed, moreover, HFDs distinct in fat quantity (48 kJ% vs. 60 kJ% fat) and fat quality (palm oil vs. beef tallow) were applied.

1.7.1 Previous findings regarding the impact of n-3 LCPUFA-enriched HFD

In studies emphasising anti-obesogenic and anti-inflammatory effects of n-3 LCPUFA, diets with very high fat content (Janovská 2013), not well-defined fat quality (Todoric 2006), and extreme n-6/n-3 PUFA ratios (Huber 2007) have been applied frequently. However, at the TUM-Chair of Nutritional Medicine, the impact n-3 LCPUFA and/or n-6/n-3 PUFA ratio on DIO and its pathological characteristics was examined, feeding male C57BL/6J mice defined HFDs for 12 weeks (Ludwig 2013). Mice were fed a control diet with 13 kJ% fat (C), a high-fat diet (HF) or n-3 LCPUFA-enriched HFD (HF/n-3) with unbalanced (C, 9.85:1; HF, 13.5:1) or balanced (HF/n-3, 1:0.84) n-6/n-3 PUFA ratio, respectively. The moderate HFDs (48 kJ% fat) were based on soybean and palm oil. In the study by Ludwig et al. (Ludwig 2013) findings indicated that in a DIO mouse model n-3 LCPUFA exert anti-obesogenic effects and apparently improve the overall health status of obese mice. Those effects became apparent by a reduced increase in body weight and fat mass, smaller adipocytes in MAT than epididymal adipose tissue (EAT), improved insulin level, and lower hepatic TAG and plasma non-esterified fatty acids (NEFA) levels. Interestingly, the HF/n-3 animals ingested slightly more energy than HF animals but excreted less energy, indicating a n-3 LCPUFA-induced increase in energy expenditure. Compared with control, gene expression data of key enzymes involved in hepatic lipogenesis and mitochondrial or peroxisomal β -oxidation showed a significant reduction of ACC1 upon HF/n-3, a significant increase of CPT1a upon HF and a significant upregulation of acyl-coenzyme A oxidase 1 (ACOX1) in both high-fat groups, moreover, the respective levels of ACOX1 were significantly higher for HF/n-3 than for HF animals. In addition, UCP1 mRNA level was significantly increased in iBAT upon HF/n-3 compared with HF and C, indicating increased energy expenditure by DIT in these animals.

Furthermore, pathway-specific RT² Profiler™ RT-qPCR arrays for “T and B cell activation” and “Endothelial cell biology” had been carried out with samples of MAT and with mucosal tissue of the small intestine, respectively. The resulting data pointed to T and B cell activation in MAT and an alleviation of HFD-induced endothelial cell activation in the upper small intestine (USI) upon HF/n-3

compared to HF feeding. Further gene expression analyses showed a significant increase of the chemoattractants MCP1 and OPN in MAT and EAT upon both HFDs compared to control, whereby OPN mRNA levels were even more pronounced in HF/n-3 compared with HF animals. Besides that, the significantly enhanced gene expression levels of the pro-inflammatory tumor necrosis factors α (TNF α) and the anti-inflammatory IL10 upon HF/n-3 compared to control in EAT, but not in MAT, suggested n-3 LCPUFA-induced inflammatory changes preferentially in EAT. Analysing the mRNA levels of Integrin α -X (ITGAX) and mannose receptor, C type 1 (MRC1), encoding the surface markers CD11c (marker for the pro-inflammatory M1 macrophage subtype) and CD206 (marker for the anti-inflammatory M2 macrophage subtype) in MAT and EAT, respectively, significantly increased expression levels were observed upon HF/n-3 compared to controls. In addition, the array result for interferon regulatory factor 4 (IRF4), which participates in the regulation of alternative macrophage priming (Eguchi 2013), displayed enhanced expression in HF/n-3 animals compared to HF animals. However, no clear pro- or anti-inflammatory potential could be demonstrated for n-3 LCPUFA in MAT or EAT, although changes of plasma SAA levels and mRNA levels of cell adhesion molecules (ICAM1 and VCAM1) in the small intestine indicated an alleviation of HF-induced systemic inflammation and intestinal endothelial cell activation upon HF/n-3. Moreover, analysis of immune cell infiltration in adipose tissue was missing (findings from this thesis were published in Ludwig et al.) and the higher energy expenditure upon HF/n-3 than HF feeding cannot be explained by the results so far.

1.7.2 Previous findings regarding the impact of methyl-donor supplemented HFD

In another feeding trial carried out at the TUM-Chair of Nutrition Physiology, it was assessed whether NAFLD, induced by HFD over 8 weeks, can be reversed in mice by additional 4 weeks of dietary methyl-donor supplementation (MDS; Dahlhoff 2014). Mice were fed a control diet with 11 kJ% fat (C^A) or a soybean oil / beef tallow-based HFD with 60 kJ% fat (HF^A) for 12 weeks. In the study by Dahlhoff et al. (Dahlhoff 2014) findings indicated that in a DIO mouse model therapeutical MDS failed to reverse NAFLD, but it prevented the progression of hepatic steatosis due to a reduction of hepatic TAG and NEFA content. Increased activation of AMPK α and the upregulation of enzymes involved in fatty acid β -oxidation in the liver upon HF^A / methyl-donor supplemented diet (HFMS) suggested an increase in catabolic pathways that prevent further hepatic lipid accumulation. For both high-fat groups, the gene expression of CPT1a was significantly upregulated compared to control and Western blot analysis showed a significant increase in P-AMPK α and P-AMPK α /AMPK α ratio, whereby total AMPK α content remained unaffected. When comparing HFMS mice and HF^A mice, significant higher levels of P-AMPK α and P-AMPK α /AMPK α ratio, and a significantly enhanced β -hydroxyacyl CoA dehydrogenase activity were found upon HFMS in the liver.

The hepatic C1-metabolism, enzymes involved in this metabolic process were found to be modulated by methyl-donors and n-3 LCPUFA (Dahlhoff 2014, Huang 2012), is of prime importance in hepatic lipid homeostasis providing methyl-groups for the biosynthesis of phosphatidylcholine. Thus, the beneficial effect of MSD supplementation on the progression of hepatic lipid accumulation in obese mice, which were observed in the study by Dahlhoff et al. might most likely be explained by the restored repression of phosphatidylcholine synthesis. In this context, AMPK was considered to link C1-metabolism and β -oxidation.

However, analysis of *de novo* lipogenesis (DNL), another metabolic process that defines hepatic TAG accumulation and is controlled by AMPK, was missing (findings from this thesis were published in Dahlhoff et al.). Noteworthy, the HF^A used in the study by Dahlhoff et al. differed from the HF used in the study by Ludwig et al. in terms of fat quantity and quality (Ludwig 2013).

2 Aim of the thesis

The literature on high-fat diet (HFD)-induced obesity with n-3 long-chain polyunsaturated fatty acid (LCPUFA) intervention is complex and due to the lack of dietary standards to model diet-induced obesity (DIO), its findings are hardly comparable. The DIO mouse model used in this thesis is characterised by well-defined diet composition and study design, and it provides an opportunity for mechanistic examination of the pathways involved in the favourable effects of n-3 LCPUFA-enriched HFD (HF/n-3) in a broad tissue context. Preliminary findings of this mouse study (cf. 1.7.1) that indicated differential inflammatory, metabolic, and vascular changes upon HFDs (HF and HF/n-3), differing in their fat quality and their n-6/n-3 PUFA ratio, warrants further investigations, especially to further clarify the molecular mechanisms that are involved in the immunomodulatory and anti-obesity effects of n-3 LCPUFA. Moreover, for a better understanding of the impact of fat quantity and quality of the HFD on DIO phenotype, expression data of an additional mouse study using another HFD (HF^A; cf. 1.7.2) will be used for comparative analyses.

Thus, the pursued aims of this thesis, which analysed the effects of long-term HFD feeding, were

1) to determine the inflammatory potential of the defined soybean / palm oil based HF (48 kJ% fat) in different tissue and to explore whether its partial substitution with n-3 LCPUFA can modulate adipose tissue inflammation. Therefore, immune cell infiltration, especially by macrophage, should be examined by RT-qPCR and immunohistochemical analyses and the macrophage phenotype should be characterised in the visceral fat depots epididymal and mesenteric adipose tissue (EAT and MAT), and even in interscapular brown adipose tissue (iBAT), since certain immune cells can play a role in thermogenesis.

2) to analyse the impact of the HFDs on endothelial cell biology in the small intestine and to examine whether potential adverse effects of HF can be improved by n-3 LCPUFA. Proteins involved in the regulation of nitric oxide bioavailability and in the maintenance of vascular integrity were among the target genes. Moreover, in order to get first physiological insights on endothelial function, plasma albumin levels should be measured.

3) to characterise the anti-obesogenic effect of n-3 LCPUFA during high-fat feeding by analysing lipid metabolism and diet-induced thermogenesis (DIT) in the small intestine, the liver and iBAT.

4) to investigate the effects of different fat quantity, quality and substitution / supplementation on hepatic lipid metabolism in DIO by comparative analyses of expression data from two different mouse feeding studies that used distinct HFDs.

3 Methods

3.1 Study designs

The data presented in this thesis were obtained from analyses of two mouse feeding studies, whereby part of the findings were already published in Ludwig et al. and Dahlhoff et al. as a result of cooperative collaborations. Emphasis was laid on the study by Ludwig et al. (Ludwig 2013) analysing the impact of n-3 LCPUFA and/or n-6/n-3 PUFA ratio in a DIO mouse model (Figure 5), which was designed at the TUM-Chair of Nutritional Medicine (Prof. Dr. Hauner; Dr. Bernhard Bader). However, data obtained from a second feeding trial carried out at the TUM-Chair of Nutrition Physiology (Prof. Dr. Daniel), were taken for comparative analyses. The study by Dahlhoff et al. (Dahlhoff 2014) examined the impact of MDS in another DIO mouse model (Figure 6) using a HFD distinct in fat quantity and quality.

3.1.1 Feeding trial analysing the impact of n-3 LCPUFA and/or n-3/n-6 PUFA ratio on DIO

The first trial (Figure 5) was performed as described by Ludwig et al. (Ludwig 2013). In brief, six-week-old male C57BL/6J mice were obtained from Charles River Laboratories and single-housed under controlled, specific-pathogen-free (SPF) conditions at constant temperature (22 °C) and humidity with a 12 h light / dark cycle. They had ad libitum access to food and water. Upon arrival, C57BL/6J mice were adapted on a control diet (C) for two weeks. At the age of eight weeks, mice were randomly assigned to two cohorts, which differ in feeding time. One cohort was fed for 6 weeks and the other one for 12 weeks. Each cohort was further divided into three dietary groups (n=12 mice per group): C with 13 kJ% fat (already used for adaptation), HFD with 48 kJ% fat (HF), and HFD enriched with n-3 LCPUFA concentrate (EPAX 1050-TG; rich in EPA and DHA) with 48 kJ% fat (HF/n-3). For more detailed information on diet composition (Table 1) and fatty acid pattern (Table 2) see chapter 3.2. At the end of the feeding period, animals were euthanised in the postprandial state by carbon dioxide and cervical dislocation. Blood was withdrawn from the inferior vena cava and plasma was stored in heparinised tubes. For analysis, adipose tissue depots (mesenteric, epididymal, interscapular brown), liver, spleen and small intestinal mucosa [USI and lower small intestine (LSI)] were sampled, weighed, snap-frozen in liquid nitrogen and stored at -80 °C. All procedures applied throughout this study were conducted according to the German guidelines for animal care and approved by the district Oberbayern ethics committee.

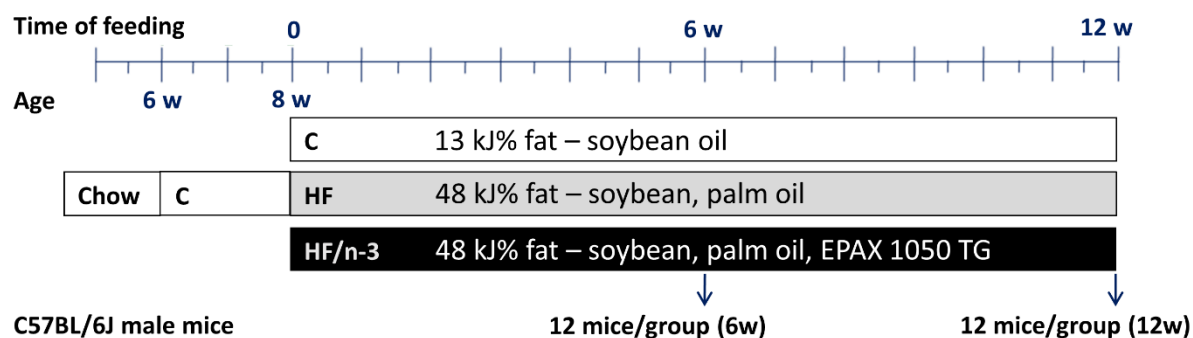


Figure 5. Study design of feeding trial analysing the impact of n-3 LCPUFA and/or n-6/n-3 PUFA ratio on DIO. 72 male C57BL/6J mice aged 6 weeks were adapted on control diet for 2 weeks. Mice were then randomly assigned to three groups and fed different diets: control diet with 13 kJ% fat (C), HFD with 48 kJ% fat (HF), and HFD enriched with n-3 LCPUFA concentrate (EPAX 1050-TG; rich in EPA and DHA) with 48 kJ% fat (HF/n-3). Mice were sacrificed after 6 or 12 weeks for dissection and organ sampling.

3.1.2 Feeding trial analysing the impact of methyl-donor supplementation on DIO

The second trial (Figure 6) was performed as described by Dahlhoff et al. (Dahlhoff 2014). In brief, eight-week-old male C57BL/6NCRl mice were obtained from Charles River Laboratories and maintained in a 12 h light / dark cycle with unlimited access to food and water. Upon arrival, the mice were fed standard laboratory chow (Ssniff Spezialdiäten; cat. no. E1534) for two weeks. The following 12-week feeding trial was bipartite including at first a 8-week period to achieve DIO associated with NAFLD in mice (DIO-phase) followed by a 4-week period of MDS (MDS-phase). At the age of ten weeks, the beginning of DIO-phase, mice were randomly assigned to two cohorts (n=23 mice per group), which were fed control diet with 11 kJ% fat (C^A) or HFD with 60 kJ% fat (HF^A) for 8 weeks. At the end of the DIO-phase (8-week trial), five animals of each dietary group were analysed to determine the status of obesity and NAFLD. For the MDS-phase, C^A mice were divided into a control group (C^A) and a C^A / methyl-donor supplemented group (CMS), and the HF^A mice were divided into a high-fat group (HF^A) and a HF^A / methyl-donor supplemented (HFMS) group, respectively (n=9 mice per group) and were fed further 4 weeks (12-week trial). For more detailed information on diets see chapter 3.2, Table 3 - Table 5. At the end of the feeding period, animals were euthanised in a non-fasting state by isoflurane and cervical dislocation. For analysis, the liver was sampled, snap-frozen in liquid nitrogen and stored at -80 °C. All procedures applied throughout this study were conducted according to the German guidelines for animal care and approved by the district Oberbayern ethics committee.

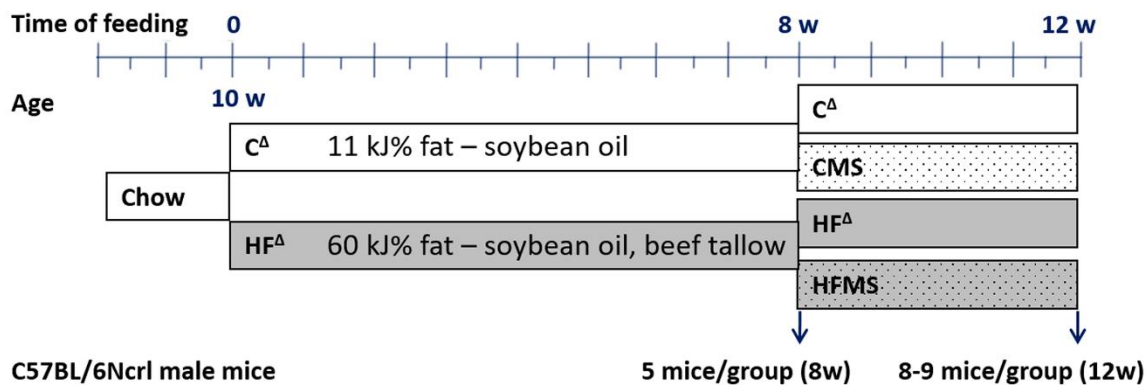


Figure 6. Study design of feeding trial analysing the impact of methyl-donor supplementation on DIO. 46 male C57BL/6Ncr1 mice aged 8 weeks were fed chow diet for 2 weeks. Mice were then randomly assigned to control diet (C^{Δ}) or HFD (HF^{Δ}) and fed for 8 weeks. This phase called diet-induced obesity (DIO)-phase was followed by the methyl-donor supplementation (MDS)-phase in which the groups were further divided into non-MDS groups (C^{Δ} and HF^{Δ}) and MDS groups (CMS and HFMS). The mice were fed additional 4 weeks before dissection and sampling (12-week trial). Five animals of the C^{Δ} and HF^{Δ} group were already dissected and sampled after the DIO-phase (8-week trial).

3.2 Diets

All diets were purified experimental diets manufactured as pellets. Diets were sterilised with 25 kGy γ -radiation by Isotron Deutschland and stored in the dark at either -20°C (long-term) or 4°C (short-term).

The trial that analysed the impact of n-3 LCPUFA and/or n-6/n-3 PUFA ratio on DIO (cf. 3.1.1) used soybean / palm oil-based diets purchased from Ssniff Spezialdiäten: control diet (C) with 13 kJ% fat (cat. no. S5745-E720) or isocaloric HFDs (HF and HF/n-3) with 48 kJ% fat (HF; cat. no. S5745-E722 and HF/n-3; cat. no. S5745-E725), for HF/n-3, SFA and MUFA were partially substituted by n-3 LCPUFA EPA and DHA (EPAX 1050-TG; kindly provided by Goerlich Pharma International). Compositions of diets were nearly constant among diets. Fat and starch content were the only variables (C - 5 % soybean oil and 47.8 % corn starch; HF - 5 % soybean oil, 20 % palm oil, and 27.8 % corn starch; HF/n-3 - 5 % soybean oil, 11.25 % palm oil, 8.75 % EPAX 1050 TG, and 27.8 % corn starch). For more detailed information on soybean / palm oil-based diets see Table 1 and Table 2.

The trial that analysed the impact of MDS on DIO (cf. 3.1.2) used soybean oil / beef tallow-based diets purchased from Ssniff Spezialdiäten: control diets (C^{Δ} and CMS) with 11 kJ% fat (C^{Δ} ; cat. no. E15000-04) or HFDs (HF^{Δ} and HFMS) with 60 kJ% fat (HF^{Δ} ; cat. no. E15741-34). Compositions of diets were nearly constant among diets. Fat and carbohydrate content were the most variable contents (C^{Δ} and CMS - 4 % soybean oil, 46.8 % corn starch, and 10.8 % sugar / dextrine; HF^{Δ} and HFMS - 3.1 %

soybean oil, 31.5 % beef tallow, 2.2 % corn starch, and 22.4 % sugar / dextrine). Methyl-donor supplemented diets (CMS and HFMS) contained additionally 15 g/kg choline chloride, 15 g/kg betaine, 7.5 g/kg methionine, 15 mg/kg folic acid, 1.5 mg/kg vitamin B12 and 150 mg/kg ZnSO₄. For more detailed information on soybean oil / beef tallow-based diets see Table 3 - Table 5.

Table 1. Composition of the soybean / palm oil-based diets

Cat. no.: S5745-	E720	E722	E725
Nutrient	C	HF	HF/n-3
Lipids (%)			
Soybean oil	5.00	5.00	5.00
Palm oil	-	20.00	11.25
EPAX 1050 TG (DHA / EPA)	-	-	8.75
Cholesterol	0.013	0.038	0.021
Carbohydrates (%)			
Corn starch	47.79	27.79	27.79
Maltodextrin	5.60	5.60	5.60
Sucrose	5.00	5.00	5.00
Cellulose	5.00	5.00	5.00
Protein (%)			
Caseine	24.00	24.00	24.00
Antioxidants (%)			
Butylhydroxytoluene	0.015	0.015	0.015
dl- α -tocopheryl acetate	0.018	0.018	0.018
Others (%)			
L-cystine	0.20	0.20	0.20
Vitamins	1.20	1.20	1.20
Minerals & trace elements	6.00	6.00	6.00
Choline-chloride	0.20	0.20	0.20
Metabolizable energy (MJ/kg)	15.50	19.80	19.80
Fat (kJ%)	13.00	48.00	48.00
Carbohydrates (kJ%)	64.00	34.00	34.00
Protein (kJ%)	23.00	18.00	18.00

Shown are w/w or energy% (en%) macronutrients and other ingredients in diets used in the study by Ludwig et al. (Ludwig 2013). C, control diet; HF, HFD; HF/n-3, HFD enriched with n-3 LCPUFA (DHA / EPA). Nutrient composition was nearly kept constant across different diets except for carbohydrate and fat components. Metabolizable energy was calculated according to Atwater in MJ/kg (provided by Ssniff Spezialdiäten).

Table 2. Fatty acid pattern of the soybean / palm oil-based diets

Cat. no.: S5745-		E720	E722	E725
Fatty acid species		mass%		
		C	HF	HF/n-3
Lauric acid	12:0	0.07	0.13	0.09
Myristic acid	14:0	0.30	0.88	0.66
Pentadecanoic acid	15:0	0.04	0.05	0.07
Palmitic acid	16:0	11.37	36.70	23.91
Palmitoleic acid	16:1	0.12	0.15	0.30
Heptadecanoic acid	17:0	0.09	0.10	0.18
Heptadecenoic acid	17:1	0.05	-	0.07
Stearic acid	18:0	3.60	4.18	4.00
Elaidic acid	18:1	0.08	0.14	0.07
Oleic acid	18:1	23.47	35.81	26.08
cis-Vaccenic acid	18:1	1.53	0.87	1.11
18:2 Isomer	18:2	0.38	0.20	0.14
Linoleic acid	18:2	n-6 50.85	18.07	16.00
γ -Linolenic acid	18:3	n-6 -	-	0.12
Conjugated Linoleic acid	18:2	0.11	-	-
18:3 Isomer	18:3	0.39	0.09	0.10
Linolenic acid	18:3	n-3 5.16	1.34	1.40
Stearidonic acid	18:4	n-3 -	-	0.16
Arachidic acid	20:0	0.35	0.38	0.48
Eicosenoic acid	20:1	0.22	0.15	0.83
Eicosadienoic acid	20:2	n-6 -	-	0.21
Heneicosanoic acid	21:0	-	-	0.04
Eicosatrienoic acid	20:3	n-6 -	-	0.09
Arachidonic acid	20:4	n-6 -	-	0.90
Eicosatrienoic acid	20:3	n-3 -	-	0.14
Eicosapentaenoic acid (EPA)	20:5	n-3 -	-	4.05
Behenic acid	22:0	0.48	0.16	0.27
Cetoleic acid	22:1	0.11	-	0.11
Erucic acid	22:1	-	-	0.12
Docosatetraenoic acid	22:4	n-6 -	-	0.11
Docosapentaenoic acid	22:5	n-6 -	-	0.77
Docosapentaenoic acid	22:5	n-3 -	-	0.88
Docosahexaenoic acid (DHA)	22:6	n-3 -	-	15.05
Tricosanoic acid	23:0	0.04	-	-
Lignoceric acid	24:0	0.17	0.09	0.13
Nervonic acid	24:1	0.36	-	0.36
SFA		16.55	42.66	29.83
MUFA		25.95	37.14	29.05
PUFA		56.90	19.70	40.12
n-3 PUFA		5.16	1.34	21.68
n-6 PUFA		50.85	18.07	18.19
ratio n-6/n-3 PUFA		9.85	13.50	0.84
ratio SFA/PUFA		0.29	2.17	0.74

Cx:n indicates the length of the fatty acid with x carbons containing n double bonds. C, control diet; HF, HFD; HF/n-3, HFD enriched with n-3 LCPUFA (DHA / EPA); MUFA, monounsaturated fatty acids; PUFA, polyunsaturated fatty acids; SFA, saturated fatty acids.

Table 3. Composition of the soybean oil / beef tallow-based diets

Cat. no.:	E15000-04	E15741-34
Nutrient	C ^Δ (CMS)	HF ^Δ (HFMS)
Lipids (%)		
Soybean oil	4.00	3.10
Beef tallow	-	31.00
Carbohydrates (%)		
Corn starch	46.80	2.20
Sugar / dextrin	10.80	22.40
Cellulose	5.00	6.00
Protein (%)		
Caseine	24.00	27.70
Others (%)		
L-cystine	0.20	0.35
Vitamins	1.00	1.00
Minerals & trace elements	6.00	6.00
Choline-chloride	0.20	0.25
Metabolizable energy (MJ/kg)	15.00	21.40
Fat (kJ%)	11.00	60.00
Carbohydrates (kJ%)	66.00	21.00
Protein (kJ%)	23.00	19.00

Shown are w/w or energy% (en%) macronutrients and other ingredients in diets used in the study by Dahlhoff et al. (Dahlhoff 2014). C^Δ, control diet; CMS, C^Δ / methyl-donor supplemented diet; HF^Δ, HFD; HFMS, HF^Δ / methyl-donor supplemented diet. Nutrient composition was nearly kept constant across different diets except for carbohydrate and fat components. Metabolizable energy was calculated according to Atwater in MJ/kg (provided by Ssniff Spezialdiäten).

Table 4. Fatty acid pattern of the soybean oil / beef tallow-based diets

Cat. no.:	E15000-04	E15741-34
Fatty acid species	mass%	
	C ^Δ (CMS)	HF ^Δ (HFMS)
C12:0	-	0.10
C14:0	0.48	3.33
C16:0	10.84	26.13
C17:0	-	1.23
C18:0	4.58	18.19
C20:0	0.48	0.13
C16:1	0.48	2.53
C18:1	25.78	39.41
C20:1	-	0.03
C18:2	51.08	7.68
C18:3	6.27	1.07
C20:4	-	0.23
SFA	16.38	49.11
MUFA	26.26	41.97
PUFA	57.35	8.98
ratio SFA/PUFA	0.29	5.47

C^Δ, control diet; CMS, C^Δ / methyl-donor supplemented diet; Cys, cysteine; HF^Δ, HFD; HFMS, HF^Δ / methyl-donor supplemented diet; MUFA, monounsaturated fatty acids; PUFA, polyunsaturated fatty acids; SFA, saturated fatty acids

Table 5. Amino acid, vitamin and trace element pattern of soybean oil / beef tallow-based diets

	C ^A	CMS	HF ^A	HFMS
Amino acids [g/kg]				
Lysine	17.1	17.1	19.8	19.8
Methionine	7.3	14.8	8.3	15.8
Cystine	0.9	0.9	4.6	4.6
Met+Cys	8.2	15.7	12.8	20.3
Threonine	9.3	9.3	10.7	10.7
Tryptophan	2.7	2.7	3.1	3.1
Arginine	7.6	7.6	8.8	8.8
Histidine	6.6	6.6	7.6	7.6
Valine	14.2	14.2	16.4	16.4
Isoleucine	10.9	10.9	12.5	12.5
Leucine	20.5	20.5	23.6	23.6
Phenylalanine	11.1	11.1	12.9	12.9
Phe+Tyr	22.2	22.2	25.7	25.7
Glycine	4.3	4.3	5	5
Glutamic acid	46.9	46.9	54.1	54.1
Aspartic acid	15.5	15.5	17.9	17.9
Proline	23.9	23.9	27.6	27.6
Alanine	6.8	6.8	7.9	7.9
Serine	12.4	12.4	14.3	14.3
Vitamins [mg/kg]				
Vitamin A	15000 IU	15000 IU	15000 IU	15000 IU
Vitamin D3	1500 IU	1500 IU	1500 IU	1500 IU
Vitamin E	150	150	150	150
Vitamin K (as menadione)	20	20	20	20
Vitamin C	30	30	30	30
Thiamin (B1)	16	16	16	16
Riboflavin (B2)	16	16	16	16
Pyridoxine (B6)	18	18	18	18
Cobalamin (B12)	0.03	1.53	0.03	1.53
Nicotinic acid	49	49	45	45
Pantothenic acid	56	56	55	55
Folic acid	19	34	19	34
Biotin	0.31	0.31	0.31	0.31
Choline chloride	1040	16040	2300	17300
Inositol	80	80	80	80
Betaine	-	15000	-	15000
Trace elements [mg/kg]				
Iron	166	166	139	139
Manganese	98	98	82	82
Zinc	65	65	56	56
Zinc sulfate	-	150	-	150
Copper	14	14	12	12
Iodine	1.2	1.2	0.97	0.97
Selenium	0.14	0.14	0.13	0.13
Cobalt	0.15	0.15	0.13	0.13

Nutrient composition is expressed as [w/w], except it is delineated differently. C^A, control diet; CMS, C^A / methyl-donor supplemented diet; Cys, cysteine; HF^A, HFD; HFMS, HF^A / methyl-donor supplemented diet; IU, international unit; Met, methionine; Phe, phenylalanine; Tyr, tyrosine.

3.3 Fat intake

Values that were used for the calculation of fat intake, such as food intake (g/wk), energy intake (kJ/wk) and energy excretion (kJ/wk) were taken from Ludwig et al. (Ludwig 2013), whereby single values were used instead of mean values except for the calculation of the assimilation efficiency. Further values needed, such as metabolizable energy (MJ/kg) and energy% fat of the diets, are given in Table 1 (cf. 3.2). It was assumed that fat contains 37.67 kJ energy per gram fat. Assimilation efficiency was included in the calculation.

Values were calculated as follows:

energy intake (kJ/wk) = food intake (g/wk) * metabolizable energy (MJ/kg)

fat intake (g/wk) = [energy intake (kJ/wk) * energy% fat] / 37.67 kJ/g

assimilation efficiency = [energy intake (kJ/wk) - energy excretion (kJ/wk)] / energy intake (kJ/wk)

Calculation of body weight adjusted fat intake based on the publication by Kless et al. (Kless 2017).

Formula obtained from linear regression analysis between fat intake and final body weight to obtain the calculated fat intake y (g/wk) for both high-fat groups

HF: $y = 0.007264$ (1/wk) * final body weight (g) + 0.3901 (g/wk);

HF/n-3: $y = 0.004916$ (1/wk) * final body weight (g) + 0.5608 (g/wk)

Residual (g/wk) = calculated fat intake (g/wk) - fat intake (g/wk)

Body weight adjusted fat intake (g/wk) = calculated fat intake of medium body weight (group-specific mean value of calculated fat intake; g/wk) + residual (g/wk)

3.4 RNA and protein isolation

To obtain homogenous tissue samples, tissues were separately ground in frozen state with liquid nitrogen and stored at -80 °C. Tissue powder aliquots (30 mg or 80 mg for RNA isolation and 50 to 100 mg for protein isolation) were homogenised, using the ART-MICCRA D-8 homogeniser (Micra ART Labortechnik), in Qiazol® lysis reagent (Qiagen) or radioimmunoprecipitation assay (RIPA) buffer (recipe cf. 3.14.1) added with proteinase and phosphatase inhibitors (Sigma-Aldrich and Roche) for RNA or protein extraction, respectively. mRNA or total RNA (including small RNAs) was extracted with chloroform (1/5 volume), after the homogenate was incubated for 5 min at room temperature. After an additional incubation on room temperature for 3 min a centrifugation with 12000 x g was performed at 4 °C for 15 min. The aqueous phase was transferred, added with 1 volume of cold ethanol and further purified with mRNeasy® mini kit or the miRNeasy® mini kit (Qiagen) according to the manufacturer's instructions, respectively. To avoid DNA contamination, on-column DNase I (Qiagen) digestion was performed. The RNA concentration of the eluate was determined with

NanoDrop ND-1000 UV-Vis spectrophotometer (Peqlab) and quality confirmed with the RNA 6000 Nano kit on an Agilent 2100 Bioanalyzer (Agilent Technologies) according to the manufacturer's instructions and expressed as RNA integrity number (RIN), which was always above a value of five. RNA was used in real-time quantitative polymerase chain reaction (RT-qPCR) assays (cf. 3.7). For protein extraction, homogenates were incubated 1 hour on ice and afterwards centrifuged with 2000 x g at 4 °C for 2 min to remove cell debris. In case of iBAT, an additional centrifugation with 16000 x g was performed at 4 °C for 15 min. Protein concentration of extracts was then determined by bicinchoninic acid (BCA) method (Smith 1985; Pierce Thermo Scientific) in a 96-well plate with a bovine serum albumin (BSA) standard at 562 nm using an UV-Vis spectrophotometer (Tecan). Finally, extracts were diluted with sodium dodecyl sulfate polyacrylamide gel electrophoresis (SDS-PAGE) sample buffer (recipe cf. 3.14.1), boiled at 95 °C for 5 min for denaturation and stored at -80 °C until use in SDS-PAGE and Western blotting (cf. 3.8).

3.5 Primer design and primer testing

Oligonucleotides / primers used for differential gene expression analysis, were either commercially available as QuantiTect® primer assays (Qiagen) or as RT² qPCR Primer Assay (Qiagen / SABioscience), or custom-designed primer pairs, i.e. forward and reverse primers, selected according to strict criteria (cf. 9.1, for primer details). Before starting primer design, Ensembl genome browser (www.ensembl.org) databases were checked for alternative transcript variants. Areas of primer annealing were chosen in Ensemble genome browser, primer characteristics specified like this: exon-exon spanning primer and an amplicon size of 100-150 bp. A suitable primer was picked and further analysed with OligoCalc (www.basic.northwestern.edu/biotools/oligocalc.html). Primers should be between 18-25 bp long with a G-C base pair content of 40-70 % and should have a melting temperature (T_m ; salt-adjusted) of 60-64 °C and T_m (nearest neighbor) of 56-58 °C. Furthermore, primer pairs were checked for self-complementarity and "blasted" with BLAST to exclude annealing to non-specific target sequences. Next, primer sequences were checked for heterodimer formation by IDT OligoAnalyzer (<http://eu.idtdna.com/analyzer/applications/oligoanalyzer>). Finally, the sequences were checked for target specificity with University of California, Santa Cruz (UCSC) in silico PCR (<http://genome.ucsc.edu>). Primers were synthesised commercially by Metabion international AG. In a final step, specificity and specific annealing temperature were tested in RT-qPCR and verified with agarose gel electrophoresis (cf. 3.6).

3.6 Agarose gel electrophoresis

Agarose gel electrophoresis was performed to verify molecular sizes of RT-qPCR products and to evaluate primer specificity. A 2 % agarose gel in 0.5 % Tris / borate / EDTA (TBE) buffer (recipe cf. 3.14.3) was cast in a suitable chamber (Biometra). Ethidium bromide or Roti®-Safe GelStain (Carl Roth) was added to the agarose-TBE solution to allow visualisation under UV-light (Intas) by intercalation into nucleic acids. Samples were diluted with Orange G dye (5:1; recipe cf. 3.14.3) before being applied to the gel. For size reference, GeneRuler™ 50 bp DNA Ladder (Fermentas) was used.

3.7 Gene expression analysis

Expression of specific target genes was evaluated with RT-qPCR. For each sample, 10 ng of extracted RNA was needed per reaction using the QuantiTect® quantitative, real-time one-step RT-PCR kit (Qiagen) following the supplier's protocol. Primers used were designed (cf. 3.5) or purchased from Qiagen (cf. 9.1). RT-qPCR was performed using SYBR Green I dye and a realplex4 Mastercycler eppgradient S (Eppendorf). The following thermal cycling conditions were used: 30 min at 50 °C (cDNA synthesis), 15 min at 95 °C (inactivation of reverse transcriptase (RT)) followed by 40 cycles at 95 °C for 15 s, 60 °C (55 °C for Qiagen primers) for 30 s and 72 °C for 30 s. The PCR was concluded with a melting curve analysis of the PCR product (1.75 °C/min). C_q -values were retrieved from the realplex 2.0 software (CalQplex algorithm; Eppendorf) and analysed according to the $\Delta\Delta C_q$ -method (Livak 2001). To normalise data, the following genes were used as invariant controls: iBAT, cyclophilin B (CypB) and heat shock protein 90 (cytosolic) and class B member 1 (Hsp90 α b1); liver, hypoxanthine-guanine phosphoribosyltransferase1 (Hprt1) and β -actin (Actb); USI, glyceraldehyd-3-phosphat-dehydrogenase (Gapdh), Actb and Hprt1; LSI, CypB and Hsp90 α b1; EAT, Gapdh and Actb; MAT, Hprt1 and Actb; spleen, Gapdh and Hprt1; liver (feeding trial by Dahlhoff et al.), Gapdh and Hprt1. For all groups, data were expressed as mean \pm standard error relative to control samples. As RT-qPCR assay controls non-template assays and (-)-RT assays were included for every primer used. Finally, target specificity was analysed by melting curve analysis and agarose gel electrophoresis (cf. 3.6).

3.8 SDS-PAGE and Western blot

Protein expression was analysed in the small intestine and iBAT, and livers from both feeding studies. Equal amounts of protein (30-80 μ g/lane) were loaded on a 7.5, 10 or 12.5 % sodium dodecyl sulfate (SDS) polyacrylamide gel (recipe cf. 3.14.1) and separated by electrophoresis (SDS-PAGE). An appropriate protein standard ladder served as reference. Subsequently, proteins were blotted on to

a 0.2 µm Protran™ nitrocellulose membrane (GE Healthcare Life Sciences) using the tank blot Eco-Mini system (Biometra). The membrane was washed with Tris-buffered saline (TBS, recipe cf. 3.14.2) and blocked with 2 % ECL Advance™ blocking reagent (GE Healthcare Life Sciences). After washing with TBS + Tween-20 (TBS-T), membranes were incubated with primary antibody at 4 °C overnight in TBS-T + 2 % BSA or 2 % ECL Advance™ blocking reagent, depending on antibody. Detection was performed with the Odyssey Infrared Detection system (LI-COR Biosciences) using an IRDye800CW-conjugated goat anti-rabbit or IRDye680RD-conjugated donkey anti-mouse secondary antibody (LI-COR Biosciences). Staining for citrate synthase (CS) served as mitochondrial loading control. Expression of β-ACTIN, HSP90 or HPRT was measured as an invariant control. Densitometric analysis was performed using Odyssey application software version 3.0 (LI-COR Biosciences). Antibodies used in this thesis are listed in the materials sections (cf. 9.2).

Recruitment of iBAT was represented as UCP1 content in total iBAT and calculated as follows: [UCP1 expression * dilution factor for protein content * (total iBAT in mg / weighed portion of iBAT for protein isolation in mg)] (normalised values were used).

The relative protein expression capacity index was calculated as follows: $\{[(\text{protein expression} * \text{total iBAT in mg}) / \text{body mass in mg}] * 100 \%$ (normalised values were used).

3.9 Chemical analysis

To determine triacylglycerol (TAG) content in iBAT, grounded tissues were homogenised in HB-buffer (recipe cf. 3.14.4). TAG was extracted as follows; supernatants were collected after centrifugation with 23100 x g at 4 °C for 15 min and incubated at 70 °C for 5 min. After incubation on ice for 5 min and another centrifugation with 23100 x g at 4 °C for 15 min the TAG concentrations were determined in the samples using the serum triglyceride determination kit from Sigma-Aldrich, following the manufacturer's instructions. For measurement in 96-well plates, the reaction volume was scaled down (1/8 for reagents and 1/2 for samples). Results were normalised to total weight and total protein content of the tissue (determined by BCA method).

3.10 Para-formaldehyde fixed and paraffin-embedded tissue sections

For histological analyses, pieces of VATs (EAT and MAT), iBAT and spleen were fixed in 4 % paraformaldehyde overnight, washed in phosphate-buffered saline twice and then kept in 70 % ethanol for one week. Tissues were subsequently dehydrated in ethanol and xylene of different concentrations with a TP1020 Tissue Processor (Leica Microsystems) and embedded in pre-warmed

Paraplast®paraffin at 60 °C on a Mikrom AP280-1/2/3 automatic embedding station (Microm / Thermo Fisher Scientific).

3.11 Immunohistochemical stainings and morphometry

For immunohistochemistry of paraformaldehyde-fixed paraffin-embedded EAT, MAT and iBAT, 6- μ m-thick sections of each tissue were dewaxed and stained with specific primary antibodies, followed by antigen signal detection using corresponding specific secondary antibodies combined with the Bond Polymer Refine Detection kit (Leica Microsystems) and a polymeric horseradish peroxidase linker antibody conjugate with 3,3'-diaminobenzidine tetrahydrochloride. Stainings were performed with the support of the research group of Prof. Dr. Heikenwalder (TUM, Institute of Virology, Munchen) using an automated IHC stainer (Leica Microsystems). Finally, sections were counterstained with hematoxylin. Primary antibodies (cf. 9.2) against macrophage antigens, T or B cell antigens, and proliferation marker, as well as apoptosis antibodies were applied. Tissue sections were observed with a DMI 4000 B microscope and Leica Application Suite version 3.7 (Leica Microsystems). Digital images were taken with a Leica DFC490 camera at x200 magnification for VATs sections and at x400 magnification for iBAT sections. Furthermore, close-ups from representative CLS in iBAT were taken at x630 magnification and measurements of total section area were performed using the polygon and measurement tool in ImageJ (Open Source; Wayne Rasband (NIH)).

The number of CLS or solitary cells was counted in the whole area of each stained section and expressed as the mean number per mm² of tissue section, not including those observed within vessels and adipose tissue lymphoid aggregates. A minimum of 2 complete sections of each animal (n=4-5/group) was analysed.

Important to note, specific definitions are lacking with regard to the number of macrophages typically composing a CLS (West 2009). Following an initial description of CLS (Weisberg 2003), these structures are defined as macrophages aggregates completely surrounding adipocytes. These aggregates, which contain up to 15 macrophages, have been termed CLS and postulated to represent the vestigial lipid droplets of dead adipocytes (Cinti 2005b). In other papers, CLS were defined as three or more cells stained positively for a macrophage-specific marker surrounding an adipocyte (Kolak 2007, Wentworth 2010, Altintas 2011). For this thesis, the latter classification was used and cells that were stained positive for an immune cell marker, but did not correspond to this classification were defined as solitary cells. Moreover, subgroups of CLS have been defined based on differences in their morphological characteristics, which were as follows: "CLS" - circular regions with continuous rim of macrophages; "cluster" - clusters of macrophages, which form multinucleated giant cells; "others" - three or more CLS-associated macrophages, which do not form such distinct

patterns but surround an adipocyte. Total counts as well as the counts of the subgroups were expressed as the mean number per mm² of tissue section. Furthermore, the subgroups were presented as percentage of total counts (cf. Figure 10).

For T cell differentiation marker expression analysis, 6- μ m-thick cryosections from splenic tissue embedded in OCT TissueTek freezing medium (Sakura Finetek) were cut with a Cryo-Star HM 560 MV (Microm / Thermo Fisher Scientific), fixed briefly in acetone and processed for staining with the following primary antibodies (cf. 9.2) and antigen signal detection system, using corresponding specific secondary antibodies combined with the Bond Polymer Refine Red Detection kit (Leica Microsystems). Fast Red served as substrate chromogen and hematoxylin was used for counterstaining. Stainings were carried out with the support of the research group of Prof. Dr. Heikenwalder (TUM, Institute of Virology, Munchen) using an automated IHC stainer (Leica Microsystems). Tissue sections were observed with a DMI 4000 B microscope and Leica Application Suite version 3.7 (Leica Microsystems) and digital images were taken with a Leica DFC490 camera at x100 magnification. Antigen signal-positive stained areas were quantified using Image-Pro Plus version 7.0 software (Media Cybernetics), and expressed as a percentage of total section area. The complete section of four to six animals per group was analysed.

3.12 ELISA

MCP1 plasma levels were determined using heparin stabilised plasma and the commercially available mouse MCP-1 ELISA Ready-SET-Go! Set (eBiosciences), following the supplier's instructions.

Plasma albumin levels were determined using the commercially available mouse Albumin ELISA Quantitation Set and the ELISA Starter Accessory Kit (Bethyl Laboratories), following the supplier's instructions. The initial standard dilution was divided into 2 steps (300000 and 10000 ng/ml) for better handling of the high concentrated standard (30 mg/ml). Moreover, the heparin stabilised plasma samples were diluted 1:10⁶ before measurement.

3.13 Statistical measurements

All data were expressed as means \pm standard error of the means (SEM). Statistical analyses were performed using Prism 5 (GraphPad Software). Differences were considered statistically significant with *p < 0.05, **p < 0.01, ***p < 0.001 compared with control group or high-fat groups. For normal distributed samples, one-way ANOVA was used to detect differences between dietary groups with Tukey's post-test to identify significant differences. In case of no normal distribution or n < 5, Kruskal-Wallis test and Dunn's post-test were applied.

Exception: Figure 8C and Figures 10A and 10C; only the high-fat groups were compared ($n < 5$). Thus, Mann Whitney test was used to detect differences between dietary groups and to identify significant differences.

In addition, outliers were detected by using Grubb's test (GraphPad Software) and excluded from analysis.

For immunohistochemical analyses, the detection of positive-stained cells were made in duplicates and mean values were used for statistical analyses.

Pearson correlation coefficient (r) was employed to investigate correlations (two-tailed test) and tests for linear trend were calculated by using linear regression models.

All data were analysed using Prism 5 (GraphPad Software).

3.14 Buffer recipes

3.14.1 Protein isolation and SDS-PAGE

Radio-immunoprecipitation assay (RIPA) buffer

0.05 M Tris / HCl, pH 8
0.15 M NaCl
1 mM EDTA, pH 8
0.2 % SDS
1 % NP-40
0.25 % Na-Deoxycholate
in H₂O, to pH 7.4

Stacking gel stock (5 %)

58.5 ml H₂O
25 ml 0.5 M Tris / HCl, pH 6.8
1 ml 10 % SDS
16.5 ml 30 % acrylamide / bis-acrylamide
+ spatula tip of bromophenolblue
H₂O ad 100 ml

Per gel
2ml stacking gel stock
2 μ l TEMED
15 μ l 10 % (w/v) APS

10 x (glycine) Running buffer

250 mM Tris / HCl
2 M glycine
1 % (w/v) SDS
in H₂O, to pH 8.3

5 x Sample buffer ("Laemmli buffer")

310 mM Tris / HCl
5 % SDS
25 % glycerol
50 mM DTT
2.5 mM EDTA
in H₂O, to pH 6.8
+ \approx 1 mg bromophenolblue

Separating gel stock (10 %)

2.5 ml H₂O
1.5 ml 1.5 M Tris / HCl, pH 8.8
60 μ l 10 % SDS
2 ml 30 % acrylamide / bis-acrylamide
H₂O ad 6 ml

Per gel
6ml separating gel stock
2 μ l TEMED
62 μ l 10 % (w/v) APS

3.14.2 Western blot

Transfer buffer

20 mM Tris / HCl
150 mM glycine
20 % methanol
0.02 % SDS
in H₂O, to pH 8.3

10 x Tris-buffered saline (TBS)

200 mM Tris
1.37 M NaCl
in H₂O, to pH 7.6

1 x TBS + Tween-20® (TBS-T)

100 ml 10 x TBS
0.1 % Tween-20®
H₂O ad 1 l

3.14.3 Agarose gel electrophoresis

5 x Tris / borate / EDTA (TBE) buffer

0,45 M Tris / HCl
0,44 M boric acid
1 M EDTA, pH 8
in H₂O, to pH 8

50 x Tris / acetate / EDTA (TAE) buffer

2 M Tris / HCl
5.7 % acetic acid
0.5 M EDTA, pH 8
in H₂O, to pH 8

Orange G dye

25 ml glycerol
0.25 g Orange G
5 ml TAE (10 x)
H₂O ad 1 l

3.14.4 TAG analysis

HB buffer

10 mM NaH₂PO₄
1 mM EDTA, pH 7.4
1 % polyoxyethylen (10) tridecyl ether
In H₂O, to pH 7.4

4 Results

4.1 Changes in inflammatory status upon HF and HF/n-3 (48 kJ% fat)

Obesity is associated with a chronic adipose tissue inflammatory state, whereby the expansion of the fat depots leads to immune cell infiltration (Weisberg 2003, Kintscher 2008, Winer 2011) and recruitment as well as macrophage differentiation and activation in adipose tissues (Odegaard 2008). There are different macrophage subsets with differential functions, the pro-inflammatory M1 and the anti-inflammatory M2 macrophages (Murray 2011), which can switch their phenotype (Lumeng 2007). Moreover, they can form aggregates, so-called CLS that surround dying adipocytes, which are identified by the absence of perilipin staining (Cinti 2005b).

For this thesis, since a clear definition of CLS is lacking (West 2009), CLS were defined as adipocytes surrounded by three or more cells stained positively for a macrophage-specific marker. Furthermore, cells that were stained positive for an immune cell marker, but did not correspond to aforementioned classification were defined as solitary cells.

4.1.1 Inflammatory status of MAT and EAT

4.1.1.1 T and B cells

Preliminary results, obtained by a pathway specific RT-qPCR array for “T and B cell activation” with MAT samples, already indicated T and B cell activation upon HF/n-3 (Ludwig 2013). However, no statistical analysis was possible because pooled samples were used for measurements. Moreover, the mRNA level of OPN, a T cell-derived chemoattractant for macrophages (Weber 1996), showed the most striking upregulation in HF/n-3 mice compared to control and HF mice. An increase in OPN expression was observed in MAT and in EAT (Ludwig 2013). These findings might indicate an increase in T cell number upon HF/n-3.

Hence, the presence of T lymphocyte was further analysed in MAT and EAT by RT-qPCR, but also immunohistochemical analyses. The surface markers CD4, CD8 α and CD86, identifying helper T lymphocytes, cytotoxic/suppressor T lymphocytes and immune cells involved in the priming of T cells, respectively, were used for gene expression analysis to identify different T cell subsets and the costimulatory marker CD86. In addition, immunohistochemical analyses of VATs were performed to assess markers for T cells and B cells and proliferation and apoptosis markers. Changes on proliferation and apoptosis were explored to make an assumption on cellular turnover within adipose tissue. Cell death of adipocytes, for example, might lead to increased immune cell infiltration (Cinti 2005b). For immunohistochemical analyses, antibodies specific for CD3, protein tyrosine

phosphatase, receptor type, C (PTPRC = B220), antigen KI-67 (KI67) and cleaved caspase 3 (CL-CASP3) were used for detection and positive-stained cells were quantified.

Significantly decreased CD8 α mRNA levels were detected upon HF/n-3 in MAT, whereas the expression of CD4 showed only a tendency for downregulation in HF/n-3 mice compared to control (Figure 7A). In EAT only the gene expression level of CD4 was analysed. It was significantly elevated upon HF/n-3 compared to control and HF feeding (Figure 7B). However, in both VATs CD86 mRNA levels were not regulated (Figures 7A and B). Moreover, immunohistochemical analyses in MAT revealed a significant downregulation of CD3-positive cells upon HF compared to control and a significant increase of CL-CASP3-positive cells upon HF/n-3 compared with HF, whereas B220- and KI67-stainings showed no regulation (Figure 7C). In EAT significantly more CD3-positive cells were observed in HF/n-3 mice compared to HF mice (Figure 7D). However, the expression levels of B220, KI67 and CL-CASP3 were not examined in EAT.

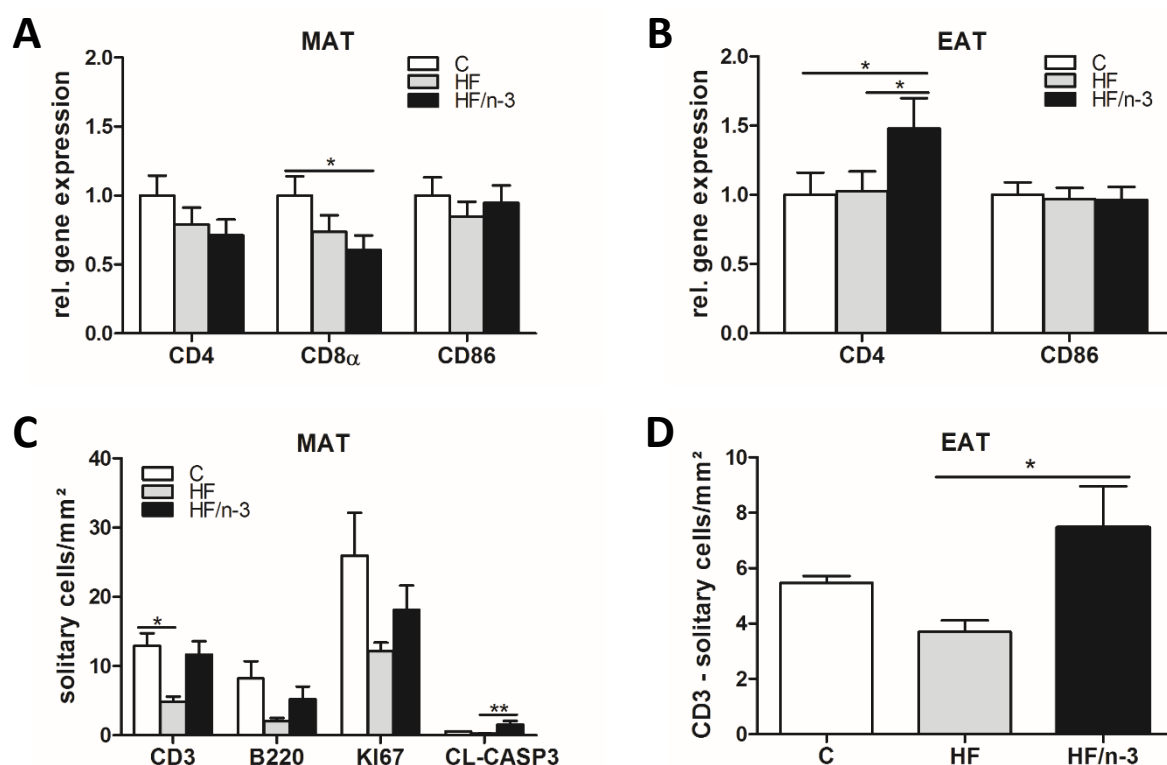


Figure 7. Differential mRNA expression of genes encoding T lymphocyte and co-stimulatory markers, and immunohistochemical detection and quantification of T cells and B cells as well as proliferation and apoptosis markers in VATs. All data are means \pm SE and were collected from mice after 12 weeks of feeding either control (C), HFD (HF), or n-3 long-chain polyunsaturated fatty acid (LCPUFA)-enriched HFD (HF/n-3). **(A and B)** Gene expression of T cell and co-stimulatory markers in MAT (n=8-9) and in EAT (n=10-12). Shown are the gene expression levels of CD4, CD8 α and CD86 in MAT **(A)** and of CD4 and CD86 in EAT **(B)**. Data were retrieved by RT-qPCR, normalised to Hprt1 and Actb (MAT) or to Gapdh and Actb (EAT), and calculated relative to controls. **(C and D)** Immunohistochemical detection and quantification of CD3, protein tyrosine phosphatase, receptor type, C (PTPRC = B220), antigen KI-67 (KI67) and cleaved caspase 3 (CL-CASP3) in MAT (n=4) and of

CD3 in EAT (n=3-4). Number of solitary cells positively-stained for T cell marker CD3, B cell marker B220, proliferation marker KI67 and apoptosis marker CL-CASP3 in MAT (C) and for T cell marker CD3 in EAT (D) is expressed as solitary cells per mm² of tissue section. Statistical analysis was performed using one-way ANOVA and Tukey post-test. In case of no normal distribution or n < 5, data were tested by Kruskal-Wallis and Dunn's post-test. In addition, outliers were detected by using Grubb's test and excluded from statistical data analysis. *p < 0.05, **p < 0.01, ***p < 0.001, significant differences compared with control or between groups as indicated.

4.1.1.2 Macrophages

T lymphocyte infiltration in the enlarged WAT, a primary event in adipose tissue inflammation, is followed by macrophage recruitment (Kintscher 2008), whereby FFA attract them into adipose tissue (Suganami 2007, Kosteli 2010).

Adipose tissue macrophages (ATMs) co-express F4/80 and CD11b, which are encoded by EGF-like module-containing mucin-like hormone receptor-like 1 (EMR1) and immune cell marker integrin α -G (ITGAM), respectively, whereby especially the macrophage marker F4/80 is used to identify ATMs (Lumeng 2007). Moreover, macrophages are further classified according to their state of activation / polarization into pro-inflammatory M1 macrophages and anti-inflammatory M2 macrophages (Gordon 2010). ITGAX, MRC1 and C-type lectin domain family 10, member A (CLEC10a) are known to encode CD11c (marker for M1 macrophage subset), CD206 and CD301 (markers for M2 macrophage subset), respectively (Fujisaka 2009). However, CD11c is in addition used as dendritic cell marker (Lumeng 2007).

RT-qPCR analyses and immunohistochemical detections in CLS were performed for these markers to characterise macrophage polarization / infiltration in MAT and EAT. Besides that, comparisons were made between MAT and EAT, as we have already observed differential effects for T cell infiltration.

In MAT, only upon HF/n-3 significantly increased EMR1 mRNA levels were observed compared to control, whereas in EAT significantly higher EMR1 mRNA levels were measured upon HF/n-3 and HF than in control (Figures 8A and B). ITGAM mRNA expression was significantly elevated in EAT and MAT upon HF/n-3 compared with control diet, whereas its expression was also significantly increased upon HF/n-3 compared to HF in MAT. Similar gene expression changes were detected for CLEC10a. Measurements of CLEC10a showed a significant upregulation upon HF/n-3 compared with controls in EAT and MAT, and a significant increase upon HF/n-3 compared to HF was found in EAT (Figure 8A and B). Gene expression levels of ITGAX and MRC1 were previously measured (Ludwig 2013) and showed similar results. Surprisingly, for all immune cell markers, the highest mRNA levels were observed for the HF/n-3 mice, whereby ITGAX showed the highest fold changes compared to control (MAT: 2.44- fold; EAT: 6.62-fold).

To assess the presence of macrophages in CLS and the number of solitary cells in MAT and EAT, immunohistochemical analyses (Figure 9) and quantifications (Figures 8C and D) were performed, using primary antibodies specific for F4/80, CD11c, and CD206. F4/80-positive CLS staining was almost absent in MAT of control animals (Figure 8C and Figure 9A), whereas F4/80-positive CLS were substantially more frequent in MAT upon HF/n-3 than upon HF (Figure 8C and Figures 9B and C). Similarly, compared with control, only for HF/n-3 mice, F4/80-positive CLS density was significantly higher in EAT, although HF mice showed the same trend but did not reach statistical significance due to higher standard deviations (Figures 8D and 9D-F). Notably, the F4/80-positive CLS densities were about twofold higher in EAT than in MAT upon HF/n-3 and even 22.5-fold elevated upon HF (Figures 8C and D). CD11c-positive-stained CLS in MAT were significantly more abundant in HF/n-3 mice compared to control mice (Figures 8C and 10G-I). A similar finding was observed for EAT (Figures 8D and 10J-L). The density of CD11c-positive-stained CLS was only slightly higher in EAT than in MAT upon HF/n-3 (Figures 8C and D and 10I and L). For the M2 macrophage marker CD206 (Figures 8C and D and 10M-R), we observed a significant elevation of CD206-positive CLS in MAT upon HF/n-3 compared with C, whereas in EAT there was only a trend for higher CLS density upon both HFDs compared with control ($p=0.1462$).

Furthermore, for positive-stained cells, which are not localised in CLS, so-called solitary cells, a significant increase in F4/80-positive solitary cells and a significant decrease in CD11c-positive solitary cells were observed in EAT upon HF/n-3 compared to control (Figure 8F). In MAT, only the CD206-positive solitary cells were significantly downregulated for the HF animals compared to control (Figure 8E). The same observation was made for EAT (Figure 8F). Moreover, control animals showed the highest counts for CD11c- or CD206-positive solitary cells in EAT (Figure 8F).

Immunohistochemical stainings are used for the detection of CLS, but co-expression analyses are commonly applied to determine the phenotype of macrophages. Nevertheless, in this thesis, a correlation-based approach was applied to examine co-expressed macrophage markers in order to get an idea about the phenotype of the macrophages localised to CLS. In EAT, for both high-fat groups, a significant correlation could be observed between the macrophage marker F4/80 and the CD206 receptor, a marker of the anti-inflammatory phenotype, within CLS (HF, $r=0.9568$, $p=0.0002$; HF/n-3, $r=0.8643$, $p=0.0056$). However, the linear regression analysis in EAT revealed disparities between correlation levels of F4/80 and the CD11c receptor, a marker of the pro-inflammatory phenotype, within CLS. The HF animals displayed a significant positive correlation ($r=0.9860$, $p<0.0001$), whereas the HF/n-3 mice showed a nearly significant negative correlation between these markers ($r=-0.6922$, $p=0.0571$), suggesting a difference in the predominant phenotype for HF and HF/n-3 animals.

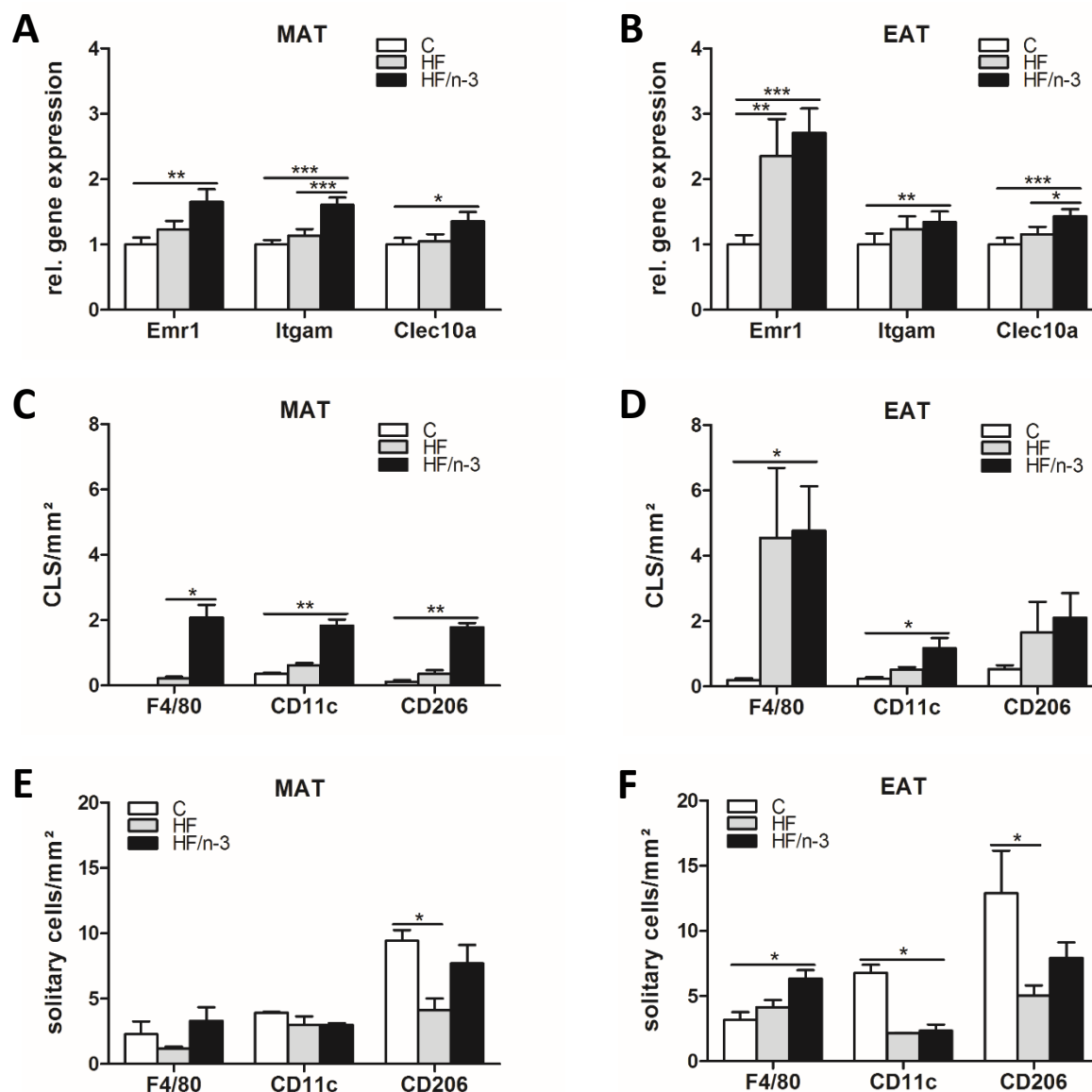


Figure 8. Differential mRNA expression of genes encoding M1 and M2 macrophage markers and their immunohistochemical detection and quantification in crown-like structures (CLS) or as solitary cells in VATs. All data are means \pm SE and were collected from mice after 12 weeks of feeding either control (C), HFD (HF), or n-3 long-chain polyunsaturated fatty acid (LCPUFA)-enriched HFD (HF/n-3). **(A and B)** Gene expression of macrophage markers in MAT (n=8-10) and in EAT (n=8-12). Shown are the gene expression levels of EGF-like module-containing mucin-like hormone receptor-like 1 (Emr1; F4/80), integrin α -M (Itgam) and C-type lectin domain family 10, member A (Clec10a) in MAT **(A)** and in EAT **(B)**. Data were retrieved by RT-qPCR, normalised to Hprt1 and Actb (MAT) or to Gapdh and Actb (EAT), and calculated relative to controls. **(C-F)** Immunohistochemical detection (cf. Figure 9) and quantification of CLS and of solitary cells, which are positive for F4/80, CD11c or CD206 in MAT and EAT (n=3-4). Number of positive-stained CLS in MAT **(C)** and in EAT **(D)** and of positive-stained solitary cells in MAT **(E)** and in EAT **(F)** was expressed as CLS or solitary cells per mm² of tissue section. Statistical analysis was performed using one-way ANOVA and Tukey post-test. In case of no normal distribution or n < 5, data were tested by Kruskal-Wallis and Dunn's post-test (three groups) or Mann Whitney test (two groups). In addition, outliers were detected by using

Grubb's test and excluded from statistical data analysis. * $p < 0.05$, ** $p < 0.01$, *** $p < 0.001$, significant differences compared with control or between groups as indicated.

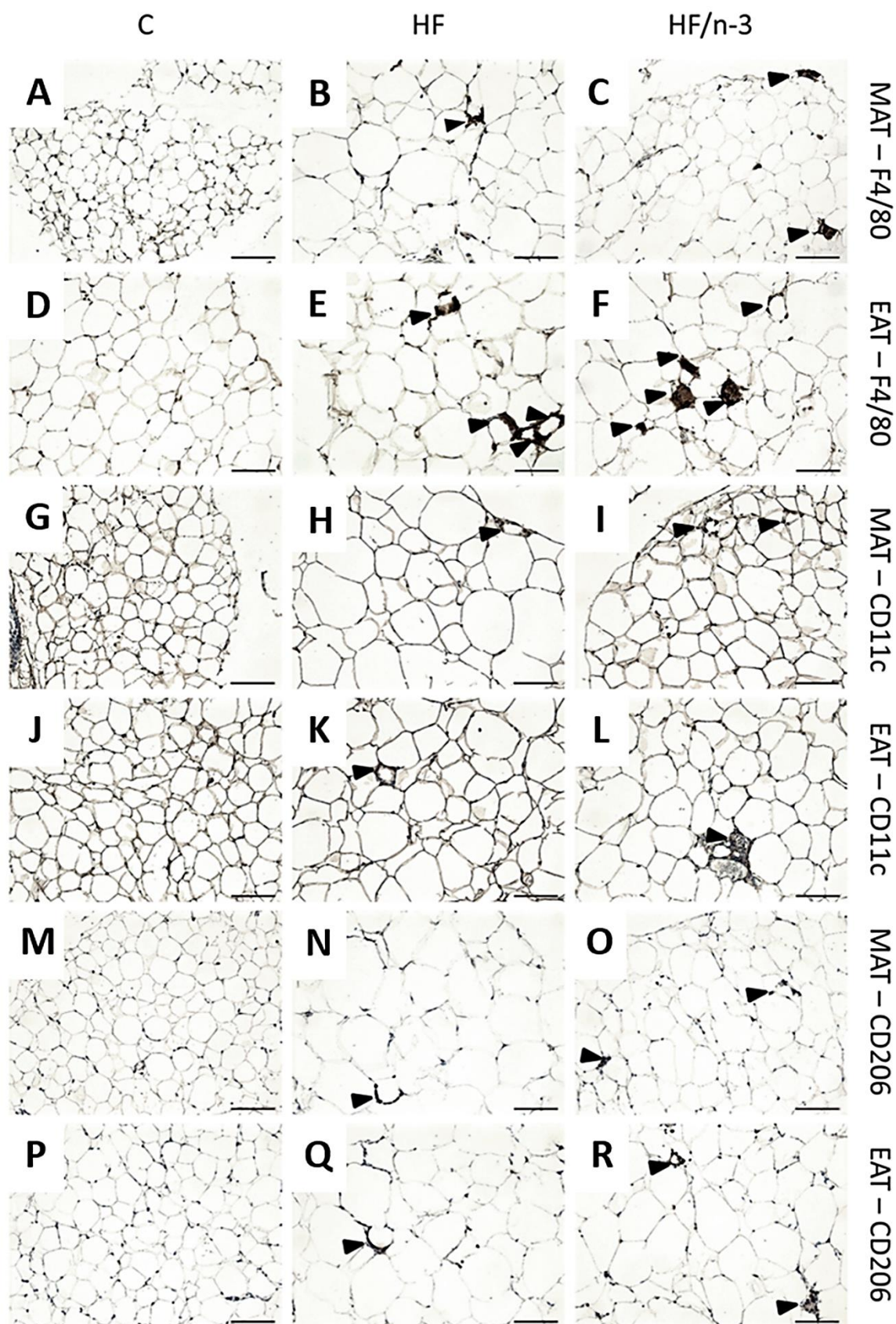


Figure 9. Immunohistochemical analysis of macrophage-associated M1 and M2 marker expression in crown-like structures (CLS) of VATs. Shown are microscopic images of paraformaldehyde-fixed paraffin sections of MAT and EAT from mice fed HF (B, E, H, K, N, and Q), HF/n-3 (C, F, I, L, O, and R), and control diet (A, D, G, J, M, and P) stained with primary antibodies specific for F4/80 (A–F), CD11c

(G–L), or CD206 (M–R). For antigen signal detection, corresponding specific secondary antibodies combined with horseradish peroxidase-based detection system were applied, followed by counterstaining with hematoxylin. Arrowheads point to positive-stained cells in CLS surrounding adipocytes. Scale bar indicates 100 μ m.

In this thesis, different morphological characteristics were observed for CLS. Thus, based on the morphologically distinct subgroups, F4/80-positive-stained CLS were defined as follows: “CLS” - circular regions with continuous rim of macrophages (cf. Figure 9K); “cluster” - clusters of macrophages, which form multinucleated giant cells (Cinti 2005b; cf. Figure 9F); “others” - three or more CLS-associated macrophages, which do not form such distinct patterns but surround an adipocyte.

In MAT the total count of CLS but also the number of all CLS subgroups were significantly upregulated in HF/n-3 animals compared to HF animals (Figure 10A), whereas in EAT only the total count of F4/80-positive-stained CLS and its subgroup termed „others“ were significantly enhanced in HF/n-3 compared to control mice (Figure 10B). Notably, expressing the different subgroups of CLS as percentage of total counts of F4/80-positive-stained CLS, for the control group, most of the CLS found in EAT, the number being rather low compared to the high-fat groups (Figure 10B), were assigned to the subgroup termed „cluster“. Perhaps even more interesting was the finding that the subgroup termed „cluster“ was observed significantly more frequently in MAT from HF/n-3 animals than from HF animals (Figure 10C), whereas in EAT these structures were significantly downregulated in the HF animals compared to controls (Figure 10D). In general, looking at the structures that could be assigned to the subgroups termed „cluster“ or „CLS“ and comparing the high-fat groups, it might be assumed that „cluster“ are prevalent in the VATs from the HF/n-3 mice and „CLS“ dominate those from HF mice. However, for both high-fat groups, even more than 80 % of the structures could not be assigned to the subgroups termed „cluster“ or „CLS“ in EAT (Figure 10D) and the share was 60 % in MAT (Figure 10C).

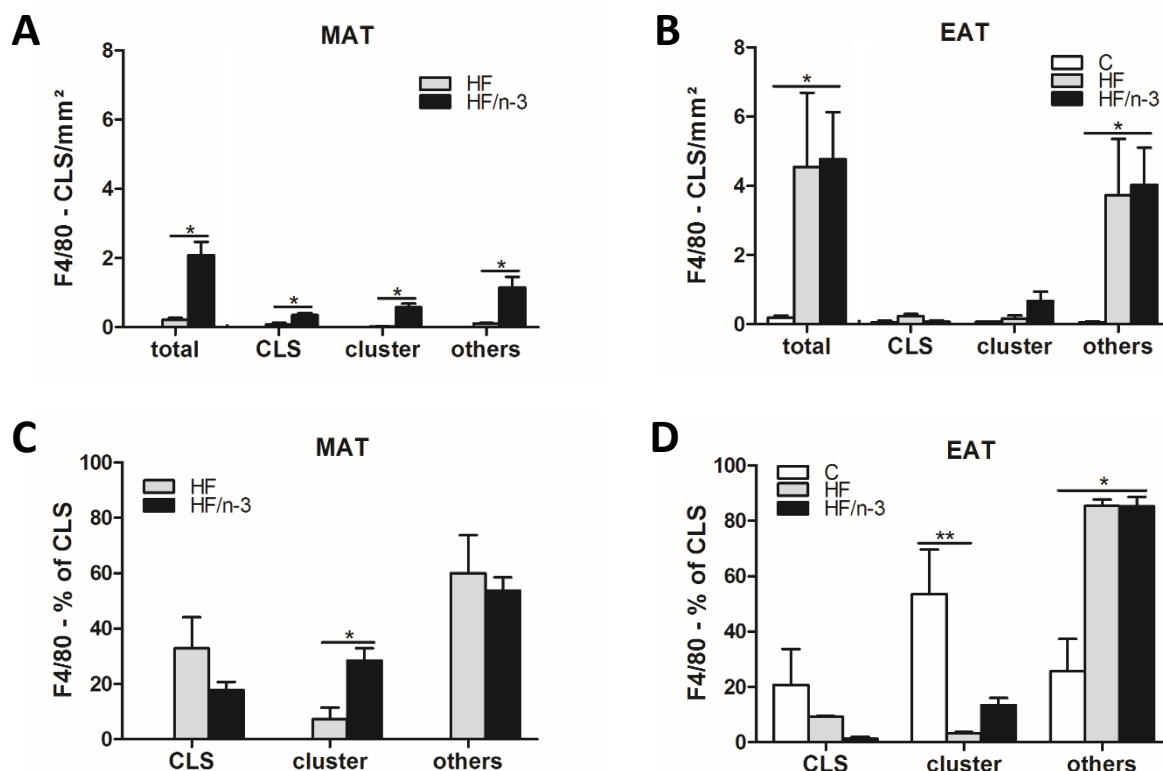


Figure 10. Subdivision of crown-like structures (CLS) of VATs according to their appearance. All data are means \pm SE and were collected from mice after 12 weeks of feeding either control (C), HFD (HF), or n-3 long-chain polyunsaturated fatty acid (LCPUFA)-enriched HFD (HF/n-3). After immunohistochemical detection (cf. Figure 9 A-F) and quantification of F4/80-positive-stained CLS (cf. Figure 8 C and D) in MAT and EAT the CLS were further subdivided into subgroups of CLS according to their appearance and presented in two different ways. **(A and B)** Total count of F4/80-positive-stained CLS (“total”) and subgroups of CLS in MAT **(A)** and EAT **(B)** are expressed as CLS per mm² of tissue section. **(C and D)** Subgroups of CLS are expressed as percentage of total counts of F4/80-positive-stained CLS in MAT **(C)** and in EAT **(D)**. The subgroups of CLS were defined based on differences in their morphological characteristics, which were as follows: “CLS” - circular regions with continuous rim of macrophages; “cluster” - clusters of macrophages, which form multinucleated giant cells; “others” - three or more CLS-associated macrophages, which do not form such distinct patterns but surround an adipocyte. Statistical analysis was performed using Kruskal-Wallis and Dunn’s post-test (EAT) or Mann Whitney test (MAT). Because of the small sample size, no test for normal distribution was possible. In addition, outliers were detected by using Grubb’s test and excluded from statistical data analysis. * $p < 0.05$, ** $p < 0.01$, *** $p < 0.001$, significant differences compared with control or between groups as indicated.

Besides analysing the expression of macrophage surface markers of the pro-inflammatory M1 or anti-inflammatory M2 phenotype, informations about the polarization status of the macrophages and the general inflammation status of the adipose tissues can also be determined by cytokine measurements (Lumeng 2007). Thus, the pro-inflammatory cytokine TNF α and the M1-associated nitric oxide synthase 2 (NOS2) were examined by RT-qPCR analyses. The anti-inflammatory IL10 was

already measured and showed no regulation in MAT, whereas in EAT its mRNA level was significantly increased upon HF/n-3 compared to control (Ludwig 2013). No regulations were observed in MAT (Figure 11A), however, in EAT TNF α gene expression was significantly elevated upon HF/n-3 compared to control and NOS2 gene expression showed a significant upregulation upon HF compared to control and HF/n-3 feeding (Figure 11B). Notably, for both high-fat groups, a significant correlations could be observed between the gene expression levels of the macrophage marker EMR1 and the pro-inflammatory cytokine TNF α (HF, $r=0.8496$, $p=0.0005$; HF/n-3, $r=0.8544$, $p=0.0016$) as well as between those of EMR1 and the anti-inflammatory cytokine IL10 (HF, $r=0.8017$, $p=0.0017$; HF/n-3, $r=0.6817$, $p=0.0299$) in EAT.

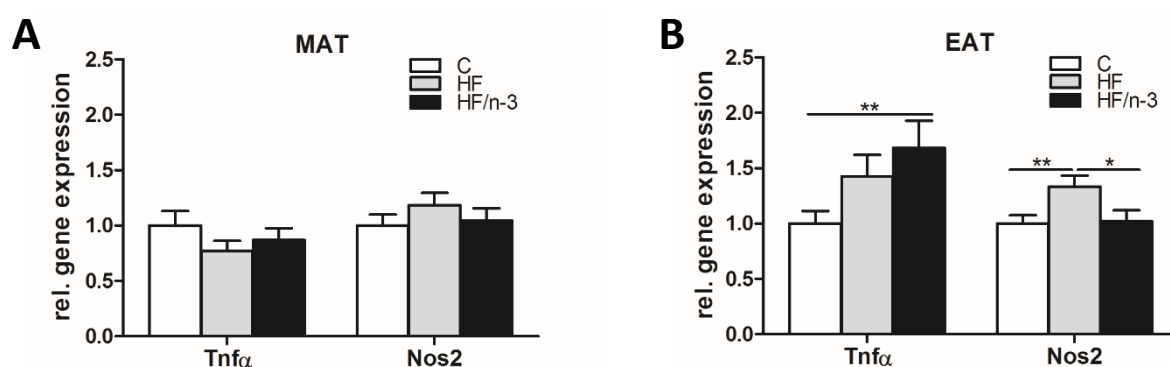


Figure 11. Gene expression of pro-inflammatory cytokines in VATs. All data are means \pm SE and were collected from mice after 12 weeks of feeding either control (C), HFD (HF), or n-3 long-chain polyunsaturated fatty acid (LCPUFA)-enriched HFD (HF/n-3). **(A and B)** Gene expression levels of Tnf α and nitric oxide synthase 2 (Nos2) in MAT **(A; n=8-10)** and in EAT **(B; n=10-12)**. Data were retrieved by RT-qPCR, normalised to Hprt1 and Actb (MAT) or to Gapdh and Actb (EAT), and calculated relative to controls. Statistical analysis was performed using one-way ANOVA and Tukey post-test. In case of no normal distribution, data were tested by Kruskal-Wallis and Dunn's post-test. In addition, outliers were detected by using Grubb's test and excluded from statistical data analysis. * $p < 0.05$, ** $p < 0.01$, *** $p < 0.001$, significant differences compared with control or between groups as indicated.

In order to receive information about whether the increased number of immune cells, found especially in EAT upon high-fat feeding, was due to an increased infiltration, target proteins involved in endothelial cell activation and growth or in the regulation of angiogenesis were analysed. Hence, classical adhesion molecules such as vascular cell adhesion molecule 1 (VCAM1) and intercellular adhesion molecule 1 (ICAM1) and TEK were examined by RT-qPCR analyses. No regulations were observed in MAT between the diets (Figure 12A), but in EAT VCAM1 gene expression was significantly elevated upon HF/n-3 compared to control and HF feeding, whereas ICAM1 and TEK were not regulated on gene expression level (Figure 12B). Additionally, a nearly significant correlation could be observed between the gene expression levels of CD4 and VCAM1 within the HF ($r=0.5757$, $p=0.0502$) and HF/n-3 group ($r=0.6192$, $p=0.0563$) in EAT.

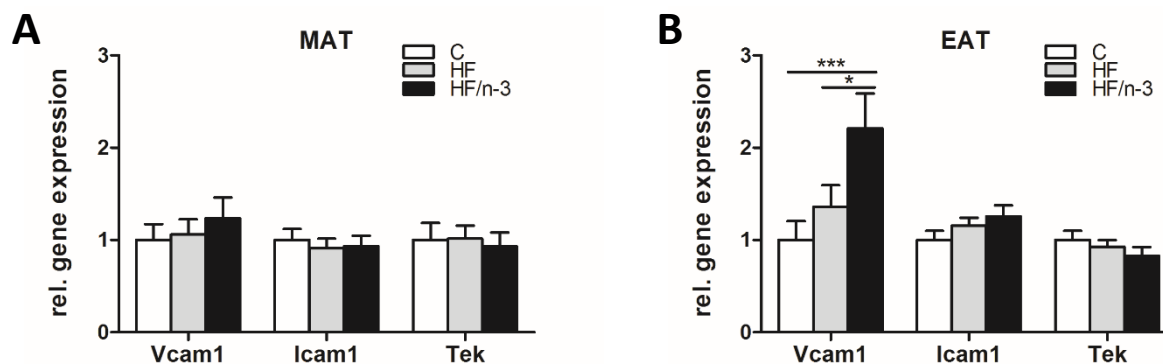


Figure 12. Expression analysis of genes involved in endothelial cell activation and growth or in the regulation of angiogenesis in VATs. All data are means \pm SE and were collected from mice after 12 weeks of feeding either control (C), HFD (HF), or n-3 long-chain polyunsaturated fatty acid (LCPUFA)-enriched HFD (HF/n-3). **(A and B)** Gene expression levels of the classical adhesion molecules vascular cell adhesion molecule 1 (Vcam1) and intercellular adhesion molecule 1 (Icam1) and endothelial-specific receptor tyrosine kinase (Tek) in MAT **(A; n=8-10)** and in EAT **(B; n=10-12)**. Data were retrieved by RT-qPCR, normalised to Hprt1 and Actb (MAT) or to Gapdh and Actb (EAT), and calculated relative to controls. Statistical analysis was performed using one-way ANOVA and Tukey post-test. In case of no normal distribution, data were tested by Kruskal-Wallis and Dunn's post-test. In addition, outliers were detected by using Grubb's test and excluded from statistical data analysis. * $p < 0.05$, ** $p < 0.01$, *** $p < 0.001$, significant differences compared with control or between groups as indicated.

4.1.2 Inflammatory status of iBAT

It has been reported, that alternatively activated macrophages in cross-talk with eosinophils can stimulate the expression of thermogenic genes in iBAT via catecholamines upon cold (Nguyen 2011, Qiu 2014). Thus, since a further aim of this thesis was to assess whether n-3 LCPUFA increase energy expenditure by inducing DIT in iBAT and since it would be interesting to explore a possible involvement of immune cells in DIT, immune cell infiltration and inflammation were also analysed in iBAT.

Similar to analyses in VATs (cf. 4.1.1.2), gene expression levels of the macrophage marker F4/80 and of surface markers that define macrophage phenotype - CD11c (M1 phenotype) or CD206 and CD301 (M2 phenotype) - (Figure 13A) as well as their immunohistochemical detection (Figure 14) and quantification in CLS (Figure 13B) or as solitary cells (Figure 13C) were examined in iBAT. Moreover, mRNA levels of pro- and anti-inflammatory markers and of the eosinophil-specific marker sialic acid binding Ig-like lectin 5 (SIGLEC5; Zhang 2007) were determined (Figure 13D and E).

Gene expression levels of the respective markers were measured and in comparison with analyses in VATs, similar changes were observed in iBAT, whereby the C_q -values of the immune cell markers (Appendix Table 21 (iBAT), Table 22 (EAT) and Table 25 (MAT)) showed in general higher values

analysing iBAT than VATs. Notably, compared with the findings in VATs (cf. Table 8), significant higher mRNA levels for EMR1, but also for ITGAX and CLEC10a were found upon both HFDs compared to control. However, the mRNA level of MRC1 was only significantly increased upon HF/n-3 (Figure 13A).

Examining the immunohistochemical analyses of iBAT, one must realise that CLS were not so visible in iBAT than in VATs. Surprisingly, with regard to CLS, for all groups the CD301-positive-stained CLS were more frequent than CLS stained with other macrophage markers applied, whereby CD301-positive-stained CLS were significantly less upon HF compared to control. However, the number of CD11c- or CD206-positive-stained CLS was not different between diets. Notably, the biggest changes were observed for F4/80-positive CLS, which were significantly more frequent upon HF/n-3 than upon HF (Figure 13B). The results of the solitary cell counts resemble those of the positive-stained CLS, with more F4/80-positive and CD11c-positive solitary cells upon HF/n-3 than HF, but the number of CD301-positive solitary cells was significantly downregulated in both high-fat groups compared to control group (Figure 13C).

Compared to findings in VATs (Figure 8), upon HF/n-3, the number of F4/80-positive CLS (BAT vs. MAT: 3.9-fold and BAT vs. EAT: 1.7-fold) and solitary cells (BAT vs. MAT: 11-fold and BAT vs. EAT: 5.6-fold) found per mm² tissue were generally more pronounced in iBAT than in VATs. Furthermore, comparing HF/n-3 with control, similarly high values were observed for the fold changes of F4/80-positive CLS and F4/80-positive solitary cells in iBAT, whereas in VATs the values for the fold changes of F4/80-positive CLS were higher than those of F4/80-positive solitary cells (MAT: not defined due to the missing values for CLS in the control group and EAT: 12.3-fold).

Besides that, the gene expression level of MCP1 was significantly higher for the high-fat groups than control, whereas the pro-inflammatory marker TNF α showed no regulation. However, mRNA levels for the anti-inflammatory markers IL10 and TGF β 1 were significantly higher for HF/n-3 than for controls but upon HF, only IL10 levels were significantly elevated compared to control (Figure 13D).

Given the involvement of M2 macrophages and eosinophils in thermogenesis, the mRNA abundance of the eosinophil-specific marker SIGLEC5 was determined and a correlation-based approach was applied to examine a possible correlation between the abundance of immune cells and the thermogenic marker UCP1. Notably, the mRNA level of SIGLEC5 was significantly enhanced for the HF/n-3 mice compared to control and HF mice (Figure 13E) and, within the HF/n-3 group, SIGLEC5 was significantly correlated with the gene expression levels of EMR1, MCR1 and CLEC10a, and even UCP1 (Table 6). Furthermore, for the HF/n-3 mice, significant correlations were observed between the gene expression levels of macrophage markers (EMR1 and MRC1) and of metabolic markers (CD36 and CPT1a; Table 6), which were associated with the M2 macrophage phenotype (Huang 2014).

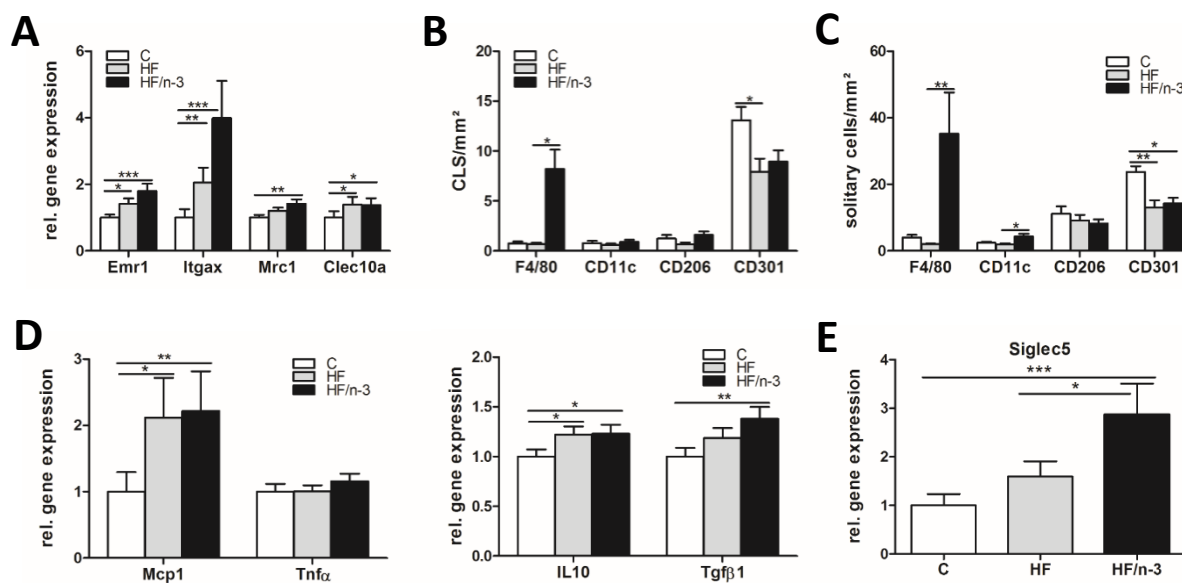


Figure 13. Differential mRNA expression of cytokines and genes encoding immune cell markers, such as M1 and M2 macrophage markers, and their immunohistochemical detection and quantification in crown-like structures (CLS) or as solitary cells in iBAT. All data are means \pm SE and were collected from mice after 12 weeks of feeding either control (C), HFD (HF), or n-3 long-chain polyunsaturated fatty acid (LCPUFA)-enriched HFD (HF/n-3). **(A)** Gene expression of macrophage markers in iBAT (n=10-12). Shown are the gene expression levels of EGF-like module-containing mucin-like hormone receptor-like 1 (Emr1; F4/80), integrin α -X (Itgax; CD11c), mannose receptor C type 1 (Mrc1; CD206) and C-type lectin domain family 10, member A (Clec10a; CD301). **(B and C)** Immunohistochemical detection (cf. Figure 14) and quantification of CLS and solitary cells, which are positive for F4/80, CD11c, CD206 or CD301 in iBAT (n=4-5). Number of positive-stained CLS **(B)** and of positive-stained solitary cells **(C)** is expressed as CLS or solitary cells per mm² of tissue section. **(D and E)** Gene expression of the pro- or anti-inflammatory chemokines / cytokines and of an eosinophil-specific marker in iBAT (n=7-12). Shown are the gene expression levels of Mcp1, Tnf α , IL10 or Tgf β 1 **(D)** and of sialic acid binding Ig-like lectin 5 (Siglec5; **E**). Gene expression data were retrieved by RT-qPCR, normalised to CypB and Hsp90 α b1, and calculated relative to controls. Statistical analysis was performed using one-way ANOVA and Tukey post-test. In case of no normal distribution or n < 5, data were tested by Kruskal-Wallis and Dunn's post-test. In addition, outliers were detected by using Grubb's test and excluded from statistical data analysis. *p < 0.05, **p < 0.01, ***p < 0.001, significant differences compared with control or between groups as indicated.

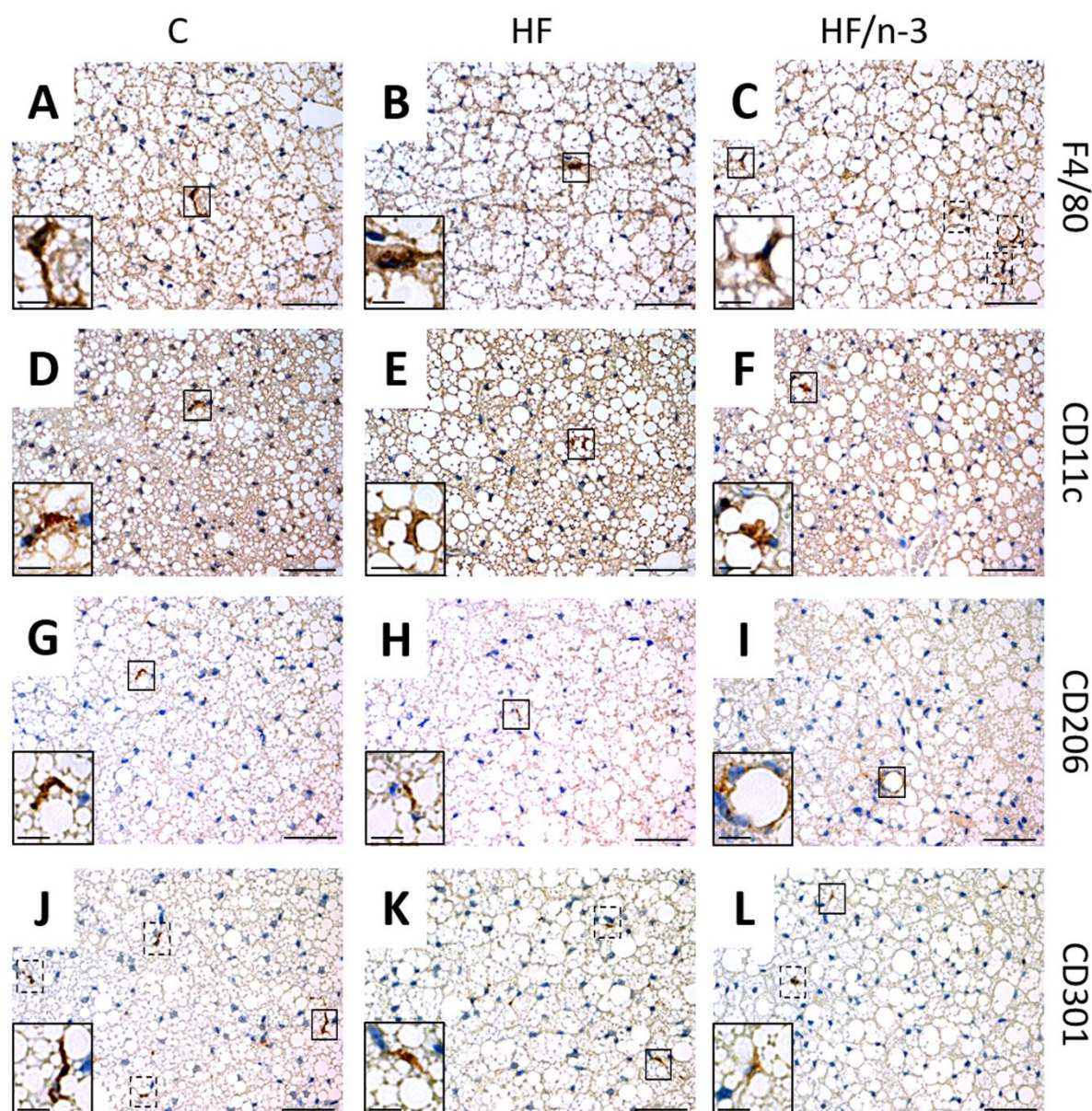


Figure 14. Immunohistochemical analysis of macrophage-associated M1 and M2 marker expression in crown-like structures (CLS) of iBAT. Shown are microscopic images of paraffin sections of iBAT from mice fed control (A, D, G, and J), HF (B, E, H, and K) or HF/n-3 diet (C, F, I, and L). They were stained with primary antibodies specific for F4/80 (A, B, and C), CD11c (D, E, and F), CD206 (G, H, and I) or CD301 (J, K, and L). For antigen detection, corresponding specific secondary antibodies combined with horseradish peroxidase-based detection system were applied, followed by counterstaining with hematoxylin. Positive-stained cells in CLS surrounding lipid droplets are highlighted with black frames (continuous or dashed line). One representative structure for each figure (black frame with continuous line) is also shown in a higher magnification as insert. Additional structures are visualised by black frames with dashed lines. Scale bars indicate 50 μm for the whole section or 20 μm for the representative structure in the lower left corner of each section.

Table 6. Correlation analysis data on macrophage phenotypes in iBAT

Gene	Gene		Total	Correlation		
				C	HF	HF/n-3
Siglec5	Emr1	p	<0.0001***	0.8431	0.0694	0.0052**
		r	0.6916	-0.06412	0.5661	0.8027
Siglec5	Mrc1	p	<0.0001***	0.6795	0.0880	0.0225*
		r	0.6480	0.1333	0.5131	0.7059
Siglec5	Clec10a	p	0.0003***	0.0826	0.6175	0.0085**
		r	0.5779	0.5207	0.1608	0.7750
Siglec5	Ucp1 [#]	p	0.0049**	0.1271	0.8127	0.0319*
		r	0.4717	-0.4657	-0.0767	0.6761
Emr1	Cpt1a	p	<0.0001***	0.7326	0.3536	0.0281*
		r	0.6740	0.1104	0.3100	0.6873
Mrc1	CD36	p	0.0001***	0.6814	0.1284	0.0287*
		r	0.6128	0.1325	0.4643	0.6854

Shown are correlations between gene expression data of immune cell markers and metabolic markers in interscapular brown adipose tissue (iBAT) after 12 weeks of feeding either control (C), HFD (HF), or n-3 long-chain polyunsaturated fatty acid (LCPUFA)-enriched HFD (HF/n-3). The expression data were generated by RT-qPCR analysis (n=7-12) and correlation analyses were performed utilizing the whole data set (total), but also analysing the data from each group separately. For the genes marked with a hash symbol, the data were obtained from Ludwig et al. (Ludwig 2013), testing for normal distribution and outliers. Normalised values were used. Outliers were detected by using Grubb's test and excluded from statistical data analysis. *p < 0.05, **p < 0.01, ***p < 0.001, indicate significant correlation. p, statistical significance; r, Pearson correlation coefficient.

4.1.3 Inflammatory status of spleen, plasma and liver

Given the T cell immunosuppressive effect in MAT upon HF/n-3 (cf. 4.1.1.1) and the significantly increased spleen mass that was observed in HF/n-3 animals (Ludwig 2013), splenic immune cell profile was examined. The spleen, like the mesenteric lymph nodes (MLN), represents a secondary lymphoid organ and is a major site of lymphocyte proliferation and immune system homeostasis (Mebius 2005).

Immunological changes in spleen were evaluated by measurements of splenic mRNA levels for the macrophage marker EMR1 and ITGAX, as well as for CD4 and CD8 α , identifying helper T lymphocytes and cytotoxic / suppressor T lymphocytes, respectively (Ellmeier 1999). EMR1 and ITGAX gene expression levels were significantly downregulated upon HF/n-3 compared to control, whereas ITGAX was also significantly decreased in HF/n-3 animals compared to HF animals in the spleen (Figure 15A). Similar to the findings in MAT, splenic CD4 and CD8 α mRNA levels were significantly lower upon HF/n-3 than HF, whereby this decrease was also observed for CD4 in HF/n-3 mice compared to

control mice (Figure 15B). Moreover, these findings were confirmed by immunohistochemical analyses of splenic tissue and the quantification of T cell marker-positive stained areas in the splenic white pulps, using primary antibodies specific for mouse T cell markers CD4 and CD8 α (Figures 15C and D). These analyses revealed a significant reduction of positive-stained T cell areas in the splenic white pulps of HF/n-3 mice compared with HF mice. In addition, immunohistochemical analysis and quantification of CD3-positive stained areas in spleen also showed a trend for lower T cell marker expression in HF/n-3 animals (Figure 15E).

Accordingly, previous findings showed that systemically increased SAA levels, which were observed in HF animals, were prevented upon HF/n-3 (Ludwig 2013). However, further analysis of plasma inflammatory markers revealed only a tendency of slightly higher MCP1 levels upon both HFDs compared to control (Figure 15F). Moreover, inflammatory hepatic conditions that might induce the increased production of SAA, following the exposure to bacterial LPS and the activation of NF κ B (Lv 2013), were not found. The mRNA levels of the macrophage marker EMR1 and of TNF α were not regulated upon HFDs in the liver (Appendix Table 23).

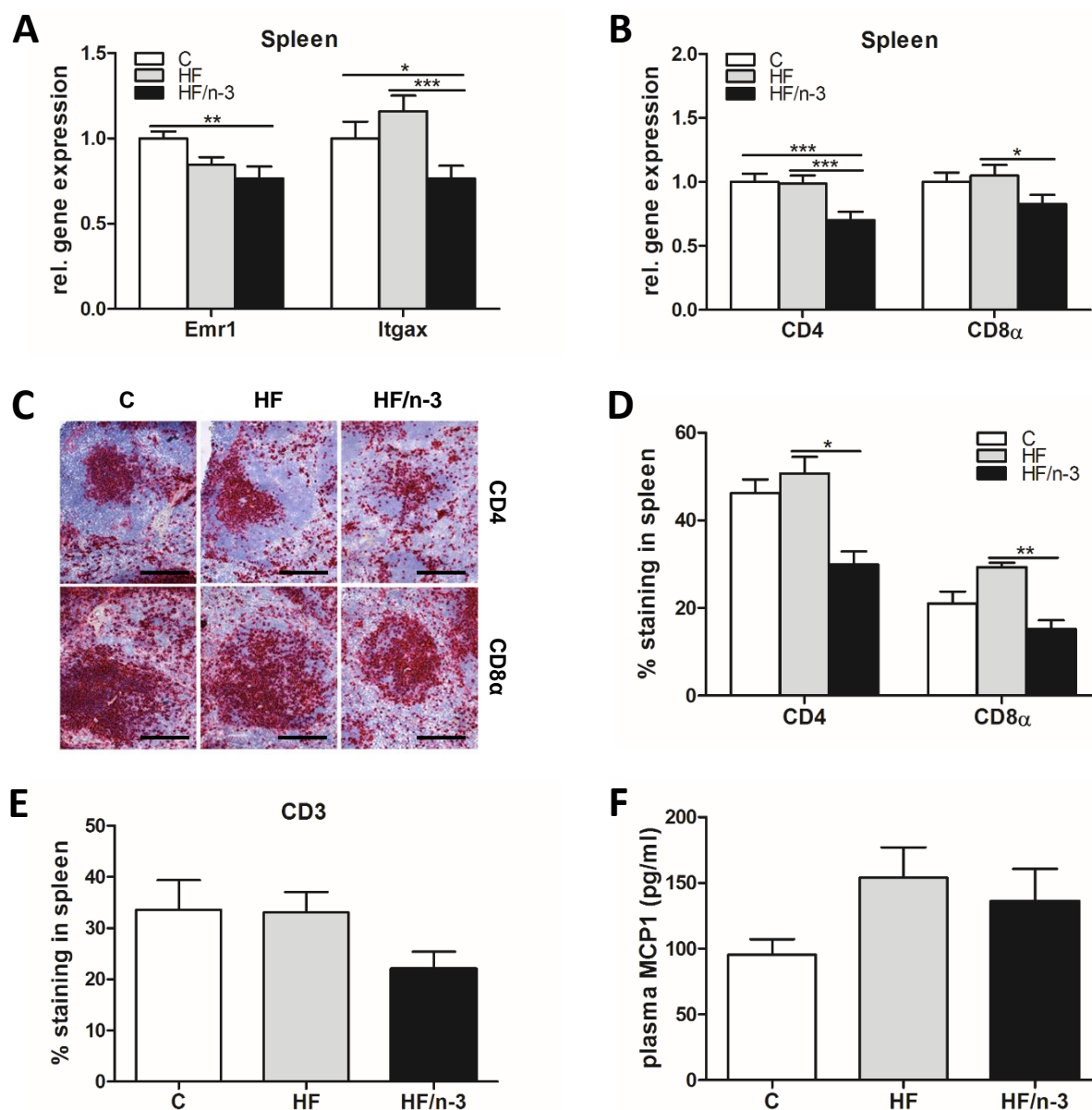


Figure 15. Gene expression analysis of immune cell markers, the immunohistochemical detection and quantification of T cells in spleen and MCP1 measurement in plasma. All data are means \pm SE and were collected from mice after 12 weeks of feeding either control (C), HFD (HF), or n-3 long-chain polyunsaturated fatty acid (LCPUFA)-enriched HFD (HF/n-3). **(A and B)** Gene expression of macrophage markers and T cell markers in spleen (n=10-12). Shown are the gene expression levels of EGF-like module-containing mucin-like hormone receptor-like 1 (Emr1) and integrin α -X (Itgax; **A**) or CD4 and CD8 α (**B**). Data were retrieved by RT-qPCR, normalised to Gapdh and Hprt1, and calculated relative to controls. **(C-E)** Immunohistochemical detection of T cells in splenic white pulps and their quantification (n=4-6). Shown are representative digital images of CD4- and CD8 α -positive stained areas of the splenic white pulps taken from stained cryosections (**C**). For immunohistochemistry, CD4- and CD8 α -specific antibodies and an antigen detection system based on Fast Red were used. Scale bar indicates 200 μ m. Area of splenic white pulps positively stained for CD4 and CD8 α (**D**) or for CD3 (**E**) was quantified, related to section area and expressed in percent. **(F)** Plasma monocyte chemoattractant protein-1 (MCP1) level was quantified with a commercially available ELISA kit. Statistical analysis was performed using one-way ANOVA and Tukey post-test. In case of no normal

distribution or $n < 5$, data were tested by Kruskal-Wallis and Dunn's post-test. In addition, outliers were detected by using Grubb's test and excluded from statistical data analysis. * $p < 0.05$, ** $p < 0.01$, *** $p < 0.001$, significant differences compared with control or between groups as indicated.

4.2 Gene expression analysis indicating inflammatory and vascular changes in small intestine upon HF and HF/n-3 (48 kJ% fat)

Diet-induced inflammation affects adipose tissues, the liver and even the intestine (Li 2008), indicating a possible connectivity between MAT / mesenteric lymph nodes, the intestine and the liver. Moreover, LPS penetrating the intestine due to HFD-induced disruption of the intestinal barrier function might promote local and systemic inflammation (de La Serre 2010, Cani 2008). However, in this context only the intestinal epithelial barrier was studied, whereas the impact of HFD on intestinal endothelial integrity was less recognised and investigated, although LPS will have to enter the microcirculation to result in systemic inflammation. The endothelium plays an important role in many physiological functions, which vary along the vascular tree. Its activation, for example via inflammatory mediators or bacterial products, can result in inflammation-induced increase in endothelial permeability (Aird 2007), whereas chemokines as well as ROS can impair (Granger 2010) and n-3 LCPUFA are said to improve vascular endothelial function, partly due to their different effects on NO bioavailability (Balakumar 2012).

In this thesis, besides analysing inflammatory processes in the upper (USI) and lower small intestine (LSI), a potential evocation of endothelial dysfunction in mice by the fat quantity and quality of the HFDs used, and the impact of those on vascular integrity was further explored using intestinal mucosal scrapings. Thus, the regulation of NO synthesis was assessed in USI. Furthermore, the gene expression levels of proteins involved in the maintenance of vascular integrity were examined by RT-qPCR analysis. Finally, the albumin content in blood plasma was determined in order to get first physiological insights on potential differential effects of the diets used, which differed in n-6/n-3 ratios, on endothelial function.

4.2.1 Small intestine and inflammation

Preliminary gene expression data indicated endothelial activation upon HF feeding analysing mucosal scrapings of the USI and suggested a higher inflammatory potential of HF compared to HF/n-3.

To validate the aforementioned hypothesis that the HFDs have differential effects on intestinal inflammation, immune cell markers and cytokines were examined separately in the USI and the LSI by RT-qPCR and correlation analyses. Surprisingly, only few inflammatory changes could be observed in the USI. ITGAM and ITGAX (Appendix Table 27) showed no regulation, but the gene expression

level of CD86, which is expressed on antigen-presenting cells and provides co-stimulatory signals necessary for T cell activation and survival (Kong 2011), was significantly enhanced upon HF compared to control and HF/n-3 (Figure 16A). Moreover, the mRNA levels of cytokines like MCP1 and TGF β 1 were also significantly upregulated in HF mice compared to controls, whereby the partial substitution of palm oil with n-3 LCPUFA resulted in a downward trend. Furthermore, a significant decreased gene expression for NOS2 could be observed upon HF/n-3 compared to control in USI (Figure 16B).

Compared to the USI, inflammatory changes were even less pronounced in the LSI. Only the gene expression of NOS2 was significantly downregulated in HF/n-3 mice compared to control and HF mice, whereas the mRNA levels of TGF β 1 (Figure 16C), EMR1 and ITGAX (Appendix Table 24) were not regulated. However, for the HF/n-3 animals, the gene expression levels of TGF β 1 significantly correlated with those of EMR1 and ITGAX (Table 7), indicating a non-inflamed mucosa (Smith 2011) upon HF/n-3 in LSI.

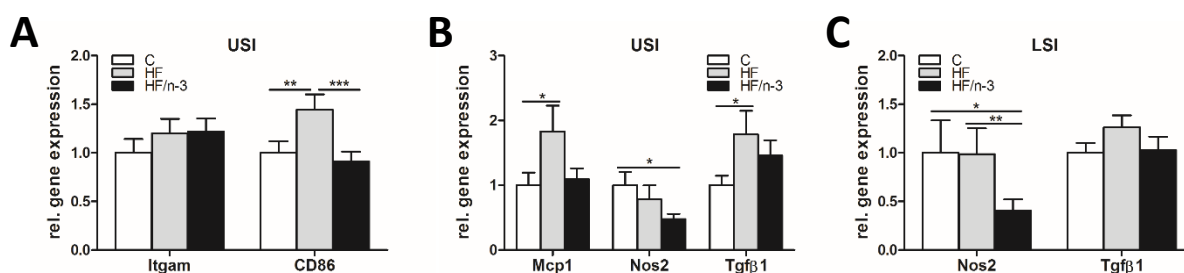


Figure 16. Gene expression of immune cell markers and cytokines in upper (USI) and lower small intestine (LSI). All data are means \pm SE and were collected from mice after 12 weeks of feeding either control (C), HFD (HF), or n-3 long-chain polyunsaturated fatty acid (LCPUFA)-enriched HFD (HF/n-3). **(A and B)** Gene expression data of the immune cell marker integrin α -G (Itgam) and CD86 **(A)** and of the cytokines monocyte chemoattractant protein-1 (Mcp1), nitric oxide synthase 2 (Nos2) and transforming growth factor β 1 (Tgf β 1; **B**) in USI (n=7-11). **(C)** Gene expression data of Nos2 and Tgf β 1 in LSI (n=9-12). Data were retrieved by RT-qPCR, normalised to Hprt1, Gapdh and Actb (USI) or CypB and Hsp90 α b1 (LSI), and calculated relative to controls. Statistical analysis was performed using one-way ANOVA and Tukey post-test. In case of no normal distribution, data were tested by Kruskal-Wallis and Dunn's post-test. In addition, outliers were detected by using Grubb's test and excluded from statistical data analysis. *p < 0.05, **p < 0.01, ***p < 0.001, significant differences compared with control or between groups as indicated.

Table 7. Correlation analysis of the cytokine TGFβ1 and immune cell markers in LSI

Gene	Gene		Total	Correlation		
				C	HF	HF/n-3
Tgfβ1	Emr1	p	0.0019**	0.1217	0.5422	0.0083**
		r	0.5368	0.4949	0.2196	0.7764
Tgfβ1	Itgax	p	<0.0001***	0.2708	0.1195	0.0058**
		r	0.6452	0.3643	0.5246	0.7969

Shown are correlations between gene expression data of chemokines / cytokines and immune cell markers in lower small intestine (LSI) after 12 weeks of feeding either control (C), HFD (HF), or n-3 long-chain polyunsaturated fatty acid (LCPUFA)-enriched HFD (HF/n-3). The expression data were generated by RT-qPCR analysis (n=8-12) and correlation analyses were performed utilizing the whole data set (total), but also analysing the data from each group separately. Normalised values were used. Outliers were detected by using Grubb's test and excluded from statistical data analysis. *p < 0.05, **p < 0.01, ***p < 0.001, indicate significant correlation. p, statistical significance; r, Pearson correlation coefficient.

4.2.2 Summary of the findings regarding inflammatory status

Findings obtained so far from RT-qPCR and immunohistochemical analyses that examined immune cell markers, chemokine and cytokines in MAT and EAT (Table 8), as well as in iBAT, spleen, liver, blood plasma, USI and LSI (Table 9) are listed below. Significant gene and protein expression changes upon both HFDs compared to control and those upon HF/n-3 compared to HF are represented as arrows to give an overview of the changes induced by HFDs that differ in their fat quality.

Table 8. Summary of inflammatory changes in MAT and EAT

MAT / Function	Gene / Protein (IHC)	Regulation			EAT/ Function	Gene / Protein (IHC)	Regulation		
		HF C	HF/n-3 C	HF/n-3 HF			HF C	HF/n-3 C	HF/n-3 HF
T cell	CD4	—	—	—	T cell	CD4	—	↑	↑
	CD8α	—	↓	—					
	CD3	↓	—	—		CD3	—	—	↑
Co-stimulation	CD86	—	—	—	Co-stimulation	CD86	—	—	—
B cell	B220	—	—	—					
Macrophage	Emr1	—	↑	—	Macrophage	Emr1	↑	↑	—
	F4/80 (CLS)	—	—	↑		F4/80 (CLS)	—	↑	—
	F4/80 (solitary cell)	—	—	—		F4/80 (solitary cell)	—	↑	—
	Itgax*	—	↑	↑		Itgax*	—	↑	—
	CD11c (CLS)	—	↑	—		CD11c (CLS)	—	↑	—
	CD11c (solitary cell)	—	—	—		CD11c (solitary cell)	—	↓	—
	Itgam	—	↑	↑		Itgam	—	↑	—
	Mrc1*	—	↑	—		Mrc1*	—	—	↑
	CD206 (CLS)	—	↑	—		CD206 (CLS)	—	—	—
	CD206 (solitary cell)	↓	—	—		CD206 (solitary cell)	↓	—	—
	Clec10a	—	↑	—		Clec10a	—	↑	↑
	Chemokine	Mcp1*	↑	↑	—	Chemokine	Mcp1*	↑	↑
Spp1 (Opn)*		—	↑	↑		Spp1 (Opn)*	↑	↑	↑
Cytokine	Tnfa	—	—	—	Cytokine	Tnfa	—	↑	—
	Nos2	—	—	—		Nos2	↑	—	↓
	IL10*	—	—	—		IL10*	—	↑	—
Adhesion	Vcam1	—	—	—	Adhesion	Vcam1	—	↑	↑
	Icam1	—	—	—		Icam1	—	—	—
Angiogenesis	Tek	—	—	—	Angiogenesis	Tek	—	—	—
Proliferation	KI67	—	—	—					
Apoptosis	CL-CASP3	—	—	↑					

Regulation of gene (1st letter in capital) or protein (only capitals or bold type; immunohistochemistry (IHC)) expression of immune cell markers, chemokines and cytokines, as well as markers related to adhesion, angiogenesis, proliferation and apoptosis by HFD (HF) and n-3 long-chain polyunsaturated fatty acid (LCPUFA)-enriched HFD (HF/n-3) in mesenteric (MAT) and epididymal adipose tissue (EAT). Comparisons between HF and control diet (black), HF/n-3 and control diet (red) or HF/n-3 and HF (green) are shown. Upward- and downward-oriented arrows indicate upregulation or downregulation, respectively, and unregulated processes are represented by a dash symbol. For the genes rated by asterisks, the data were obtained from Ludwig et al. (Ludwig 2013), testing for normal distribution and outliers.

Table 9. Summary of inflammatory changes in iBAT, spleen, liver, plasma, USI and LSI

iBAT / Function	Gene / Protein (IHC)	Regulation			Spleen / Function	Gene / Protein (IHC)	Regulation				
		HF	HF/n-3	HF/n-3			HF	HF	HF/n-3	HF/n-3	
		C	C	HF			C	C	HF		
Macrophage	Emr1	↑	↑	—	T cell	CD4	—	↓	↓		
	F4/80 (CLS)	—	—	↑		CD4	—	—	↓		
	F4/80 (solitary cell)	—	—	↑		CD8α	—	—	↓		
	Itgax	↑	↑	—		CD8α	—	—	↓		
	CD11c (CLS)	—	—	—		CD3	—	—	—		
	CD11c (solitary cell)	—	—	↑		Macrophage	Emr1	—	↓	—	
	Mrc1	—	↑	—			Itgax	—	↓	↓	
	CD206 (CLS)	—	—	—			<hr/>				
	CD206 (solitary cell)	—	—	—			Liver / Function	Gene / Protein	Regulation		
	Clec10a	↑	↑	—			Macrophage	Emr1	—	—	—
CD301 (CLS)	↓	—	—	Cytokine	Tnfa		—	—	—		
CD301 (solitary cell)	↓	↓	—	<hr/>							
Eosinophil	Siglec5	—	↑	↑	Plasma / Function	Gene / Protein (ELISA)	Regulation				
Chemokine	Mcp1	↑	↑	—		Acute-phase protein	SAA*	↑	—	↓	
	Cytokine	Tnfa	—	—		Chemokine	MCP1	—	—	—	
	IL10	↑	↑	—	<hr/>						
	Tgfβ1	—	↑	—	USI / Function	Gene / Protein	Regulation				
<hr/>			<hr/>			<hr/>					
Co-stimulation	CD86	↑	—	↓	Macrophage	Emr1	—	—	—		
Macrophage	Itgax	—	—	—		Itgax	—	—	—		
	Itgam	—	—	—	Cytokine	Nos2	—	↓	↓		
Chemokine	Mcp1	↑	—	—		Tgfβ1	—	—	—		
Cytokine	Nos2	—	↓	—	Adhesion	Vcam1*	—	—	—		
	Tgfβ1	↑	—	—		Icam1*	—	—	—		
Adhesion	Vcam1*	—	—	—	Angiogenesis	Tek*	—	—	—		
	Icam1*	↑	—	—							
Angiogenesis	Tek*	↑	—	—	<hr/>						

Regulation of gene (1st letter in capital) or protein (only capitals or bold type; immunohistochemistry (IHC) or ELISA) expression of immune cell markers, chemokines and cytokines, as well as markers related to adhesion and angiogenesis by HFD (HF) and n-3 long-chain polyunsaturated fatty acid (LCPUFA)-enriched HFD (HF/n-3) in interscapular brown adipose tissue (iBAT), spleen, liver, blood plasma and upper (USI) and lower small intestine (LSI). Comparisons between HF and control diet (black), HF/n-3 and control diet (red) or HF/n-3 and HF (green) are shown. Upward- and downward-oriented arrows indicate upregulation or downregulation, respectively, and unregulated processes are represented by a dash symbol. For the genes rated by asterisks, the data were obtained from Ludwig et al. (Ludwig 2013), testing for normal distribution and outliers.

4.2.3 Small intestine, vasculature and NO biology

Endothelial dysfunction is characterised by reduced NO availability secondary to an enhanced oxidative stress production and subsequent impaired vasodilatory response, and it is associated with hyperpermeability. The generation of NO is highly regulated, inter alia, by phosphorylation of eNOS, cofactors and substrate availability or the localisation of eNOS. However, in pathogenic conditions involving vascular oxidative stress and inflammation, ROS and the formation of peroxynitrite (ONOO⁻) would lead to eNOS uncoupling and the subsequent eNOS contribution to superoxide production (Félétou 2011, Figure 17A).

Since physiologic levels of NO appear to play an important role in the maintenance of endothelial function, in this thesis, the possible different regulation of NO bioavailability by HFDs differing in fat quality was assessed in USI by RT-qPCR and correlation analyses. Thus, genes involved in the control of NO generation such as NOS3, arginase 2 (ARG2), which compete with NOS3 for its substrate L-arginine, and caveolin 1 (CAV1), which can bind NOS3 and thereby inhibit its activity, were examined. Notably, the mRNA expression levels of ARG2 and CAV1, both negative regulators of NOS3, were significantly increased upon HF compared to control or HF/n-3, respectively, whereas the gene expression level of NOS3 showed no regulation (Figure 17B).

In addition, given that oxidative stress induces eNOS uncoupling, the gene expression levels of gp91PHOX and p47PHOX (NAD(P)H oxidase subunits), which produce superoxide and of enzymes that act as antioxidants, like superoxide dismutase (SOD) or catalase (CAT), were examined by RT-qPCR and partly validated on protein level by Western blot analysis. The gene expression levels of cytochrome b-245, beta polypeptide (gp91PHOX) and neutrophil cytosolic factor 1 (p47PHOX) showed no regulation (Figure 17C), however, the mRNA levels of SOD1 and CAT were significantly upregulated upon HF/n-3 compared to control and HF feeding and SOD1 levels were also significantly higher for HF than for control in USI (Figure 17D). Nevertheless, the protein level of CAT showed no significant changes, and only a trend of an increase was observed upon HF/n-3 in USI, whereas in LSI the expression of CAT was significantly enhanced in HF/n-3 animals compared to controls (Figure 17E). Remarkably, in USI, a significant correlation was observed between the gene expression levels of SOD1 and CAT for the HF/n-3 animals (Table 10), indicating a balanced antioxidative defence system upon HF/n-3. Conversely, for the HF animals, the gene expression level of eNOS correlate with those of the NAD(P)H oxidase subunit gp91PHOX and the immune cell marker CD86 (Table 10), possible sources of oxidative stress and inflammation.

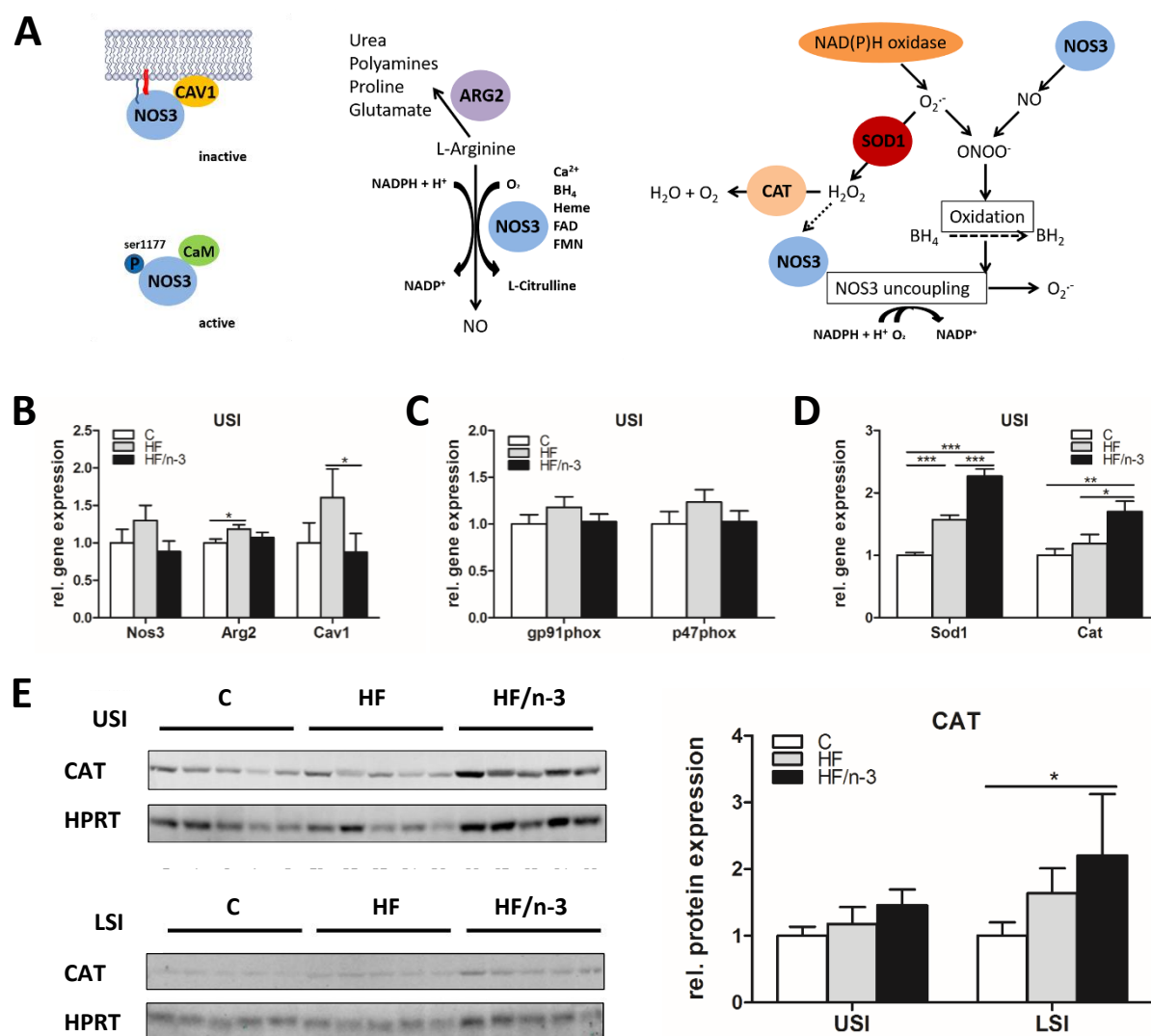


Figure 17. mRNA and protein expression of genes that play a role in the regulation of nitric oxide bioavailability in small intestine. All data are means \pm SE and were collected from mice after 12 weeks of feeding either control (C), HFD (HF), or n-3 long-chain polyunsaturated fatty acid (LCPUFA)-enriched HFD (HF/n-3). **(A)** Schematic presentation of the control of NO bioavailability. **(B)** Gene expression data of nitric oxide synthase 3 (Nos3), arginase 2 (Arg2) and caveolin 1 (Cav1) in USI (n=8-11). **(C and D)** Gene expression data of the NAD(P)H oxidase subunits gp91phox and p47phox **(C)** and of superoxide dismutase 1 (Sod1) and catalase (Cat; **D**) in USI (n=8-11). Gene expression data were retrieved by RT-qPCR, normalised to Hprt1, Gapdh and Actb, and calculated relative to controls. **(E)** Western blot analysis of CAT in USI and LSI (n=4-5). Shown are their protein expression levels relative to controls. HPRT was used for protein normalisation. Statistical analysis was performed using one-way ANOVA and Tukey post-test. In case of no normal distribution or n < 5, data were tested by Kruskal-Wallis and Dunn's post-test. In addition, outliers were detected by using Grubb's test and excluded from statistical data analysis. *p < 0.05, **p < 0.01, ***p < 0.001, significant differences compared with control or between groups as indicated.

Table 10. Correlation analysis data on the regulation of nitric oxide bioavailability in USI

Gene	Gene		Total	Correlation		
				C	HF	HF/n-3
Sod1	Cat	p	0.0006***	0.6895	0.7346	0.0217*
		r	0.6009	-0.1449	0.1158	0.7825
gp91phox	Nos3	p	0.0060**	0.1752	0.0310*	0.1339
		r	0.4977	0.4654	0.6483	-0.5774
CD86	Nos3	p	0.0028**	0.3401	0.0208*	0.5646
		r	0.5355	0.3376	0.6818	-0.2414

Shown are correlations between the mRNA level of nitric oxide synthase 3 (Nos3) and the gene expression data of oxidative markers or immune cell markers in upper small intestine (USI) after 12 weeks of feeding either control (C), HFD (HF), or n-3 long-chain polyunsaturated fatty acid (LCPUFA)-enriched HFD (HF/n-3). The expression data were generated by RT-qPCR analysis (n=8-12) and correlation analyses were performed utilizing the whole data set (total), but also analysing the data from each group separately. Normalised values were used. Outliers were detected by using Grubb's test and excluded from statistical data analysis. *p < 0.05, **p < 0.01, ***p < 0.001, indicate significant correlation. p, statistical significance; r, Pearson correlation coefficient.

4.2.4 Small intestine, endothelial permeability and serum albumin level

Impaired vascular integrity, which is observed in inflammation or chronic disease states, is characterised by leakage of fluid, proteins, or small molecules. Moreover, it clinically manifests as accumulation of plasma-like, protein-rich fluid in the extravascular space leading to edema. Furthermore, blood fluid, solutes and even circulating cells can cross the endothelium via two routes: transcellular or paracellular. The latter is responsible for the majority of endothelial leakage of blood fluid and protein under pathophysiological conditions, which takes place in the microvessels (Yuan 2010). It must also be noted that basal vessel permeability differs according to the type of tissue examined. The fenestrated endothelium, which is found in the gastrointestinal tract, is characterised by the presence of transcellular pores, which are spanned by a diaphragm (Sarin 2010).

Hence, to assess changes in intestinal integrity endothelial cell markers, junctional proteins and a fenestration marker were examined by RT-qPCR analyses using RNA from intestinal mucosal scrapings. Additionally, blood plasma albumin level after 6 and 12 weeks of feeding as well as hepatic albumin gene level were determined to find indications for changes in systemic microvascular permeability.

Endothelial cell markers like CD31 and CDH5 were significantly upregulated upon HF compared to control feeding, whereas the gene expression of claudin5 (CLDN5) showed no regulation in the USI (Figure 18A). It should be noted that all these proteins are found in intercellular junctions and define the paracellular pathway. OCLN, another junction protein was not regulated on gene expression

level, however, the mRNA level of the fenestration marker plasmalemma vesicle-associated protein (PLVAP), a fenestral diaphragm protein, was significantly upregulated in the USI of HF animals compared to control and HF/n-3 animals (Figure 18B).

Notably, for HF and control animals, a significant correlation was observed between the gene expression levels of CDH5 and CAV1 or PLVAP, which are proteins defining paracellular and transcellular pathways, in USI (Table 11). Both proteins, CAV1 and PLVAP, were found to be involved in lymphocyte transmigration (Keuschnigg 2009). Thus, it was further investigated whether their mRNA levels are related to those of immune cell markers and oxidative stress markers. For HF and control mice, the gene expression levels of both proteins were significantly correlated with the mRNA level of p47PHOX, whereas, only for the HF animals, they were significantly correlated with CD86. However, a significant correlation was even observed between the mRNA levels of PLVAP and CAV1 in USI within HF and control group (Table 11).

Table 11. Correlation analysis data on genes involved in the regulation of the transcellular pathway in USI

Gene	Gene		Correlation			
			Total	C	HF	HF/n-3
Cdh5	Cav1	p	<0.0001***	<0.0001***	0.0019**	0.5190
		r	0.7727	0.9421	0.8221	0.2692
Cdh5	Plvap	p	<0.0001***	0.0001***	<0.0001***	0.2085
		r	0.8889	0.9267	0.9263	0.4986
CD86	Cav1	p	0.0006***	0.1131	0.0094**	0.3604
		r	0.5981	0.5324	0.7391	-0.3747
CD86	Plvap	p	<0.0001***	0.0526	0.0136*	0.9714
		r	0.7251	0.6265	0.7138	-0.01525
p47phox	Cav1	p	0.0003***	0.0353*	0.0143*	0.8670
		r	0.6283	0.6665	0.7105	0.07118
p47phox	Plvap	p	<0.0001***	0.0075**	0.0056**	0.6614
		r	0.7490	0.7819	0.7696	0.1848
Cav1	Plvap	p	<0.0001***	0.0003***	0.0005***	0.1726
		r	0.8366	0.9064	0.8683	0.5342

Shown are correlations between the mRNA levels of plasmalemma vesicle-associated protein (Plvap) or caveolin 1 (Cav1) and the gene expression data of endothelial, immune cell or oxidative markers in upper small intestine (USI) after 12 weeks of feeding either control (C), HFD (HF), or n-3 long-chain polyunsaturated fatty acid (LCPUFA)-enriched HFD (HF/n-3). The expression data were generated by RT-qPCR analysis (n=8-12) and correlation analyses were performed utilizing the whole data set (total), but also analysing the data from each group separately. Normalised values were used. Outliers were detected by using Grubb's test and excluded from statistical data analysis. *p < 0.05, **p < 0.01, ***p < 0.001, indicate significant correlation. p, statistical significance; r, Pearson correlation coefficient.

Surprisingly, for LSI, which already showed less pronounced inflammatory changes compared to USI, the mRNA expression of OCLN was significantly enhanced upon HF compared to control feeding, whereas the expression of endothelial marker CD31 showed no changes after 12 weeks of feeding (Figure 18C). At the earlier timepoint of feeding, at 6 weeks, no regulation was observed for the mRNA levels of CDH5 or OCLN in LSI (Figure 18D).

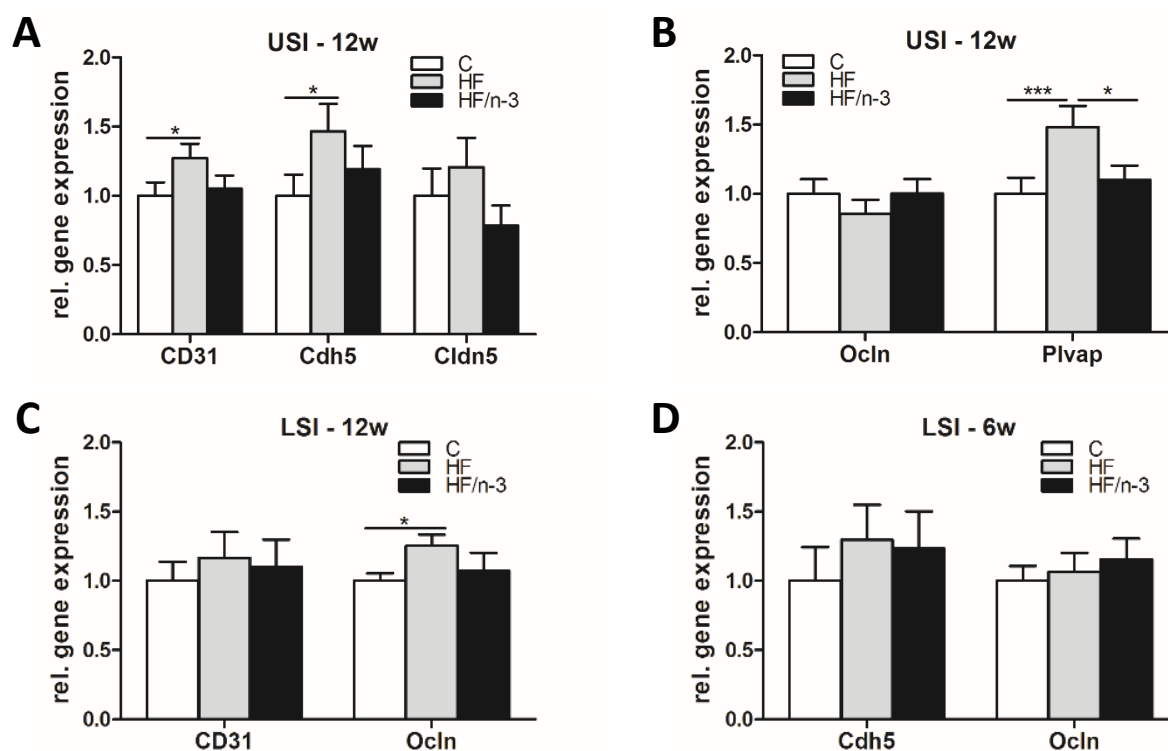


Figure 18. Gene expression of endothelial cell markers, junctional and plasmalemma vesicle-associated proteins in upper (USI) and lower small intestine (LSI). All data are means \pm SE and were collected from mice after 12 weeks or 6 weeks of feeding either control (C), HFD (HF), or n-3 long-chain polyunsaturated fatty acid (LCPUFA)-enriched HFD (HF/n-3). (**A and B**) Gene expression of endothelial markers platelet endothelial cell adhesion molecule 1 (CD31), cadherin 5 (Cdh5) and claudin 5 (Cldn5; **A**), and of the tight junction protein occludin (Ocln) and the fenestration marker plasmalemma vesicle-associated protein (Plvap; **B**) in USI (n=8-11). (**C and D**) Gene expression of CD31 and Ocln in LSI after 12 weeks (**C**; n=9-11) and of Cdh5 and Ocln after 6 weeks of feeding (**D**; n=11-12). Data were retrieved by RT-qPCR, normalised to Hprt1, Gapdh and Actb (USI) or CypB and Hsp90ab1 (LSI 6w or 12w), and calculated relative to controls. Statistical analysis was performed using one-way ANOVA and Tukey post-test. In case of no normal distribution, data were tested by Kruskal-Wallis and Dunn's post-test. In addition, outliers were detected by using Grubb's test and excluded from statistical data analysis. *p < 0.05, **p < 0.01, ***p < 0.001, significant differences compared with control or between groups as indicated.

Finally, the plasma level of albumin, the main plasma protein regulating the colloidal osmotic pressure of blood and binding / transporting fatty acids (Rozga 2013), was determined after 6 and 12

weeks of the feeding. Labeled albumin is used frequently as tracer for monitoring microvascular permeability (Bates 2010).

Plasma level of albumin was not regulated in the 12-week feeding trial (Figure 19A). However, in order to test whether this finding was explained by a possible long-term compensation process, we also measured the plasma albumin level from mice of the 6-week feeding trial, showing a significant decrease upon both HFDs compared to control (Figure 19B). Moreover, in liver, where albumin is produced (Ballmer 2001), the gene expression level of albumin was significantly decreased in HF/n-3 animals compared to control and HF animals in the 6-week feeding trial (Figure 19C).

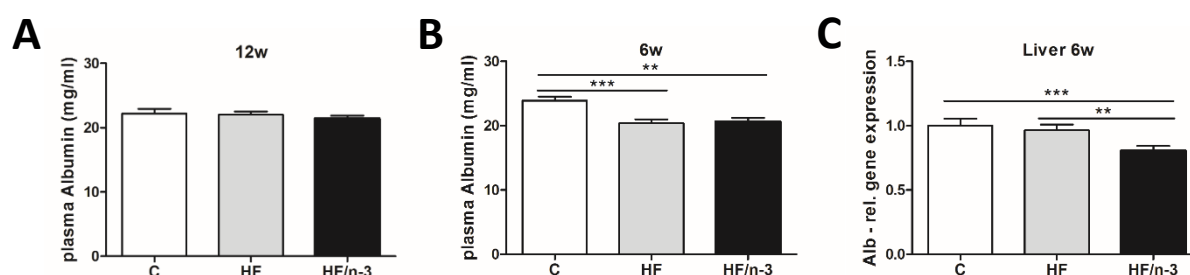


Figure 19. Albumin measurement in plasma and gene expression of albumin in liver. All data are means \pm SE and were collected from mice after 6 weeks or 12 weeks of feeding either control (C), HFD (HF), or n-3 long-chain polyunsaturated fatty acid (LCPUFA)-enriched HFD (HF/n-3). **(A and B)** Plasma albumin level was quantified with commercially available ELISA kits after 12 weeks (**A**; n=10-12) or 6 weeks of feeding (**B**; n=12). **(C)** Gene expression data of albumin (Alb) in liver (n=10-12). Data were retrieved by RT-qPCR, normalised to Hprt1 and Actb, and calculated relative to controls. Statistical analysis was performed using one-way ANOVA and Tukey post-test. In case of no normal distribution, data were tested by Kruskal-Wallis and Dunn's post-test. In addition, outliers were detected by using Grubb's test and excluded from statistical data analysis. * $p < 0.05$, ** $p < 0.01$, *** $p < 0.001$, significant differences compared with control or between groups as indicated.

4.3 Changes in fatty acid uptake and metabolism upon HFDs

The immune response and metabolic regulation are highly integrated and the proper function of each is dependent on the other, so the next point to be investigated was the differential effect of HFDs on fatty acid and energy metabolism. Fatty acids taken up by nutrition are either oxidised for energy generation, which already begins in the small intestine, or are released. Some of them enter the portal vein directly reaching the liver, the others form TAG, enter the lymphatic system packaged as chylomicrons and reach the vascular circulation through the thoracic duct (Yáñez 2011). In obesity, fat can accumulate in the liver in excessive amounts. In this context, hepatic TAG accumulation results from an imbalance of FFA uptake from circulation, DNL, fatty acid oxidation and TAG export via VLDL particles to peripheral fat stores (Rui 2014). Moreover, iBAT plays a central role in regulating energy homeostasis via thermogenesis that is regulated by UCP1 (Cannon 2004).

In order to characterise the n-3 LCPUFA-mediated fat mass-reducing effect that was observed in HF/n-3 mice compared to HF mice by previous analyses of this study (Ludwig 2013), the contribution of the small intestine, liver and iBAT to fatty acid metabolism and energy expenditure was further analysed. Moreover, given that the outcome of DIO is determined by the fat quantity and quality of the HFD, mice from the study by Dahlhoff et al. (Dahlhoff 2014) were examined and data on hepatic lipid metabolism were used for comparative analysis.

4.3.1 Changes in fatty acid oxidation in small intestine upon HF and HF/n-3 (48 kJ% fat)

Alterations in the expression of genes involved in the regulation of fat oxidation in the intestine are considered to contribute to the anti-obesogenic effect of n-3 LCPUFA (van Schothorst 2009). In this thesis the mRNA levels of genes involved in mitochondrial and peroxisomal β -oxidation and in ω -oxidation, such as CPT1a, ACOX1 and cytochrome P450, family 4, subfamily a, polypeptide 10 (CYP4a10), respectively, were analysed in USI and LSI. The expression level for each of them was significantly increased in the USI for both high-fat groups. Remarkably, the HF/n-3 animals even showed a significantly increased expression compared to the HF animals (Figure 20A). In the LSI, these genes were only significantly upregulated in the HF/n-3 animals, except for CYP4a10, which also showed a significant increase in the HF group compared to control (Figure 20B). However, this upregulation of CYP4a10 was only minor compared to the HF/n-3 group, showing a mRNA level that was almost 9-fold higher than in the HF group (Figure 20B; HF vs. C: 1.71-fold; HF/n-3 vs. C: 14.73-fold). Interestingly, the fold changes for CYP4a10 were even more pronounced in the USI (Figure 20A; HF vs. C: 7.01-fold; HF/n-3 vs. C: 42.65-fold and HF/n-3 vs. HF: 6.08-fold).

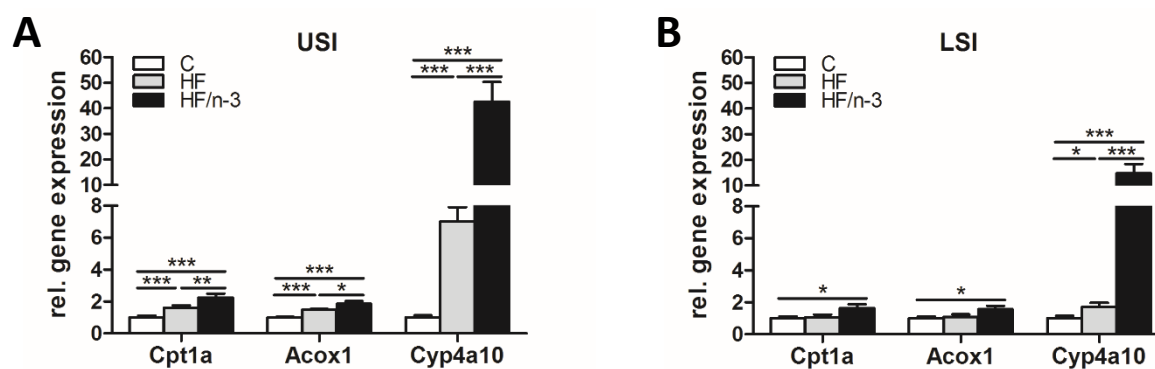


Figure 20. Expression of genes involved in lipid metabolism in upper (USI) and lower small intestine (LSI). All data are means \pm SE and were collected from mice after 12 weeks of feeding either control (C), HFD (HF), or n-3 long-chain polyunsaturated fatty acid (LCPUFA)-enriched HFD (HF/n-3). **(A and B)** Gene expression data of carnitine palmitoyl transferase 1a (Cpt1a), acyl-coenzyme A oxidase 1 (Acox1) and cytochrome P450, family 4, subfamily a, polypeptide 10 (Cyp4a10), which represent genes involved in mitochondrial and peroxisomal β -oxidation as well as ω -oxidation in USI **(A; n=7-11)** and in LSI **(B; n=8-12)**. Data were retrieved by RT-qPCR, normalised to Hprt1, Gapdh and Actb (USI) or CypB and Hsp90 α b1 (LSI), and calculated relative to controls. Statistical analysis was performed using one-way ANOVA and Tukey post-test. In case of no normal distribution, data were tested by Kruskal-Wallis and Dunn's post-test. In addition, outliers were detected by using Grubb's test and excluded from statistical data analysis. * $p < 0.05$, ** $p < 0.01$, *** $p < 0.001$, significant differences compared with control or between groups as indicated.

4.3.2 Fatty acid metabolism in liver

Previous findings from the study by Ludwig et al. demonstrated a significant reduction in hepatic TAG levels in mice fed HF/n-3 compared to HF and suggested altered lipid handling (Ludwig 2013). In order to further characterise the changes in hepatic TAG content, fatty acid metabolism was analysed in the livers from these mice. In addition, we examined hepatic DNL in mice from the study by Dahlhoff et al. (Dahlhoff 2014) that reported improved hepatic lipid accumulation upon dietary MDS. To get an idea about the impact of fat quantity and quality on hepatic lipid metabolism, a subsequent comparative analysis was performed with the data from these feeding studies, since, in comparison to the moderate, soybean / palm oil-based HF (48 kJ% fat) used in the study by Ludwig et al., the soybean oil / beef tallow-based HF^A (60 kJ% fat) used in the study by Dahlhoff et al. showed differences in fat quantity and quality.

4.3.2.1 Impact of HF and HF/n-3 (48 kJ% fat) on hepatic lipid metabolism

In the study by Ludwig et al. the previous analysis of key regulators and enzymes involved in hepatic lipogenesis and β -oxidation indicated reduced lipogenesis and increased peroxisomal β -oxidation for

the HF/n-3 mice compared to control and HF mice. Moreover, the mRNA level of CPT1a, operating in mitochondrial β -oxidation, showed a significant upregulation upon HF compared to control (Ludwig 2013). Hence, in this thesis the impact of HF and HF/n-3 on hepatic lipid handling was further explored by expression analyses of genes involved in peroxisomal β -oxidation, ω -oxidation, lipolysis, and DNL, namely enoyl-Coenzyme A hydratase (LPBE), CYP4a10, hormone sensitive lipase (HSL) and ACC2, respectively. Surprisingly, the analysis of LPBE revealed only a significant upregulation for the HF/n-3 mice compared to control and HF mice, although, previous measurements showed significantly increased mRNA levels of ACOX1, another gene involved in peroxisomal β -oxidation, for both high-fat groups compared to control, whereby the respective levels were significantly higher for HF/n-3 than for HF mice (Ludwig 2013). Furthermore, the gene expression of CYP4a10 - the enzyme with the biggest fold change in the small intestine - was significantly upregulated in the liver upon both HFDs. Notably, HF/n-3 animals showed significant higher expression levels than HF animals (HF vs. C: 1.59-fold; HF/n-3 vs. C: 4.03-fold and HF/n-3 vs. HF: 2.53-fold), but the fold changes of hepatic CYP4a10 were not as pronounced as those observed in the small intestine. For HSL, the first enzyme involved in lipolysis, the mRNA level was also significantly increased for the HF/n-3 group compared to control, whereas the mRNA level for ACC2 was significantly downregulated upon HF/n-3 compared to control and HF (Figure 21A). Similar results were observed previously for ACC1 (Ludwig 2013).

On protein expression level, DNL was characterised in the liver by analysing ACC1_2 and its regulator AMPK α . Activated AMPK can phosphorylate ACC and inhibit DNL (Hardie 2011). Thus, protein levels for total AMPK α and phospho-AMPK α (Thr172) as well as for total ACC1_2 and their phosphorylated forms P-ACC1 (Ser76) and P-ACC2 (Ser219/Ser221) were determined by Western blot analyses. In addition, the ratios for P-AMPK α and total AMPK α and P-ACC1 or P-ACC2 and total ACC1_2 were quantified. Interestingly, for HF mice, significantly reduced expression of total AMPK α , but no changes for P-AMPK α were observed, resulting in an increased P-AMPK α /AMPK α ratio. Moreover, a tendency for an increased activation of AMPK α was observed for the HF/n-3 group (Figure 21B). These findings suggest increased activation of AMPK α , but reduced total content of AMPK α for the HF group in the liver. However, significantly reduced expression levels for total ACC1_2 were measured for both high-fat groups compared to control, whereby HF/n-3 animals showed a significant downregulation compared to HF animals. Furthermore, the expression levels of the phosphorylated ACC proteins were only significantly decreased upon HF/n-3, and P-ACC1/ACC1_2 and P-ACC2/ACC1_2 ratios were not significantly different between the dietary groups (Figure 21C).

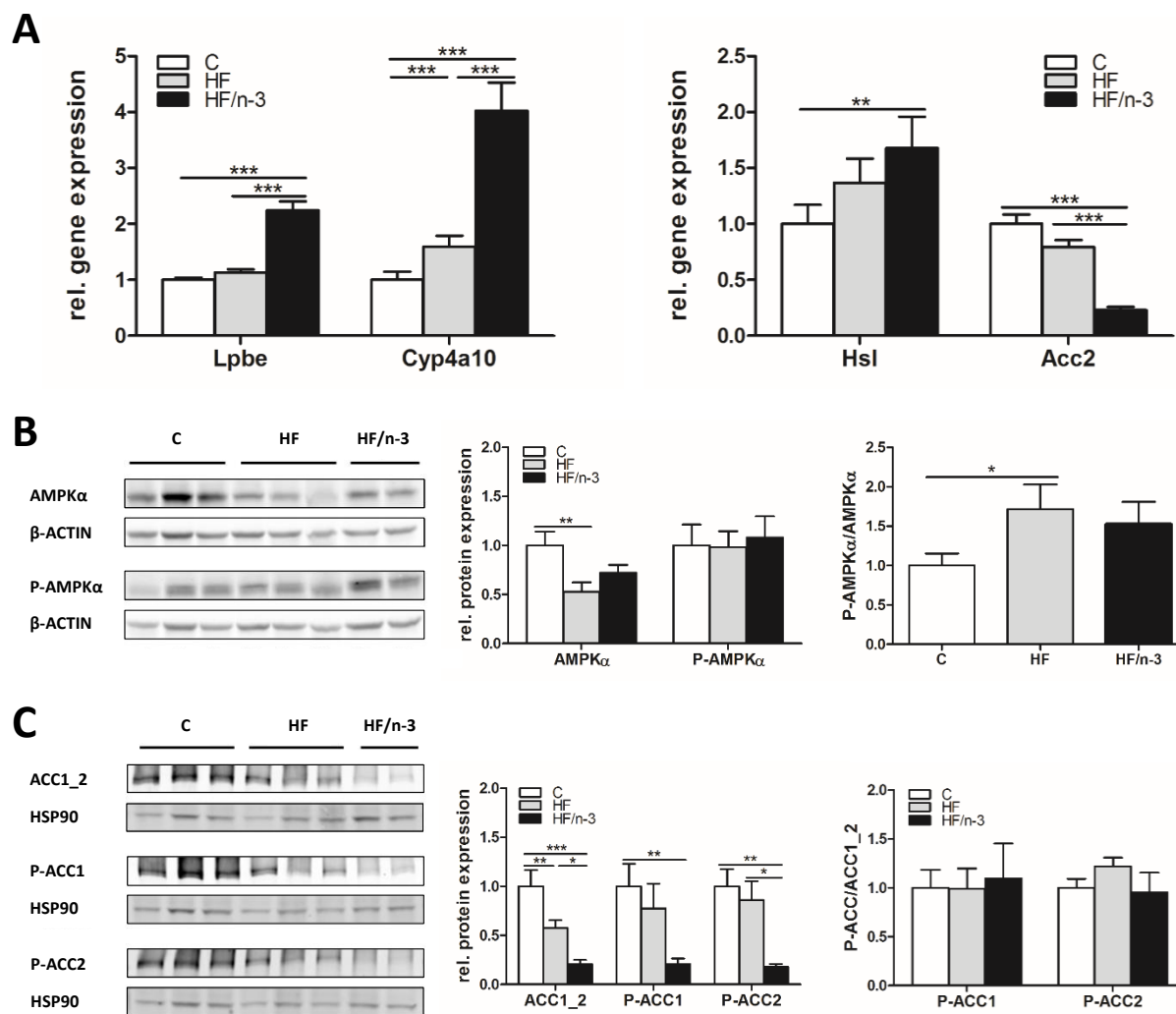


Figure 21. Gene and protein expression of enzymes involved in lipid metabolism in liver. All data are means \pm SE and were collected from mice after 12 weeks of feeding either control (C), HFD (HF), or n-3 long-chain polyunsaturated fatty acid (LCPUFA)-enriched HFD (HF/n-3). **(A)** Expression data for genes involved in peroxisomal β -oxidation, ω -oxidation, lipolysis and *de novo* lipogenesis, namely enoyl-Coenzyme A hydratase (Lpbe), cytochrome P450, family 4, subfamily a, polypeptide 10 (Cyp4a10), hormone sensitive lipase (Hsl) and acetyl-CoA carboxylase 2 (Acc2), respectively (n=10-11). Data were retrieved by RT-qPCR, normalised to Hprt1 and Actb, and calculated relative to controls. **(B and C)** Western blot analysis of AMP-activated protein kinase α (AMPK α ; **B**) and acetyl-CoA carboxylases (ACC1_2) and their representative phosphorylations (**C**) in liver (n=5-6). Separate gels were run for quantification of total AMPK α and P-AMPK α (Thr172) and ACC1_2, P-ACC1 (Ser76) and P-ACC2 (Ser219/Ser221), respectively. Shown are the protein expression levels relative to controls and the ratios for the phosphorylated forms to total protein expression levels (normalised values were used). β -ACTIN or HSP90 was used for protein normalisation. Statistical analysis was performed using one-way ANOVA and Tukey post-test. In case of no normal distribution, data were tested by Kruskal-Wallis and Dunn's post-test. In addition, outliers were detected by using Grubb's test and excluded from statistical data analysis. *p < 0.05, **p < 0.01, ***p < 0.001, significant differences compared with control or between groups as indicated.

In order to confirm a possible interaction between activated AMPK α and ACC, correlation analyses were performed. For the HF/n-3 animals, a significant correlation was found between P-AMPK α /AMPK α and P-ACC1/ACC1_2 ratios (Table 12), but not between P-AMPK α /AMPK α and P-ACC2/ACC1_2 ratios in the liver (data not shown). It is known that ACC2 is the isoform of ACC, which is involved in the regulation of mitochondrial fatty acid oxidation, whereas ACC1 maintains the regulation of fatty acid synthesis (Hardie 2011).

Noteworthy, further correlation analyses illustrated a significant negative correlation between P-ACC2/ACC1_2 ratios and the gene expression levels of ACC1 and ACC2, respectively, for control and HF/n-3 animals. Furthermore, a nearly significant correlation could also be observed between P-ACC2/ACC1_2 ratios and the gene expression levels of CPT1a upon HF/n-3 in the liver (Table 12).

Table 12. Correlation analysis data on the regulation of acetyl-CoA carboxylase in liver

Protein (WB)	Gene / Protein (WB)	Correlation				
		Total	C	HF	HF/n-3	
P-AMPKα/AMPKα	P-ACC1/ACC1_2	p	0.0919	0.8065	0.7077	0.0435*
		r	0.4354	-0.1298	0.2923	0.8244
P-ACC2/ACC1_2	Acc1 [#]	p	0.7806	0.0686	0.3027	0.0398*
		r	0.07302	-0.7778	-0.5088	-0.8957
P-ACC2/ACC1_2	Acc2	p	0.1188	0.0493*	0.4521	0.0055**
		r	0.3928	-0.8129	-0.3842	-0.9722
P-ACC2/ACC1_2	Cpt1a [#]	p	0.8616	0.0169*	0.2533	0.0786
		r	-0.04423	-0.8920	-0.5547	0.7614

Shown are correlations between targets involved in *de novo* lipogenesis, mitochondrial fatty acid oxidation or the master regulator AMPK α in the liver after 12 weeks of feeding either control (C), HFD (HF), or n-3 long-chain polyunsaturated fatty acid (LCPUFA)-enriched HFD (HF/n-3). The expression data were generated by RT-qPCR (n=8-12) or Western blot (WB) analysis (n=5-6), whereby protein expression data (only capitals or bold type) are presented as ratios for the phosphorylated forms and total protein expression levels. Correlation analyses were performed utilizing the whole data set (total), but also analysing the data from each group separately. For the genes marked with a hash symbol, the data were obtained from Ludwig et al. (Ludwig 2013), testing for normal distribution and outliers. Normalised values were used. Outliers were detected by using Grubb's test and excluded from statistical data analysis. *p < 0.05, **p < 0.01, ***p < 0.001, indicate significant correlation. p, statistical significance; r, Pearson correlation coefficient.

4.3.2.2 Impact of HF^A and HFMS (60 kJ% fat) on hepatic lipid metabolism

In the study by Dahlhoff et al. previous findings suggested that dietary methyl-donors can prevent further hepatic lipid accumulation in DIO mice by activating AMPK α , thereby mediating increased fatty acid utilization. However, for both high-fat groups - with and without dietary MDS - the gene expression of CPT1a was significantly upregulated compared to control and, moreover, Western blot analysis showed a significant increase in P-AMPK α and P-AMPK α /AMPK α ratio with significant higher levels found in HFMS than in HF^A livers. In contrast to the HF mice from the study by Ludwig et al., total AMPK α content remained unaffected upon HF^A (Dahlhoff 2014, Ludwig 2013).

Nonetheless, analysis of DNL, another metabolic process that defines hepatic TAG accumulation and is partly controlled by AMPK, was missing.

4.3.2.2.1 Impact of HF^A and HFMS (60 kJ% fat) on hepatic *de novo* lipogenesis

To characterise hepatic DNL in mice from the study by Dahlhoff et al. for subsequent comparison with the results regarding hepatic DNL obtained from the analysis of mice from the study by Ludwig et al. (cf. 4.3.2.1), the gene expression levels of ACC1 and ACC2 were analysed by RT-qPCR (Figure 22A). In addition, protein expression of total ACC1 (265 kDa) and ACC2 (280 kDa), and their phosphorylated forms P-ACC1 (Ser76) and P-ACC2 (Ser219/Ser221) were determined by Western blot analyses (Figures 22B and C), and the ratios for P-ACC1 and total ACC1 protein, as well as for P-ACC2 and total ACC2 were quantified.

The mRNA levels for ACC1 and ACC2 were significantly lower in CMS, HF^A and HFMS mice compared to control mice (Figure 22A). Interestingly, in mice fed HFMS, significantly reduced protein expression levels were measured for total and phosphorylated ACC1. For P-ACC1, significantly reduced expression levels were also observed in CMS and HF^A animals compared to control, but total ACC1 protein expression showed only a tendency for lower levels. Moreover, the P-ACC1/ACC1 ratios did not change (Figure 22B). For hepatic ACC2 protein expression, in comparison to control mice, significantly lower levels for total ACC2 were only found in HFMS mice, but not in CMS and HF^A mice, which showed only a tendency for lower levels, whereas significantly reduced levels were determined for P-ACC2 upon CMS and HFMS. Noteworthy, P-ACC2/ACC2 ratios were not significantly different between the dietary groups (Figure 22C).

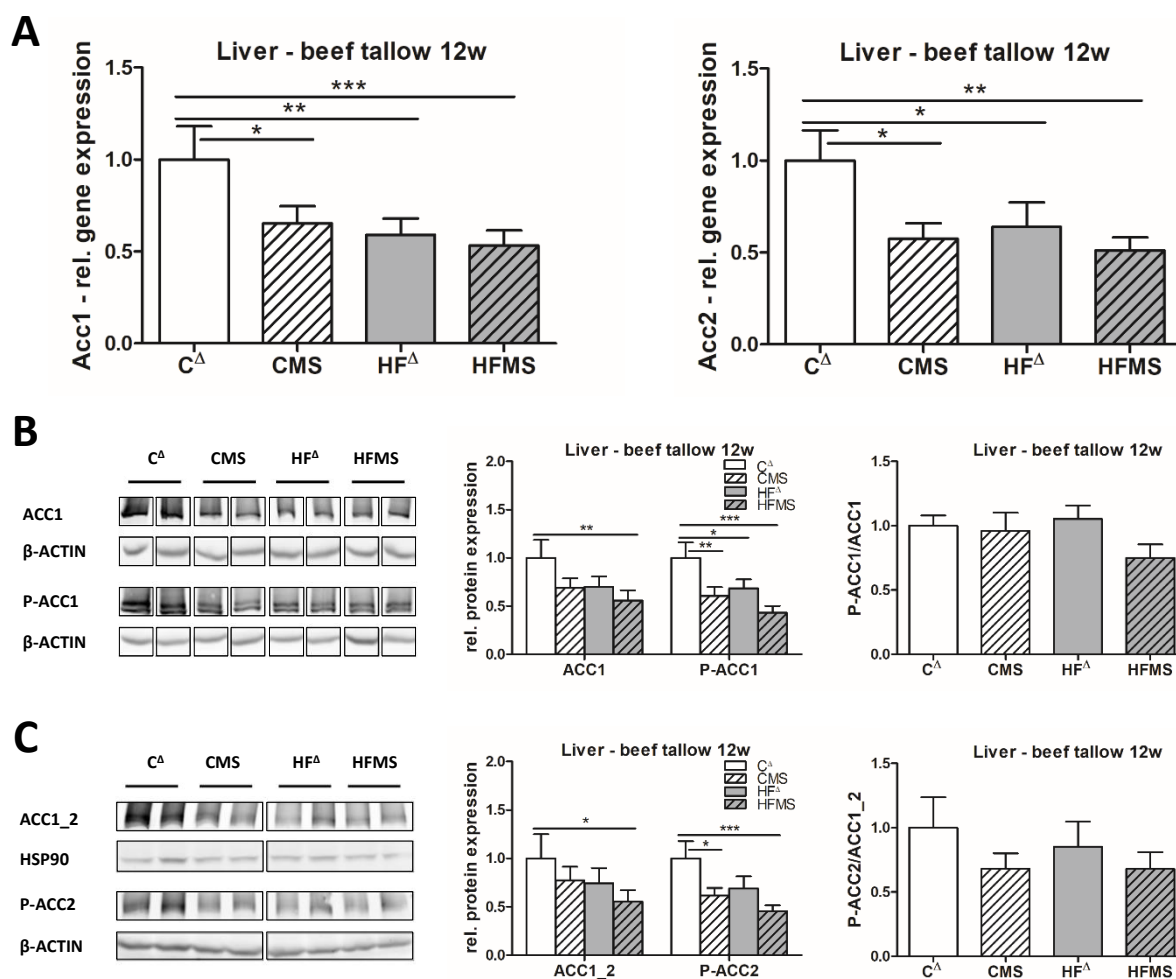


Figure 22. Gene and protein expression of enzymes involved in *de novo* lipogenesis in livers from mice fed soybean oil / beef tallow-based HFDs. All data are means \pm SE and were collected from mice after 12 weeks of feeding either control (C^Δ) or HFD (HF^Δ ; 60 kJ% fat) based on soybean oil and beef tallow, or 4-week dietary methyl-donor supplementation (CMS or HFMS). **(A)** Gene expression data for acetyl-CoA carboxylase 1 and 2 (Acc1 and Acc2) in liver ($n=8-9$). Data were retrieved by RT-qPCR, normalised to Hprt1 and Gapdh, and calculated relative to controls. **(B and C)** Western blot analysis of ACC1 and its representative phosphorylation P-ACC1 (Ser76; **B**) and of ACC1_2 and P-ACC2 (Ser219/Ser221; **C**) in liver ($n=7-9$). Separate gels were run for quantification of total ACC1 and ACC1_2, or P-ACC1 (Ser76) and P-ACC2 (Ser219/Ser221), respectively. Shown are their protein expression levels relative to controls and the ratios for the phosphorylated forms and total protein expression levels (normalised values were used). β -ACTIN or HSP90 was used for protein normalisation. Statistical analysis was performed using one-way ANOVA and Tukey post-test. In case of no normal distribution, data were tested by Kruskal-Wallis and Dunn's post-test. In addition, outliers were detected by using Grubb's test and excluded from statistical data analysis. * $p < 0.05$, ** $p < 0.01$, *** $p < 0.001$, significant differences compared with control or between groups as indicated.

4.3.2.2.2 Comparison of data on hepatic lipid metabolism generated by analysing the material of feeding studies that used differential HFDs

Finally the data on the regulation of hepatic metabolism that were generated by analysing the material of two different feeding trials, the study by Ludwig et al. (Ludwig 2013) and the study by Dahlhoff et al. (Dahlhoff 2014), were summarised in Table 13. The feeding trials not only differed in the aim of the study, the analysis of the impact of different kinds of substitution / supplementation (n-3 LCPUFA vs. methyl-donors) on DIO, moreover, the HFDs that were used in the studies also differed in fat quantity (48 kJ% vs. 60 kJ% fat) and fat quality (palm oil vs. beef tallow).

Table 13. Data on the regulation of hepatic metabolism by HFDs that differ in fat quantity, fat quality and substitution / supplementation

A. Partial substitution of palm oil with n-3 LCPUFA B. Methyl-donor supplementation

Function	Gene / Protein (WB)	Regulation			Function	Gene / Protein (WB)	Regulation			
		HF C	HF/n-3 C	HF/n-3 HF			CMS C ^Δ	HF ^Δ C ^Δ	HFMS C ^Δ	HFMS HF ^Δ
FA oxidation	Cpt1a*	↑	—	—	FA oxidation	Cpt1a [#]	—	↑	↑	—
DNL	Acc1*	—	↓	↓	DNL	Acc1	↓	↓	↓	—
	Acc2	—	↓	↓		Acc2	↓	↓	↓	—
	ACC1_2	↓	↓	↓		ACC1	—	—	↓	—
Regulation	P-ACC1	—	↓	—	Regulation	P-ACC1	↓	↓	↓	—
	P-ACC2	—	↓	↓		P-ACC2	—	—	↓	—
	P-ACC1/ACC1_2	—	—	—		P-ACC1/ACC1	—	—	—	—
	P-ACC2/ACC1_2	—	—	—		P-ACC2/ACC1_2	—	—	—	—
	AMPKα	↓	—	—		AMPKα[#]	—	—	—	—
	P-AMPKα	—	—	—		P-AMPKα[#]	↑	↑	↑	↑
	P-AMPKα/ AMPKα	↑	—	—		P-AMPKα/ AMPKα[#]	↑	↑	↑	↑

Regulation of gene (1st letter in capital) or protein (only capitals or bold type; Western blot) expressions of enzymes involved in fatty acid oxidation and *de novo* lipogenesis, and the further regulation of these enzymes by (A) HF (48 kJ% fat, palm oil) and partial substitution of palm oil with n-3 LCPUFA (HF/n-3) or (B) HF^Δ (60 kJ% fat, beef tallow) and methyl-donor supplementation (HFMS). Comparisons between HFDs (HF or HF^Δ) and corresponding control diets (C or C^Δ; black), substituted / supplemented HFD and corresponding control diet (red), substituted / supplemented HFD and corresponding HFD (green) or methyl-donor supplemented control diet (CMS) and corresponding control diet (yellow) are shown. Upward- and downward-oriented arrows indicate upregulation or downregulation, respectively, and unregulated processes are represented by a dash symbol. For the genes rated by asterisks, the data were obtained from Ludwig et al. (Ludwig 2013), for those marked

with a hash symbol, the data was obtained from Dahlhoff et al. (Dahlhoff 2014), testing for normal distribution and outliers. DNL, *de novo* lipogenesis; FA, fatty acid; WB, Western blot.

4.3.3 Impact of HF and HF/n-3 (48 kJ% fat) on iBAT

Hitherto, data of the present study indicated that the upregulation of fatty acid oxidation in small intestine and liver, as well as the reduction of hepatic DNL might contribute to the n-3 LCPUFA-mediated fat mass-reducing effect and the improved health status of the HF/n-3 mice compared to HF mice. However, the results so far can not completely explain the increased energy expenditure upon HF/n-3, a finding that is based on previous results that indicated significant lower final body mass, despite higher energy assimilation than in HF animals (Ludwig 2013).

It has been described that the energy consumed can be stored or can be used for physiological needs and physical activity, whereby the majority is used for metabolic processes, or is lost due to the production of heat (Tseng 2010, Lowell 2000). The BAT contributes to the regulation of energy homeostasis by burning calories to produce heat. It was proposed that induction of brown fat thermogenesis reduced the increase in obesity expected from the level of energy intake (Rothwell 1979). In comparison to cold-induced thermogenesis, specific food compounds, such as PUFA, trigger DIT. They induce thermogenesis, inter alia, impinging on UCP1 expression / activity (Sadurskis 1995, Oudart 1997). It must be kept in mind that DIT, in absolute terms, not only includes the heat production in iBAT (facultative DIT), but also the energy cost due to absorption, digestion and storage of nutrients (obligatory DIT; Oudart 1997).

Based on previous results that showed significantly increased UCP1 mRNA levels in iBAT upon HF/n-3 compared to HF (Ludwig 2013), the potential contribution of DIT to the anti-obesogenic effect of n-3 LCPUFA was further examined in iBAT.

4.3.3.1 iBAT mass, lipid droplets and lipid metabolism

First, iBAT mass and TAG content in total iBAT was further characterised, followed by analysis of gene and protein expressions and processes that are related to thermogenic capacity of iBAT.

At the end of the 12-week feeding, significantly increased iBAT mass was measured for both high-fat groups compared to control (Table 14), whereas TAG content in total iBAT showed only a significant increase for the HF mice, and the TAG content in HF/n-3 mice was only close at the significance level (Table 14). Noteworthy, for HF mice, the protein content pro gram of iBAT mass and the TAG content pro gram of protein was significantly upregulated in iBAT compared to control mice. Comparing iBAT mass with TAG content, a significant correlation could be observed within the control ($r=0.9582$, $p=0.0102$) and HF/n-3 group ($r=0.9193$, $p=0.0272$), but due to the higher scattering no correlation

was found within the HF group ($r=0.7493$, $p=0.1449$). Surprisingly, analysis of iBAT tissue morphology in hematoxylin and eosin-stained paraffin sections by light microscopy indicated increased lipid droplet size in iBAT for both high-fat groups (Figure 23A). These enlarged lipid droplets might be explained by increased storage of TAG in iBAT.

Table 14. iBAT mass, triacylglycerol and protein content

Mass	C	HF	HF/n-3
iBAT (mg) [#]	179.3 ± 21.2	312 ± 15.5 ^a	246.8 ± 18.2 ^{a,b}
Subgroup (n=5)			
TAG (mg) / g iBAT	92.6 ± 9.3	118.1 ± 13.7	118.4 ± 12.7
TAG (mg) in total iBAT	20.7 ± 1.6	40.7 ± 6.9 ^a	32.1 ± 5.6
Protein (mg) / g iBAT	49.2 ± 3.6	37.0 ± 1.3 ^a	45.4 ± 2.0
Protein (mg) in total iBAT	11.2 ± 1.1	12.5 ± 0.7	11.9 ± 1.2
TAG (mg) / protein (mg)	1.9 ± 0.1	3.3 ± 0.5 ^a	2.6 ± 0.2

All data are means ± SE and were collected from mice after 12 weeks of feeding either control (C), HFD (HF), or n-3 long-chain polyunsaturated fatty acid (LCPUFA)-enriched HFD (HF/n-3). Statistical analysis was performed using one-way ANOVA and Tukey post-test. In case of no normal distribution, data were tested by Kruskal-Wallis and Dunn's post-test. In addition, outliers were detected by using Grubb's test and excluded from statistical data analysis. For iBAT mass, marked with a hash symbol, the data were obtained from Ludwig et al. (Ludwig 2013). Index letters a and b indicate a significant difference ($p < 0.05$) compared with C and HF group, respectively. iBAT, interscapular brown adipose tissue; TAG, triacylglycerol.

To further analyse differences in TAG / lipid deposition in iBAT, we assessed whether the lipid storage in iBAT can be explained by changes in expression levels of genes and proteins involved in lipid uptake, DNL, TAG storage or synthesis, glycerol-3-phosphate generation and glucose uptake or glycolysis. First gene expression analyses were performed. mRNA levels of LPL and CD36 were significantly increased upon HF/n-3 compared with control, and LPL levels were also significantly higher upon HF/n-3 than HF, indicating increased lipid uptake in iBAT for the HF/n-3 mice. ANGPTL4, an inhibitor of LPL activity (Lafferty 2013), was found to be significantly upregulated on gene expression level in both high-fat groups compared to control group (Figure 23B). In order to characterise the regulation of LPL, correlation analysis was performed. Negative correlations were found between the mRNA levels for LPL and ANGPTL4 within the HF/n-3 group ($r=-0.8822$, $p=0.0007$) and the HF group ($r=-0.5410$, $p=0.0857$), whereas, only for the HF/n-3 animals, this correlation was significant (Table 15). Interestingly, in MAT, a significant positive correlation could be observed

between the mRNA levels for LPL and ANGPTL4 within the HF/n-3 group ($r=0.7481$, $p=0.0328$). In the context of increased lipid droplets in both high-fat groups, for the mRNA level of the lipid droplet protein perilipin 5 (PLIN5) significantly elevated levels were only measured for the HF/n-3 animals compared to controls. Furthermore, significantly decreased ACC1 and ACC2 mRNA levels, which were substantially stronger in HF/n-3 mice than in HF mice, were detected for both high-fat groups compared to control (Figure 23C). Thus, expression data indicated a downregulation of DNL and an upregulation of lipid deposition in iBAT upon HF/n-3.

Since increased lipid deposition could be explained by an upregulation of TAG synthesis, the expression of genes involved in this process was analysed. The mRNA levels of 1-acylglycerol-3-phosphate O-acyltransferase 9 (AGPAT9) and diglyceride acyltransferase 2 (DGAT2) were significantly higher for HF/n-3 than for control. DGAT2 mRNA expression was even significantly elevated upon HF/n-3 compared to HF, whereas DGAT1 mRNA levels were significantly lower for HF than for control and HF/n-3 (Figure 23D). To examine whether genes involved in glycerol-3-phosphate generation for TAG synthesis were regulated (Festuccia 2003), gene expression levels for GYK, lactate dehydrogenase (LDHB) and phosphoenolpyruvate carboxykinase 1 (PCK1) were analysed. For HF/n-3, significantly elevated GYK and LDHB mRNA levels were detected compared to HF, whereas GYK levels were even significantly higher for HF/n-3 than for control mice. However, PCK1 expression showed no regulation (Figure 23E). Considering the role of glucose uptake and glycolysis in iBAT, GLUT4 mRNA levels were found to be significantly lower in HF/n-3 than in HF and control mice, and GLUT4 levels were also significantly reduced upon HF compared to control. GLUT1 gene expression showed no regulation. Moreover, hexokinase 2 (HK2) mRNA levels significantly decreased upon HF/n-3 compared to control (Figure 23F).

For some of the analysed genes in iBAT, such as LPL, CD36, PLIN, DGAT2, GYK, PCK1 and ACC1_2, it is known that their expression can be regulated by the transcription factors PPAR α or PPAR γ (Rakhshandehroo 2007, Tontonoz 2008). Furthermore, activated AMPK α can switch on catabolic pathways, such as fatty acid oxidation, and switch off ATP-consuming, anabolic pathways, such as DNL (Hardie 2011). Therefore, protein levels for total AMPK α and P-AMPK α (Thr172) were determined by Western blot analysis, and the ratios for P-AMPK α and total AMPK α were quantified. Significantly reduced expression levels of total AMPK α and P-AMPK α were found for both high-fat groups compared to controls, but the ratio was only significantly increased for HF/n-3 mice compared to control and HF mice (Figure 23G). Noteworthy, these findings indicated an increased activation of AMPK α upon HF/n-3, but reduced total content of AMPK α in both high-fat groups in iBAT.

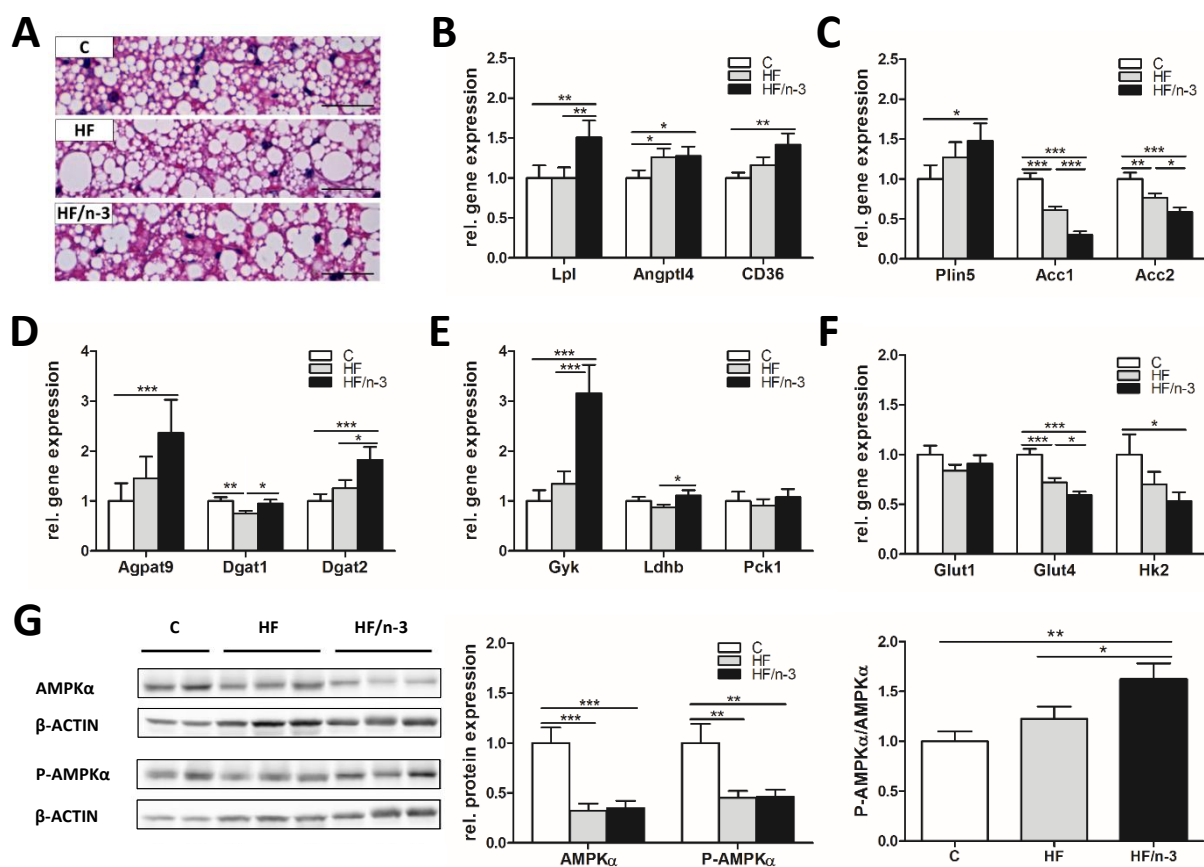


Figure 23. Light microscopy of lipid droplets and expression of genes involved in lipid and glucose metabolism in iBAT. All data are means \pm SE and were collected from mice after 12 weeks of feeding either control (C), HFD (HF), or n-3 long-chain polyunsaturated fatty acid (LCPUFA)-enriched HFD (HF/n-3). **(A)** Representative microscopic images of hematoxylin and eosin-stained paraffin sections of iBAT from C, HF, or HF/n-3 animals after 12 weeks of feeding. Scale bar indicates 50 μ m. **(B)** Gene expression data of lipoprotein lipase (Lpl), angiopoietin-like 4 (Angptl4) and fatty acid translocase (CD36), genes involved in lipid uptake, in iBAT (n=10-12). **(C)** Gene expression data of the lipid droplet protein perilipin 5 (Plin5) and of Acc1 and Acc2, which represent *de novo* lipogenesis, in iBAT (n=10-12). **(D)** Gene expression data of 1-acylglycerol-3-phosphate O-acyltransferase 9 (Agpat9) and diglyceride acyltransferase 1 or 2 (Dgat1 and Dgat2), genes involved in TAG synthesis, in iBAT (n=9-12). **(E)** Gene expression data of glycerol kinase (Gyk), lactate dehydrogenase (Ldhb) and phosphoenolpyruvate carboxykinase 1 (Pck1), genes involved in glyceol-3-phosphate generation, in iBAT (n=9-12). **(F)** Gene expression data of glucose transporter 1 or 4 (Glut1 and Glut4) and of hexokinase 2 (Hk2), genes representing glucose uptake and glycolysis, in iBAT (n=10-12). Gene expression data were retrieved by RT-qPCR, normalised to CypB and Hsp90 α b1, and calculated relative to controls. **(G)** Western blot analyses of AMPK α and P-AMPK α in iBAT (n=5-6). Separate gels were run for quantification of total AMPK α and P-AMPK α (Thr172). Shown are the protein expression levels relative to controls and the ratios for the phosphorylated forms and total protein expression levels (normalised values were used). β -ACTIN was used for protein normalisation. Statistical analysis was performed using one-way ANOVA and Tukey post-test. In case of no normal distribution, data were tested by Kruskal-Wallis and Dunn's post-test. In addition, outliers were detected by using Grubb's test and excluded from statistical data analysis. * $p < 0.05$, ** $p < 0.01$, *** $p < 0.001$, significant differences compared with control or between groups as indicated.

To characterise processes in iBAT, which ensure that fatty acids needed for β -oxidation and/or activation of UCP1 are released from lipid droplets, lipolysis was further explored in iBAT. Hence, gene expression levels of HSL and G0/G1 switch 2 (G0S2), an inhibitor for ATGL, were analysed by RT-qPCR (Figure 24A). Moreover, protein levels of adipose triglyceride lipase (ATGL), HSL (Figure 24B), including the phosphorylated forms of HSL (Figure 24C) P-HSL (Ser660), P-HSL (Ser563) and P-HSL (Ser565), and the lipid droplet component PLIN (Figure 24B), were determined by Western blot analyses. The phosphorylations of HSL on Ser660 or Ser563 activate, whereas its phosphorylation on Ser565 inhibits lipolysis by reducing HSL phosphorylation at Ser563 (Nielsen 2014). In addition, the ratios for the phosphorylated forms and total HSL were quantified (Figure 24D).

The mRNA level of HSL showed no changes, but the mRNA level for G0S2 was significantly reduced in the HF mice compared to controls, whereas the HF/n-3 mice showed only a trend (Figure 24A). Notably, on protein level, significantly reduced expressions of HSL and ATGL were observed for the high-fat mice compared to controls (Figure 24B), whereas PLIN was not regulated. Compared to controls, P-HSL (Ser660) and of P-HSL (Ser565) levels were also significantly downregulated upon both HFDs, but P-HSL (Ser563) was only significantly lower expressed in HF/n-3 iBAT (Figure 24C). Finally, these changes resulted in significant lower P-HSL/HSL ratios for HF/n-3 mice than for control or for HF mice (Figure 24D).

Thus, the data indicated that the supply of FFA for mitochondria seems not to be sustained by increased lipolysis of TAG for the HF/n-3 mice.

To further characterise the potential relationship of genes and proteins involved in the regulation of TAG synthesis and hydrolysis and their interplay, correlation analyses were performed using data from this study (Table 15). PPAR γ is known to be involved in the regulation of TAG uptake and storage (Tontonoz 2008) as also shown in Table 15 by significant correlations between the gene expression levels of PPAR γ 2 and LPL, GYK, DGAT1 or DGAT2. As mentioned before, a significant negative correlation was also observed between the gene expression levels of ANGPTL4 and LPL within the HF/n-3 group (Table 15). Furthermore, significant correlations between the gene expression levels of DGAT2 and HSL (Table 15) suggest a dynamic interplay between TAG synthesis and hydrolysis.

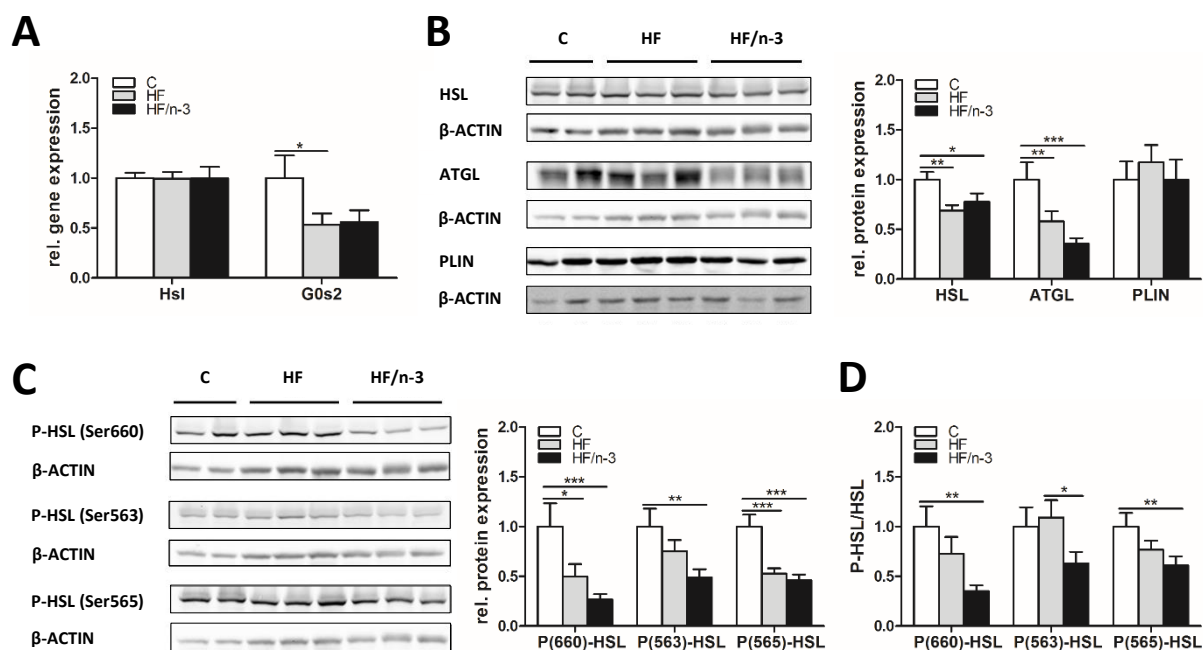


Figure 24. Gene and protein expression of markers involved in lipolysis in iBAT. All data are means \pm SE and were collected from mice after 12 weeks of feeding either control (C), HFD (HF), or n-3 long-chain polyunsaturated fatty acid (LCPUFA)-enriched HFD (HF/n-3). **(A)** Gene expression data of hormone sensitive lipase (Hsl) and G0/G1 switch 2 (G0s2), an inhibitor for ATGL, in iBAT (n=10-12). Data were retrieved by RT-qPCR, normalised to CypB and Hsp90ab1, and calculated relative to controls. **(B and C)** Western blot analyses of HSL, adipose triglyceride lipase (ATGL) and perilipin (PLIN; **B**) and of representative phosphorylations of HSL (**C**) in iBAT (n=5-6). Shown are their protein expression levels relative to controls. **(D)** Data of Western blot analyses, which represent the activation states (n=5-6). Separate gels were run for quantification of total HSL and P-HSL (Ser660), P-HSL (Ser563) and P-HSL (Ser565), respectively, whereby the blot of P-HSL (Ser565) was reincubated with ATGL. Shown are the ratios for the phosphorylated forms of HSL and its total protein expression level (normalised values were used). β -ACTIN was used for protein normalisation. Statistical analysis was performed using one-way ANOVA and Tukey post-test. In case of no normal distribution, data were tested by Kruskal-Wallis and Dunn's post-test. In addition, outliers were detected by using Grubb's test and excluded from statistical data analysis. * $p < 0.05$, ** $p < 0.01$, *** $p < 0.001$, significant differences compared with control or between groups as indicated.

Table 15. Correlation analysis data on genes and proteins involved in the regulation of triacylglycerol synthesis and hydrolysis and their interplay in iBAT

Gene	Gene		Total	Correlation		
				C	HF	HF/n-3
Ppar γ 2	Lpl	p	<0.0001***	<0.0001***	0.0078**	0.0288*
		r	0.7009	0.9216	0.7233	0.6851
Ppar γ 2	Gyk	p	0.0113*	0.0010**	0.3817	0.0364*
		r	0.4355	0.8216	0.2931	0.6638
Ppar γ 2	Dgat1	p	0.0642	0.0734	0.6832	0.0369*
		r	0.3311	0.5346	0.1392	0.6970
Ppar γ 2	Dgat2	p	0.0001***	<0.0001***	0.0935	0.0303*
		r	0.6102	0.9248	0.5056	0.6807
Angptl4	Lpl	p	0.1809	0.2165	0.0857	0.0007***
		r	-0.2426	-0.4051	-0.5410	-0.8822
Dgat2	Hsl	p	0.0174*	0.1847	0.0022**	0.0473*
		r	0.4115	0.4319	0.7902	0.6377

Shown are correlations between targets related to the control of triacylglycerol uptake, synthesis and hydrolysis and targets involved in these processes in the interscapular brown adipose tissue (iBAT) after 12 weeks of feeding either control (C), HFD (HF), or n-3 long-chain polyunsaturated fatty acid (LCPUFA)-enriched HFD (HF/n-3). The expression data were generated by RT-qPCR (n=8-12) and correlation analyses were performed utilizing the whole data set (total), but also analysing the data from each group separately. Normalised values were used. Outliers were detected by using Grubb's test and excluded from statistical data analysis. *p < 0.05, **p < 0.01, ***p < 0.001, indicate significant correlation. p, statistical significance; r, Pearson correlation coefficient.

4.3.3.2 Thermogenic capacity of iBAT

Previously, we reported that the mRNA level for UCP1 was significantly upregulated in iBAT of HF/n-3 mice (Ludwig 2013). Increased UCP1 levels may indicate that DIT in iBAT is involved in the anti-obesogenic effect of n-3 LCPUFA. To further explore this preliminary finding in this thesis, protein expression levels of UCP1 and CS were determined (Figure 25A). In addition, the expression levels of genes involved in energy metabolism, such as the fatty acid binding protein 3 (FABP3), CPT1a, CS, and p47PHOX, as a representative respiratory chain component, were analysed (Figure 25C). Moreover, the gene expression levels of key transcription factors for energy metabolism and mitochondrial biogenesis, PPAR α and peroxisome proliferator-activated receptor γ coactivator 1- α and - β (PGC1a and PGC1b) were measured (Figure 25C).

Significantly elevated UCP1 and CS protein levels were found in iBAT upon HF/n-3 compared to control and HF (Figure 25A), but the UCP1/CS ratio was not significantly different (data not shown). Notably, considering the significant lower protein content found in iBAT for the HF mice (cf. 4.3.3.1, Table 14), the UCP1 and CS protein levels were still significantly elevated upon HF/n-3 compared to

control and HF, however, for the HF mice, CS was even significantly downregulated compared to control mice (0.7-fold, data not shown), indicating a lower mitochondrial density in iBAT for the HF animals. Recruitment of iBAT (iBAT mass and expression of UCP1), which is represented as UCP1 content in total iBAT, was calculated (cf. 3.8), showing a significant increase for the HF/n-3 animals compared to control and HF animals (Figure 25A). Furthermore, considering the difference of iBAT mass and body mass between the dietary groups, the relative UCP1 and CS protein expression was determined as capacity index (cf. 3.8) for the respective proteins (Figure 25B). Previously, we already reported (Ludwig 2013) that the UCP1 mRNA expression capacity index is 1.7 and 1.2-fold higher for HF/n-3 mice compared to control and HF mice, respectively. Using the protein expression data from the present study UCP1 protein expression indices for HF/n-3 mice were found to be 2.9- and 1.4-fold higher than for control and HF mice, respectively. For HF mice, the value was 2-fold higher compared to control. Moreover, for CS, the values upon HF/n-3 were 2- and 1.4-fold higher compared to control and HF mice, respectively, and the values for HF were 1.4-fold higher than for control (Figure 25B).

With regard to FABP3, CPT1a and p47PHOX, mRNA levels were significantly upregulated in both high-fat groups compared to controls, whereby the significantly higher FABP3 levels for HF/n-3 than for HF mice represented the substantial highest change between the high-fat groups (Figure 25C). For key transcription factors in energy metabolism and mitochondrial biogenesis, mRNA levels for PPAR α , PGC1 α and PGC1 β were significantly enhanced upon HF/n-3 compared to controls, and, importantly, PPAR α and PGC1 β mRNA levels were even significantly higher for HF/n-3 than for HF mice (Figure 25C). In addition, the mitochondrial protein CS was also significantly enhanced on gene expression level in HF/n-3 animals compared to control and HF animals (Appendix Table 21).

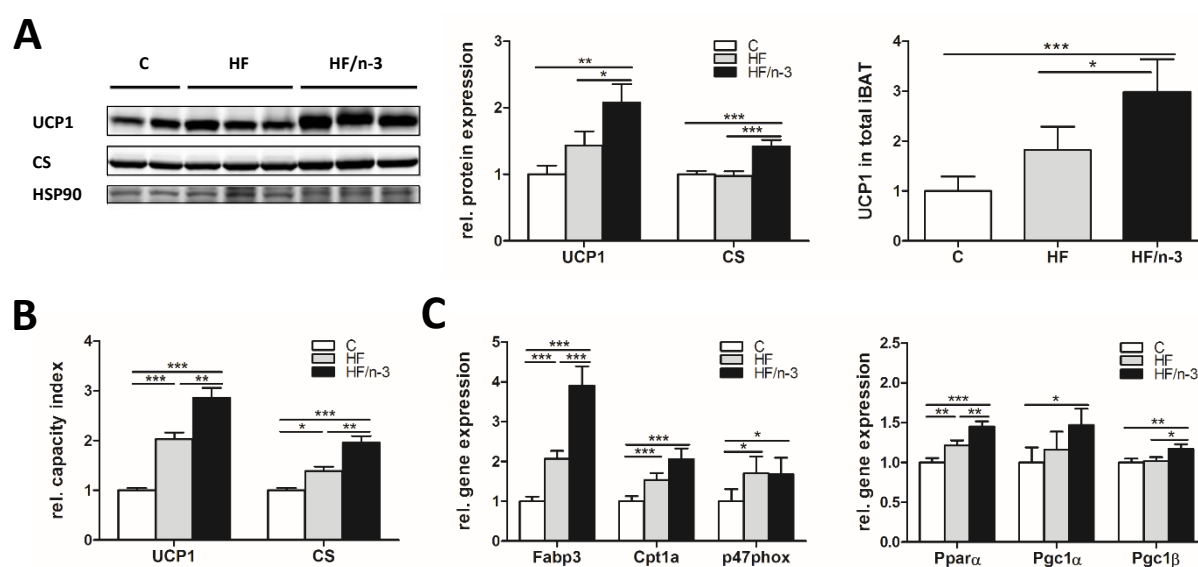


Figure 25. Protein expression of uncoupling protein 1 (UCP1) and citrate synthase (CS) and expression levels of genes involved in energy metabolism and mitochondrial biogenesis in iBAT. All

data are means \pm SE and were collected from mice after 12 weeks of feeding either control (C), HFD (HF), or n-3 long-chain polyunsaturated fatty acid (LCPUFA)-enriched HFD (HF/n-3). **(A)** Western blot analysis of UCP1 and CS in iBAT (n=5-6). Shown are the protein expression levels relative to controls and UCP1 content in total iBAT that represents recruitment of iBAT (normalised values were used). HSP90 was used for protein normalization. **(B)** Relative capacity index of UCP1 and CS (normalised values were used). **(C)** Gene expression data of fatty acid binding protein 3 (Fabp3), carnitine palmitoyltransferase 1a (Cpt1a), the NAD(P)H oxidase subunit p47phox, peroxisome proliferator activated receptor α (Ppar α) and peroxisome proliferator-activated receptor γ coactivator 1- α and - β (Pgc1 α and Pgc1 β), genes involved in energy metabolism and mitochondrial biogenesis, in iBAT (n=10-12). Data were retrieved by RT-qPCR, normalised to CypB and Hsp90 α 1, and calculated relative to controls. Statistical analysis was performed using one-way ANOVA and Tukey post-test. In case of no normal distribution, data were tested by Kruskal-Wallis and Dunn's post-test. In addition, outliers were detected by using Grubb's test and excluded from statistical data analysis. *p < 0.05, **p < 0.01, ***p < 0.001, significant differences compared with control or between groups as indicated.

4.3.3.3 Thermogenic activation and whitening of iBAT

As shown in chapter 4.3.3.2, the capacity for thermogenesis in terms of the expression of mediators of thermogenesis is given, however, thermogenesis has to be induced to contribute to energy expenditure. Thermogenesis can be activated by catecholamines via β -adrenergic receptor signalling, stimulating the expression of thermogenic genes, but also thyroid hormones and fibroblast growth factor 21 (FGF21) can play a role (Villarroya 2013b). In this context, bile acid-mediated activation of the G protein-coupled bile acid receptor (TGR5) increases intracellular cAMP levels, which lead to an increase in 5'-deiodinase (DIO2) and to local generation of triiodothyronine (Watanabe 2006). Moreover, current evidence suggested that FGF21 is an autonomous, direct activator of iBAT, whereby GPR120 activation induces the release of FGF21 (Quesada-López 2016). Thus, gene expression levels of the β 1- or β 3-adrenergic receptor (ADRB1 and ADRB3), TGR5 and DIO2, as well as GRP120 and FGF21 were assessed in iBAT of mice.

A significant upregulation of ADRB3 was found for HF compared to HF/n-3 animals (Figure 26A), whereas significantly reduced TGR5 mRNA levels were detected for HF mice compared to controls (Figure 26B). ADRB1 (Figure 26A) and DIO2 (Figure 26B) mRNA levels were not regulated. Importantly, the gene expression levels of GPR120 and FGF21 showed both a significant increase upon HF/n-3 compared to controls, whereas the expression level of GPR120 was even significantly higher upon HF/n-3 than upon HF (Figure 26C).

Furthermore, it has been shown, that adipose tissue macrophages can produce catecholamines upon their activation by eosinophil-derived IL4, and thereby sustain adaptive thermogenesis. For example, biosynthesis of catecholamines is essentially catalysed by the tyrosine hydroxylase (TH; Nguyen 2011). Worthy of note, TH is also recognised as marker for noradrenergic nerve fiber (Dinh 2015,

Nagatsu 1995). Thus, having already shown that the number of M2 macrophages and eosinophils significantly increased upon HF/n-3 (cf. 4.1.2), the protein expression level of TH was determined. However, Western blot analysis of TH revealed only a slightly increased TH expression upon HF/n-3 compared to control ($p=0.2516$; Figure 26D).

Considering that thermogenic capacity can be remarkably diminished with decreased adipose tissue vascularization, and vascular rarefaction even mediates obesity-associated BAT dysfunction, a process that is associated with the “whitening” of this tissue (Shimizu 2015), blood vessel abundance was assessed indirectly by measuring the gene expression level of endothelial cell markers, such as CDH5 and CLDN5. CDH5 was significantly upregulated upon both HFDs compared to control, but CLDN5 showed no regulation in iBAT (Figure 26E).

However, despite findings regarding enhanced potential for thermogenesis and energy expenditure, due to indications on increased amounts of mitochondria and UCP1 (cf. 4.3.3.2), as well as a potential for increased vessel density (Figure 26E), both HF/n-3 and HF mice showed enlarged lipid droplets compared to control (cf. 4.3.3.1). Furthermore, immunohistochemical analyses of BAT from HF and HF/n-3 mice showed that in the vicinity of these morphological changed brown adipocytes macrophages (F4/80 staining) were present (Figure 26F). Since these adipocytes with enlarged lipid droplet size within the iBAT tissue of HF and HF/n-3 mice resembled white adipocytes, we hypothesised that this could indicate whitening of iBAT. Thus, the mRNA levels of genes typically expressed in WAT, like the transcription factor transducin-like enhancer of split 3 (TLE3) and leptin (LEP), as well as adiponectin (ADIPOQ) were measured in iBAT. The mRNA expression levels of TLE3 and LEP were significantly increased for the high-fat groups compared to controls, whereby LEP levels were less pronounced for the HF/n-3 than for the HF animals (Figure 26G). Adiponectin was not regulated (Appendix Table 21).

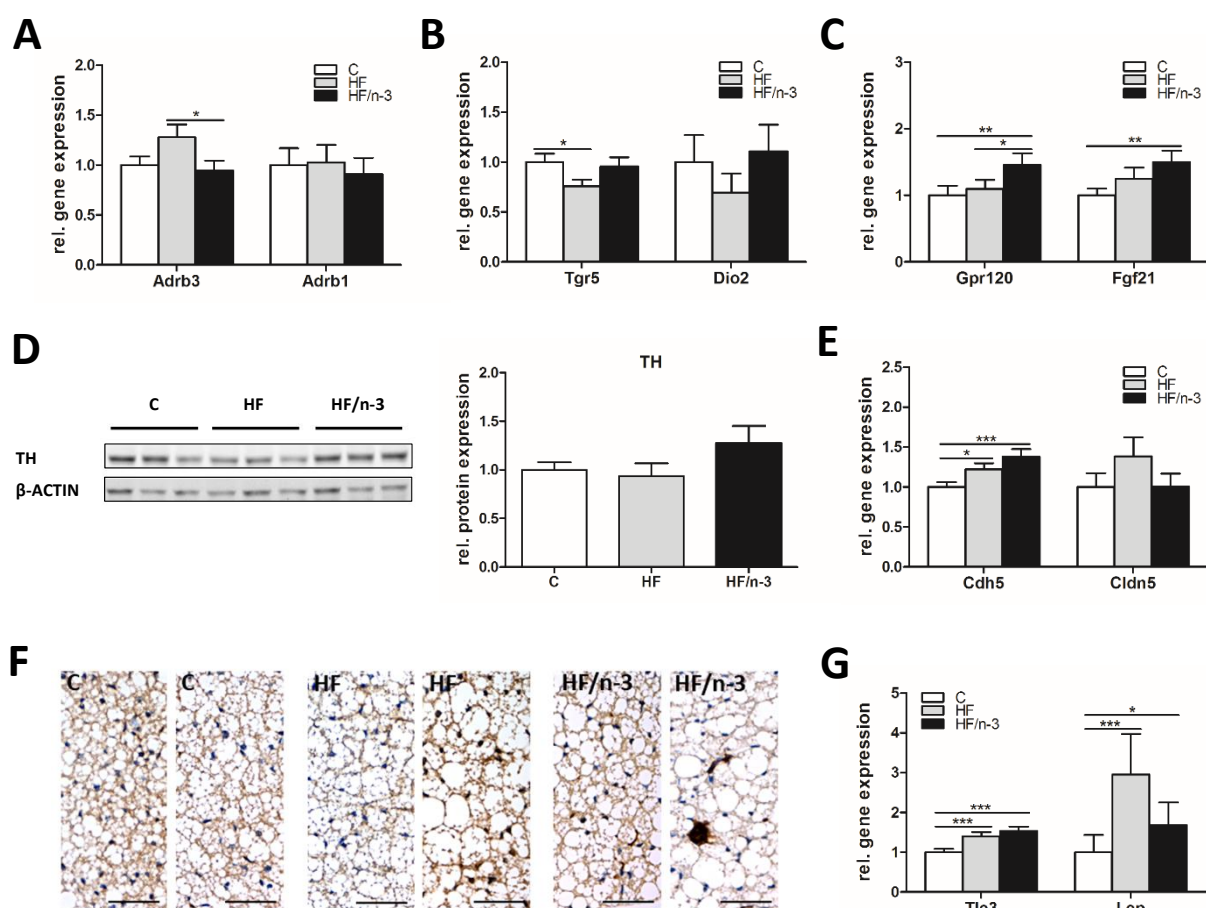


Figure 26. Gene expression of proteins that are associated with thermogenic activation and whitening of iBAT. All data are means \pm SE and were collected from mice after 12 weeks of feeding either control (C), HFD (HF), or n-3 long-chain polyunsaturated fatty acid (LCPUFA)-enriched HFD (HF/n-3). **(A-C)** Gene expression data of proteins associated with thermogenic activation in iBAT (n=9-12). Shown are the gene expression levels of β -adrenergic receptors *Adrb3* and *Adrb1* **(A)**, of the G protein-coupled bile acid receptor (*Tgr5*) and 5'-deiodinase (*Dio2*; **B**), and of the G protein-coupled receptor (*Gpr120*) and the fibroblast growth factor 21 (*Fgf21*; **C**). **(D)** Western blot analysis of tyrosine hydroxylase (TH), a catecholamine-synthesising enzyme of macrophages in iBAT (n=5-6). Shown are the protein expression levels relative to control. β -ACTIN expression was used for protein normalisation. **(E)** Gene expression data of the endothelial cell markers cadherin 5 (*Cdh5*) and claudin 5 (*Cldn5*) in iBAT (n=9-12). **(F)** Representative microscopic images of paraffin sections from iBAT stained with primary antibody specific for F4/80. Images show regions with normal average lipid droplet size (left image per diet) and with enlarged lipid droplet size (right image per diet). Scale bar indicates 50 μ m. **(G)** Gene expression data of transducin-like enhancer of split 3 (*Tle3*) and leptin (*Lep*) in iBAT (n=9-12). Gene expression data were retrieved by RT-qPCR, normalised to *CypB* and *Hsp90ab1*, and calculated relative to controls. Statistical analysis was performed using one-way ANOVA and Tukey post-test. In case of no normal distribution, data were tested by Kruskal-Wallis and Dunn's post-test. In addition, outliers were detected by using Grubb's test and excluded from statistical data analysis. * $p < 0.05$, ** $p < 0.01$, *** $p < 0.001$, significant differences compared with control or between groups as indicated

To further characterise the control of UCP1 expression and a possible interplay in the aforementioned network of transcription factors, hormones and receptors to stimulate the expression of thermogenic genes, correlation analyses were performed.

Differential correlations were observed for the groups. Significant or nearly significant correlations were found between the gene expression levels of PPAR α , GPR120 or FGF21 and UCP1 upon HF/n-3. Within the HF group, the mRNA level of FGF21 significantly correlated with the mRNA level of UCP1 and for the control group, a significant correlations was observed between PPAR γ 2 and UCP1 (Table 16). Moreover, based on data from correlation analysis, an interplay between GPR120 and FGF21 was supported by analysing the whole data set, however, within the individual groups a nearly significant correlation was only found for the HF mice.

Notably, combining the findings obtained from correlation analyses one could speculate about a relationship between different signalling pathways. An example is the significant correlation between the mRNA levels of SIGLEC5 and UCP1 upon HF/n-3 (cf. 4.1.2, Table 6), which supports a connection between alternatively activated macrophages, eosinophils and the expression of thermogenic genes in iBAT, and the correlation data obtained from the gene expression levels of GPR120 and EMR1, CLEC10a or SIGLEC5 (Table 16), which also showed significant correlations upon HF/n-3.

Table 16. Correlation analysis of signalling pathway molecules and UCP1 expression or immune cell marker proteins in iBAT

Gene	Gene		Correlation			
			Total	C	HF	HF/n-3
Ppara	Ucp1 [#]	p	0.0006***	0.6483	0.9713	0.0795
		r	0.5653	-0.1553	0.01167	0.5789
Pparγ2	Ucp1 [#]	p	0.0449*	0.0056**	0.7307	0.7516
		r	0.3461	0.7432	0.1113	-0.1150
Gpr120	Ucp1 [#]	p	0.0013**	0.2812	0.1563	0.0203*
		r	0.5424	-0.3782	0.4362	0.7144
Fgf21	Ucp1 [#]	p	<0.0001***	0.4879	0.0243*	0.0185*
		r	0.6331	0.2221	0.6422	0.7214
Gpr120	Fgf21	p	0.0002***	0.3687	0.0567	0.1656
		r	0.6043	0.3192	0.5630	0.4747
Gpr120	Emr1	p	0.1441	0.0181*	0.5595	0.0443*
		r	0.2686	-0.7231	-0.1980	0.6444
Gpr120	Clec10a	p	0.6638	0.5362	0.1437	0.0040**
		r	0.07990	-0.2227	-0.4484	0.8155
Gpr120	Siglec5	p	0.0070**	0.6072	0.3718	0.0404*
		r	0.4674	0.1859	-0.2835	0.6537

Shown are correlations between targets related to the regulation of UCP1 expression or inflammation and UCP1 or marker of immune cells, as well as correlations that support a possible interplay between these processes in the interscapular brown adipose tissue (iBAT) after 12 weeks of feeding either control (C), HFD (HF), or n-3 long-chain polyunsaturated fatty acid (LCPUFA)-enriched HFD (HF/n-3). The expression data were generated by RT-qPCR analysis (n=8-12). Correlation analyses were performed utilizing the whole data set (total), but also analysing the data from each group separately. For the genes marked with a hash symbol, the data were obtained from Ludwig et al. (Ludwig 2013), testing for normal distribution and outliers. Normalised values were used. Outliers were detected by using Grubb's test and excluded from statistical data analysis. *p < 0.05, **p < 0.01, ***p < 0.001, indicate significant correlation. p, statistical significance; r, Pearson correlation coefficient.

Moreover, to further characterise the metabolic regulation in brown adipocytes with enlarged lipid droplets, correlation analyses were performed between the mRNA level of TLE3 and those of enzymes involved in energy metabolism, since TLE3 as a co-activator of PPARγ-dependent gene expression (Villanueva 2011) is known to alter BAT phenotype and function (Villanueva 2013).

Notably, for the HF group, the gene expression levels of CPT1a, DGAT2, LPL, AGPAT9, GYK and HK2 significantly or nearly significantly negatively correlated with the gene expression level of TLE3, however, no significant correlations were found within the other groups (Table 17). In addition, a significant negative correlation was observed between the mRNA levels of TLE3 and UCP1 or TGR5 and even between TLE3 and the protein level of UCP1 within the HF group (Table 17). For the HF/n-3

group, a nearly significant inverse correlation was only detected between the mRNA levels of ADRB1 and TLE3 (Table 17).

Table 17. Correlation analysis data on the metabolic regulation in adipocytes with enlarged lipid droplets in iBAT

Gene	Gene / Protein (WB)	Correlation				
		Total	C	HF	HF/n-3	
Tle3	Cpt1a	p	0.0039**	0.8384	0.0419*	0.4434
		r	0.4820	-0.06607	-0.5935	-0.2742
Tle3	Dgat2	p	0.0378*	0.8911	0.0410*	0.5851
		r	-0.3577	0.04438	-0.5956	-0.1972
Tle3	Lpl	p	0.2918	0.9748	0.0386*	0.1009
		r	0.1862	-0.01024	-0.6015	-0.5482
Tle3	Agpat9	p	0.0110*	0.1643	0.0275*	0.6399
		r	0.4306	0.4287	-0.6320	-0.1694
Tle3	Gyk	p	0.0087**	0.8509	0.0752	0.2536
		r	0.4496	0.06088	-0.5567	-0.3988
Tle3	Hk2	p	0.0090**	0.1758	0.0031**	0.4904
		r	-0.4413	0.4184	-0.7740	-0.2476
Tle3	Tgr5	p	0.0221*	0.3486	0.0155*	0.8333
		r	-0.3914	-0.2969	-0.6774	0.07665
Tle3	Ucp1 [#]	p	0.0487*	0.5308	0.0474*	0.3041
		r	0.3406	-0.2011	-0.5814	-0.3619
Tle3	UCP1	p	0.0160*	0.9007	0.0252*	0.0686
		r	0.5738	-0.07810	-0.8674	0.7778
Tle3	Adrb1	p	0.3338	0.3614	0.1000	0.0617
		r	-0.1709	0.2895	-0.4972	-0.6089

Shown are correlations between Tle3, a transcriptional co-repressor that is associated with whitening, and targets involved in these energy metabolism in the interscapular brown adipose tissue (iBAT) after 12 weeks of feeding either control (C), HFD (HF), or n-3 long-chain polyunsaturated fatty acid (LCPUFA)-enriched HFD (HF/n-3). The expression data were generated by RT-qPCR (n=8-12) or Western blot (WB) analysis (n=5-6) and correlation analyses were performed utilizing the whole data set (total), but also analysing the data from each group separately. Gene expression data (1st letter in capital) can be distinguished from protein expression data (only capitals or bold type) because of different ways of writing. For the genes marked with a hash symbol, the data were obtained from Ludwig et al. (Ludwig 2013), testing for normal distribution and outliers. Normalised values were used. Outliers were detected by using Grubb's test and excluded from statistical data analysis. *p < 0.05, **p < 0.01, ***p < 0.001, indicate significant correlation. p, statistical significance; r, Pearson correlation coefficient.

4.3.4 Summary of results obtained from the analysis of lipid metabolism

Findings obtained so far on the expression and regulation of enzymes involved in energy metabolism in USI, LSI, liver and iBAT by RT-qPCR and Western blot analyses are summarized in Table 18 in order to give an overview of the changes induced by HFDs that differ in their fat quality. To simplify the overview, significant gene and protein expression changes upon both HFDs compared to control and those upon HF/n-3 compared to HF are represented by upward- and downward-oriented arrows indicating upregulation or downregulation, respectively, and unregulated processes are represented by a dash symbol.

Moreover, correlation analysis data on energy metabolism in iBAT are shown in Table 19. The findings from correlation analysis of mRNA levels in iBAT indicated that FGF21 is the regulator of key proteins involved in energy metabolism, namely ADRB1, CD36 and DGAT1 (Table 19A). Significant correlations were observed between the mRNA levels of FGF21 and ADRB1, CD36 or DGAT1 within all groups. In addition, especially within the HF/n-3 group, significant or nearly significant correlations were observed between the mRNA levels of the identified key proteins ADRB1, CD36 and DGAT1 (Table 19A) and between the mRNA levels of ADRB1, CD36 or DGAT1 and those of almost all other enzymes involved in energy metabolism that were analysed in iBAT (Table 19B).

Table 18. Summary of expression data of genes and proteins involved in energy metabolism and its regulation in small intestine, liver and iBAT

USI / Function	Gene / Protein	Regulation			iBAT / Function	Gene / Protein (WB)	Regulation		
		HF C	HF/n-3 C	HF/n-3 HF			HF C	HF/n-3 C	HF/n-3 HF
FA oxidation	Cpt1a	↑	↑	↑	FA uptake	Lpl	—	↑	↑
	Acox1	↑	↑	↑		CD36	—	↑	—
	Cyp4a10	↑	↑	↑	Regulation	Angptl4	↑	↑	—
					FA transport	Fabp3	↑	↑	↑
					FA oxidation	Cpt1a	↑	↑	—
						p47phox	↑	↑	—
					Thermogenesis	Ucp1*	—	↑	↑
						UCP1	—	↑	↑
						UCP1/CS	—	—	—
					Mitochondria	Cs	—	↑	↑
						CS	—	↑	↑
					Regulation	Ppara	↑	↑	↑
						Pgc1α	—	↑	—
						Pgc1β	—	↑	↑
					DNL	Acc1	↓	↓	↓
						Acc2	↓	↓	↓
					Regulation	AMPKα	↓	↓	—
						P-AMPKα	↓	↓	—
						P-AMPKα/AMPKα	—	↑	↑
					Lipid droplet	Plin5	—	↑	—
						PLIN5	—	—	—
					G-3-P generation	Gyk	—	↑	↑
						Ldhb	—	—	↑
						Pck1	—	—	—
					TAG synthesis	Agpat9	—	↑	—
						Dgat1	↓	—	↑
						Dgat2	—	↑	↑
					Lipolysis	Hsl	—	—	—
						HSL	↓	↓	—
						ATGL	↓	↓	—
					Regulation	G0s2	↓	—	—
						P(660)-HSL	↓	↓	—
						P(563)-HSL	—	↓	—
						P(565)-HSL	↓	↓	—
						P(660)-HSL/HSL	—	↓	—
						P(563)-HSL/HSL	—	—	↓
						P(565)-HSL/HSL	—	↓	—
					Glucose transport	Glut1	—	—	—
						Glut4	↓	↓	↓
					Glycolysis	Hk2	—	↓	—

LSI / Function	Gene / Protein	Regulation		
		HF C	HF/n-3 C	HF/n-3 HF
FA oxidation	Cpt1a	—	↑	—
	Acox1	—	↑	—
	Cyp4a10	↑	↑	↑

Liver / Function	Gene / Protein (WB)	Regulation		
		HF C	HF/n-3 C	HF/n-3 HF
FA oxidation	Cpt1a*	↑	—	—
	Acox1*	↑	↑	↑
	Lpbe	—	↑	↑
	Cyp4a10	↑	↑	↑
DNL	Scd1*	—	↓	↓
	Acc1*	—	↓	↓
	Acc2	—	↓	↓
	ACC1_2	↓	↓	↓
Regulation	P-ACC1	—	↓	—
	P-ACC2	—	↓	↓
	P-ACC1/ACC	—	—	—
	P-ACC2/ACC	—	—	—
	AMPKα	↓	—	—
	P-AMPKα	—	—	—
	P-AMPKα/AMPKα	↑	—	—
Lipolysis	Hsl	—	↑	—

(Table 18 continued) Regulation of gene (1st letter in capital) or protein (only capitals or bold type; Western blot) expressions of enzymes involved in energy metabolism, and the further regulation of some enzymes, by HFD (HF) and n-3 long-chain polyunsaturated fatty acid (LCPUFA)-enriched HFD (HF/n-3) in upper and lower small intestine (USI and LSI), liver and interscapular brown adipose tissue (iBAT). Comparisons between HF and control diet (black), HF/n-3 and control diet (red) or HF/n-3 and HF (green) are shown. Upward- and downward-oriented arrows indicate upregulation or downregulation, respectively, and unregulated processes are represented by a dash symbol. For the genes rated by asterisks, the data were obtained from Ludwig et al. (Ludwig 2013), testing for normal distribution and outliers. DNL, *de novo* lipogenesis; FA, fatty acid; G-3-P, glycerol-3-phosphate; TAG, triacylglycerol; WB, Western blot.

Table 19. Correlation analysis data on genes involved in energy metabolism in iBAT

A. FGF21 as regulator of possible key proteins involved in energy metabolism in iBAT

Gene	Gene		Total	Correlation		
				C	HF	HF/n-3
Fgf21	Adrb1	p	0.0004***	0.0198*	0.0055**	0.0016**
		r	0.5759	0.6590	0.7443	0.8557
Fgf21	CD36	p	<0.0001***	0.0224*	0.0111*	0.0320*
		r	0.7477	0.6490	0.7011	0.6756
Fgf21	Dgat1	p	0.0071**	0.0015*	0.0036**	0.0462*
		r	0.4664	0.8066	0.7927	0.6746
Adrb1	Dgat1	p	0.0010***	0.0055**	0.0739	0.0099**
		r	0.5552	0.7443	0.5589	0.7982
Adrb1	CD36	p	0.0044**	0.0795	0.0502	0.0112*
		r	0.4762	0.5252	0.5756	0.7573
Dgat1	CD36	p	0.0157*	0.0031**	0.0869	0.0214*
		r	0.4235	0.7745	0.5393	0.7443

B. Data set on correlations between mRNA levels of aforementioned key proteins and other proteins involved in energy metabolism

Table is shown on the next page

(A and B) Shown are correlations between targets involved in energy metabolism in the interscapular brown adipose tissue (iBAT) after 12 weeks of feeding either control (C), HFD (HF), or n-3 long-chain polyunsaturated fatty acid (LCPUFA)-enriched HFD (HF/n-3). The expression data were generated by RT-qPCR (n=8-12) and correlation analyses were performed utilizing the whole data set (total), but also analysing the data from each group separately. For the genes marked with a hash symbol, the data were obtained from Ludwig et al. (Ludwig 2013), testing for normal distribution and outliers. Normalised values were used. Outliers were detected by using Grubb's test and excluded from statistical data analysis. *p < 0.05, **p < 0.01, ***p < 0.001, indicate significant correlation. p, statistical significance; r, Pearson correlation coefficient.

Table 19 continued

B. Data set on correlations between mRNA levels of aforementioned key proteins and other proteins involved in energy metabolism

Gene	Gene		Correlation				Gene			Correlation				Gene			Correlation			
			Total	C	HF	HF/n-3				Total	C	HF	HF/n-3				Total	C	HF	HF/n-3
Ucp1 [#]	Adrb1	p	0.1306	0.0794	0.0632	0.0558	CD36	p	0.0002***	0.2802	0.1128	0.1929	Dgat1	p	0.1000	0.1575	0.0657	0.0951		
		r	0.2645	0.5253	0.5512	0.6201		r	0.6002	0.3396	0.4817	0.4491		r	0.2960	0.4350	0.5725	0.5890		
Cs	Adrb1	p	0.0158*	0.0283*	0.0200*	0.0237*	CD36	p	<0.0001***	0.7453	0.2648	0.0174*	Dgat1	p	0.0161*	0.0347*	0.0487*	0.0012**		
		r	0.4169	0.6562	0.6579	0.7018		r	0.6659	0.1110	0.3500	0.7264		r	0.4289	0.6379	0.6049	0.8920		
Lpl	Adrb1	p	0.0366*	0.0393*	0.1376	0.0419*	CD36	p	<0.0001***	0.1624	<0.0001***	0.0459*	Dgat1	p	0.0110*	0.0874	0.2766	0.0193*		
		r	0.3599	0.5998	0.4546	0.6499		r	0.7063	0.4305	0.9289	0.6409		r	0.4435	0.5140	0.3601	0.7527		
Angptl4	Adrb1	p	0.0008***	0.1161	0.0113*	0.0294*	CD36	p	0.5869	0.1301	0.0795	0.1046	Dgat1	p	0.0023**	0.4867	0.1034	0.0094**		
		r	-0.5616	-0.5014	-0.7265	-0.6833		r	-0.09977	-0.4855	-0.5502	-0.5432		r	-0.5348	-0.2350	-0.5448	-0.8015		
Agpat9	Adrb1	p	0.0083**	0.0011**	0.0135*	0.1225	CD36	p	<0.0001***	0.1003	0.0327*	0.0174*	Dgat1	p	0.0592	0.0208*	0.1752	0.0042**		
		r	0.4451	0.8193	0.6872	0.5211		r	0.6894	0.4969	0.6166	0.7263		r	0.3371	0.6548	0.4404	0.8439		
Dgat2	Adrb1	p	0.0165*	0.0657	0.0014**	0.0627	CD36	p	<0.0001***	0.5016	0.0313*	0.0197*	Dgat1	p	0.0642	0.2048	0.0788	0.0013**		
		r	0.4082	0.5470	0.8107	0.6071		r	0.6783	0.2153	0.6206	0.7166		r	0.3310	0.3942	0.5512	0.8898		
Plin5	Adrb1	p	0.0010**	0.0319*	0.0008***	0.0183*	CD36	p	0.0023**	0.9641	0.0807	0.0343*	Dgat1	p	0.3327	0.4413	0.1478	0.0483*		
		r	0.5373	0.6189	0.8316	0.7225		r	0.5047	0.0146	0.5235	0.6692		r	0.1769	0.2458	0.4668	0.6701		
Gyk	Adrb1	p	0.6042	0.0849	0.9165	0.0374*	CD36	p	<0.0001***	0.1517	0.0401*	0.0260*	Dgat1	p	0.2282	0.0985	0.9618	0.0009***		
		r	0.09364	0.5175	0.03591	0.6610		r	0.6760	0.4406	0.6242	0.6938		r	0.2229	0.4992	0.01745	0.9013		
Ldhd	Adrb1	p	0.0020**	0.0319*	0.1382	0.0159*	CD36	p	<0.0001***	0.0030**	0.3010	0.0018**	Dgat1	p	<0.0001***	<0.0001***	0.0011**	0.0001***		
		r	0.5329	0.6190	0.5032	0.7670		r	0.6760	0.7753	0.3641	0.8782		r	0.8520	0.8930	0.8695	0.9622		
Pck1	Adrb1	p	<0.0001***	0.0014**	0.0045**	0.0084**	CD36	p	0.0068**	0.3173	0.1112	0.0108*	Dgat1	p	0.0015**	0.0312*	0.1722	0.0449*		
		r	0.6532	0.8108	0.7557	0.7753		r	0.4556	0.3158	0.4836	0.7595		r	0.5390	0.6210	0.4432	0.6777		
Hsl	Adrb1	p	<0.0001***	0.0391*	0.0062**	0.0427*	CD36	p	0.0343*	0.3665	0.2520	0.0534	Dgat1	p	0.0109*	0.1347	0.0424*	0.1592		
		r	0.6409	0.6267	0.7370	0.6481		r	0.3695	0.3021	0.3588	0.6248		r	0.4509	0.4805	0.6188	0.5115		
Fabp3	Adrb1	p	0.3100	0.0112*	0.0046**	0.0557	CD36	p	<0.0001***	0.0757	0.0124*	0.0482*	Dgat1	p	0.6888	0.0173*	0.0710	0.0173*		
		r	0.1794	0.7005	0.7541	0.6203		r	0.6589	0.5309	0.6934	0.6703		r	0.07363	0.6691	0.5636	0.7607		
Cpt1a	Adrb1	p	0.0257*	0.0136*	0.0034**	0.0158*	CD36	p	<0.0001***	0.7314	0.0196*	0.0234*	Dgat1	p	0.6233	0.4382	0.1913	0.0022**		
		r	0.3822	0.6870	0.7696	0.7332		r	0.6469	0.1109	0.6596	0.7027		r	0.09024	0.2474	0.4261	0.8718		
Acc2	Adrb1	p	0.0189*	0.2081	0.2048	0.0592	CD36	p	0.1931	0.9954	0.9558	0.0572	Dgat1	p	0.2156	0.7477	0.6812	0.2047		
		r	0.4004	0.3916	0.3942	0.6136		r	-0.2288	-0.001879	0.01798	0.6174		r	0.2251	0.1040	-0.1401	0.4673		
Glut1	Adrb1	p	0.0084**	0.0142*	0.5073	0.0190*	CD36	p	0.0229*	0.0140*	0.4438	0.0043**	Dgat1	p	<0.0001***	0.0019**	0.9984	0.0406*		
		r	0.4446	0.6840	-0.2125	0.7196		r	0.3892	0.6849	0.2445	0.8120		r	0.6446	0.7973	0.0006898	0.6876		
Glut4	Adrb1	p	0.1283	0.8344	0.0668	0.3007	CD36	p	0.1635	0.5877	0.3209	0.0481*	Dgat1	p	0.0542	0.8567	0.0109*	0.3074		
		r	0.2702	0.07155	0.5451	0.3643		r	-0.2483	0.1842	0.3136	0.6359		r	0.3492	0.06184	0.7290	0.3841		
Hk2	Adrb1	p	0.0150*	0.5695	0.0194*	0.0308*	CD36	p	0.2496	0.0245*	0.0004***	0.0018**	Dgat1	p	0.0064**	0.2590	0.0351*	0.0018**		
		r	0.4138	0.1828	0.6606	0.6792		r	0.2030	0.6415	0.8559	0.8498		r	0.4722	0.3540	0.6368	0.8788		

4.4 Association between food / fat intake or fat quality and obesity or inflammatory status

Of interest with regard to nutrient gene interactions was whether weekly fat intake and moreover fat quality of the diets, since HFDs differ in their n-6/n-3 PUFA and SFA/PUFA ratios, are related to significant changes in weight-associated parameter and/or expression levels of parameter related to lipid metabolism, metabolic control and inflammation. Thus, fat intake (g/wk) was calculated for each animal (cf. 3.3), whereby the assimilation efficiency (cf. 3.3) was included in the calculation, and correlation analyses were performed. Significant correlations are listed in Table 20. Moreover, additional correlation analyses (body weight adjusted fat intake or body weight) – results are given in brackets in Table 20 – were carried out to interpret the initial results and to exclude the influence of the individual body weight of the mice (Kless 2017). For HF but also HF/n-3 animals, the body weight adjusted fat intake was calculated (cf. 3.3), however, for the HF/n-3 group, this calculation represents an explorativ approach, since no significant correlations were found between fat intake and final body weight within this group (Table 20). Nevertheless, body weight adjusted fat intake was also calculated for the HF/n-3 mice, since the results for the HF mice were very informative.

For the HF mice, significant correlations were observed between fat intake and final body weight, but also other weight-associated parameter such as fat mass (Ludwig 2013) and iBAT mass or gene expression levels of inflammation parameter in EAT (TNF α , ITGAX and EMR1) and USI (CD86) significantly correlate with fat intake. However, for most of these parameters (except CD86), a significant correlations was also found between them and final body weight, whereas statistical significance was no longer present using the values for body weight adjusted fat intake for linear regression analysis. However, CD86 nearly significantly correlated with the body weight adjusted fat intake, but not with final body weight (Table 20).

For the HF/n-3 mice, significant correlations were observed between fat intake and lean mass or pAMPK α /AMPK α , but also significant inverse correlations were found between fat intake and gene expression levels of metabolic markers in iBAT (PPAR α , DGAT1 and AGPAT9). Surprisingly, for the explorative approach, most of these parameter significantly correlated with the body weight adjusted fat intake, although the regression coefficient changed its sign from plus to minus or vice versa (Table 20).

Table 20. Correlation analysis data on the identification of associations between food / fat intake or fat quality (n-6/n-3 PUFA and SFA/PUFA ratios) and obesity or inflammatory status in iBAT, EAT and USI

Correlations between fat intake (g/wk) [body weight adjusted fat intake (g/wk), final body weight (g)] and certain parameter	Correlation				
	C	HF		HF/n-3	
weight-associated parameter					
Final body weight (g) [#]	p 0.0684	0.0055**		0.5473	
	r 0.6712	0.8651		0.2772	
Fat mass (g) [#]	p 0.0890	0.0253*	[0.6168, 0.0259*]	0.7631	[0.3648, 0.0054**]
	r 0.6376	0.7703	[-0.2105, 0.7683]	-0.1410	[0.4070, 0.9023]
Lean mass (g) [#]	p 0.2167	0.6658	[0.2800, 0.2473]	0.0046*	[0.0082**, 0.6488]
	r 0.4909	0.1822	[0.4361, 0.4636]	0.9086	[-0.8846, 0.2116]
iBAT mass (g) [#]	p 0.0879	0.0458*	[0.4711, 0.0787]	0.9039	[0.7060, 0.0258*]
	r 0.6393	0.7159	[-0.2995, 0.6538]	0.05669	[0.1759, 0.8141]
rel. gene expression of					
TNFα in EAT	p 0.5657	0.0332*	[0.7703, 0.0192*]	0.1851	[0.1601, 0.9750]
	r 0.2408	0.7468	[-0.1237, 0.7916]	-0.5663	[0.5935, 0.01474]
Itgax in EAT [#]	p 0.6715	0.0197*	[0.9629, 0.0022**]	0.4442	[0.2117, 0.1432]
	r 0.1790	0.7897	[-0.01981, 0.9014]	-0.3481	[0.5391, 0.6131]
Emr1 in EAT	p 0.5676	0.0057**	[0.3986, 0.0178*]	0.4921	[0.2073, 0.0523]
	r 0.2638	0.8640	[-0.3478, 0.7971]	-0.3145	[0.5435, 0.7497]
CD86 in USI	p 0.7183	0.0279*	[0.0536, 0.2164]	0.5108	[0.6749, 0.3420]
	r 0.1683	0.8079	[-0.7472, 0.5346]	-0.3391	[0.2203, -0.4742]
Pparaα in iBAT	p 0.9570	0.6508	[0.3779, 0.9802]	0.0485*	[0.0243*, 0.8238]
	r 0.02295	0.1908	[-0.3622, 0.01056]	-0.7576	[0.8186, 0.1043]
Dgat1 in iBAT	p 0.5363	0.0662	[0.2063, 0.1553]	0.0188*	[0.0161*, 0.6948]
	r -0.2586	0.7233	[-0.5445, 0.5990]	-0.8859	[0.8946, -0.2064]
Agpat9 in iBAT	p 0.8556	0.4791	[0.9095, 0.3693]	0.0422*	[0.0266*, 0.9483]
	r 0.07733	0.2944	[0.04836, 0.3683]	-0.7714	[0.8116, 0.03045]
ratio of rel. protein level (WB)					
pAMPKα/AMPKα in iBAT	P 0.3624	0.5022	[0.8658, 0.3316]	0.0086**	[0.0086**, 0.8202]
	r -0.8423	0.4021	[-0.1056, 0.5549]	0.9914	[-0.9914, 0.1798]

Shown are correlations between fat intake [body weight adjusted fat intake or body weight] and weight-associated parameter or the gene / protein expression levels of targets that are associated with obesity and inflammation in interscapular brown adipose tissue (iBAT), epididymal adipose tissue (EAT), and upper small intestine (USI) after 12 weeks of feeding either control (C), HFD (HF), or n-3 long-chain polyunsaturated fatty acid (LCPUFA)-enriched HFD (HF/n-3). The expression data were generated by RT-qPCR analysis (n=8-12) or Western blot (WB) analysis (n=3-5) and the values of fat

intake (n=7-8) were calculated (cf. 3.3) based on the values of food intake measured by Ludwig et al. (Ludwig 2013). Correlation analyses (fat intake) were performed analysing the data from each group separately, whereby additional correlation analyses (body weight adjusted fat intake and body weight) - results are given in brackets - were required to interpret the initial results. For the parameters marked with a hash symbol, the data were obtained from Ludwig et al. (Ludwig 2013), testing for normal distribution and outliers. Normalised expression values were used. Outliers were detected by using Grubb's test and excluded from statistical data analysis. *p < 0.05, **p < 0.01, ***p < 0.001, indicate significant correlation. p, statistical significance; PUFA, polyunsaturated fatty acids; r, Pearson correlation coefficient; SFA, saturated fatty acids; TAG, triacylglycerol; wk, week.

5 Discussion

Obesity is associated with a chronic low-grade inflammatory state (Hotamisligil 2006), whereby animal studies have postulated that LPS absorbed by the intestine due to HFD-induced disruption of the intestinal barrier function might promote local and systemic inflammation (Cani 2008, Cani 2007). Moreover, a potential crosstalk between the intestine, the adjacent MAT and the liver might affect the HFD-induced inflammatory processes and detrimental metabolic changes, which are generally thought to be induced by SFA and n-6 LCPUFA. n-3 LCPUFA, however, may rather counteract adipose tissue inflammation (Lee 2003, Calder 2013, Todoric 2006) and enhance vascular integrity and compliance (Lorente-Cebrián 2013), since n-6 LCPUFA and n-3 LCPUFA are precursors of signalling molecules with opposing effects, which modulate membrane microdomain composition, receptor signalling and gene expression (Schmitz 2008).

Apart from fat quantity and quality, feeding duration, age and gender, macronutrient composition and genetic background determine the DIO phenotypes observed in mice feeding studies, which are sometimes difficult to compare or even controversial. Due to this variability in HFDs, it was highly desirable for nutritional research to use a well-defined diet composition and study design to achieve better controlled studies and greater comparability between studies.

With this background and with the purpose to analyse the chronic effects of n-3 LCPUFA and/or the balanced or unbalanced dietary n-6/n-3 PUFA ratios on inflammation, vascular integrity and metabolism, in the present thesis a DIO mouse model was examined using male C57BL/6J mice, housed under SPF conditions, which were fed defined soybean / palm oil-based diets for 12 weeks to induce obesity. The HFDs were characterised by high-fat content (48 kJ% fat) and unbalanced or balanced n-6/n-3 PUFA ratios for the isocaloric HF and HF/n-3, respectively, whereby the HF/n-3 diet was enriched with n-3 LCPUFA. The control diet had a lower fat content (Ludwig 2013). Based on preliminary data from gene expression arrays and RT-qPCR experiments of this study, at the beginning of the present thesis, it was hypothesised that n-6 and n-3 LCPUFA have differential effects on adipose tissue inflammation, n-3 LCPUFA alleviate HF-induced endothelial cell activation in the small intestine of the mice and increase energy expenditure by inducing DIT.

Further exploring these postulated effects, the main findings of this thesis were as follows: (1) Differential effects were observed for VATs upon HFDs, whereby for HF the highest impact was observed analysing EAT and a few inflammatory markers were found to be significantly increased in USI upon HF. Moreover, for the HF/n-3 mice, both immunosuppressive and -enhancing effects were observed in adipose tissues, however, the increased number of rather anti-inflammatory ATMs upon HF/n-3 was associated with healthy adipose tissue remodelling in VATs and thermogenesis in iBAT thermogenesis. (2) Differential effects of HFDs on genes involved in vascular function were found in USI. Findings for HF mice indicated endothelial dysfunction, based on the differential regulation of

mRNA levels of proteins regulating NO bioavailability and the transcellular pathway, whereas vascular integrity seemed to be maintained upon HF/n-3, possibly due to its anti-inflammatory and anti-oxidative properties. (3) The observed anti-obesogenic effect of n-3 LCPUFA might be explained in part by the enhanced combustion of fatty acids by targeting transcriptional regulatory pathways and AMPK α , whereby FGF21 might mediate their metabolic effects in iBAT. For the HF/n-3 mice, expression data and subsequent correlation analyses suggest that HF/n-3 activates less efficient pathways for energy production in the intestine and the liver and increases ATP consumption upon the induction of a TAG / FFA cycle in iBAT, which showed increased thermogenic and oxidative potential in HF/n-3 mice.

With regard to the data of this thesis and of published data of mouse studies from other laboratories, using lard- or beef tallow-based HFDs with up to 60 kJ% fat, it is tempting to speculate that the soybean / palm oil-based HF (48 kJ% fat) used in the DIO model analysed in this thesis is too moderate to induce a strong inflammatory response and to disturb the intestinal barrier upon chronic HF feeding. Therefore, the postulated counteractive impact of HF/n-3 on adverse effects of HF on the intestinal barrier and endothelial permeability were difficult to study.

5.1 Differential effects of HFDs on inflammation

In this thesis, for the first time, a holistic, comparative and molecular approach was applied to determine chronic HF-induced inflammatory changes and the potential of HF/n-3 to counteract these effects in a DIO mouse model, whereby HF/n-3 showed lower n-6/n-3 PUFA and SFA/PUFA ratios. Different adipose tissues, VATs (EAT and MAT) and iBAT, the spleen, the liver and the small intestine were analysed, and macrophage but also the less explored T cells were characterised based on gene expression and immunohistochemical analyses of their surface markers and subsequent correlation analyses to define their distinct phenotype and biological function.

5.1.1 Moderate and tissue-specific inflammatory changes in adipose tissues upon HF

Although we could show tissue-specific inflammatory changes according to gene expression and immunohistochemical analyses upon HF, surprisingly, in this thesis, the obese HF mice did only show moderate changes in inflammatory markers compared to control and obese HF/n-3 mice. In EAT, only the significantly upregulated gene expression level of EMR1 suggested an increased macrophage number upon HF compared to control. Furthermore, the significantly increased mRNA level of iNOS upon HF compared to C and HF/n-3, as well as the significant correlation between F4/80-positive CLS and CD11c-positive CLS that was only observed within the HF group - a negative correlation was

observed within the HF/n-3 group - indicated more likely the predominance of the pro-inflammatory M1 phenotype in EAT for the HF mice compared to the HF/n-3 mice. However, no significant changes in T cell marker expression levels were observed upon HF in EAT.

Unlike other feeding trials with similar experimental settings, using HFDs with higher fat content and different fat quality (Kaneko 2011, Shaul 2010, Strissel 2007) than HF, gene expression levels of TNF α and the M1 macrophage marker ITGAX were not significantly increased in EAT upon HF compared to control feeding (cf. Table 8). Moreover, compared to the data from aforementioned HFD feeding studies, the HF-induced increase of EMR1 mRNA levels is considered rather as moderate (2-fold vs. 8-fold).

Contrary to the findings in EAT that indicated moderate inflammatory changes upon HF, no changes were observed in MAT. Surprisingly, in contrast to EAT, significantly increased mRNAs levels of the macrophage markers EMR1, ITGAX and CLEC10a were found in iBAT from HF mice. Nonetheless, cytokine expression levels do not suggest inflammatory conditions and the expression of immune cell markers was lower in iBAT compared to EAT, as evidenced by higher C_q -values.

Thus, findings from the present study indicated preferentially inflammatory processes in EAT upon long-term HF feeding compared to control. However, MAT and iBAT, which were rarely examined in other published studies, were not impaired, in agreement with previous assumptions that, under HFD conditions, MAT is the most metabolically active adipose tissue and thus the least affected (Hageman 2010) and BAT is largely resistant to inflammation (Fitzgibbons 2011), although it can be subjected to inflammation, which can downregulate the activity of iBAT, in severe obesity (Roberts-Toler 2015).

Moreover, based on correlation analyses, one can speculate that the more inflammatory phenotype observed upon HF in EAT is attributed to the higher body weight of these mice compared to the HF/n-3 mice, which were fed a HFD with lower n-6/n-3 PUFA and SFA/PUFA ratios, and is therefore a secondary effect of the increased fat intake with low fat quality (cf. Table 20).

5.1.2 Immunosuppressive effects of HF/n-3

Unlike SFA and n-6 LCPUFA, n-3 LCPUFA were reported to be beneficial in the treatment of inflammatory diseases. The anti-inflammatory and pro-resolving effects of n-3 LCPUFA might depend in large on the formation of eicosanoid lipid mediators that are less inflammatory than those derived from n-6 LCPUFA (Calder 2013). Moreover, the nature of the lipid can define the adipose tissue environment and shape ATM polarization and its inflammatory and metabolic sequelae, since it was found that lipid-induced toxicity is an important determinant of the pro-inflammatory switch in ATM polarization in adipose tissues, observed in an advanced state of obesity that is often associated with

insulin resistance (Prieur 2011). Thus, based on its balanced n-6/n-3 ratio and the lower SFA/PUFA ratio compared to HF, rather immunosuppressive effects were assumed upon HF/n-3.

Consistently, our findings from gene expression and immunohistochemical analyses indicated (1) a significant reduction of T cells in MAT and spleen upon HF/n-3 compared to HF and/or control, and (2) the promotion of a more anti-inflammatory cytokine profile and a rather less inflammatory M2-like polarization of ATMs upon HF/n-3 in MAT and iBAT compared to EAT.

Although, the impact of n-3 LCPUFA on T cells was largely analysed, to the best of our knowledge, MAT was never examined in this context in mice. Nonetheless, the significant reduction of CD4- and/or CD8 α -positive T cells found upon HF/n-3 in MAT and spleen was possibly caused by activation-induced apoptosis in Th1 cells that was reported to be stimulated by n-3 LCPUFA after their incorporation into lipid rafts or by distinct n-3 LCPUFA-induced T cell subtype activation (Kim 2010). The finding of a significant upregulation of the CASP3 protein in MAT upon HF/n-3 supports this opinion.

Furthermore, in contrast to EAT, some findings in MAT and iBAT indicated the promotion of a rather less inflammatory M2-like phenotype in macrophages in HF/n-3 mice, consistent with findings from a previous study (Titos 2011). However, the results from the present study were less conclusive since they are based on gene and immunohistochemical analyses, which are limited considering the classification of immune cells, and detailed analyses of T cells and ATMs by fluorescence-activated cell sorting analysis are warranted to define and quantitate in more detail their different activation and metabolic phenotyp. Nevertheless, and despite the upregulation of M2 and M1 markers in all adipose tissues upon HF/n-3, data from gene expression analysis indicated a rather anti-inflammatory environment in MAT and iBAT, whereas in EAT the gene expression levels of pro- and anti-inflammatory cytokines were upregulated upon HF/n-3 compared to control. In addition, CD301-positive cells predominated the CLS in iBAT.

Moreover, even though in most publications the classification of macrophages is based on the co-expression of distinct surface markers for the M1 and M2 phenotype, recent literature found that macrophages do not always rigidly adhere to these expression profiles. They rather show a mixed M1/M2 profile and a more or less inflammatory state (Shaul 2010, Xu 2013). Stemming from these findings, we finally concluded that macrophages within MAT and iBAT adopt more likely an anti-inflammatory phenotype in the HF/n-3 animals.

In addition, activated macrophages are not only categorised into M1- or M2-polarised subtypes based on their phenotype, but also in respect to the distinct mechanism of activation (Eguchi 2013), which define their different functions (Huang 2014). Thus, the significant correlations between the gene expression levels of immune cell markers and metabolic markers, such as CD36 and CPT1a found for HF/n-3 (cf. Table 6) or the upregulation of key transcription factors controlling M2

polarization like IRF4 (cf. Ludwig 2013) or PGC1 β lend further support to the assumption of a prevalence for the anti-inflammatory M2 macrophage phenotype in iBAT and MAT upon HF/n-3.

The phenotype of the macrophages (M1 and/or M2) within EAT cannot be characterised with the results presented, but the moderate upregulation (1.68-fold) of the TNF α gene expression level in HF/n-3 mice indicated only a slightly higher inflammatory state in HF/n-3 mice compared to control mice and a rather moderate one compared to the data from other feeding studies (4- to 12-fold) using HFDs with higher fat content and different fat quality (Kaneko 2011, Shaul 2010, Strissel 2007).

5.1.3 Immunoenhancing effects of HF/n-3

Findings from the present study provided so far only little evidence of differential effects on adipose tissue inflammation upon chronic HFD feeding, since only results from correlation analysis indicated the predominance of a more inflammatory macrophage phenotype in EAT for the HF mice compared to the HF/n-3 mice. Surprisingly, an increased abundance of macrophages was found upon HF/n-3 compared to control in all analysed adipose tissues and even compared to HF in MAT and iBAT revealing an immunoenhancing effect of HF/n-3. Thereby, EAT showed the strongest effect amongst adipose tissues, as evidenced by the higher number of macrophages found in EAT compared to MAT and iBAT in addition to the elevated number of T cells and the higher mRNA level of TNF α that were observed upon HF/n-3 compared to control in EAT.

Although literature that analysed the impact of n-3 PUFA and its derivatives on ATMs in DIO is rather small, and no data exists for iBAT, their impact on macrophage polarization was largely explored in *in-vitro* studies, showing potent anti-inflammatory effects. Notably, depending on the composition of the background diet and the study design, different outcomes have been observed for the number of ATMs upon n-3 PUFA intervention; a reduction (Oh 2010) or no changes, but even an increase in the number of macrophages was found in VATs (Pavlisova 2015). Nevertheless, the role of ATMs accumulation is sometimes still unclear. It was shown that the ATM number change in the course of adipose tissue remodelling in obese mice, while enhanced M1 polarization of ATMs in obese adipose tissues may interrupt the normal process of dead cell clearance and, thus, further stimulate pro-inflammatory responses (Strissel 2007). Conversely, it was reported that macrophages are also recruited to adipose tissues, if the need for lipid buffering capacity is high (Kosteli 2010) or apoptotic cells has to be cleared (Fischer-Posovszky 2011), but without activation of a pro-inflammatory state. In the context of the present study, the increase in ATMs upon HF/n-3 was considered to be associated with healthy adipose tissue remodelling and the clearance of apoptotic adipocytes (MAT and EAT), and/or lipid buffering and even thermogenesis (iBAT). This assumption is based on aforementioned findings on the prevalence for a rather anti-inflammatory macrophage phenotype in

adipose tissues upon HF/n-3 and those from RT-qPCR analysis, indicating significant higher overall levels of OPN (shown previously; Ludwig 2013) and apoptosis, as well as a significant higher number of multinucleated giant cells (“clusters”) in MAT when comparing HF/n-3 mice with HF mice. These clusters resemble the adipogenic niche for adipose tissue remodelling and restoration, which was introduced by Lee et al. and, moreover, it was found that the macrophages involved in this processes express high levels of OPN (Lee 2013). In addition, DHA has been reported to show anti-obesity activity due to its role in stimulating apoptosis (Kim 2006), a mechanism that might contribute to the significant reduction of VAT volume upon HF/n-3 compared to HF that was previously observed in the present study (Ludwig 2013).

In BAT, findings from gene expression and linear regression analyses, which indicated a significant higher number of eosinophils upon HF/n-3 compared to HF and significant correlations between eosinophils and macrophages or even the marker of thermogenesis UCP1 within the HF/n-3 group, lend further support to the concept that eosinophils and M2 macrophages might not only play an important role in regulating adaptive thermogenesis upon cold (Molofsky 2013, Nguyen 2011), but also upon HF/n-3. Thus, results from this thesis indicated for the first time that the efferent thermogenic circuit, consisting of eosinophils and alternative activated macrophages, might also be induced upon HF/n-3 in iBAT, since former publications only reported its role in the development of cold-induced beige fat, due to their contribution to catecholamine synthesis (Qiu 2014). A potential mechanism might involve the induction of the n-3 fatty acid receptor GPR120, which mediates anti-inflammatory effects (Oh 2010), as indicated by its significantly increased mRNA level upon HF/n-3 and significant correlations between GPR120 and surface markers of aforementioned immune cells. Moreover, macrophages may act through the control of sympathetic innervation and thus lipolysis to induce iBAT thermogenesis, whereby macrophages recruitment might have been initiated by the increased need for lipid buffering capacity, given the increased lipid uptake that was found upon HF/n-3 for iBAT. Noteworthy, the recent publication by Fischer et al. questioned that M2 macrophages synthesise relative amounts of catecholamines and have a direct role in adipocyte metabolism or adaptive thermogenesis upon cold or IL4 treatment (Fischer 2017).

5.1.4 Inflammatory changes in the small intestine upon HFDs

Most prior studies have focused on adipose tissue as the source of obesity-associated inflammation, whereas the intestine as another potential source has not been extensively explored, although it could be shown that HFDs and gut bacteria interact to promote pro-inflammatory changes in the small intestine (Ding 2010). In this thesis, the HFDs showed differential effects on intestinal inflammation upon long-term feeding. However, in contrast to the feeding trial by Ding et al. that

used a HFD based on soybean oil and lard (Ding 2010), findings from the present study indicated once again rather minor inflammatory changes within the small intestine upon HF compared to control. Noteworthy, HF/n-3 counteracted the significant HF-induced changes in USI, as previously shown for the cell adhesion molecule ICAM1 (Ludwig 2013), but also for MCP1 and the immune cell marker CD86, which is associated with intestinal inflammation (Plaza-Diaz 2014), suggesting that the lower fat quality of HF is associated with its stronger pro-inflammatory properties in comparison to HF/n-3. Finally, the TGF β 1 mRNA level was also significantly increased in USI upon HF feeding compared to control and HF/n-3 and might partly explain the low inflammatory tone in the small intestine of HF animals (Smith 2011).

Surprisingly, in the present study, the USI showed even bigger changes in inflammatory markers than the LSI, whereby the USI represents the duodenum and most parts of the jejunum and the LSI mostly consists of the ileum (Fatima 2009). However, given the differential inflammatory changes in the distinct regions of the small intestine upon HFDs (de Wit 2008), most studies that analysed HFD-induced intestinal inflammation (Ding 2010) or changes in the gut microbiota and intestinal permeability (de la Serre 2010) examined the ileum. These feeding studies could show HFD-induced impairments in gut barrier function and/or inflammatory changes in the intestine, whereas others could not (Kless 2015) or only if the housing conditions were changed and the jejunum was examined (Müller 2016). Thus, factors like the study design, the dietary approach (dose and composition), the duration of the diet intervention, the housing conditions and the choice of the segment of the gut (jejunum, ileum or colon) can affect the outcome and data of the feeding study and might explain to some extent the conflicting results.

5.2 Differential effects of HFDs on genes and proteins involved in vascular function in USI

All feeding studies that analysed the potential link between HFD-induced impairment in gut barrier function, LPS translocation and systemic inflammation only studied the intestinal epithelial barrier so far. In this thesis, however, using a comparative and molecular approach, the differential impact of HFDs on intestinal endothelial integrity was assessed upon long-term feeding. Furthermore, for the first time the effect of HFDs, differing in fat quality, on the regulation of NO bioavailability was examined in the small intestine, given our findings on the HF-induced pro-inflammatory phenotype of the endothelium in the mucosal scrapings of the USI and since physiologic levels of NO appear to play an important role in the maintenance of endothelial function. Macrovascular and microvascular complications associated with obesity, were found to be caused by reduced NO availability secondary to an enhanced oxidative stress production (Iantorno 2014). Thereby, reactive metabolites of both oxygen (ROS) and nitrogen (NO) have been implicated in the endothelial cell response to

inflammation, while an imbalance in favour of superoxide was associated with the pro-inflammatory phenotype of the endothelial cells and even pathological angiogenesis and increased endothelial permeability that are induced by inflammatory mediators (Cromer 2011).

5.2.1 Regulation of NO bioavailability upon HFDs in USI

Findings from RT-qPCR analyses of proteins that regulate NO bioavailability, such as CAV1 and ARG2, indicated a possible reduction in NO bioavailability in the USI from HF mice. Both genes were significantly upregulated upon HF compared to control or HF/n-3 and might result in reduced NO generation, consistent with former studies (Grayson 2013, Chung 2014), since CAV1 inactivates NOS3 by binding and ARG2 competes with NOS3 for its substrate L-arginine. These HF-induced changes could be counteracted by HF/n-3, possibly due to its anti-inflammatory and anti-oxidative properties as suggested by the findings on intestinal inflammation (cf. 5.1.4) and gene expression and correlation analyses in USI that indicated an increased and balanced antioxidant response (SOD1 and CAT) upon HF/n-3 compared to control and HF. However, in comparison with HF/n-3 mice, significantly upregulated mRNA levels were found for SOD1 but not for CAT upon HF compared to control, possibly resulting in enhanced hydrogen peroxide levels. Given that in an oxidising environment eNOS might turn itself into a source of superoxide anions (Pacher 2007), the aforementioned findings for HF animals, besides the significant correlations that were found between the mRNA levels of eNOS and proteins associated with inflammation and oxidative stress, might add to the assumption that, in contrast to HF/n-3, HF feeding disturbed the nitroso-redox balance in intestinal endothelial cells.

There is little information in the literature describing the effect of PUFA on NO bioavailability and most of it is based on *in-vitro* studies or studies that analysed the aorta. Previous reports showed increased NO generation and reduced vascular oxidative stress upon fish oil intervention, while preventing vascular endothelial dysfunction (Balakumar 2012). In addition, studies comparing the impact of n-3 and n-6 LCPUFA found higher anti-oxidative and anti-inflammatory properties upon n-3 LCPUFA intervention (Richard 2008) and revealed distinct changes in the composition and function of caveolae that house an array of cell signalling molecules and are associated with genes involved in endothelial dysfunction and inflammation (Wang 2008).

5.2.2 RT-qPCR analyses of proteins involved in the regulation of intestinal barrier integrity

As already mentioned in the context of HFD-induced intestinal inflammation (cf. 5.1.4), published studies that analysed HFD-induced changes in intestinal permeability mainly examined the ileum (de

la Serre 2010, Cani 2008, Kless 2015). However, other feeding studies reported defective intestinal barrier integrity in the jejunum, depending on housing conditions and thus intestinal bacterial diversity and composition (Müller 2016) or at early time points and without intestinal inflammation (Johnson 2015). Nonetheless, all these feeding studies analysed the epithelial barrier, whereas the microvascular endothelial barrier, which also influences intestinal permeability, was less recognised and investigated. Although, Spadoni et al. (Spadoni 2015) has characterised, for the first time, the gut-vascular barrier and its role in the control of the systemic dissemination of bacteria, HFD-induced changes of intestinal vascular integrity upon long-term feeding are largely unknown.

In this context, findings from the present study based on RT-qPCR analyses indicated changes in the transcellular pathway upon HF that might result in increased transcellular flux in USI. However, HF/n-3 could counteract this effect, since the significant HF-induced upregulation of mRNA levels for both the lipid raft protein CAV1, a critical protein for caveolae-mediated endocytosis and transcytosis, and PLVAP, a transmembrane glycoprotein that has been localised to caveolae and transendothelial channels of systemic fenestrated capillaries, could be reversed upon HF/n-3 in USI. With regard to changes in the transcellular pathway, former studies have shown that an upregulation of PLVAP is associated with VEGF-induced caveolae formation and microvascular leakage as observed in diabetic retinopathy (Wisniewska-Kruk 2016), and PLVAP was found to be increased in the gut upon infection, resulting in the systemic dissemination of bacteria (Spadoni 2015). Moreover, rats fed with a high-fat / sucrose diet showed high expression of CAV1 and endothelial hyperpermeability (Peng 2014), whereby phospho-CAV1 was thought to participate in transcellular and paracellular pathway to regulate endothelial permeability (Sun 2009).

Given that the role of junctional proteins like CDH5 (Harris 2010) in the control of endothelial permeability and angiogenesis is defined by its phosphorylation status (activity) and localisation (amount available for engagement at adherens junctions), in this thesis, mRNA expression data on junction proteins are insufficient to describe functional changes of the paracellular pathway. However, surprisingly, we could demonstrate significantly increased mRNA levels for the endothelial-specific cell-cell adhesion proteins CDH5 and CD31 (Harris 2010, Privratsky 2014), but also for TGFβ1, ICAM1, MMP9 and CAV1 in USI from HF mice compared to control mice. It is noteworthy that in the context of chronic inflammatory diseases the upregulation of these angiogenic mediators indicates pathological angiogenesis, which is associated with vascular hyperpermeability (Chidlow 2007).

Thus, based on findings from the present study and published reports on PLVAP, HF might enhance lipoprotein passage (Herrnberger 2014), leukocyte transmigration (Keuschnigg 2009) or systemic dissemination of bacteria (Spadoni 2015) within USI. In this thesis, the possibility of HF-induced leukocyte transmigration is supported by significant correlations that were found between the mRNA levels for the immune cell marker CD86 and the vesicular transport-related genes CAV1 and PLVAP

(cf. Table 11). However, physiological measurements that would allow the detection of enhanced vascular leakage were beyond the scope of the present study and measurements of plasma albumin levels were insufficient to express an opinion on that issue, since no mouse urine samples were available for analyses. Nonetheless, the hypoalbuminaemia found upon HFDs at week 6 but no longer at week 12 is worth further investigation and might indicate compensatory effects.

Noteworthy, in contrast to HF, vascular integrity seems to be maintained upon HF/n-3 in the USI, as evidenced by the unchanged gene expression levels for CAV1 and PLVAP, which may partly depend on the attenuation of raft dependent inflammatory signalling that was found to be differentially modulated by n-6 and n-3 PUFA (Wang 2008). Moreover, studies have shown that oxidative stress and CAV1 expression are related (Ousmaal 2016).

For technical reasons, mucosal scrapings, that represent an enrichment of epithelial and microvascular cells, were used for analyses of the small intestine. Thus, the observed expression level changes of some markers cannot be solely attributed to one cell type, although we tried to use mainly endothelial-specific marker. Moreover, separate analyses were performed for the upper and the lower part of the small intestine, whereby HF feeding induced more changes in the USI.

Finally, to confirm the assumptions made in the context of differential changes of endothelial function upon HFDs (5.2.1 and 5.2.2), a new feeding study is required as a next step, which is well-designed to reproduce and support essential data from the former study by performing more physiological and biochemical experiments.

5.3 Differential effects of HFDs on obesity

In this thesis, besides the analysis of the inflammatory changes and associated modifications in vascular function upon HFDs differing in n-6/n-3 PUFA and SFA/PUFA ratios, we also applied, for the first time, a holistic, comparative and molecular approach to further characterise the differential impact of HFDs on obesity upon long-term feeding. Different tissues, the small intestine, the liver and iBAT, were analysed and potential mechanisms for the n-3 LCPUFA-induced anti-obesogenic effect were explored by RT-qPCR and Western blot analyses, and subsequent correlation analyses.

5.3.1 Impact of HFDs on lipid metabolism in small intestine and liver

Data from previous *in-vivo* studies already proposed that n-3 LCPUFA can reduce HFD-induced obesity and hepatic fat accumulation by targeting transcriptional regulatory networks and by the regulation of genes involved in hepatic (Dossi 2014) and intestinal (van Schothorst 2009) lipid

metabolism. In this thesis, findings from RT-qPCR and Western blot analyses are consistent with these reports. Of note, HF/n-3 mice showed a significant upregulation of PPAR α -induced genes involved in fatty acid oxidation, whereby the most pronounced increases were found for the ω -oxidation gene CYP4a10, which is crucial for the generation of dicarboxylic fatty acids (Fiamoncini 2015). In this context, it is important to note that lipidomics data from mice analysed in the present thesis (personal communication by Dr. Tobias Ludwig, Prof. Hannelore Daniel, and Dr. Bernhard Bader, TUM) revealed significantly enhanced levels of odd-numbered medium-chain, dicarboxylic acylcarnitines and significantly lower levels of long-chain acylcarnitines in the livers from HF/n-3 mice compared to livers from control and/or HF mice. These data support the notion that HF/n-3-induced activation of PPAR α may account for the stimulation of hepatic and even intestinal lipid oxidation and the concept, that in particular ω -oxidation and peroxisomal β -oxidation were activated upon HF/n-3, considering previous findings from a mouse feeding study, which used a fish oil-based HFD (Fiamoncini 2015).

However, given the important interplay between peroxisomes and mitochondria, the intermediates that are exported from the peroxisome by a still unknown mechanism can be further oxidised to CO₂ and H₂O in mitochondria, whereby the carnitine-mediated pathway, which implies the previous conversion into acylcarnitines in peroxisomes, and the free-acid pathway are discussed (Wanders 2016). Nonetheless, there are still substantial gaps in the knowledge about peroxisome metabolism. Surprisingly, in this thesis, CPT1a, which is also modulated by PPAR α and controls mitochondrial β -oxidation, was not induced upon HF/n-3, raising the question of whether this carnitine acyltransferase is still the rate limiting step of mitochondrial β -oxidation in circumstances where fatty acids are preferentially channeled into peroxisomes for oxidation, since peroxisomes contain itself two distinct carnitine acyltransferases. In addition, medium-chain fatty acids are supposed to diffuse across the mitochondrial membrane (Wanders 2016).

Notably, since peroxisomal β -oxidation itself generates heat instead of ATP due to lack of an electron transport system (Lodhi 2014), in the present study, the enhanced fatty acids turnover in peroxisomes may partly explain the higher energy expenditure upon HF/n-3 compared to HF and the prevention of excessive hepatic lipid deposition found in HF/n-3 mice (Ludwig 2013). Furthermore, peroxisomes can perform fatty acid β -oxidation using half of the O₂ amount that would be needed for mitochondrial β -oxidation (Fiamoncini 2013).

In addition, given the role of malonyl-CoA, the product of ACC2, and of AMPK in the control of CPT1 (Hardie 2011), in this thesis, data from Western blot and linear regression analysis do not support a role of the AMPK-ACC2-CPT1 axis in providing a flux control over mitochondrial β -oxidation, although, for the HF/n-3 mice, activated AMPK α seems to be involved in the downregulation of hepatic DNL by phosphorylating ACC1 and further findings from correlation analyses even indicate an association

between posttranslational and transcriptional control of both ACC isoforms. Surprisingly, the P-ACC/ACC ratios (ACC1 and ACC2) were not altered upon both HFDs. Nevertheless, the observed significant lower hepatic mRNA levels for ACC2 and ACC1 (Ludwig 2013) in HF/n-3 mice than in HF mice, together with the significant lower ACC protein level, indicate reduced hepatic DNL upon HF/n-3. Thus, our data suggest, that HF/n-3 may prevent HF-induced hepatic lipid deposition by increasing fatty acid oxidation, especially ω -oxidation and peroxisomal β -oxidation, and by reducing DNL, whereby ACC was rather regulated on transcriptional level and not by the posttranslational regulation via AMPK α .

SREBP-1c, which is known to be involved in the dietary control of lipogenic enzyme genes, is also regulated by AMPK, whereby activated AMPK reduce SREBP-1c expression (Browning 2004), however, although it is speculated that AMPK can target nuclear proteins involved in transcriptional regulation, it is still an open question how AMPK quickly downregulate key players in liver lipid metabolism (Cantó 2010). Moreover, PUFA can directly influence gene expression by targeting SREBP-1c, suppressing its gene transcription, mRNA stability and proteolytic processing, whereby the latter option might imply the activation of AMPK as observed in hepatoma cells (Deng 2015) and might reduce feed-forward activation of the SREBP gene as found for EPA (Takeuchi 2010).

Of note, an ideal ACC inhibitor would impair lipogenesis, however, it also would avoid compensatory inhibition of fat oxidation by protein hyper-acetylation due to increased availability of acetyl-CoA to prevent hepatic lipid accumulation. In this context, it was shown that ACC inhibition targets CPT1a at the mRNA level (Chow 2014). Surprisingly, in this thesis, this regulation was observed for the control mice, whereas an inverse relationship was found for the HF/n-3 mice (cf. Table 12), indicating metabolic flexibility upon HF/n-3, whereby DNL is reduced and the activity of lipid oxidation is maintained or even increased.

Thus, in summary, the greater beneficial effect of HF/n-3, containing EPA and DHA, on reducing hepatic TAG content is rather related to enhanced combustion of fatty acids, since EPA has the highest potential to activate PPAR α , the major regulator of fatty acid oxidation, and other reports stated that n-3 LCPUFA inhibit VLDL secretion partly due to lower substrate (TAG) availability (Jump 2011).

Moreover, regardless of fat quantity (48 vs. 60 kJ% fat) and quality (SFA/PUFA ratios; 2.16:1 vs. 5.4:1), in this thesis, data from two independent mouse feeding studies (Ludwig 2013, Dahlhoff 2014) showed that both HFDs, HF (Ludwig 2013) and HF^A (Dahlhoff 2014), change the expression levels of lipogenic genes, indicating a reduction of hepatic DNL. Considering the aforementioned findings gained with the HF/n-3 mice, this effect might present a long-term adaptation to HFDs as already stated in another publication (Jump 2011), although the extent of the expression changes might depend on PUFA, fat and carbohydrate content of the diet (Ferramosca 2014). Noteworthy, given

that upon HF the ACC protein content was reduced, whereas for the HF^Δ mice the ACC mRNA levels were changed, the mechanisms seem to differ across studies. However, in both feeding studies, ACC was rather not controlled by the posttranslational regulation via AMPK α , since the P-ACC/ACC ratios for ACC1 and ACC2 showed no alterations, although Western blot analyses indicated the activation of AMPK α upon HF and HF^Δ. Surprisingly, for the HF mice, the total level of AMPK α showed a significant reduction compared to control mice.

5.3.2 Impact of HFDs on iBAT energy metabolism - increased thermogenic and oxidative potential in iBAT upon HF/n-3

Besides increased fatty acid oxidation in the small intestine and the liver, BAT is deemed important in the combat of obesity, since uncoupled respiration wastes food energy. However, only a handful of studies have investigated the impact of HFD on iBAT upon long-term feeding and even less have analysed DIT in iBAT considering the fat composition of the HFDs. Nonetheless, emerging evidence suggested that a fish oil diet rich in n-3 LCPUFA promotes BAT thermogenesis (Bargut 2016b), although the underlying mechanisms remain poorly described. Importantly, it has to be taken into consideration that the mechanism of DIT, referring to increased energy expenditure that accompanies food intake, includes uncoupling of mitochondrial respiration through UCP1, but also the activation of futile metabolic cycles (Bonet 2017). Both might account for the anti-obesogenic effect of HF/n-3 and therefore were examined in this thesis.

In this regard, findings from this thesis indicate enhanced thermogenic and oxidative potential in iBAT upon HF/n-3 compared to HF. Increases in iBAT mass, UCP1 content, and mitochondrial and vascular density, features that characterise cold-induced iBAT activation (Cannon 2004), were observed for iBAT from HF/n-3 mice. Although iBAT mass was significantly increased upon both HFDs, the mRNA and protein levels of UCP1 and the mitochondrial marker CS were only significantly upregulated upon HF/n-3 compared to control and even HF; importantly, these increased expression levels were even observed taking in account iBAT mass or protein content. Furthermore, the mRNA levels of PGC1 α and PGC1 β , as regulatory factors for mitochondrial biogenesis, were also significantly increased upon HF/n-3. Conversely, the HF mice showed significant lower protein and mitochondrial densities in iBAT, suggested by the reduced protein level of CS (CS per gram of protein), and, in addition, the TAG content in total iBAT or per gram of protein (cf. Table 14) was significantly elevated upon HF compared to control. Thus, in contrast to the HF/n-3 mice, the iBAT mass increase of HF mice might be related to lipid accumulation resulting from lower oxidative potential or dysfunctional lipid metabolism.

These results are in line with Bargut et al. (Bargut 2016b) reporting an induction of thermogenic markers in iBAT upon feeding a fish oil-based HFD, whereby energy expenditure could be increased by partial and even more by total substitution of lard with fish oil.

Noteworthy, although an enhanced level of UCP1 is often used as a surrogate measure of BAT activity, it will not necessarily result in increased energy expenditure as shown by Festuccia et al. (Festuccia 2011), analysing the impact of the PPAR γ agonist thiazolidinedione (TZD) on BAT. Despite the increased capacity for UCP1-mediated uncoupled respiration upon TZD treatment, BAT mitochondrial number and energy expenditure were not changed, moreover, the brown adipocytes displayed a whitened phenotype, which was explained by the TZD effects in promoting lipogenesis and in dampening the β -adrenergic-mediated activation of adipocytes (Festuccia 2011).

Interestingly, in the present thesis, this morphological change in iBAT, which was observed in obesity and was associated with lipid accumulation and dysfunctional BAT (Bargut 2016a), was not only found in HF mice but also in HF/n-3 mice, although former studies observed rather reduced lipid accumulation upon fish oil-based HFD compared to lard-based HFD (Bargut 2016b). Nonetheless, in the study by Bargut et al., the differences in iBAT lipid content were not as pronounced comparing the lard / fish oil-based HFD with the lard-based HFD and finally, both HFDs rich in fish oil showed increased energy expenditure. Unfortunately, the study by Bargut et al. does not provide data for the dietary lipid composition (Bargut 2016b).

Finally, in the present study, data from RT-qPCR analysis do not support an inactive state for iBAT from HF/n-3 mice compared to the HF mice, but rather suggest an increase in fatty acid uptake (LPL and CD36), efficient fatty acid oxidation (CPT1a, PPAR α and FABP3; Vergnes 2011) and ultimately enhanced lipid turnover in iBAT for the HF/n-3 mice.

Furthermore, in contrast to findings from the study by Festuccia et al. (Festuccia 2011), in the present study, data from RT-qPCR analysis do not a priori indicate reduced sympathetic activity upon HF/n-3. The mRNA levels of ADRB1 and ADRB3, which regulate the thermogenic functions of brown adipocytes (Collins 2012), were not reduced. In addition, the data showed a slight rise in the protein level of TH and suggest an increased abundance of eosinophils and of alternative activated macrophages upon HF/n-3, which might indicate higher sympathetic nerve activity (Tang 2015) and thermogenic function of iBAT in HF/n-3 mice compared to control and HF mice, considering other reports that stated general beneficial effects of n-3 LCPUFA on the autonomic nervous system (La Rovere 2015) and a contribution of immune cells in the regulation of brown adipocyte activity upon cold (Nguyen 2011, Qiu 2014). However, the latter was questioned recently by Fischer et al. (Fischer 2017).

On top of that, two further adrenergic-independent brown fat activator pathways were analysed, which can play a role in the activation of iBAT upon HF/n-3; bile acids that act through TGR5

(Watanabe 2006) or the hepatic factor FGF21, whose expression can also be induced in brown adipocytes by GPR120 (Quesada-López 2016). Compared to the HF mice, we found that the HF/n-3 mice had higher mRNA levels for TGR5 and GPR120, and that those were significantly upregulated compared to controls.

Moreover, for the HF/n-3 mice, in addition to the aforementioned possibly increased lipid uptake, the plasma NEFA levels were significantly diminished compared to control and HF mice, and the HF-induced body weight gain was partly prevented. Given the reports, which have suggested that the activation of iBAT is accompanied by increased lipid uptake (Bartelt 2011), these findings support a lipid-lowering effect of the HF/n-3 that might involve iBAT. Furthermore, the differential regulation of LPL activity found upon HF/n-3 in MAT and iBAT would suggest that fatty acids were shuffled towards activated iBAT (Dijk 2015). Comparing the mRNA levels of ANGPTL4 and LPL (Lafferty 2013), findings from linear regression analyses showed a significant correlation in MAT ($r=0.7481$, $p=0.0328$) and a significant inverse correlation in iBAT ($r=-0.8822$, $p=0.0007$) within the HF/n-3 group.

Finally, even the findings on mitochondrial and vascular density give no indication of obesity-linked BAT dysfunction for the HF/n-3 mice (Shimizu 2015).

To conclude, there is no a priori reason to expect an inactive iBAT for the HF/n-3 mice. In contrast to the HF mice, the increased lipid accumulation observed upon HF/n-3 might be an effect of on overall high lipid load rather than of an inability of iBAT to combust the fatty acids. However, based on the linear regression analyses, which show significant inverse correlations between the mRNA levels of the white adipocyte marker TLE3, that was reported to antagonise thermogenesis (Villanueva 2013), and enzymes related to energy metabolism, including UCP1 (cf. Table 17), we assume a less active state of iBAT for the HF mice compared to HF/n-3 mice upon long-term feeding, which may depend on the reduced mitochondrial protein content associated with HF.

5.3.3 Induction of a TAG / FFA cycle in iBAT upon HF/n-3

Since the net balance among the synthesis, oxidation, and hydrolysis of TAG in adipocytes determines the net quantity of cellular fat content, RT-qPCR and Western blot analyses were performed to further characterise iBAT energy metabolism. In this thesis, for the first time, expression data indicate the induction of a second thermogenic pathway that relies on futile cycling of TAG (lipolysis and fatty acid re-esterification) upon long-term HF/n-3 feeding in iBAT.

Considering that adipocyte lipolysis is a complex process that is tightly controlled through integration of multiple and diverse hormonal and biochemical signals to prevent the spillover of lipids and lipotoxicity when fatty acid demand is low, we further characterised lipolysis by Western blot analyses, since lipolysis is regulated by several co-activation mechanism that include post-

translational phosphorylation of the lipases or co-regulatory proteins such as G0S2 (Nielsen 2014). Notably, in this thesis, the data indicate a downregulation of the lipolytic pathway upon both HFDs compared to control in iBAT. Surprisingly, although their mRNA levels were not changed, the protein levels of the lipases ATGL and HSL were significantly reduced, indicating posttranslational modifications upon HFDs. One explanation might be proteasome-mediated degradation as already described for adipose ATGL in obese mice, however, the level of lipases does not always correlate with its cellular hydrolase activity (Dai 2013). In addition, findings on the phosphorylation status of HSL indicated reduced lipolysis by the β -adrenergic cAMP-PKA-HSL pathway (Ser660) upon HF/n-3, whereas the mRNA level of G0S2, a negative regulator of ATGL (Nielsen 2014), was found to be reduced upon both HFDs compared to control. However, due to time constraints, the regulation of ATGL, such as its AMPK-dependent activation, was not further analysed, although ATGL-catalysed lipolysis may be required for brown adipose phenotype, since it was found to promote fatty acid oxidation and re-esterification, inducing the cycling between DAG and TAG (Ahmadian 2011, Ahmadian 2009).

Nonetheless, in this thesis, findings from linear regression analyses (cf. Table 15) that showed for both high-fat groups significant correlations between lipolysis (HSL) and fatty acid re-esterification (DGAT2), and the increased mRNA level of GYK (Mazzucotelli 2007) upon HF/n-3, add to the assumption of HF/n-3-induced futile cycling of TAG in iBAT. Furthermore, the upregulation of the energy-demanding fatty acid re-esterification, creating a substrate cycle upon HF/n-3 could help to explain the induction of mitochondrial biogenesis and the activation of AMPK α (P-AMPK α /AMPK α ratio) as well as the significantly reduced NEFA levels in plasma (Ludwig 2013) that were observed for the HF/n-3 mice compared to HF and control mice, since the data of this thesis indicate that the fatty acids, which were preferentially channeled into iBAT upon HF/n-3, remain in this tissue for oxidation or storage (cf. Table 19).

These findings are in line with those from recent studies, analysing WAT but not iBAT. They suggested the involvement of a futile substrate cycle based on TAG lipolysis and re-esterification in the anti-obesity effect of n-3 LCPUFA, whereby UCP1 was not induced (Janovská 2013, Flachs 2013). Notably, the TAG / FFA substrate cycling in adipose tissues creates an efficient buffer system that provides fatty acids in time of metabolic need, thus allowing sufficient fatty acid flux without non-physiological increase in cellular NEFA (Flachs 2013). In this regard, it should be noted that long-chain acyl-CoA themselves can modulate fatty acid supply via feedback inhibition of lipolysis (Sanders 2015).

5.3.4 Balanced energy metabolism in iBAT upon HF/n-3

Finally, considering that a shift in the balance among activities of the major metabolic pathways, those contributing to TAG / FFA cycle and those involved in associated metabolic fluxes like mitochondrial β -oxidation and DNL or in fatty acid uptake and citric acid cycle might affect cellular lipid content (TAG and NEFA), in this thesis, gene expression data and subsequent correlation analyses indicate a balanced energy metabolism upon HF/n-3 in iBAT.

Upon long-term feeding, the expression profile of genes involved in the regulation of lipid metabolism was profoundly altered in iBAT upon HF/n-3 compared to control and HF. In addition to the aforementioned significant upregulation of UCP1, FGF21, a direct activator of iBAT (Quesada-López 2016), and of genes related to mitochondrial biogenesis (PGC1 α and PGC1 β), fatty acid uptake (LPL and CD36) and fatty acid oxidation (FABP3, CPT1a and PPAR α), genes involved in glycerol-3-phosphate generation (GSK and LDHB) and TAG synthesis (DGAT1, DGAT2 and AGPAT9) were also found to be induced upon HF/n-3. Notably, correlation analyses indicate that, for the HF/n-3 mice, the increased expression levels of PPAR α , DGAT1 and AGPAT9 are direct effects of the increased fat intake and probably the improved fat quality of HF/n-3 compared to HF, however, the actual effect was masked by the influence of the final body weight (cf. Table 20).

No change in the mRNA levels of HSL (lipolysis) and GLUT1 (glucose uptake) were detected, whereas the mRNA levels of ACC1 and ACC2 (DNL) as well as GLUT4 and HK2 (glucose metabolism) were significantly reduced upon HF/n-3.

Moreover, findings from correlation analyses in iBAT examining the coordinated regulation of mRNA levels of enzymes related to metabolic pathways and a relationship between ADRB1 and UCP1 or metabolic enzymes (cf. Table 19) suggest that a TAG / FFA cycle or even UCP1-mediated thermogenesis (Flachs 2013) are induced in iBAT upon HF/n-3 in order to result in increased energy expenditure.

Noteworthy is that, within the HF/n-3 group, the mRNA levels of ADRB1, CD36 and DGAT1 show a significant correlation with FGF21 mRNA level and also with the mRNA levels of almost all other enzymes involved in energy metabolism.

However, these findings make it difficult to dissect the possible impact of TAG / FFA cycle activation and mitochondrial uncoupling on whole body energy balance, if the HF/n-3-induced modulations of energy metabolism-related gene expression levels in iBAT will finally translate into functional thermogenic activity. Notably, activity of the TAG / FFA cycle might also play a crucial role in transformation of WAT to BAT, as reported by Barneda et al. (Barneda 2013).

5.3.5 Pathways induced in iBAT upon HF/n-3

In the present thesis, activation of PPAR α , PPAR γ 2 and AMPK α could be the pathways to mediate the effects of chronic HF/n-3 feeding in iBAT, whereby also the HF/n-3-induced increase in FGF21 and immune cells might be involved in regulating the activity of iBAT.

As noted above (cf. 5.3.2), UCP1-mediated thermogenesis can not be induced by the PPAR γ agonist TZD alone (Festuccia 2011). It also requires PPAR α , which contributes to thermogenic activation of BAT by coordinately regulating lipid catabolism and thermogenic gene expression via induction of PGC-1 α (Hondares 2011). In the present study, as n-3 LCPUFA are ligands of PPAR α and PPAR γ 2 (Jump 2008), findings from correlation analyses in iBAT (cf. Tables 15 and 16) indicate that, for the HF/n-3 mice, PPAR α activation participates in UCP1 expression and PPAR γ 2 could be responsible for the changes in genes involved in lipid uptake and storage, because these genes are transcriptional targets of PPAR γ 2 (Tontonoz 2008).

Moreover, a complex interplay of intracellular regulation pathways, including PPAR α and PPAR γ 2 and AMPK α , may generate the conditions for the activation of a TAG / FFA cycle, since the gene expression of PPAR α was significantly increased and the activation of AMPK α (P-AMPK α /AMPK α ratio) was induced in iBAT upon HF/n-3. Notably, given its important role in regulating cellular energy balance, mediating the responses to environmental or dietary changes, AMPK α might be involved in the regulation of lipolysis and the TAG / FFA cycle or might even modulate the coupling between lipolysis and fatty acid re-esterification, consistent with findings previously obtained from the analysis of metabolic effects elicited by combined interventions, including n-3 LCPUFA, in WAT (Flachs 2013). Furthermore, AMPK activity results from a local energy deficit (van Dam 2015). Thus, the HF/n-3-induced activation of AMPK α (P-AMPK α /AMPK α ratio), identified in the present thesis, might occur as a consequence rather than being a cause of BAT activation, as UCP1-dependent uncoupling and the energy-demanding TAG / FFA cycle leads to decreased intracellular energy levels. In addition, as stated before (cf. 5.1.3) the number of M2 macrophages and eosinophils might be increased upon HF/n-3 in order to support the formation of metabolic active adipocytes (Masoodi 2015), since ATMs that are recruited to iBAT, possibly due to enhanced local lipid fluxes, can buffer local increases in lipid concentration (Kosteli 2010) and even contribute to iBAT activity upon cold (Nguyen 2011, Qiu 2014), although the latter was questioned recently by Fischer et al. (Fischer 2017). Furthermore, n-3 LCPUFA act as ligands of GPR120 and, as recently reported, GPR120 may not only be the mediator in anti-inflammatory and insulin-sensitising effects (Oh 2010), but even in the energy metabolism of brown adipocytes, since n-3 LCPUFA-mediated GPR120 activation can induce the release of FGF21 resulting in the promotion of iBAT activity (Quesada-López 2016). In this thesis, it was found that mRNA levels for GPR120 and FGF21 were significantly increased upon HF/n-3 compared to control and HF feeding. Thus, based on findings from correlation analyses, FGF21 may

be essential for the HF/n-3-induced changes in the gene expression levels of enzymes related to energy metabolism (CD36, DGAT1, UCP1 and ADRB1) and, given its impact on sympathetic nerve activity (Owen 2014) and its potential as metabolic hormone (Jin 2016), FGF21 might also influence the sympathetic innervation of iBAT and fine tune multiorgan crosstalk. Moreover, due to its dual role, GPR120 may connect inflammation and metabolism in iBAT.

Finally, in this thesis, findings suggest that n-3 LCPUFA exert their favourable effects on obesity by targeting distinct pathways, such as PPAR α , PPAR γ 2 and AMPK α in iBAT, but also in liver and small intestine, in order to increase energy expenditure, whereby FGF21, as downstream target of PPARs and as activator of several downstream signalling pathways including AMPK α (Jin 2016), may mediate these effects. Various changes in gene and protein expression profiles were observed for the HF/n-3 mice compared to the HF mice, whereby the changes in the liver and the small intestine suggested enhanced endosomal ω -oxidation and peroxisomal β -oxidation, and those in iBAT indicated the induction of an energy-demanding TAG / FFA cycling and possibly UCP1-dependent thermogenesis upon HF/n-3. However, although the thermogenic and oxidative capacity of iBAT was induced upon HF/n-3, a new feeding study is required for additional measurements of iBAT activity and lipid content to examine whether the upregulation of the thermogenic capacity / machinery in iBAT translates into physiologically functional thermogenesis.

5.4 Conclusion and perspectives

The mouse feeding study analysed in this thesis provided an opportunity for mechanistic examination of the pathways involved in the favourable effects of a n-3 LCPUFA-enriched HFD in DIO, whereby the differential inflammatory, metabolic, and vascular changes upon HFDs, which differed in their fat quality (n-6/n-3 PUFA and SFA/PUFA ratios), could be analysed. The expression data of this thesis support findings from former studies that found numerous beneficial impacts of n-3 LCPUFA on health, including lipid-lowering and anti-inflammatory actions and their ability to maintain vascular function. Moreover, our data indicated that the HF/n-3 with a balanced n-6/n-3 ratio and lower SFA/PUFA ratio than HF could exert both immunoenhancing and -suppressive effects in different tissues, suggesting a more complex role of ATMs in obese adipose tissues. Thus, the unexpected increased content of macrophages in VATs and iBAT upon HF/n-3 compared to HF and control feeding - highest numbers were observed in EAT - was considered important for healthy adipose tissue remodelling, whereby the rather anti-inflammatory macrophages could play a valuable role in the clearance of apoptotic adipocytes, lipid buffering or even iBAT thermogenesis. However, only little evidence of differential effects of the HFDs on adipose tissue inflammation were found upon chronic feeding, although the data suggest a predominance of a more pro-inflammatory

macrophage phenotype upon HF compared to HF/n-3 in EAT, which has to be supported by further measurements. Furthermore, for the HF mice, rather minor inflammatory changes were observed in USI and even less in LSI, but also in the other tissues examined. It is therefore tempting to speculate that the soybean / palm oil-based HF (48 kJ% fat) is too moderate to induce a strong inflammatory response and to disturb the intestinal barrier function upon long-term feeding. Nonetheless, in this thesis, gene expression data showed differential changes in proteins, which regulate NO bioavailability and the transcellular pathway, upon HFDs in the intestine, suggesting favourable effects on vascular integrity for HF/n-3 that might involve the anti-oxidative potential of n-3 LCPUFA. For further physiological experiments, the potential compensatory effect upon chronic feeding must be kept in mind, since hypoalbuminaemia was found upon HFDs at week 6 but no longer at week 12. In addition, although the physiological and metabolic confirmation for the enhanced iBAT activity upon HF/n-3 compared to HF feeding is still pending, the HF/n-3-induced modulations of energy metabolism-related gene expression levels in iBAT indicated the contribution of TAG / FFA cycling and even UCP1-dependent mitochondrial uncoupling to the enhanced energy expenditure observed upon HF/n-3. In this context, HF/n-3 might exert its beneficial effect on obesity and obesity-related fatty liver by targeting distinct pathways, such as PPAR α , PPAR γ 2 and AMPK α in iBAT, but also in liver and intestine, in order to enhance fatty acid oxidation and to induce mechanism of DIT, effects that might be mediated by the metabolic hormone FGF21. Moreover, it was suggested that the increased lipid uptake by iBAT upon HF/n-3 might contribute its hypolipidemic effect, whereby iBAT seems to play an outstanding role in the storage and combustion of fatty acids.

However, the assumptions made in this thesis, based on findings from RT-qPCR, Western blot and immunohistochemical analyses, have to be confirmed by physiological and functional analyses, whereby new feeding studies have to be carried out. A possible impact of HF on endothelial dysfunction and vascular permeability has to be evaluated by the Evans blue extravasation method and blood flow measurements. Detailed analyses of immune cells by fluorescence-activated cell sorting analysis are warranted to define and quantitate in more detail the different activation and metabolic phenotypes. Furthermore, iBAT activity and lipid content have to be determined by measuring supraclavicular skin temperature or using different positron emission tomography-computed tomography tracers in combination with magnetic resonance spectroscopy techniques (Schilperoort 2016).

Overall, manipulation of dietary fat quality, in terms of reducing the SFA content and the n-6/n-3 PUFA ratio of the HFD, is a possible avenue for positive manipulation of energy metabolism and metabolic inflammation in obese mice. However, mixed results as well as the lack of consistency and findings across human studies (Buckley 2009) make it difficult to confirm these findings in humans. Various factors including differences in study design, dose and composition of the n-3 PUFA

intervention, composition of the background diet and the duration of the intervention as well as the gut microbiome could be confounding the results from animal and human studies.

Translating these discoveries into recommendations for human intake of n-3 LCPUFA as preventive strategy or even as combination therapy for obesity will ultimately require a more complete understanding of the individual effects of each fatty acid on inflammation and the regulation of energy metabolism, and of the different possible targets of n-3 LCPUFA to combat obesity, taking into account the valuable contribution of our results to explore potential mechanism. Given the differential physiological functions of DHA and EPA (Mozaffarian 2012) and the diversity of bioactive metabolites, including pro-resolving mediators like resolvins and protectins or immunomodulatory branched fatty acid esters of hydroxy fatty acids (Kuda 2017), the pleiotropic effects of fatty acids add another layer of complexity toward understanding the anti-obesogenic and anti-inflammatory impact of n-3 LCPUFA. In addition to targeting iBAT activity, as analysed in this study, n-3 LCPUFA might also increase the differentiation of brown adipocytes in white fat depots, as shown for EPA (Zhao 2014). Thereby, EPA might promote brown adipogenesis by modulating miRNAs (Kim 2016). In addition, a recent study revealed that the gut microbiota, which composition was found to be changed depending on dietary fat composition (Lam 2015) and thus might partly explain the differential impact of HFDs on intestinal barrier disruption and associated systemic inflammation (Kaliannan 2015), might also play a role in the emergence of thermogenic brown fat cells within white fat depots (Suárez-Zamorano 2015), adding insight into the microbiota-fat signalling axis.

6 Appendix

Table 21. Changes in gene expression upon soybean / palm oil-based HFDs in iBAT

Function	C _q -value	Gene	Fold change		
			HF vs. C	HF/n-3 vs. C	HF/n-3 vs. HF
FA transport	19-21	Lpl	1.00	1.51**	1.50**
	19-20	CD36	1.16	1.42**	1.22
	19-22	Fabp3	2.07***	3.91***	1.89***
FA metabolism	16-18	Ucp1 [#]	1.12	1.59***	1.42***
	25-28	Cpt1a	1.54***	2.06***	1.34
	23-26	Lpbe	0.90	0.87	0.96
	19-22	Acc1	0.61***	0.30***	0.49***
	20-22	Acc2	0.76**	0.59***	0.77*
	25-28	Agpat9	1.46	2.37***	1.62
	26-27	Dgat1	0.75**	0.95	1.27*
	18-21	Dgat2	1.26	1.83***	1.45*
	23-26	Gyk	1.34	3.16***	2.35***
	21-22	Ldhd	0.87	1.11	1.27*
	26-27	Glut1	0.84	0.91	1.09
	21-23	Glut4	0.72***	0.59***	0.82*
	25-27	Hk2	0.70	0.54*	0.76
	19-20	Cs	1.09	1.25***	1.14*
	20-22	Pck1	0.91	1.08	1.19
	28-31	p47phox	1.70*	1.68*	0.98
	23-26	Hsl	1.00	1.00	1.00
	20-23	Plin5	1.27	1.48*	1.16
	23-27	gOs2	0.53*	0.56	1.06
	22-25	Angptl4	1.26*	1.28*	1.01
Inflammation	27-29	Emr1	1.41*	1.79***	1.27
	28-33	Itgax	2.06**	3.99***	1.94
	26-27	Mrc1	1.20	1.42**	1.18
	29-32	Clec10a	1.39*	1.38*	0.99
	32-36	Siglec5	1.60	2.87***	1.80*
	25-26	Tgfβ1	1.19	1.38**	1.16
	29-31	Tnfα	1.01	1.16	1.15
	31-33	IL10	1.22*	1.23*	1.01
28-32	Mcp1	2.12*	2.22**	1.05	
Endothelium	27-31	Cdh5	1.22*	1.38***	1.13
	23-26	Cldn5	1.38	1.01	0.73
Innervation	25-27	Adrb1	1.03	0.91	0.88
	25-27	Adrb3	1.28	0.94	0.74*
	31-32	Tgr5	0.76*	0.95	1.26
	25-28	Dio2	0.70	1.10	1.59
	25	Gpr120	1.09	1.46**	1.33*
31-33	Fgf21	1.25	1.50**	1.20	

Function	C _q -value	Gene	Fold change		
			HF vs. C	HF/n-3 vs. C	HF/n-3 vs. HF
Transcription	29-31	Tle3	1.40***	1.54***	1.10
	22-23	Ppar γ 2	1.03	1.04	1.01
	22-24	Ppara α	1.21**	1.45***	1.19**
	25-28	Pgc1 α	1.16	1.47*	1.27
	23-25	Pgc1 β	1.02	1.17**	1.15*
Adipokines	20-23	AdipoQ	0.97	1.08	1.11
	24-29	Lep	2.95***	1.68*	0.57

Shown are the results of gene expression analysis in interscapular brown adipose tissue (iBAT) after 12 weeks of feeding either control (C), HFD (HF), or n-3 long-chain polyunsaturated fatty acid (LCPUFA)-enriched HFD (HF/n-3), using RT-qPCR (n=7-12). mRNA expression levels are depicted as relative fold changes. Data were analysed with $\Delta\Delta C_q$ method and normalised to CypB and Hsp90 α b1 gene expression. Fold changes were calculated relative to C and HF group. For the genes marked with a hash symbol, the data was obtained from Ludwig et al. (Ludwig 2013), testing for normal distribution and outliers. Statistical analysis was performed using one-way ANOVA and Tukey post-test. In case of no normal distribution, data were tested by Kruskal-Wallis and Dunn's post-test. In addition, outliers were detected by using Grubb's test and excluded from statistical data analysis. *p < 0.05, **p < 0.01, ***p < 0.001, significant differences compared with control or between groups as indicated. FA, fatty acid; HFD, high-fat diet.

Table 22. Changes in gene expression upon soybean / palm oil-based HFDs in EAT

Function	C _q -value	Gene	Fold change		
			HF vs. C	HF/n-3 vs. C	HF/n-3 vs. HF
Inflammation	24-28	Emr1	2.35**	2.71***	1.15
	24-27	Itgam	1.24	1.34**	1.08
	24-29	Itgax [#]	2.85	6.62***	2.32
	23-24	Mrc1 [#]	0.97	1.17	1.21*
	26-28	Clec10a	1.16	1.43***	1.23*
	28-31	CD4	1.03	1.48*	1.44*
	28-30	CD86	0.97	0.96	0.99
	27-29	Nos2	1.33**	1.02	0.76*
	28-31	Tnf α	1.43	1.68**	1.18
	31-34	IL10 [#]	1.45	1.71*	1.18
	24-28	Mcp1 [#]	3.08**	2.61**	0.85
	25-31	Spp1 (Opn) [#]	2.60*	8.04***	3.09**
	Endothelium	26-29	Vcam1	1.36	2.21***
27-29		Icam1	1.15	1.26	1.09
25-26		Tek	0.93	0.83	0.89

Shown are the results of gene expression analysis in epididymal adipose tissue (EAT) after 12 weeks of feeding either control (C), HFD (HF), or n-3 long-chain polyunsaturated fatty acid (LCPUFA)-enriched HFD (HF/n-3), using RT-qPCR (n=8-12). mRNA expression levels are depicted as relative fold

changes. Data were analysed with $\Delta\Delta C_q$ method and normalised to Actb and Gapdh gene expression. Fold changes were calculated relative to C and HF group. For the genes marked with a hash symbol, the data was obtained from Ludwig et al. (Ludwig 2013), testing for normal distribution and outliers. Statistical analysis was performed using one-way ANOVA and Tukey post-test. In case of no normal distribution, data were tested by Kruskal-Wallis and Dunn's post-test. In addition, outliers were detected by using Grubb's test and excluded from statistical data analysis. *p < 0.05, **p < 0.01, ***p < 0.001, significant differences compared with control or between groups as indicated. HFD, high-fat diet.

Table 23. Changes in gene expression upon soybean / palm oil-based HFDs in liver

Function	C _q -value	Gene	Fold change		
			HF vs. C	HF/n-3 vs. C	HF/n-3 vs. HF
12 weeks					
Inflammation	26-27	Emr1	1.04	1.17	1.12
	31-35	Tnfa	1.23	0.92	0.75
FA metabolism	21-23	Cpt1a [#]	1.26*	1.01	0.80
	19-21	Acox1 [#]	1.29**	1.78***	1.38***
	22-25	Lpbe	1.13	2.25***	1.99***
	20-24	Cyp4a10	1.59***	4.03***	2.53***
	20-28	Scd1 [#]	0.71	0.06***	0.09***
	24-27	Acc1 [#]	0.83	0.51***	0.61***
	19-23	Acc2	0.79	0.23***	0.29***
	25-28	Hsl	1.37	1.68**	1.23
6 weeks					
Endothelium	14-15	Alb	0.96	0.81***	0.84**

Shown are the results of gene expression analysis in liver after 12 weeks or 6 weeks of feeding either control (C), HFD (HF), or n-3 long-chain polyunsaturated fatty acid (LCPUFA)-enriched HFD (HF/n-3), using RT-qPCR (n=9-12). mRNA expression levels are depicted as relative fold changes. Data were analysed with $\Delta\Delta C_q$ method and normalised to Hprt1 and Actb gene expression. Fold changes were calculated relative to C and HF group. For the genes marked with a hash symbol, the data was obtained from Ludwig et al. (Ludwig 2013), testing for normal distribution and outliers. Statistical analysis was performed using one-way ANOVA and Tukey post-test. In case of no normal distribution, data were tested by Kruskal-Wallis and Dunn's post-test. In addition, outliers were detected by using Grubb's test and excluded from statistical data analysis. *p < 0.05, **p < 0.01, ***p < 0.001, significant differences compared with control or between groups as indicated. FA, fatty acid; HFD, high-fat diet.

Table 24. Changes in gene expression upon soybean / palm oil-based HFDs in LSI

Function	C _q -value	Gene	Fold change		
			HF vs. C	HF/n-3 vs. C	HF/n-3 vs. HF
12 weeks					
Inflammation	26-31	Itgax	1.28	1.15	0.90
	28-32	Emr1	1.20	1.13	0.94
	22-27	Nos2	0.99	0.40*	0.41**
	26-29	Tgfβ1	1.26	1.03	0.81
Stress	21-23	Sod1	1.18	1.43**	1.21
	24-27	Tnfsf10	0.95	0.91	0.95
Endothelium	26-29	CD31	1.17	1.10	0.94
	29-30	Vcam1 [#]	1.22	1.07	0.88
	30-32	Icam1 [#]	0.97	1.01	1.04
	28-31	Tek [#]	1.17	0.98	0.83
Junction	24-26	Ocln	1.26*	1.11	0.88
FA metabolism	22-26	Cpt1a	1.06	1.62*	1.52
	21-25	Acox1	1.09	1.56*	1.43
	24-29	Cyp4a10	1.71*	14.73***	8.63***
6 weeks					
Endothelium	34-36	Cdh5	1.30	1.23	0.95
Junction	24-25	Ocln	1.07	1.16	1.09

Shown are the results of gene expression analysis in lower small intestine (LSI) after 12 weeks or 6 weeks of feeding either control (C), HFD (HF), or n-3 long-chain polyunsaturated fatty acid (LCPUFA)-enriched HFD (HF/n-3), using RT-qPCR (n=8-12). mRNA expression levels are depicted as relative fold changes. Data were analysed with $\Delta\Delta C_q$ method and normalised to CypB and Hsp90α1 gene expression. Fold changes were calculated relative to C and HF group. For the genes marked with a hash symbol, the data was obtained from Ludwig et al. (Ludwig 2013), testing for normal distribution and outliers. Statistical analysis was performed using one-way ANOVA and Tukey post-test. In case of no normal distribution, data were tested by Kruskal-Wallis and Dunn's post-test. In addition, outliers were detected by using Grubb's test and excluded from statistical data analysis. *p < 0.05, **p < 0.01, ***p < 0.001, significant differences compared with control or between groups as indicated. FA, fatty acid; HFD, high-fat diet.

Table 25. Changes in gene expression upon soybean / palm oil-based HFDs in MAT

Function	C _q -value	Gene	Fold change		
			HF vs. C	HF/n-3 vs. C	HF/n-3 vs. HF
Inflammation	24-27	Emr1	1.23	1.65**	1.34
	25-27	Itgam	1.14	1.61***	1.41***
	25-29	Itgax [#]	1.07	2.44***	2.29**
	23-25	Mrc1 [#]	1.17	1.56***	1.33
	28-30	Clec10a	1.05	1.35*	1.29
	24-29	CD4	0.79	0.71	0.90
	25-30	CD8 α	0.74	0.60*	0.82
	25-28	CD86	0.85	0.95	1.12
	28-30	Nos2	1.18	1.04	0.88
	28-30	Tnf α	0.77	0.87	1.12
	31-33	IL10 [#]	1.09	0.98	0.89
	25-28	Mcp1 [#]	1.66*	1.60*	0.96
	25-31	Spp1 (Opn) [#]	1.68	5.27***	3.14**
	Endothelium	24-26	Vcam1	1.06	1.23
26-29		Icam1	0.91	0.93	1.02
25-27		Tek	1.01	0.93	0.92
FA uptake	18-21	Lpl	1.05	0.99	0.94
	23-25	Angptl4	1.52*	1.51	0.99

Shown are the results of gene expression analysis in mesenteric adipose tissue (MAT) after 12 weeks of feeding either control (C), HFD (HF), or n-3 long-chain polyunsaturated fatty acid (LCPUFA)-enriched HFD (HF/n-3), using RT-qPCR (n=8-10). mRNA expression levels are depicted as relative fold changes. Data were analysed with $\Delta\Delta C_q$ method and normalised to Actb and Hprt1 gene expression. Fold changes were calculated relative to C and HF group. For the genes marked with a hash symbol, the data was obtained from Ludwig et al. (Ludwig 2013), testing for normal distribution and outliers. Statistical analysis was performed using one-way ANOVA and Tukey post-test. In case of no normal distribution, data were tested by Kruskal-Wallis and Dunn's post-test. In addition, outliers were detected by using Grubb's test and excluded from statistical data analysis. *p < 0.05, **p < 0.01, ***p < 0.001, significant differences compared with control or between groups as indicated. FA, fatty acid; HFD, high-fat diet.

Table 26. Changes in gene expression upon soybean / palm oil-based HFDs in spleen

Function	C _q -value	Gene	Fold change		
			HF vs. C	HF/n-3 vs. C	HF/n-3 vs. HF
Inflammation	24-25	Emr1	0.84	0.77**	0.91
	24-26	Itgax	1.16	0.76*	0.66***
	24-25	CD4	0.99	0.70***	0.71***
	25-26	CD8 α	1.05	0.83	0.79*

Shown are the results of gene expression analysis in spleen after 12 weeks of feeding either control (C), HFD (HF), or n-3 long-chain polyunsaturated fatty acid (LCPUFA)-enriched HFD (HF/n-3), using RT-qPCR (n=10-12). mRNA expression levels are depicted as relative fold changes. Data were analysed with $\Delta\Delta C_q$ method and normalised to Gapdh and Hprt1 gene expression. Fold changes were calculated relative to C and HF group. Statistical analysis was performed using one-way ANOVA and Tukey post-test. In case of no normal distribution, data were tested by Kruskal-Wallis and Dunn's post-test. In addition, outliers were detected by using Grubb's test and excluded from statistical data analysis. *p < 0.05, **p < 0.01, ***p < 0.001, significant differences compared with control or between groups as indicated. HFD, high-fat diet.

Table 27. Changes in gene expression upon soybean / palm oil-based HFDs in USI

Function	C _q -value	Gene	Fold change		
			HF vs. C	HF/n-3 vs. C	HF/n-3 vs. HF
Inflammation	28-31	Itgam	1.20	1.22	1.02
	26-29	Itgax	1.15	1.09	0.95
	29-31	CD86	1.45**	0.91	0.63***
	27-30	Nos2	0.78	0.48*	0.61
	26-28	Tgf β 1	1.79*	1.46	0.82
	31-34	Mcp1	1.83*	1.10	0.60
NO bioavailability	28-30	Nos3	1.30	0.88	0.68
	20-22	Arg2	1.18*	1.07	0.90
	27-30	Cav1	1.61	0.88	0.55*
Stress	27-29	gp91phox	1.18	1.03	0.87
	27-29	p47phox	1.24	1.03	0.83
	20-22	Sod1	1.57***	2.27***	1.44***
	21-23	Cat	1.18	1.70**	1.43*
	24-26	Tnfsf10	0.87	0.67***	0.77*
	27-30	Mmp9	2.82***	2.12***	0.75
Endothelium	27-29	CD31	1.27*	1.05	0.83
	29-31	Vcam1 [#]	1.76	1.27	0.72
	30-31	Icam1 [#]	1.58*	1.09	0.69
	29-31	Tek [#]	1.71*	1.21	0.71
	24-26	Plvap	1.48***	1.10	0.74*

Function	C _q -value	Gene	Fold change		
			HF vs. C	HF/n-3 vs. C	HF/n-3 vs. HF
Junction	35-37	Cdh5	1.47*	1.19	0.81
	31-33	Cldn5	1.21	0.79	0.65
	24-26	Ocln	0.86	1.00	1.17
FA metabolism	22-26	Cpt1a	1.61***	2.24***	1.39**
	20-22	Acox1	1.47***	1.86***	1.26*
	23-29	Cyp4a10	7.01***	42.65***	6.08***

Shown are the results of gene expression analysis in upper small intestine after 12 weeks of feeding either control (C), HFD (HF), or n-3 long-chain polyunsaturated fatty acid (LCPUFA)-enriched HFD (HF/n-3), using RT-qPCR (n=7-11). mRNA expression levels are depicted as relative fold changes. Data were analysed with $\Delta\Delta C_q$ method and normalised to Actb, Gapdh and Hprt1 gene expression. Fold changes were calculated relative to C and HF group. For the genes marked with a hash symbol, the data was obtained from Ludwig et al. (Ludwig 2013), testing for normal distribution and outliers. Statistical analysis was performed using one-way ANOVA and Tukey post-test. In case of no normal distribution, data were tested by Kruskal-Wallis and Dunn's post-test. In addition, outliers were detected by using Grubb's test and excluded from statistical data analysis. *p < 0.05, **p < 0.01, ***p < 0.001, significant differences compared with control or between groups as indicated. FA, fatty acid; HFD, high-fat diet, NO, nitric oxide.

Table 28. Changes in gene expression upon soybean oil / beef tallow-based HFDs in liver

Tissue	Function	C _q -value	Gene	Fold change			
				HF ^Δ vs. C ^Δ	CMS vs. C ^Δ	HFMS vs. C ^Δ	HFMS vs. HF ^Δ
Liver	FA Metabolism	21-23	Cpt1a [#]	1.59***	0.90	1.68***	1.05
		23-25	Acc1	0.59**	0.65*	0.53***	0.90
		23-25	Acc2	0.64*	0.58*	0.51**	0.74

Shown are the results of gene expression analysis in liver after 12 weeks (n=8-9) of feeding either control (C^Δ) or HFD (HF^Δ; 60 kJ% fat) based on soybean oil and beef tallow, or 4-week dietary methyl-donor supplementation (CMS or HFMS), using RT-qPCR. mRNA expression levels are depicted as relative fold changes. Data were analysed with $\Delta\Delta C_q$ method and normalised to Gapdh and Hprt1 expression. Fold changes were calculated relative to C^Δ and HF^Δ group. For the genes marked with a hash symbol, the data was obtained from Dahlhoff et al. (Dahlhoff 2014), testing for normal distribution and outliers. Statistical analysis was performed using one-way ANOVA and Tukey post-test. In case of no normal distribution, data were tested by Kruskal-Wallis and Dunn's post-test. In addition, outliers were detected by using Grubb's test and excluded from statistical data analysis. *p < 0.05, **p < 0.01, ***p < 0.001, significant differences compared with control or between groups as indicated. FA, fatty acid; HFD, high-fat diet.

7 References

- Abu-Elheiga L, Matzuk MM, Abo-Hashema KA, Wakil SJ. Continuous fatty acid oxidation and reduced fat storage in mice lacking acetyl-CoA carboxylase 2. *Science* 291(5513):2613-2616, 2001
- Ahmadian M, Abbott MJ, Tang T, Hudak CS, Kim Y, Bruss M, Hellerstein MK, Lee HY, Samuel VT, Shulman GI, Wang Y, Duncan RE, Kang C, Sul HS. Desnutrin/ATGL is regulated by AMPK and is required for a brown adipose phenotype. *Cell Metab* 13(6):739-748, 2011
- Ahmadian M, Duncan RE, Varady KA, Frasson D, Hellerstein MK, Birkenfeld AL, Samuel VT, Shulman GI, Wang Y, Kang C, Sul HS. Adipose overexpression of desnutrin promotes fatty acid use and attenuates diet-induced obesity. *Diabetes* 58(4):855-866, 2009
- Aird WC. Phenotypic heterogeneity of the endothelium: I. Structure, function, and mechanisms. *Circ Res* 100(2):158-173, 2007
- Altintas MM, Azad A, Nayer B, Contreras G, Zaias J, Faul C, Reiser J, Nayer A. Mast cells, macrophages, and crown-like structures distinguish subcutaneous from visceral fat in mice. *J Lipid Res* 52(3):480-488, 2011
- Amado-Azevedo J, Valent ET, Van Nieuw Amerongen GP. Regulation of the endothelial barrier function: a filum granum of cellular forces, Rho-GTPase signaling and microenvironment. *Cell Tissue Res* 355(3):557-576, 2014
- Angulo P. Obesity and nonalcoholic fatty liver disease. *Nutr Rev* 65(6 Pt 2):S57-63, 2007
- Atkins GB, Jain MK, Hamik A. Endothelial differentiation: molecular mechanisms of specification and heterogeneity. *Arterioscler Thromb Vasc Biol* 31(7):1476-1484, 2011
- Augustin HG, Koh GY, Thurston G, Alitalo K. Control of vascular morphogenesis and homeostasis through the angiopoietin-Tie system. *Nat Rev Mol Cell Biol* 10(3):165-177, 2009
- Baker RG, Hayden MS, Ghosh S. NF- κ B, inflammation, and metabolic disease. *Cell Metab* 13(1):11-22, 2011
- Bakker W, Eringa EC, Sipkema P, van Hinsbergh VW. Endothelial dysfunction and diabetes: roles of hyperglycemia, impaired insulin signaling and obesity. *Cell Tissue Res* 335(1):165-189, 2009
- Balakumar P, Taneja G. Fish oil and vascular endothelial protection: bench to bedside. *Free Radic Biol Med* 53(2):271-279, 2012
- Ballmer PE. Causes and mechanisms of hypoalbuminaemia. *Clin Nutr* 20(3):271-273, 2001
- Bargut TC, Aguila MB, Mandarim-de-Lacerda CA. Brown adipose tissue: Updates in cellular and molecular biology. *Tissue Cell* 48(5):452-460, 2016a
- Bargut TC, Silva-e-Silva AC, Souza-Mello V, Mandarim-de-Lacerda CA, Aguila MB. Mice fed fish oil diet and upregulation of brown adipose tissue thermogenic markers. *Eur J Nutr* 55(1):159-169, 2016b
- Barneda D, Frontini A, Cinti S, Christian M. Dynamic changes in lipid droplet-associated proteins in the "browning" of white adipose tissues. *Biochim Biophys Acta* 1831(5):924-933, 2013

- Bartelt A, Bruns OT, Reimer R, Hohenberg H, Ittrich H, Peldschus K, Kaul MG, Tromsdorf UI, Weller H, Waurisch C, Eychmüller A, Gordts PL, Rinninger F, Bruegelmann K, Freund B, Nielsen P, Merkel M, Heeren J. Brown adipose tissue activity controls triglyceride clearance. *Nat Med* 17(2):200-205, 2011
- Bates DO. Vascular endothelial growth factors and vascular permeability. *Cardiovasc Res* 87(2):262-271, 2010
- Belvitch P, Dudek SM. Role of FAK in S1P-regulated endothelial permeability. *Microvasc Res* 83(1):22-30, 2012
- Bonet ML, Mercader J, Palou A. A nutritional perspective on UCP1-dependent thermogenesis. *Biochimie* 134:99-117, 2017
- Brisset AC, Isakson BE, Kwak BR. Connexins in vascular physiology and pathology. *Antioxid Redox Signal* 11(2):267-282, 2009
- Brose N, Rosenmund C. Move over protein kinase C, you've got company: alternative cellular effectors of diacylglycerol and phorbol esters. *J Cell Sci* 115(Pt 23):4399-4411, 2002
- Browning JD, Horton JD. Molecular mediators of hepatic steatosis and liver injury. *J Clin Invest* 114(2):147-152, 2004
- Buckley JD, Howe PR. Anti-obesity effects of long-chain omega-3 polyunsaturated fatty acids. *Obes Rev* 10(6):648-659, 2009
- Buettner R, Parhofer KG, Woenckhaus M, Wrede CE, Kunz-Schughart LA, Schölmerich J, Bollheimer LC. Defining high-fat-diet rat models: metabolic and molecular effects of different fat types. *J Mol Endocrinol* 36(3):485-501, 2006
- Buettner R, Schölmerich J, Bollheimer LC. HFDs: modeling the metabolic disorders of human obesity in rodents. *Obesity (Silver Spring)* 15(4):798-808, 2007
- Cade WT. Diabetes-related microvascular and macrovascular diseases in the physical therapy setting. *Phys Ther* 88(11):1322-1335, 2008
- Calder PC. Immunoregulatory and anti-inflammatory effects of n-3 polyunsaturated fatty acids. *Braz J Med Biol Res* 31(4):467-490, 1998
- Calder PC. Omega-3 polyunsaturated fatty acids and inflammatory processes: nutrition or pharmacology? *Br J Clin Pharmacol* 75(3):645-662, 2013
- Cani PD, Amar J, Iglesias MA, Poggi M, Knauf C, Bastelica D, Neyrinck AM, Fava F, Tuohy KM, Chabo C, Waget A, Delmée E, Cousin B, Sulpice T, Chamontin B, Ferrières J, Tanti JF, Gibson GR, Casteilla L, Delzenne NM, Alessi MC, Burcelin R. Metabolic endotoxemia initiates obesity and insulin resistance. *Diabetes* 56(7):1761-1772, 2007
- Cani PD, Bibiloni R, Knauf C, Waget A, Neyrinck AM, Delzenne NM, Burcelin R. Changes in gut microbiota control metabolic endotoxemia-induced inflammation in HFD-induced obesity and diabetes in mice. *Diabetes* 57(6):1470-1481, 2008
- Cannon B, Nedergaard J. Brown adipose tissue: function and physiological significance. *Physiol Rev* 84(1):277-359, 2004

- Cantó C, Auwerx J. AMP-activated protein kinase and its downstream transcriptional pathways. *Cell Mol Life Sci* 67(20):3407-3423, 2010
- Catalano KJ, Stefanovski D, Bergman RN. Critical role of the mesenteric depot versus other intra-abdominal adipose depots in the development of insulin resistance in young rats. *Diabetes* 59(6):1416-1423, 2010
- Chidlow JH Jr, Shukla D, Grisham MB, Kevil CG. Pathogenic angiogenesis in IBD and experimental colitis: new ideas and therapeutic avenues. *Am J Physiol Gastrointest Liver Physiol* 293(1):G5-G18, 2007
- Chow JD, Lawrence RT, Healy ME, Dominy JE, Liao JA, Breen DS, Byrne FL, Kenwood BM, Lackner C, Okutsu S, Mas VR, Caldwell SH, Tomsig JL, Cooney GJ, Puigserver PB, Turner N, James DE, Villén J, Hoehn KL. Genetic inhibition of hepatic acetyl-CoA carboxylase activity increases liver fat and alters global protein acetylation. *Mol Metab* 3(4):419-431, 2014
- Chung JH, Moon J, Lee YS, Chung HK, Lee SM, Shin MJ. Arginase inhibition restores endothelial function in diet-induced obesity. *Biochem Biophys Res Commun* 451(2):179-183, 2014
- Cinti S. The adipose organ. *Prostaglandins Leukot Essent Fatty Acids* 73(1):9-15, 2005a
- Cinti S. Transdifferentiation properties of adipocytes in the adipose organ. *Am J Physiol Endocrinol Metab* 297(5):E977-986, 2009
- Cinti S, Mitchell G, Barbatelli G, Murano I, Ceresi E, Faloia E, Wang S, Fortier M, Greenberg AS, Obin MS. Adipocyte death defines macrophage localization and function in adipose tissue of obese mice and humans. *J Lipid Res* 46(11):2347-2355, 2005b
- Collins S. β -Adrenoceptor Signaling Networks in Adipocytes for Recruiting Stored Fat and Energy Expenditure. *Front Endocrinol (Lausanne)* 2:102, 2012
- Cromer WE, Mathis JM, Granger DN, Chaitanya GV, Alexander JS. Role of the endothelium in inflammatory bowel diseases. *World J Gastroenterol* 17(5):578-593, 2011
- Dahlhoff C, Worsch S, Sailer M, Hummel BA, Fiamoncini J, Uebel K, Obeid R, Scherling C, Geisel J, Bader BL, Daniel H. Methyl-donor supplementation in obese mice prevents the progression of NAFLD, activates AMPK and decreases acyl-carnitine levels. *Mol Metab* 3(5):565-580, 2014
- Dai Z, Qi W, Li C, Lu J, Mao Y, Yao Y, Li L, Zhang T, Hong H, Li S, Zhou T, Yang Z, Yang X, Gao G, Cai W. Dual regulation of adipose triglyceride lipase by pigment epithelium-derived factor: a novel mechanistic insight into progressive obesity. *Mol Cell Endocrinol* 377(1-2):123-134, 2013
- de La Serre CB, Ellis CL, Lee J, Hartman AL, Rutledge JC, Raybould HE. Propensity to HFD-induced obesity in rats is associated with changes in the gut microbiota and gut inflammation. *Am J Physiol Gastrointest Liver Physiol* 299(2):G440-448, 2010
- de Wit NJ, Boekschoten MV, Bachmair EM, Hooiveld GJ, de Groot PJ, Rubio-Aliaga I, Daniel H, Müller M. Dose-dependent effects of dietary fat on development of obesity in relation to intestinal differential gene expression in C57BL/6J mice. *PLoS One* 6(4):e19145, 2011

- de Wit NJ, Bosch-Vermeulen H, de Groot PJ, Hooiveld GJ, Bromhaar MM, Jansen J, Müller M, van der Meer R. The role of the small intestine in the development of dietary fat-induced obesity and insulin resistance in C57BL/6J mice. *BMC Med Genomics* 1:14, 2008
- Deng X, Dong Q, Bridges D, Raghov R, Park EA, Elam MB. Docosahexaenoic acid inhibits proteolytic processing of sterol regulatory element-binding protein-1c (SREBP-1c) via activation of AMP-activated kinase. *Biochim Biophys Acta* 1851(12):1521-1529, 2015
- DiGirolamo M, Fine JB, Tagra K, Rossmanith R. Qualitative regional differences in adipose tissue growth and cellularity in male Wistar rats fed ad libitum. *Am J Physiol* 274(5 Pt 2):R1460-1467, 1998
- Dijk W, Heine M, Vergnes L, Boon MR, Schaart G, Hesselink MK, Reue K, van Marken Lichtenbelt WD, Olivecrona G, Rensen PC, Heeren J, Kersten S. ANGPTL4 mediates shuttling of lipid fuel to brown adipose tissue during sustained cold exposure. *Elife* 4: e08428, 2015
- Ding S, Chi MM, Scull BP, Rigby R, Schwerbrock NM, Magness S, Jobin C, Lund PK. HFD: bacteria interactions promote intestinal inflammation which precedes and correlates with obesity and insulin resistance in mouse. *PLoS One* 5(8):e12191, 2010
- Dinh CH, Szabo A, Yu Y, Camer D, Zhang Q, Wang H, Huang XF. Bardoxolone methyl prevents fat deposition and inflammation in brown adipose tissue and enhances sympathetic activity in mice fed a high-fat diet. *Nutrients* 7(6):4705-4723, 2015
- Dossi CG, Tapia GS, Espinosa A, Videla LA, D'Espessailles A. Reversal of high-fat diet-induced hepatic steatosis by n-3 LCPUFA: role of PPAR- α and SREBP-1c. *J Nutr Biochem* 25(9):977-984, 2014
- Dronavalli S, Duka I, Bakris GL. The pathogenesis of diabetic nephropathy. *Nat Clin Pract Endocrinol Metab* 4(8):444-452, 2008
- Dvorak HF. Vascular permeability to plasma, plasma proteins, and cells: an update. *Curr Opin Hematol* 17(3):225-229, 2010
- Eckel RH, Grundy SM, Zimmet PZ. The metabolic syndrome. *Lancet* 365(9468):1415-1428, 2005
- Eguchi J, Kong X, Tenta M, Wang X, Kang S, Rosen ED. Interferon regulatory factor 4 regulates obesity-induced inflammation through regulation of adipose tissue macrophage polarization. *Diabetes* 62(10):3394-3403, 2013
- Elgazar-Carmon V, Rudich A, Hadad N, Levy R. Neutrophils transiently infiltrate intra-abdominal fat early in the course of high-fat feeding. *J Lipid Res* 49(9):1894-1903, 2008
- Ellmeier W, Sawada S, Littman DR. The regulation of CD4 and CD8 coreceptor gene expression during T cell development. *Annu Rev Immunol* 17:523-554, 1999
- Fatima J, Iqbal CW, Houghton SG, Kasperek MS, Duenes JA, Zheng Y, Sarr MG. Hexose transporter expression and function in mouse small intestine: role of diurnal rhythm. *J Gastrointest Surg* 13(4):634-641, 2009
- Faty A, Ferré P, Commans S. The acute phase protein Serum Amyloid A induces lipolysis and inflammation in human adipocytes through distinct pathways. *PLoS One* 7(4):e34031, 2012

- Feldmann HM, Golozoubova V, Cannon B, Nedergaard J. UCP1 ablation induces obesity and abolishes diet-induced thermogenesis in mice exempt from thermal stress by living at thermoneutrality. *Cell Metab* 9(2):203-209, 2009
- Féletou M. The Endothelium: Part 1: Multiple functions of the endothelial cells-focus on endothelium-derived vasoactive mediators. San Rafael (CA): Morgan & Claypool Life Sciences, 2011
- Ferramosca A, Conte A, Damiano F, Siculella L, Zara V. Differential effects of high-carbohydrate and high-fat diets on hepatic lipogenesis in rats. *Eur J Nutr* 53(4):1103-1114, 2014
- Festuccia WT, Blanchard PG, Deshaies Y. Control of brown adipose tissue glucose and lipid metabolism by PPAR γ . *Front Endocrinol* 2:84, 2011
- Festuccia WT, Kawashita NH, Garofalo MA, Moura MA, Brito SR, Kettelhut IC, Migliorini RH. Control of glyceroneogenic activity in rat brown adipose tissue. *Am J Physiol Regul Integr Comp Physiol* 285(1):R177-182, 2003
- Feuerer M, Herrero L, Cipolletta D, Naaz A, Wong J, Nayer A, Lee J, Goldfine AB, Benoist C, Shoelson S, Mathis D. Lean, but not obese, fat is enriched for a unique population of regulatory T cells that affect metabolic parameters. *Nat Med* 15(8):930-939, 2009
- Fiamoncini J, Lima TM, Hirabara SM, Ecker J, Gorjão R, Romanatto T, ELolimy A, Worsch S, Laumen H, Bader B, Daniel H, Curi R. Medium-chain dicarboxylic acylcarnitines as markers of n-3 PUFA-induced peroxisomal oxidation of fatty acids. *Mol Nutr Food Res* 59(8):1573-1583, 2015
- Fiamoncini J, Turner N, Hirabara SM, Salgado TM, Marçal AC, Leslie S, da Silva SM, Deschamps FC, Luz J, Cooney GJ, Curi R. Enhanced peroxisomal β -oxidation is associated with prevention of obesity and glucose intolerance by fish oil-enriched diets. *Obesity (Silver Spring)* 21(6):1200-1207, 2013
- Fischer K1, Ruiz HH, Jhun K, Finan B, Oberlin DJ, van der Heide V, Kalinovich AV, Petrovic N, Wolf Y, Clemmensen C, Shin AC, Divanovic S, Brombacher F, Glasmacher E, Keipert S, Jastroch M, Nagler J, Schramm KW, Medrikova D, Collden G, Woods SC, Herzig S, Homann D, Jung S, Nedergaard J, Cannon B, Tschöp MH, Müller TD, Buettner C. Alternatively activated macrophages do not synthesize catecholamines or contribute to adipose tissue adaptive thermogenesis. *Nat Med* 23(5):623-630, 2017
- Fischer-Posovszky P, Wang QA, Asterholm IW, Rutkowski JM, Scherer PE. Targeted deletion of adipocytes by apoptosis leads to adipose tissue recruitment of alternatively activated M2 macrophages. *Endocrinology* 152(8):3074-3081, 2011
- Fitzgibbons TP, Kogan S, Aouadi M, Hendricks GM, Straubhaar J, Czech MP. Similarity of mouse perivascular and brown adipose tissues and their resistance to diet-induced inflammation. *Am J Physiol Heart Circ Physiol* 301(4):H1425-1437, 2011
- Flachs P, Horakova O, Brauner P, Rossmeisl M, Pecina P, Franssen-van Hal N, Ruzickova J, Sponarova J, Drahotka Z, Vlcek C, Keijer J, Houstek J, Kopecky J. Polyunsaturated fatty acids of marine origin upregulate mitochondrial biogenesis and induce beta-oxidation in white fat. *Diabetologia* 48(11):2365-2375, 2005
- Flachs P, Rossmeisl M, Kuda O, Kopecky J. Stimulation of mitochondrial oxidative capacity in white fat independent of UCP1: a key to lean phenotype. *Biochim Biophys Acta* 1831(5):986-1003, 2013

- Frayn KN, Karpe F, Fielding BA, Macdonald IA, Coppack SW. Integrative physiology of human adipose tissue. *Int J Obes Relat Metab Disord* 27(8):875-888, 2003
- Fujisaka S, Usui I, Bukhari A, Ikutani M, Oya T, Kanatani Y, Tsuneyama K, Nagai Y, Takatsu K, Urakaze M, Kobayashi M, Tobe K. Regulatory mechanisms for adipose tissue M1 and M2 macrophages in diet-induced obese mice. *Diabetes* 58(11):2574-2582, 2009
- Geraldes P, King GL. Activation of protein kinase C isoforms and its impact on diabetic complications. *Circ Res* 106(8):1319-1331, 2010
- Goldberg IJ, Eckel RH, Abumrad NA. Regulation of fatty acid uptake into tissues: lipoprotein lipase- and CD36-mediated pathways. *J Lipid Res* 50 Suppl:S86-90, 2009
- Gordon S, Martinez FO. Alternative activation of macrophages: mechanism and functions. *Immunity* 32(5):593-604, 2010
- Gorjão R, Verlengia R, Lima TM, Soriano FG, Boaventura MF, Kanunfre CC, Peres CM, Sampaio SC, Otton R, Folador A, Martins EF, Curi TC, Portioli EP, Newsholme P, Curi R. Effect of docosahexaenoic acid-rich fish oil supplementation on human leukocyte function. *Clin Nutr* 25(6):923-938, 2006
- Goyens PL, Spilker ME, Zock PL, Katan MB, Mensink RP. Compartmental modeling to quantify alpha-linolenic acid conversion after longer term intake of multiple tracer boluses. *J Lipid Res* 46(7):1474-1483, 2005
- Granger DN, Senchenkova E. Inflammation and the microcirculation. San Rafael (CA): Morgan & Claypool Life Sciences, 2010
- Grayson TH, Chadha PS, Bertrand PP, Chen H, Morris MJ, Senadheera S, Murphy TV, Sandow SL. Increased caveolae density and caveolin-1 expression accompany impaired NO-mediated vasorelaxation in diet-induced obesity. *Histochem Cell Biol* 139(2):309-321, 2013
- Hageman RS, Wagener A, Hantschel C, Svenson KL, Churchill GA, Brockmann GA. High-fat diet leads to tissue-specific changes reflecting risk factors for diseases in DBA/2J mice. *Physiol Genomics* 42(1):55-66, 2010
- Hao Q, Lillefosse HH, Fjaere E, Myrmet LS, Midtbø LK, Jarlsby RH, Ma T, Jia B, Petersen RK, Sonne SB, Chwalibog A, Frøyland L, Liaset B, Kristiansen K, Madsen L. High-glycemic index carbohydrates abrogate the antiobesity effect of fish oil in mice. *Am J Physiol Endocrinol Metab* 302(9):E1097-1112, 2012
- Hardie DG. Sensing of energy and nutrients by AMP-activated protein kinase. *Am J Clin Nutr* 93(4):891S-6, 2011
- Harms M, Seale P. Brown and beige fat: development, function and therapeutic potential. *Nat Med* 19(10):1252-1263, 2013
- Hariri N, Thibault L. HFD-induced obesity in animal models. *Nutr Res Rev* 23(2):270-299, 2010
- Harris ES, Nelson WJ. VE-cadherin: at the front, center, and sides of endothelial cell organization and function. *Curr Opin Cell Biol* 22(5):651-658, 2010

- Hauner H. Secretory factors from human adipose tissue and their functional role. *Proc Nutr Soc* 64(2): 163-169, 2005
- Herrnberger L, Hennig R, Kremer W, Hellerbrand C, Goepferich A, Kalbitzer HR, Tamm ER. Formation of fenestrae in murine liver sinusoids depends on plasmalemma vesicle-associated protein and is required for lipoprotein passage. *PLoS One* 9(12):e115005, 2014
- Hondares E, Rosell M, Díaz-Delfín J, Olmos Y, Monsalve M, Iglesias R, Villarroya F, Giralt M. Peroxisome proliferator-activated receptor α (PPAR α) induces PPAR γ coactivator 1 α (PGC-1 α) gene expression and contributes to thermogenic activation of brown fat: involvement of PRDM16. *J Biol Chem* 286(50):43112-43122, 2011
- Hotamisligil GS. Inflammation and metabolic disorders. *Nature* 444(7121):860-867, 2006
- Hu G, Place AT, Minshall RD. Regulation of endothelial permeability by Src kinase signaling: vascular leakage versus transcellular transport of drugs and macromolecules. *Chem Biol Interact* 171(2):177-189, 2008
- Huang SC, Everts B, Ivanova Y, O'Sullivan D, Nascimento M, Smith AM, Beatty W, Love-Gregory L, Lam WY, O'Neill CM, Yan C, Du H, Abumrad NA, Urban JF Jr, Artyomov MN, Pearce EL, Pearce EJ. Cell-intrinsic lysosomal lipolysis is essential for alternative activation of macrophages. *Nat Immunol* 15(9): 846-855, 2014
- Huang T, Wahlqvist ML, Li D. Effect of n-3 polyunsaturated fatty acid on gene expression of the critical enzymes involved in homocysteine metabolism. *Nutr J* 11:6, 2012
- Huber J, Löffler M, Bilban M, Reimers M, Kadl A, Todoric J, Zeyda M, Geyeregger R, Schreiner M, Weichhart T, Leitinger N, Waldhäusl W, Stulnig TM. Prevention of HFD-induced adipose tissue remodeling in obese diabetic mice by n-3 polyunsaturated fatty acids. *Int J Obes (Lond)* 31(6):1004-1013, 2007
- Iantorno M, Campia U, Di Daniele N, Nistico S, Forleo GB, Cardillo C, Tesaro M. Obesity, inflammation and endothelial dysfunction. *J Biol Regul Homeost Agents* 28(2):169-176, 2014
- Ibrahim MM. Subcutaneous and visceral adipose tissue: structural and functional differences. *Obes Rev* 11(1):11-18, 2010
- Janovská P, Flachs P, Kazdová L, Kopecký J. Anti-obesity effect of n-3 polyunsaturated fatty acids in mice fed HFD is independent of cold-induced thermogenesis. *Physiol Res* 62(2):153-161, 2013
- Jiang WG, Bryce RP, Horrobin DF, Mansel RE. Regulation of tight junction permeability and occludin expression by polyunsaturated fatty acids. *Biochem Biophys Res Commun* 244(2):414-420, 1998
- Jin L, Lin Z, Xu A. Fibroblast Growth Factor 21 Protects against Atherosclerosis via Fine-Tuning the Multiorgan Crosstalk. *Diabetes Metab J* 40(1):22-31, 2016
- Johnson AM, Costanzo A, Gareau MG, Armando AM, Quehenberger O, Jameson JM, Olefsky JM. High fat diet causes depletion of intestinal eosinophils associated with intestinal permeability. *PLoS One* 10(4):e0122195, 2015
- Jump DB. Fatty acid regulation of hepatic lipid metabolism. *Curr Opin Clin Nutr Metab Care* 14(2):115-120, 2011

- Jump DB, Botolin D, Wang Y, Xu J, Demeure O, Christian B. Docosahexaenoic acid (DHA) and hepatic gene transcription. *Chem Phys Lipids* 153(1):3-13, 2008
- Jurisc G, Detmar M. Lymphatic endothelium in health and disease. *Cell Tissue Res* 335(1):97-108, 2009
- Kahn SE, Hull RL, Utzschneider KM. Mechanisms linking obesity to insulin resistance and type 2 diabetes. *Nature* 444(7121):840-846, 2006
- Kaliannan K, Wang B, Li XY, Kim KJ1, Kang JX. A host-microbiome interaction mediates the opposing effects of omega-6 and omega-3 fatty acids on metabolic endotoxemia. *Sci Rep* 5:11276, 2015
- Kaneko H, Anzai T, Horiuchi K, Morimoto K, Anzai A, Nagai T, Sugano Y, Maekawa Y, Itoh H, Yoshikawa T, Okada Y, Ogawa S, Fukuda K. Tumor necrosis factor- α converting enzyme inactivation ameliorates HFD-induced insulin resistance and altered energy homeostasis. *Circ J* 75(10):2482-2490, 2011
- Kennedy AJ, Ellacott KL, King VL, Hasty AH. Mouse models of the metabolic syndrome. *Dis Model Mech* 3(3-4):156-166, 2010
- Keuschnigg J, Henttinen T, Auvinen K, Karikoski M, Salmi M, Jalkanen S. The prototype endothelial marker PAL-E is a leukocyte trafficking molecule. *Blood* 114(2):478-484, 2009
- Kim HK, Della-Fera M, Lin J, Baile CA. Docosahexaenoic acid inhibits adipocyte differentiation and induces apoptosis in 3T3-L1 preadipocytes. *J Nutr* 136(12):2965-2969, 2006
- Kim J, Okla M, Erickson A, Carr T, Natarajan SK, Chung S. Eicosapentaenoic Acid Potentiates Brown Thermogenesis through FFAR4-dependent Up-regulation of miR-30b and miR-378. *J Biol Chem* 291(39):20551-20562, 2016
- Kim W, Khan NA, McMurray DN, Prior IA, Wang N, Chapkin RS. Regulatory activity of polyunsaturated fatty acids in T-cell signaling. *Prog Lipid Res* 49(3):250-261, 2010
- Kintscher U, Hartge M, Hess K, Foryst-Ludwig A, Clemenz M, Wabitsch M, Fischer-Posovszky P, Barth TF, Dragun D, Skurk T, Hauner H, Blüher M, Unger T, Wolf AM, Knippschild U, Hombach V, Marx N. T-lymphocyte infiltration in visceral adipose tissue: a primary event in adipose tissue inflammation and the development of obesity-mediated insulin resistance. *Arterioscler Thromb Vasc Biol* 28(7):1304-1310, 2008
- Kless C, Müller VM, Schüppel VL, Lichtenegger M, Rychlik M, Daniel H, Klingenspor M, Haller D. Diet-induced obesity causes metabolic impairment independent of alterations in gut barrier integrity. *Mol Nutr Food Res* 59(5):968-978, 2015
- Kless C, Rink N, Rozman J, Klingenspor M. Proximate causes for diet-induced obesity in laboratory mice: a case study. *Eur J Clin Nutr* 71(3):306-317, 2017
- Kolak M, Westerbacka J, Velagapudi VR, Wågsäter D, Yetukuri L, Makkonen J, Rissanen A, Häkkinen AM, Lindell M, Bergholm R, Hamsten A, Eriksson P, Fisher RM, Oresic M, Yki-Järvinen H. Adipose tissue inflammation and increased ceramide content characterize subjects with high liver fat content independent of obesity. *Diabetes* 56(8):1960-1968, 2007

- Komarova Y, Malik AB. Regulation of endothelial permeability via paracellular and transcellular transport pathways. *Annu Rev Physiol* 72:463-493, 2010
- Kong W, Yen JH, Ganea D. Docosahexaenoic acid prevents dendritic cell maturation, inhibits antigen-specific Th1/Th17 differentiation and suppresses experimental autoimmune encephalomyelitis. *Brain Behav Immun* 25(5):872-882, 2011
- Kosteli A, Sugaru E, Haemmerle G, Martin JF, Lei J, Zechner R, Ferrante AW Jr. Weight loss and lipolysis promote a dynamic immune response in murine adipose tissue. *J Clin Invest* 120(10):3466-3479, 2010
- Kuda O. Bioactive metabolites of docosahexaenoic acid. *Biochimie* 136:12-20, 2017
- Kumashiro N, Erion DM, Zhang D, Kahn M, Beddow SA, Chu X, Still CD, Gerhard GS, Han X, Dziura J, Petersen KF, Samuel VT, Shulman GI. Cellular mechanism of insulin resistance in nonalcoholic fatty liver disease. *Proc Natl Acad Sci U S A* 108(39):16381-16385, 2011
- La Rovere MT, Christensen JH. The autonomic nervous system and cardiovascular disease: role of n-3 PUFAs. *Vascul Pharmacol* 71:1-10, 2015
- Lafferty MJ, Bradford KC, Erie DA, Neher SB. Angiopoietin-like protein 4 inhibition of lipoprotein lipase: evidence for reversible complex formation. *J Biol Chem* 288(40):28524-28534, 2013
- Lam YY, Ha CW, Hoffmann JM, Oscarsson J, Dinudom A, Mather TJ, Cook DI, Hunt NH, Caterson ID, Holmes AJ, Storlien LH. Effects of dietary fat profile on gut permeability and microbiota and their relationships with metabolic changes in mice. *Obesity (Silver Spring)* 23(7):1429-1439, 2015
- Lavie CJ, Milani RV, Mehra MR, Ventura HO. Omega-3 polyunsaturated fatty acids and cardiovascular diseases. *J Am Coll Cardiol* 54(7):585-594, 2009
- Lee JY, Plakidas A, Lee WH, Heikkinen A, Chanmugam P, Bray G, Hwang DH. Differential modulation of Toll-like receptors by fatty acids: preferential inhibition by n-3 polyunsaturated fatty acids. *J Lipid Res* 44(3):479-486, 2003
- Lee YH, Petkova AP, Granneman JG. Identification of an adipogenic niche for adipose tissue remodeling and restoration. *Cell Metab* 18(3):355-367, 2013
- Lemonnier D. Effect of age, sex, and sites on the cellularity of the adipose tissue in mice and rats rendered obese by a high-fat diet. *J Clin Invest* 51(11):2907-2915, 1972
- Li H, Lelliott C, Hakansson P, Ploj K, Tuneld A, Verolin-Johansson M, Benthem L, Carlsson B, Storlien L, Michaelsson E. Intestinal, adipose, and liver inflammation in diet-induced obese mice. *Metabolism* 57(12):1704-1710, 2008
- Livak KJ, Schmittgen TD. Analysis of relative gene expression data using real-time quantitative PCR and the 2⁻($\Delta\Delta C_T$) Method. *Methods* 25(4):402-408, 2001
- Lodhi IJ, Semenkovich CF. Peroxisomes: a nexus for lipid metabolism and cellular signaling. *Cell Metab* 19(3):380-392, 2014

- Lorente-Cebrián S, Costa AG, Navas-Carretero S, Zabala M, Martínez JA, Moreno-Aliaga MJ. Role of omega-3 fatty acids in obesity, metabolic syndrome, and cardiovascular diseases: a review of the evidence. *J Physiol Biochem* 69(3):633-651, 2013
- Lowell BB, Spiegelman BM. Towards a molecular understanding of adaptive thermogenesis. *Nature* 404(6778):652-660, 2000
- Ludwig T, Worsch S, Heikenwalder M, Daniel H, Hauner H, Bader BL. Metabolic and immunomodulatory effects of n-3 fatty acids are different in mesenteric and epididymal adipose tissue of diet-induced obese mice. *Am J Physiol Endocrinol Metab* 304(11):E1140-1156, 2013
- Lumeng CN, Bodzin JL, Saltiel AR. Obesity induces a phenotypic switch in adipose tissue macrophage polarization. *J Clin Invest* 117(1):175-184, 2007
- Lv Y, Zhang X, Sun Y, Zhang S. Activation of NF- κ B contributes to production of pig-major acute protein and serum amyloid A in pigs experimentally infected with porcine circovirus type 2. *Res Vet Sci* 95(3):1235-1240, 2013
- Martinez FO, Sica A, Mantovani A, Locati M. Macrophage activation and polarization. *Front Biosci* 13:453-461, 2008
- Masoodi M, Kuda O, Rossmeisl M, Flachs P, Kopecky J. Lipid signaling in adipose tissue: Connecting inflammation & metabolism. *Biochim Biophys Acta* 1851(4):503-518, 2015
- Masters SL, Latz E, O'Neill LA. The inflammasome in atherosclerosis and type 2 diabetes. *Sci Transl Med* 3(81):81ps17, 2011
- Matsuzawa Y, Shimomura I, Nakamura T, Keno Y, Tokunaga K. Pathophysiology and pathogenesis of visceral fat obesity. *Ann N Y Acad Sci* 748:399-406, 1995
- Mazzucotelli A, Viguerie N, Tiraby C, Annicotte JS, Mairal A, Klimcakova E, Lepin E, Delmar P, Dejean S, Tavernier G, Lefort C, Hidalgo J, Pineau T, Fajas L, Clément K, Langin D. The transcriptional coactivator peroxisome proliferator activated receptor (PPAR)gamma coactivator-1 alpha and the nuclear receptor PPAR alpha control the expression of glycerol kinase and metabolism genes independently of PPAR gamma activation in human white adipocytes. *Diabetes* 56(10):2467-2475, 2007
- Mebius RE, Kraal G. Structure and function of the spleen. *Nat Rev Immunol* 5(8):606-616, 2005
- Mensink GB, Schienkiewitz A, Haftenberger M, Lampert T, Ziese T, Scheidt-Nave C. Overweight and obesity in Germany: results of the German Health Interview and Examination Survey for Adults (DEGS1). *Bundesgesundheitsblatt Gesundheitsforschung Gesundheitsschutz* 56(5-6):786-794, 2013
- Molofsky AB, Nussbaum JC, Liang HE, Van Dyken SJ, Cheng LE, Mohapatra A, Chawla A, Locksley RM. Innate lymphoid type 2 cells sustain visceral adipose tissue eosinophils and alternatively activated macrophages. *J Exp Med* 210(3):535-549, 2013
- Mosser DM, Edwards JP. Exploring the full spectrum of macrophage activation. *Nat Rev Immunol* 8(12):958-969, 2008
- Mozaffarian D, Wu JH. (n-3) fatty acids and cardiovascular health: are effects of EPA and DHA shared or complementary? *J Nutr* 142(3):614S-625S, 2012

- Müller VM, Zietek T, Rohm F, Fiamoncini J, Lagkouvardos I, Haller D, Clavel T, Daniel H. Gut barrier impairment by HFD in mice depends on housing conditions. *Mol Nutr Food Res* 60(4):897-908, 2016
- Murray PJ, Wynn TA. Protective and pathogenic functions of macrophage subsets. *Nat Rev Immunol* 11(11):723-737, 2011
- Musiek ES, Brooks JD, Joo M, Brunoldi E, Porta A, Zanoni G, Vidari G, Blackwell TS, Montine TJ, Milne GL, McLaughlin B, Morrow JD. Electrophilic cyclopentenone neuroprostanes are anti-inflammatory mediators formed from the peroxidation of the omega-3 polyunsaturated fatty acid docosahexaenoic acid. *J Biol Chem* 283(29):19927-19935, 2008
- Nagatsu T. Tyrosine hydroxylase: Human isoforms, structure and regulation in physiology and pathology. *Essays Biochem* 30:15-35, 1995
- Nettleton JA, Jebb S, Risérus U, Koletzko B, Fleming J. Role of dietary fats in the prevention and treatment of the metabolic syndrome. *Ann Nutr Metab* 64(2):167-178, 2014
- Newberry EP, Kennedy SM, Xie Y, Sternard BT, Luo J, Davidson NO. Diet-induced obesity and hepatic steatosis in L-Fabp / mice is abrogated with SF, but not PUFA, feeding and attenuated after cholesterol supplementation. *Am J Physiol Gastrointest Liver Physiol* 294(1):G307-314, 2008
- Nguyen KD, Qiu Y, Cui X, Goh YP, Mwangi J, David T, Mukundan L, Brombacher F, Locksley RM, Chawla A. Alternatively activated macrophages produce catecholamines to sustain adaptive thermogenesis. *Nature* 480(7375):104-108, 2011
- Nielsen TS, Jessen N, Jørgensen JO, Møller N, Lund S. Dissecting adipose tissue lipolysis: molecular regulation and implications for metabolic disease. *J Mol Endocrinol* 52(3):R199-222, 2014
- Nishimura S, Manabe I, Nagasaki M, Eto K, Yamashita H, Ohsugi M, Otsu M, Hara K, Ueki K, Sugiura S, Yoshimura K, Kadowaki T, Nagai R. CD8+ effector T cells contribute to macrophage recruitment and adipose tissue inflammation in obesity. *Nat Med* 15(8):914-920, 2009
- Nomiyama T, Perez-Tilve D, Ogawa D, Gizard F, Zhao Y, Heywood EB, Jones KL, Kawamori R, Cassis LA, Tschöp MH, Bruemmer D. Osteopontin mediates obesity-induced adipose tissue macrophage infiltration and insulin resistance in mice. *J Clin Invest* 117(10):2877-2888, 2007
- Obstfeld AE, Sugaru E, Thearle M, Francisco AM, Gayet C, Ginsberg HN, Ables EV, Ferrante AW Jr. C-C chemokine receptor 2 (CCR2) regulates the hepatic recruitment of myeloid cells that promote obesity-induced hepatic steatosis. *Diabetes* 59(4):916-925, 2010
- Odegaard JI, Chawla A. Mechanisms of macrophage activation in obesity-induced insulin resistance. *Nat Clin Pract Endocrinol Metab* 4(11):619-626, 2008
- Oh DY, Talukdar S, Bae EJ, Imamura T, Morinaga H, Fan W, Li P, Lu WJ, Watkins SM, Olefsky JM. GPR120 is an omega-3 fatty acid receptor mediating potent anti-inflammatory and insulin-sensitizing effects. *Cell* 142(5):687-698, 2010
- Ohinata H, Saha SK, Ohno T, Hata N, Misawa Y, Kuroshima A. Effect of dietary docosahexaenoic acid on in vitro thermogenesis and fatty acid compositions of brown adipose tissue. *Jpn J Physiol* 48(3):189-196, 1998

- Olefsky JM, Glass CK. Macrophages, inflammation, and insulin resistance. *Annu Rev Physiol* 72:219-246, 2010
- Oudart H, Groscolas R, Calgari C, Nibbelink M, Leray C, Le Maho Y, Malan A. Brown fat thermogenesis in rats fed HFDs enriched with n-3 polyunsaturated fatty acids. *Int J Obes Relat Metab Disord* 21(11):955-962, 1997
- Ouellet V, Labbé SM, Blondin DP, Phoenix S, Guérin B, Haman F, Turcotte EE, Richard D, Carpentier AC. Brown adipose tissue oxidative metabolism contributes to energy expenditure during acute cold exposure in humans. *J Clin Invest* 122(2):545-552, 2012
- Ousmaal Mel F, Martínez MC, Andriantsitohaina R, Chabane K, Gaceb A, Mameri S, Giaimis J, Baz A. Increased monocyte/neutrophil and pro-coagulant microparticle levels and overexpression of aortic endothelial caveolin-1 β in dyslipidemic sand rat, *Psammomys obesus*. *J Diabetes Complications* 30(1):21-29, 2016
- Owen BM, Ding X, Morgan DA, Coate KC, Bookout AL, Rahmouni K, Kliewer SA, Mangelsdorf DJ. FGF21 acts centrally to induce sympathetic nerve activity, energy expenditure, and weight loss. *Cell Metab* 20(4):670-677, 2014
- Ozcan U, Cao Q, Yilmaz E, Lee AH, Iwakoshi NN, Ozdelen E, Tuncman G, Görgün C, Glimcher LH, Hotamisligil GS. Endoplasmic reticulum stress links obesity, insulin action, and type 2 diabetes. *Science* 306(5695):457-461, 2004
- Pacher P, Beckman JS, Liaudet L. Nitric oxide and peroxynitrite in health and disease. *Physiol Rev* 87(1):315-424, 2007
- Pavlisova J, Bardova K, Stankova B, Tvrzicka E, Kopecky J, Rossmeisl M. Corn oil versus lard: Metabolic effects of omega-3 fatty acids in mice fed obesogenic diets with different fatty acid composition. *Biochimie pii: S0300-9084(15)00209-6*, 2015
- Peng XL, Qu W, Wang LZ, Huang BQ, Ying CJ, Sun XF, Hao LP. Resveratrol ameliorates high glucose and high-fat/sucrose diet-induced vascular hyperpermeability involving Cav-1/eNOS regulation. *PLoS One* 9(11):e113716, 2014
- Plaza-Diaz J, Gomez-Llorente C, Fontana L, Gil A. Modulation of immunity and inflammatory gene expression in the gut, in inflammatory diseases of the gut and in the liver by probiotics. *World J Gastroenterol* 20(42):15632-15649, 2014
- Porcheray F, Viaud S, Rimaniol AC, Léone C, Samah B, Dereuddre-Bosquet N, Dormont D, Gras G. Macrophage activation switching: an asset for the resolution of inflammation. *Clin Exp Immunol* 142(3):481-489, 2005
- Poudyal H, Panchal SK, Diwan V, Brown L. Omega-3 fatty acids and metabolic syndrome: effects and emerging mechanisms of action. *Prog Lipid Res* 50(4):372-387, 2011
- Prieur X, Mok CY, Velagapudi VR, Núñez V, Fuentes L, Montaner D, Ishikawa K, Camacho A, Barbarroja N, O'Rahilly S, Sethi JK, Dopazo J, Orešič M, Ricote M, Vidal-Puig A. Differential lipid partitioning between adipocytes and tissue macrophages modulates macrophage lipotoxicity and M2/M1 polarization in obese mice. *Diabetes* 60(3):797-809, 2011

- Privratsky JR, Newman PJ. PECAM-1: regulator of endothelial junctional integrity. *Cell Tissue Res* 355(3):607-619, 2014
- Qiu Y, Nguyen KD, Odegaard JI, Cui X, Tian X, Locksley RM, Palmiter RD, Chawla A. Eosinophils and type 2 cytokine signaling in macrophages orchestrate development of functional beige fat. *Cell* 157(6):1292-1308, 2014
- Quesada-López T, Cereijo R, Turatsinze JV, Planavila A, Cairó M, Gavaldà-Navarro A, Peyrou M, Moure R, Iglesias R, Giralt M, Eizirik DL, Villarroya F. The lipid sensor GPR120 promotes brown fat activation and FGF21 release from adipocytes. *Nat Commun* 7:13479, 2016
- Rakhshandehroo M, Sanderson LM, Matilainen M, Stienstra R, Carlberg C, de Groot PJ, Müller M, Kersten S. Comprehensive analysis of PPARalpha-dependent regulation of hepatic lipid metabolism by expression profiling. *PPAR Res* 2007:26839, 2007
- Rausch ME, Weisberg S, Vardhana P, Tortoriello DV. Obesity in C57BL/6J mice is characterized by adipose tissue hypoxia and cytotoxic T-cell infiltration. *Int J Obes (Lond)* 32(3):451-463, 2008
- Reddy NL, Tan BK, Barber TM, Randeve HS. Brown adipose tissue: endocrine determinants of function and therapeutic manipulation as a novel treatment strategy for obesity. *BMC Obesity* 1:13, 2014
- Rial E, Poustie A, Nicholls DG. Brown adipose tissue mitochondria: the regulation of the 32,000-Mr uncoupling protein by fatty acids and purine nucleotides. *Eur J Biochem* 173(1-2):197-203, 1983
- Richard D, Kefi K, Barbe U, Bausero P, Visioli F. Polyunsaturated fatty acids as antioxidants. *Pharmacol Res* 57(6):451-455, 2008
- Rigor RR, Shen Q, Pivetti CD, Wu MH, Yuan SY. Myosin light chain kinase signaling in endothelial barrier dysfunction. *Med Res Rev* 33(5):911-933, 2013
- Roberts OL, Dart C. cAMP signalling in the vasculature: the role of Epac (exchange protein directly activated by cAMP). *Biochem Soc Trans* 42(1):89-97, 2014
- Roberts-Toler C, O'Neill BT, Cypess AM. Diet-induced obesity causes insulin resistance in mouse brown adipose tissue. *Obesity (Silver Spring)* 23(9):1765-1770, 2015
- Rothwell NJ, Stock MJ. A role for brown adipose tissue in diet-induced thermogenesis. *Nature* 281(5726):31-35, 1979
- Rozga J, Piątek T, Małkowski P. Human albumin: old, new, and emerging applications. *Ann Transplant* 18:205-217, 2013
- Rui L. Energy metabolism in the liver. *Compr Physiol* 4(1):177-197, 2014
- Russell FD, Bürgin-Maunders CS. Distinguishing health benefits of eicosapentaenoic and docosahexaenoic acids. *Mar Drugs* 10(11):2535-2559, 2012
- Russo GL. Dietary n-6 and n-3 polyunsaturated fatty acids: from biochemistry to clinical implications in cardiovascular prevention. *Biochem Pharmacol* 77(6):937-946, 2009

- Ruzickova J, Rossmeisl M, Prazak T, Flachs P, Sponarova J, Veck M, Tvrzicka E, Bryhn M, Kopecky J. Omega-3 PUFA of marine origin limit diet-induced obesity in mice by reducing cellularity of adipose tissue. *Lipids* 39(12):1177-1185, 2004
- Sadurskis A, Dicker A, Cannon B, Nedergaard J. Polyunsaturated fatty acids recruit brown adipose tissue: increased UCP content and NST capacity. *Am J Physiol Endocrinol Metab* 269(2 Pt 1):E351-360, 1995
- Sampath H, Ntambi JM. Polyunsaturated fatty acid regulation of genes of lipid metabolism. *Annu Rev Nutr* 25:317-340, 2005
- Sanders MA, Madoux F, Mladenovic L, Zhang H, Ye X, Angrish M, Mottillo EP, Caruso JA, Halvorsen G, Roush WR, Chase P, Hodder P, Granneman JG. Endogenous and Synthetic ABHD5 Ligands Regulate ABHD5-Perilipin Interactions and Lipolysis in Fat and Muscle. *Cell Metab* 22(5):851-860, 2015
- Sarin H. Physiologic upper limits of pore size of different blood capillary types and another perspective on the dual pore theory of microvascular permeability. *J Angiogenes Res* 2:14, 2010
- Scarpulla RC, Vega RB, Kelly DP. Transcriptional integration of mitochondrial biogenesis. *Trends Endocrinol Metab* 23(9):459-466, 2012
- Schäffler A, Scholmerich J, Buchler C. Mechanisms of disease: adipocytokines and visceral adipose tissue--emerging role in intestinal and mesenteric diseases. *Nat Clin Pract Gastroenterol Hepatol* 2(2):103-111, 2005
- Schilperoort M, Hoeke G, Kooijman S, Rensen PC. Relevance of lipid metabolism for brown fat visualization and quantification. *Curr Opin Lipidol* 27(3):242-248, 2016
- Schmitz G, Ecker J. The opposing effects of n-3 and n-6 fatty acids. *Prog Lipid Res* 47(2):147-155, 2008
- Sell H, Berger JP, Samson P, Castriota G, Lalonde J, Deshaies Y, Richard D. Peroxisome proliferator-activated receptor gamma agonism increases the capacity for sympathetically mediated thermogenesis in lean and ob/ob mice. *Endocrinology* 145(8):3925-3934, 2004
- Serhan CN, Chiang N, Van Dyke TE. Resolving inflammation: dual anti-inflammatory and pro resolution lipid mediators. *Nat Rev Immunol* 8(5):349-361, 2008
- Shaul ME, Bennett G, Strissel KJ, Greenberg AS, Obin MS. Dynamic, M2-like remodeling phenotypes of CD11c+ adipose tissue macrophages during HFD--induced obesity in mice. *Diabetes* 59(5):1171-1181, 2010
- Shikano M, Masuzawa Y, Yazawa K, Takayama K, Kudo I, Inoue K. Complete discrimination of docosahexaenoate from arachidonate by 85 kDa cytosolic phospholipase A2 during the hydrolysis of diacyl- and alkenylacylglycerophosphoethanolamine. *Biochim Biophys Acta* 1212(2):211-216, 1994
- Shimizu I, Walsh K. The whitening of brown fat and its implications for weight management in obesity. *Curr Obes Rep* 4(2):224-229, 2015
- Simopoulos AP. Importance of the omega-6/omega-3 balance in health and disease: evolutionary aspects of diet. *World Rev Nutr Diet* 102:10-21, 2011
- Singh M. Essential fatty acids, DHA and human brain. *Indian J Pediatr* 72(3):239-242, 2005

- Smith PD, Smythies LE, Shen R, Greenwell-Wild T, Gliozzi M, Wahl SM. Intestinal macrophages and response to microbial encroachment. *Mucosal Immunol* 4(1):31-42, 2011
- Smith PK, Krohn RI, Hermanson GT, Mallia AK, Gartner FH, Provenzano MD, Fujimoto EK, Goetze NM, Olson BJ, Klenk DC. Measurement of protein using bicinchoninic acid. *Anal Biochem* 150(1):76-85, 1985
- Spadoni I, Zagato E, Bertocchi A, Paolinelli R, Hot E, Di Sabatino A, Caprioli F, Bottiglieri L, Oldani A, Viale G, Penna G, Dejana E, Rescigno M. A gut-vascular barrier controls the systemic dissemination of bacteria. *Science* 350(6262):830-834, 2015
- Spector AA, Yorek MA. Membrane lipid composition and cellular function. *J Lipid Res* 26(9):1015-1035, 1985
- Stanford KI, Middelbeek RJ, Townsend KL, An D, Nygaard EB, Hitchcox KM, Markan KR, Nakano K, Hirshman MF, Tseng YH, Goodyear LJ. Brown adipose tissue regulates glucose homeostasis and insulin sensitivity. *J Clin Invest* 123(1):215-223, 2013
- Stapleton PA, James ME, Goodwill AG, Frisbee JC. Obesity and vascular dysfunction. *Pathophysiology* 15(2):79-89, 2008
- Strissel KJ, Stancheva Z, Miyoshi H, Perfield JW II, DeFuria J, Jick Z, Greenberg AS, Obin MS. Adipocyte death, adipose tissue remodeling, and obesity complications. *Diabetes* 56(12):2910-2918, 2007
- Stulnig TM, Huber J, Leitinger N, Imre EM, Angelisova P, Nowotny P, Waldhausl W. Polyunsaturated eicosapentaenoic acid displaces proteins from membrane rafts by altering raft lipid composition. *J Biol Chem* 276(40):37335-37340, 2001
- Suárez-Zamorano N, Fabbiano S, Chevalier C, Stojanović O, Colin DJ, Stevanović A, Veyrat-Durebex C, Tarallo V, Rigo D, Germain S, Iliavska M, Montet X, Seimbille Y, Hapfelmeier S, Trajkovski M. Microbiota depletion promotes browning of white adipose tissue and reduces obesity. *Nat Med* 21(12):1497-1501, 2015
- Suganami T, Tanimoto-Koyama K, Nishida J, Itoh M, Yuan X, Mizuarai S, Kotani H, Yamaoka S, Miyake K, Aoe S, Kamei Y, Ogawa Y. Role of the Toll-like receptor 4/NF-kappaB pathway in saturated fatty acid-induced inflammatory changes in the interaction between adipocytes and macrophages. *Arterioscler Thromb Vasc Biol* 27(1):84-91, 2007
- Sun Y, Hu G, Zhang X, Minshall RD. Phosphorylation of caveolin-1 regulates oxidant-induced pulmonary vascular permeability via paracellular and transcellular pathways. *Circ Res* 105(7):676-685, 2009
- Suzuki T. Regulation of intestinal epithelial permeability by tight junctions. *Cell Mol Life Sci* 70(4):631-659, 2013
- Svenson KL, Von Smith R, Magnani PA, Suetin HR, Paigen B, Naggert JK, Li R, Churchill GA, Peters LL. Multiple trait measurements in 43 inbred mouse strains capture the phenotypic diversity characteristic of human populations. *J Appl Physiol* 102(6):2369-2378, 2007
- Takeuchi Y, Yahagi N, Izumida Y, Nishi M, Kubota M, Teraoka Y, Yamamoto T, Matsuzaka T, Nakagawa Y, Sekiya M, Iizuka Y, Ohashi K, Osuga J, Gotoda T, Ishibashi S, Itaka K, Kataoka K, Nagai R, Yamada N, Kadowaki T, Shimano H. Polyunsaturated fatty acids selectively suppress sterol regulatory element-

- binding protein-1 through proteolytic processing and autoloop regulatory circuit. *J Biol Chem* 285(15):11681-11691, 2010
- Tang L, Okamoto S, Shiuchi T, Toda C, Takagi K, Sato T, Saito K, Yokota S, Minokoshi Y. Sympathetic nerve activity maintains an anti-inflammatory state in adipose tissue in male mice by inhibiting TNF- α gene expression in macrophages. *Endocrinology* 156(10):3680-3694, 2015
- Tchkonia T, Thomou T, Zhu Y, Karagiannides I, Pothoulakis C, Jensen MD, Kirkland JL. Mechanisms and metabolic implications of regional differences among fat depots. *Cell Metab* 17(5):644-656, 2013
- Tchoukalova YD, Votruba SB, Tchkonia T, Giorgadze N, Kirkland JL, Jensen MD. Regional differences in cellular mechanisms of adipose tissue gain with overfeeding. *Proc Natl Acad Sci U S A* 107(42):18226-18231, 2010
- Tilg H, Moschen AR. Adipocytokines: mediators linking adipose tissue, inflammation and immunity. *Nat Rev Immunol* 6(10):772-783, 2006
- Titos E, Rius B, González-Pérez A, López-Vicario C, Morán-Salvador E, Martínez-Clemente M, Arroyo V, Clària J. Resolvin D1 and its precursor docosahexaenoic acid promote resolution of adipose tissue inflammation by eliciting macrophage polarization toward an M2-like phenotype. *J Immunol* 187(10):5408-5418, 2011
- Todoric J, Löffler M, Huber J, Bilban M, Reimers M, Kadl A, Zeyda M, Waldhäusl W, Stulnig TM. Adipose tissue inflammation induced by HFD in obese diabetic mice is prevented by n-3 polyunsaturated fatty acids. *Diabetologia* 49(9):2109-2119, 2006
- Tontonoz P, Spiegelman BM. Fat and beyond: the diverse biology of PPAR γ . *Annu Rev Biochem* 77:289-312, 2008
- Trayhurn P. Hypoxia and adipose tissue function and dysfunction in obesity. *Physiol Rev* 93(1):1-21, 2013
- Tseng Y, Cypess AM, Kahn R. Cellular bioenergetics as a target for obesity therapy. *Nat Rev Drug Discov* 9(6):465-482, 2010
- van Dam AD, Kooijman S, Schilperoort M, Rensen PC, Boon MR. Regulation of brown fat by AMP-activated protein kinase. *Trends Mol Med* 21(9):571-579, 2015
- van Schothorst EM, Flachs P, Franssen-van Hal NL, Kuda O, Bunschoten A, Molthoff J, Vink C, Hooiveld GJ, Kopecky J, Keijer J. Induction of lipid oxidation by polyunsaturated fatty acids of marine origin in small intestine of mice fed a HFD. *BMC Genomics* 10:110, 2009
- Vergnes L, Chin R, Young SG, Reue K. Heart-type fatty acid-binding protein is essential for efficient brown adipose tissue fatty acid oxidation and cold tolerance. *J Biol Chem* 286(1):380-390, 2011
- Villanueva CJ, Vergnes L, Wang J, Drew BG, Hong C, Tu Y, Hu Y, Peng X, Xu F, Saez E, Wroblewski K, Hevener AL, Reue K, Fong LG, Young SG, Tontonoz P. Adipose subtype-selective recruitment of TLE3 or Prdm16 by PPAR γ specifies lipid storage versus thermogenic gene programs. *Cell Metab* 17(3):423-435, 2013

- Villanueva CJ, Waki H, Godio C, Nielsen R, Chou WL, Vargas L, Wroblewski K, Schmedt C, Chao LC, Boyadjian R, Mandrup S, Hevener A, Saez E, Tontonoz P. TLE3 is a dual-function transcriptional coregulator of adipogenesis. *Cell Metab* 13(4):413-427, 2011
- Villarroya F, Vidal-Puig A. Beyond the sympathetic tone: the new brown fat activators. *Cell Metab* 17(5):638-643, 2013b
- Villarroya J, Cereijo R, Villarroya F. An endocrine role for brown adipose tissue? *Am J Physiol Endocrinol Metab* 305(5):E567-572, 2013a
- Violante S, Ijlst L, Te Brinke H, Koster J, Tavares de Almeida I, Wanders RJ, Ventura FV, Houten SM. Peroxisomes contribute to the acylcarnitine production when the carnitine shuttle is deficient. *Biochim Biophys Acta* 1831(9):1467-1474, 2013
- Vitali A, Murano I, Zingaretti MC, Frontini A, Ricquier D, Cinti S. The adipose organ of obesity-prone C57BL/6J mice is composed of mixed white and brown adipocytes. *J Lipid Res* 53(4):619-629, 2012
- Wanders RJ, Komen J, Kemp S. Fatty acid omega-oxidation as a rescue pathway for fatty acid oxidation disorders in humans. *FEBS J* 278(2):182-194, 2011
- Wanders RJ, Waterham HR, Ferdinandusse S. Metabolic Interplay between Peroxisomes and Other Subcellular Organelles Including Mitochondria and the Endoplasmic Reticulum. *Front Cell Dev Biol* 3:83, 2016
- Wang L, Lim EJ, Toborek M, Hennig B. The role of fatty acids and caveolin-1 in tumor necrosis factor alpha-induced endothelial cell activation. *Metabolism* 57(10):1328-1339, 2008
- Watanabe M, Houten SM, Matakai C, Christoffolete MA, Kim BW, Sato H, Messaddeq N, Harney JW, Ezaki O, Kodama T, Schoonjans K, Bianco AC, Auwerx J. Bile acids induce energy expenditure by promoting intracellular thyroid hormone activation. *Nature* 439(7075):484-489, 2006
- Weber GF, Cantor H. The immunology of Eta-1/osteopontin. *Cytokine Growth Factor Rev* 7(3):241-248, 1996
- Weisberg SP, McCann D, Desai M, Rosenbaum M, Leibel RL, Ferrante AW Jr. Obesity is associated with macrophage accumulation in adipose tissue. *J Clin Invest* 112(12):1796-1808, 2003
- Wentworth JM, Naselli G, Brown WA, Doyle L, Phipson B, Smyth GK, Wabitsch M, O'Brien PE, Harrison LC. Pro-inflammatory CD11c+CD206+ adipose tissue macrophages are associated with insulin resistance in human obesity. *Diabetes* 59(7):1648-1656, 2010
- West DB, York B. Dietary fat, genetic predisposition, and obesity: lessons from animal models. *Am J Clin Nutr* 67(3 Suppl):505S-512S, 1998
- West M. Dead adipocytes and metabolic dysfunction: recent progress. *Curr Opin Endocrinol Diabetes Obes* 16(2):178-182, 2009
- WHO 2015, Fact sheet N°311, Obesity and overweight
(<http://www.who.int/mediacentre/factsheets/fs311/en/>)

- Winer DA, Winer S, Shen L, Wadia PP, Yantha J, Paltser G, Tsui H, Wu P, Davidson MG, Alonso MN, Leong HX, Glassford A, Caimol M, Kenkel JA, Tedder TF, McLaughlin T, Miklos DB, Dosch HM, Engleman EG. B cells promote insulin resistance through modulation of T cells and production of pathogenic IgG antibodies. *Nat Med* 17(5):610-617, 2011
- Wisniewska-Kruk J, van der Wijk AE, van Veen HA, Gorgels TG, Vogels IM, Versteeg D, Van Noorden CJ, Schlingemann RO, Klaassen I. Plasmalemma vesicle-associated protein has a key role in blood-retinal barrier loss. *Am J Pathol* 186(4):1044-1054, 2016
- Wu D, Molofsky AB, Liang HE, Ricardo-Gonzalez RR, Jouihan HA, Bando JK, Chawla A, Locksley RM. Eosinophils sustain adipose alternatively activated macrophages associated with glucose homeostasis. *Science* 332(6026):243-247, 2011
- Wu J, Boström P, Sparks LM, Ye L, Choi JH, Giang AH, Khandekar M, Virtanen KA, Nuutila P, Schaart G, Huang K, Tu H, van Marken Lichtenbelt WD, Hoeks J, Enerbäck S, Schrauwen P, Spiegelman BM. Beige adipocytes are a distinct type of thermogenic fat cell in mouse and human. *Cell* 150(2):366-376, 2012a
- Wu L, Parekh VV, Gabriel CL, Bracy DP, Marks-Shulman PA, Tamboli RA, Kim S, Mendez-Fernandez YV, Besra GS, Lomenick JP, Williams B, Wasserman DH, Van Kaer L. Activation of invariant natural killer T cells by lipid excess promotes tissue inflammation, insulin resistance, and hepatic steatosis in obese mice. *Proc Natl Acad Sci U S A* 109(19):E1143-1152, 2012b
- Xu X, Grijalva A, Skowronski A, van Eijk M, Serlie MJ, Ferrante AW Jr. Obesity activates a program of lysosomal-dependent lipid metabolism in adipose tissue macrophages independently of classic activation. *Cell Metab* 18(6):816-830, 2013
- Yáñez JA, Wang SW, Knemeyer IW, Wirth MA, Alton KB. Intestinal lymphatic transport for drug delivery. *Adv Drug Deliv Rev* 63(10-11):923-942, 2011
- Yki-Jarvinen H. Ectopic fat accumulation: an important cause of insulin resistance in humans. *J R Soc Med* 95 Suppl 42:39-45, 2002
- Yoshioka M, Bolduc C, Raymond V, St-Amand J. High-fat meal-induced changes in the duodenum mucosa transcriptome. *Obesity (Silver Spring)* 16(10):2302-2307, 2008
- Yu R, Kim CS, Kwon BS, Kawada T. Mesenteric adipose tissue-derived monocyte chemoattractant protein-1 plays a crucial role in adipose tissue macrophage migration and activation in obese mice. *Obesity (Silver Spring)* 14(8):1353-1362, 2006
- Yuan SY, Rigor RR. Regulation of endothelial barrier function. San Rafael (CA): Morgan & Claypool Life Sciences, 2010
- Yudkin JS, Eringa E, Stehouwer CD. "Vasocrine" signalling from perivascular fat: a mechanism linking insulin resistance to vascular disease. *Lancet* 365(9473):1817-1820, 2005
- Zhang M, Angata T, Cho JY, Miller M, Broide DH, Varki A. Defining the in vivo function of Siglec-F, a CD33-related Siglec expressed on mouse eosinophils. *Blood* 109(10):4280-4287, 2007
- Zhao M, Chen X. Eicosapentaenoic acid promotes thermogenic and fatty acid storage capacity in mouse subcutaneous adipocytes. *Biochem Biophys Res Commun* 450(4):1446-1451, 2014

8 Abbreviations

AA	arachidonic acid
ACC	acetyl-CoA carboxylase
ACOX1	acyl-CoA oxidase 1
ACTb	β -actin
ad	up to
ADIPOQ	adiponectin
ADRB	β -adrenergic receptor
AGPAT9	1-acylglycerol-3-phosphate O-acyltransferase 9
AJ	adherens junction
ALA	α -linolenic acid
ALB	albumin
AMP	adenosine monophosphat
AMPK	AMP-activated protein kinase
ANGPTL4	angiopoietin-like 4
ANOVA	analysis of variance, statistical test
APS	ammonium persulfate
ARG2	arginase 2
ATGL	adipose triglyceride lipase
ATM	adipose tissue macrophage
ATP	adenosine triphosphate
B220	protein tyrosine phosphatase, receptor type, C (=PTPRC)
BAT	brown adipose tissue
BCA	bicinchoninic acid, protein quantification assay
BH ₄	tetrahydrobiopterin, enzymatic cofactor
BMI	body mass index
bp	base pair
BSA	bovine serum albumin
C	control diet / group (Ludwig 2013)
C ^Δ	control diet / group (Dahlhoff 2014)
°C	degree Celsius, unit
C57BL/6J	inbred wild type mouse strain used in the study by Ludwig et al. (Ludwig 2013)
C57BL/6NCrl	inbred wild type mouse strain used in the study by Dahlhoff et al. (Dahlhoff 2014)
Ca ²⁺	calcium
CaM	calmodulin
cAMP	cyclic adenosine monophosphate
CAT	catalase
cat. no.	catalog number
CAV1	caveolin 1
CD11b	cluster of differentiation antigen 11b (=ITGAM)
CD11c	cluster of differentiation antigen 11c (=ITGAX)
CD206	cluster of differentiation antigen 206 (=MRC1)
CD3	cluster of differentiation antigen 3
CD301	cluster of differentiation antigen 301 (=CLEC10a)
CD31	platelet-endothelial cell adhesion molecule 1 (=PECAM1)
CD36	fatty acid translocase

CD4	cluster of differentiation antigen 4
CD8 α	cluster of differentiation antigen 8 α
CD86	cluster of differentiation antigen 86
CDH5	cadherin 5
cDNA	complementary deoxyribonucleic acid
C/EBP β	CCAAT / enhancer binding protein
cf.	compare
ChREBP	carbohydrate regulatory element binding protein
CLDN5	claudin 5
CL-CASP3	cleaved caspase 3
CLEC10a	C-type lectin domain family 10, member A (=CD301)
CLS	crown-like structures
“CLS”	subgroup of CLS (macrophages surrounding adipocyte)
CMS	C ^A / methyl-donor supplemented diet / group (Dahlhoff 2014)
COX	cyclooxygenase
CPT1a	carnitine palmitoyltransferase 1a
C _q -values	threshold cycle value in RT-qPCR
CS	citrate synthase
CYP450	cytochrome P450
CYP4a10	cytochrome P450, family 4, subfamily a, polypeptide 10
CYPB	cyclophilin B
Cys	cysteine
Da	dalton, unit
DAG	diacylglycerol
$\Delta\Delta C_q$	method to quantify gene expression after RT-qPCR
DGAT	diglyceride acyltransferase
DHA	docosahexaenoic acid
DIO2	5'-deiodinase
DIO	diet-induced obesity
DIT	diet-induced thermogenesis
DANN	deoxyribonucleic acid
DNL	<i>de novo</i> lipogenesis
DTT	dithiotreitol
EAT	epididymal adipose tissue
ECL	blocking reagent
ECM	extracellular matrix
EDP	epoxydocosapentaenoic acid
EDTA	ethylenediaminetetraacetic acid
EEQ	epoxyeicosatetraenoic acid
EET	epoxyeicosatrienoic acid
e.g.	for example
ELISA	enzyme-linked immunosorbent assay
ELOVL	elongation of very long-chain fatty acids protein (elongase)
EMR1	EGF-like module-containing mucin-like hormone receptor-like 1 (=F4/80)
en%	energy%
eNOS	endothelial nitric oxide synthase (=NOS3)
EPA	eicosapentaenoic acid

EPAX 1050-TG	n-3 LC-PUFA concentrate used in the study by Ludwig et al. (Ludwig 2013)
ER	endoplasmic reticulum
et al.	and others
F4/80	macrophage surface molecule (=EMR1)
FA	fatty acid
FABP3	fatty acid binding protein 3
FACS	fluorescence-activated cell sorting
FADS	fatty acid desaturase
FFA	free fatty acids
FGF21	fibroblast growth factor 21
Fig.	figure
Fw	forward
g	gram, unit
x g	times Earth's gravitational force, unit
G0S2	G0/G1 switch 2
G-3-P	glycerol-3-phosphate
GAPDH	glyceraldehyd-3-phosphat-dehydrogenase
G-C	guanine-cytosine
GDP	guanosine diphosphate
GLUT	glucose transporter
gp91PHOX	cytochrome b-245, beta polypeptide (subunit of NAD(P)H oxidase)
GPR120	G protein-coupled receptor 120
GYK	glycerol kinase
h	hour, unit
H ⁺	proton
HB	buffer for triacylglycerol analysis
HDoHE	hydroxydocosahexaenoic acid
HEPE	hydroxyeicosapentaenoic acid
HETE	hydroxyeicosatetraenoic acid
HF	high-fat diet / group (Ludwig 2013)
HF ^Δ	high-fat diet / group (Dahlhoff 2014)
HFD	high-fat diet
HFMS	HF ^Δ / methyl-donor supplemented diet / group (Dahlhoff 2014)
HF/n-3	n-3 LCPUFA-enriched HFD / group (Ludwig 2013)
HIF1 α	hypoxia-inducible factor 1
HK2	hexokinase 2
HNF-4 α	hepatic nuclear factor 4 α
HPEPE	hydroperoxyeicosapentaenoic acid
HPETE	hydroperoxyeicosatetraenoic acid
HPRT1	hypoxanthine-guanine phosphoribosyltransferase 1
HSL	hormone sensitive lipase
Hsp90	heat shock protein 90
Hsp90ab1	heat shock protein 90 (cytosolic) and class B member 1
iBAT	interscapular brown adipose tissue
ICAM1	intercellular adhesion molecule 1
i.e.	that is to say
IHC	Immunohistochemistry

IL	Interleukin
IRF4	interferon regulatory factor 4
ITGAM	integrin α -G (=CD11b)
ITGAX	integrin α -X (=CD11c)
IU	international unit
kGy	kilogray, unit
KI67	antigen KI-67
kJ	kilojoule, unit
LA	linoleic acid
LCPUFA	long-chain polyunsaturated fatty acid
LDHB	lactate dehydrogenase
LEP	leptin
LOX	lipoxygenase
LPBE	enoyl-Coenzyme A hydratase
LPL	lipoprotein lipase
LPS	lipopolysaccharide
LSI	lower small intestine
LXR α	liver X receptor α
M	mol, unit
m ²	square metre, unit
M1	type 1 macrophage
M2	type 2 macrophage
MAT	mesenteric adipose tissue
MCP1	monocyte chemoattractant protein-1
MDS	methyl-donor supplementation
Met	methionine
MetS	metabolic syndrome
min	minute, unit
MLN	mesenteric lymph nodes
MLX	max-like factor X
MMP9	matrix metalloproteinase 9
MRC1	mannose receptor, C type 1 (=CD206)
mRNA	messenger RNA
MUFA	monounsaturated fatty acid
n	number per group
n-3 LCPUFA	n-3 long-chain polyunsaturated fatty acid
n-6 LCPUFA	n-6 long-chain polyunsaturated fatty acid
NAD(P)H oxidase	nicotinamide adenine dinucleotide (phosphate)-oxidase
NAFLD	non-alcoholic fatty liver disease
NEFA	non-esterified fatty acids
NF κ B	nuclear factor κ B
NF κ Bp65	nuclear factor NF κ B p65 subunit
NLRP3	Nod-like receptor family pyrin domain containing 3
NMR	nuclear magnetic resonance
NO	nitric oxide
NOS2	nitric oxide synthase 2
NOS3	(endothelial) nitric oxide synthase 3 (=eNOS)

NP-40	Nonidet P-40®
OCLN	occludin
ONOO ⁻	peroxynitrite
OPN	osteopontin
p	statistical significance
P	phospho or phosphate
P-ACC	phosphorylated acetyl-CoA carboxylase
P-AMPK	phosphorylated AMP-activated protein kinase
P-HSL	phosphorylated hormone sensitive lipase
P-NFκBp65	phosphorylated nuclear factor NFκB p65 subunit
p47PHOX	neutrophil cytosolic factor 1 (subunit of NAD(P)H oxidase)
PCK1	phosphoenolpyruvate carboxykinase 1
PCR	polymerase chain reaction
PGC1	peroxisome proliferative activated receptor, gamma, coactivator 1
Phe	phenylalanine
PKA	protein kinase A
PLIN	perilipin
PLVAP	plasmalemma vesicle-associated protein
PPAR	peroxisome proliferator activated receptor
PUFA	polyunsaturated fatty acids
r	Pearson correlation coefficient
rev	reverse
RIN	RNA integrity number
RIPA	radioimmunoprecipitation assay buffer
RNA	ribonucleic acid
ROS	reactive oxygen species
RT	reverse transcription / transcriptase
RT-qPCR	real-time quantitative polymerase chain reaction
RXR	retinoic acid X receptor
s	second, unit
SAA	serum amyloid A
SCAT	subcutaneous adipose tissue
SDS	sodium dodecyl sulfate
SDS-PAGE	sodium dodecyl sulfate polyacrylamide gel electrophoresis
SEM	standard error of the means
Ser	serine
SFA	saturated fatty acid
SI	small intestine
SIGLEC5	sialic acid binding Ig-like lectin 5
SOD	superoxide dismutase
SPF	specific-pathogen-free
SREBP1	sterol regulatory element binding protein 1
TAE	Tris / acetate / EDTA buffer
TAG	triacylglycerols
TBE	Tris / borate / EDTA buffer
TBS	Tris-buffered saline
TBS-T	Tris-buffered saline + Tween-20®

TEC	transendothelial channel
TEK	endothelial-specific receptor tyrosine kinase
TEMED	tetramethylethylenediamine
TGF β	transforming growth factor β
TGR5	G protein-coupled bile acid receptor
TH	tyrosine hydroxylase
Thr	threonine
TJ	tight junction
TLE3	transducin-like enhancer of split 3
T _m	melting temperature
TNF α	tumor necrosis factors α
TNFSF10	tumor necrosis factor (ligand) superfamily, member 10
Tris	tris hydroxymethyl aminomethane
TSE	TSE Systems, company
TUM	Technische Universität München
Tyr	thyrosine
TZD	thiazolidinedione (PPAR γ agonist)
UCP1	uncoupling protein 1
USI	upper small intestine
VAT	visceral white adipose tissue
VCAM1	vascular cell adhesion molecule 1
VLDL	very low-density lipoprotein
vs.	versus
VVO	vesiculo-vacuolar organelle
w	week
w/w	weight in weight
WAT	white adipose tissue
WB	Western blot
wk	week

9 Materials

9.1 Primers

Gene	Gene name	Primer sequence (5'-3')		Amplicon in bp
Adrb1	β 1-adrenergic receptor	fw	CGT CCG TCG TCT CCT TCT AC	275
		rev	CAT GAT GAT GCC CAG TGT CTT	
Adrb3	β 3-adrenergic receptor	fw	CAG CCA GCC CTG TTG AAG	61
		rev	CCT TCA TAG CCA TCA AAC CTG	
Acc1	Acetyl-Coenzyme A carboxylase α	Qiagen order no. QT01554441		76
Acc2	Acetyl-Coenzyme A carboxylase β	fw	AGG GTC ATA GAG AAG GTG CTC A	140
		rev	AGA TCC TCG GGC GTC ACC AT	
Acox1	Acyl-Coenzyme A oxidase 1	fw	GAG ATG GAT AAT GGC TAC CTG AAG	139
		rev	AAA CCA TGG TCC CAT ATG TCA GC	
Actb	β -Actin	fw	CCA CTG CCG CAT CCT CTT CC	137
		rev	GCC ACA GGA TTC CAT ACC CAA GA	
Alb	Albumin	fw	CTG TGA CAA ATC CCT TCA CAC TCT	128
		rev	GCA GGA AAC ATT CGT TTC TTT CGG	
Arg2	Arginase 2	fw	TCC AGG TTG GGA TGC CAC CTA	180
		rev	TCC TCC CAT GGT GAC ACA GCT	
Cat	Catalase	fw	GCC TCG CAG AGA CCT GAT GT	141
		rev	TCT GTC AAA GTG TGC CAT CTC G	
Cav1	Caveolin 1	fw	CGA CGT GGT CAA GAT TGA CTT TGA	154
		rev	TGC CAT TGG GAT GCC GAA GAT	
Cdh5	Cadherin 5	fw	CCC ACT ATG TGG GAA AGA TCA AGT	172
		rev	ATG AGG GCA GTA AGG AAG TAC TCA	
CD4	Cluster of differentiation 4	fw	TAG AGG AGG TTC GCC TTC GC	146
		rev	CCT CCT CTT TCC TGT TCT CCA GC	
CD8α	Cluster of differentiation 8 α	fw	AGA AAG TGA ACT CTG CTG CTA CCA A	93
		rev	AAT CTT CTG GTC TCT GGG GCT G	
CD31	Platelet endothelial cell adhesion molecule 1	fw	GCA GCA CTC TTG CAG TCA GA	141
		rev	GGT TTC TGT TTG GCC TTG GCT TTC	
CD86	Cluster of differentiation 86	Qiagen order no. QT01055250		63
Cldn5	Claudin 5	fw	TAG GAT GGG TGG GCT TGA TCC	172
		rev	AGC GCC AGC ACA GAT TCA TAC A	
Clec10a	C-type lectin domain family 10, member A	Qiagen order no. QT00151011		101
Cpt1a	Carnitine palmitoyltransferase 1a	fw	GTC CCA GCT GTC AAA GAT ACC G	244
		rev	ATG GCG TAG TAG TTG CTG TTA ACC	
Cs	Citrate synthase	fw	CTG AGG AAG ACT GAC CCT CG	206
		rev	TTC ATC TCC GTC ATG CCA TA	
Cyp4a10	Cytochrome P450, family 4, subfamily a, polypeptide 10	fw	CTA AGC CCA ACC CGA TTT GC	111
		rev	TTG CCT GTG GAG GTA GAA CTG G	
CypB	Cyclophilin B	fw	TCG TCT TTG GAC TCT TTG GAA	118
		rev	TCC TTG ATG ACA CGA TGG AA	

Gene	Gene name	Primer sequence (5'-3')	Amplicon in bp
Dgat1	Diglyceride acyltransferase 1	fw TCC AGA CAA CCT GAC CTA CCG rev ACC ATC CAC TGT TGG ATC AG	174
Dgat2	Diglyceride acyltransferase 2	Qiagen order no. QT00134477	128
Dio2	5'-Deiodinase	fw ACA GGT TAA ACT GGG TGA AGA TGC rev CAG TTG CCT AGT GAA AGG TGG T	193
Emr1	EGF-like module containing, mucin-like hormone receptor-like 1	Qiagen order no. QT00099617	87
Fabp3	Fatty acid binding protein 3	fw ATC CAT GTG CAG AAG TGG AA rev CAC TGC CAT GAG TGA GAG TCA	91
Fgf21	Fibroblast growth factor 21	fw TGG AAT GGA TGA GAT CTA GAG TTG G rev GAG CTC CAG GAG ACT TTC TGG A	251
G0s2	G0/G1 switch 2	fw ACT GCA CCC TAG GCC CAG C rev GCA CAC TGC CCA GCA CGT	173
Gapbh	Glyceraldehyde 3- phosphate dehydrogenase	fw CCT GGA GAA ACC TGC CAA GTA TG rev GAG TGG GAG TTG CTG TTG AAG TC	132
gp91phox	Cytochrome b-245, beta polypeptide	fw TTG GGT CAG CAC TGG CTC TG rev TGG CGG TGT GCA GTG CTA TC	204
Gpr120	G protein-coupled receptor 120	fw CGG CGG GGA CCA GGA AAT TC rev ACC AGT CCC GGC ACC AGG A	111
Glut1	Glucose transporter 1	fw CGT CAG GGC GTG GAG GTC rev CAC CTT CTT GCT GCT GGG ATC	122
Glut4	Glucose transporter 4	fw TGT TGC GGA TGC TAT GGG TCC T rev CAC CTC CTG CTC TAA AAG GGA AG	163
Gyk	Glycerol kinase	fw CAA ATG CAA GCA GGA CGA TG rev AGG CCC CAG CTT TCA TTA GG	144
Hk2	Hexokinase 2	fw AGA GAA CAA GGG CGA GGA GC rev GGA GGA AGC GGA CAT CAC AAT	137
Hprt1	Hypoxanthine guanine phosphoribosyl transferase	fw GTC GTG ATT AGC GAT GAT GAA CC rev GTC TTT CAG TCC TGT CCA TAA TCA G	124
Hsl	Hormone sensitive lipase	fw GAA CTA AGT GGA CGC AAG CC rev TTG ACA TCA GAG GGT GTG GA	239
Hsp90ab1	Heat shock protein 90 α , class B member 1	fw AGG AGG GTC AAG GAA GTG GT rev TTT TTC TTG TCT TTG CCG CT	215
Icam1	Intercellular adhesion molecule 1	fw GTC TAC AAC TTT TCT GCT CCG GT rev GCT CAC AAG AAC CAC CTT CGA C	114
IL10	Interleukin-10	Qiagen order no. QT00106169	103
Itgam	Integrin alpha M	Qiagen order no. QT00156471	139
Itgax	Integrin alpha X	fw GCA GGA GTG TCC AAA GCA AGA C rev CTG AAG CTG GCT CAT CAC AGC	121
Ldhb	Lactate dehydrogenase	fw ATG GTG AAG GGA ATG TAC GGC rev GCT TCT GAT TGA TGA CGC TGG T	97
Lep	Leptin	fw ACA TTT CAC ACA CGC AGT CGG rev AGG CAG GCT GGT GAG GAC CT	140

Gene	Gene name	Primer sequence (5'-3')		Amplicon in bp
Lpbe	Enoyl-Coenzyme A hydratase	fw	GCT TGC CCA ACA TGG ACA GTG	103
		rev	GCC TGG ACT GAA CGG ACA CAA G	
Lpl	Lipoprotein lipase	Qiagen order no. QT01750469		108
Mcp1	Monocyte chemoattractant protein-1	fw	GCT CAG CCA GAT GCA GTT AAC G	142
		rev	GCT TGG TGA CAA AGA CTA CAG CTT	
Mmp9	Matrix metalloproteinase 9	fw	CTA GTG AGA GAC TCT ACA CGG A	122
		rev	GCG GTA ACC ATC CGA GCG G	
Mrc1	Mannose receptor, C type 1	fw	GCC AGG ACG AAA GGC GGG AT	147
		rev	GGA GTT GTT GTG GGC TCT GGT G	
Nos2	Nitric oxide synthase 2	fw	CCG AGC GTC AAA GAC CTG CA	118
		rev	AGG AAC CTA CCA GCT CAC TCT G	
Nos3	Nitric oxide synthase 3	SABioscience order no. PPM03801A		124
Ocln	Occludin	fw	CAC GAC AGG TGG GGA GTC	76
		rev	TTG ATC TGA AGT GAT AGG TGG ATA TT	
p47phox	Neutrophil cytosolic factor 1	fw	CGG CAC CCA GGT GGT TTG AT	163
		rev	TCA GTG GGC AGT TTC AGG TCA T	
Pck1	Phosphoenolpyruvate carboxykinase 1	fw	GTG CCT GTG GGA AGA CTA ACT T	116
		rev	CCT TAA GTT GCC TTG GGC ATC	
Pgc1α	Peroxisome proliferative activated receptor, gamma, coactivator 1 α	fw	GGA CGG AAG CAA TTT TTC AA	217
		rev	GAG TCT TGG GAA AGG ACA CG	
Pgc1β	Peroxisome proliferative activated receptor, gamma, coactivator 1 β	fw	CGA GCT CTT CCA GAT TGA CAG T	134
		rev	TGC AGG ATG GTG TGT CGC CTT	
Plin5	Perilipin 5	fw	AAC TGG ACC AGC AGA ATG TGG T	152
		rev	ACT ACA CAC ACA GTG CTC AGC A	
Plvap	Plasmalemma vesicle-associated protein	fw	GGA AAC AGT CAT GCA GCA ACT G	97
		rev	TAT GTA GGT GAT CAG GTC GCC T	
Pparaα	Peroxisome proliferator activated receptor α	fw	CCA GTA CTT AGG AAG CTG TCC G	150
		rev	TAT TCG ACA CTC GAT GTT CAG GG	
Pparγ2	Peroxisome proliferator activated receptor γ 2	fw	ACT CTG GGA GAT TCT CCT GTT GTC	84
		rev	CAT GGT GGT TTC TTG TGA AGT GCT	
Siglec5	Sialic acid binding Ig-like lectin 5	Qiagen order no. QT00297556		87
Sod1	Superoxide dismutase 1	fw	CGG CGG ATG AAG AGA GGC AT	125
		rev	ACG GCC AAT GAT GGA ATG CTC T	
Tek	Endothelial-specific receptor tyrosine kinase	fw	GAT GTG ACC AGA GAA TGG GCG AA	145
		rev	AGG AAG GAT GCT TGT TGA CGC AT	
Tgfβ1	Transforming growth factor β 1	Qiagen order no. QT00145250		145
Tgr5	G protein-coupled bile acid receptor 1	fw	CAG GAG GCC ATA AAC TTC CA	126
		rev	GTC AGC TCC CTG TTC TTT G	
Tle3	Transducin-like enhancer of split 3	fw	TGG TGA GCT TTG GAG CTG TT	95
		rev	CGG TTT CCC TCC AGG AAT	
Tnfa	Tumor necrosis factor α	Qiagen order no. QT00104006		112

Gene	Gene name	Primer sequence (5'-3')		Amplicon in bp
Tnfsf10	Tumor necrosis factor (ligand) superfamily, member 10	fw	ACC AAC GAG ATG AAG CAG CTG	122
		rev	ATG TGC AAG CAG GGT CTG TTC AA	
Vcam1	Vascular cell adhesion molecule 1	fw	CGT GGA CAT CTA CTC TTT CCC CA	98
		rev	TGT CTG GAG CCA AAC ACT TGA CC	

9.2 Antibodies

Antibody	Application	Description	Company
ACC1/2	WB; (BSA) 1:1000	monoclonal, rabbit anti-mouse	3676, Cell Signaling/New England Biolabs, Frankfurt am Main, Germany
ACC1	WB; (BSA) 1:1000	monoclonal, rabbit anti-mouse	04-322, Merck Millipore, Billerica, MA, USA
AMPK α	WB; (BSA) 1:1000	polyclonal, rabbit anti-mouse	2532, Cell Signaling/New England Biolabs, Frankfurt am Main, Germany
ATGL	WB; (BSA) 1:1000	monoclonal, rabbit anti-mouse	2138, Cell Signaling/New England Biolabs, Frankfurt am Main, Germany
β -ACTIN	WB; (BSA) 1:1000	polyclonal, rabbit anti-mouse	4967, Cell Signaling/New England Biolabs, Frankfurt am Main, Germany
B220	IHC-P; 1:3000	monoclonal, rat anti-mouse	553084, BD Biosciences, Heidelberg, Germany
CL-CASP3 (Asp175)	IHC-P; 1:300	polyclonal, rabbit anti-mouse	9661, Cell Signaling/New England Biolabs, Frankfurt am Main, Germany
CAT	WB; (BSA) 1:1000	polyclonal, goat anti-mouse	sc-34285, Santa Cruz, Heidelberg, Germany
CD3	IHC-P/IHC-F; 1:300	monoclonal, rabbit anti-mouse	RM-9107-S0, NeoMarkers, Fremont, CA, USA
CD4	IHC-F; 1:50	monoclonal, rat anti-mouse	550278, BD Biosciences, Heidelberg, Germany
CD8 α	IHC-F; 1:200	monoclonal, rat anti-mouse	553027, BD Biosciences, Heidelberg, Germany
CD11c	IHC-P; 1:5000	monoclonal, hamster anti-mouse	553799, BD Biosciences, Heidelberg, Germany
CD206	IHC-P; 1:1500	polyclonal, rabbit anti-human	18704-1-AP, Proteintech, Chicago, IL, USA
CD301	IHC-P; 1:40	monoclonal, rat anti-mouse	LS-C123200, LifeSpan Biosciences, Seattle, WA, USA
CS	WB; (BSA) 1:5000	polyclonal, rabbit anti-mouse	ab96600, Abcam, Cambridge, UK
F4/80	IHC-P; 1:120	monoclonal, rat anti-mouse	T-2006, BMA Biomedicals, Augst, Switzerland
HPRT	WB; (BSA) 1:1000	polyclonal, rabbit anti-mouse	sc-20975, Santa Cruz, Heidelberg, Germany
HSL	WB; (BSA) 1:1000	polyclonal, rabbit anti-mouse	4107, Cell Signaling/New England Biolabs, Frankfurt am Main, Germany
HSP90	WB; (BSA) 1:1000	monoclonal, mouse anti-mouse	SMC-149, StressMarq Biosciences Inc, Cadboro Bay, Victoria, Canada
KI67	IHC-P; 1:200	monoclonal, rabbit anti-mouse	RM-9106-S0, NeoMarkers, Fremont, CA, USA

Antibody	Application	Description	Company
NFκBp65	WB; (BSA) 1:1000	polyclonal, rabbit anti-mouse	3034, Cell Signaling/New England Biolabs, Frankfurt am Main, Germany
phospho-ACC1 (Ser76)	WB; (ECL) 1:500	polyclonal, rabbit anti-mouse	07-303, Merck Millipore, Billerica, MA, USA
phospho-ACC2 (Ser219/Ser221)	WB; (BSA) 1:500	polyclonal, rabbit anti-mouse	sc-30446, Santa Cruz, Heidelberg, Germany
phospho-AMPKα (Thr172)	WB; (BSA) 1:500	monoclonal, rabbit anti-mouse	2535, Cell Signaling/New England Biolabs, Frankfurt am Main, Germany
phospho-HSL (Ser660)	WB; (BSA) 1:1000	polyclonal, rabbit anti-mouse	4126, Cell Signaling/New England Biolabs, Frankfurt am Main, Germany
phospho-HSL (Ser563)	WB; (BSA) 1:1000	polyclonal, rabbit anti-mouse	4139, Cell Signaling/New England Biolabs, Frankfurt am Main, Germany
phospho-HSL (Ser565)	WB; (BSA) 1:1000	polyclonal, rabbit anti-mouse	4137, Cell Signaling/New England Biolabs, Frankfurt am Main, Germany
phospho-NFκBp65 (Ser536)	WB; (BSA) 1:500	polyclonal, rabbit anti-mouse	3031, Cell Signaling/New England Biolabs, Frankfurt am Main, Germany
PLIN	WB; (BSA) 1:3500	monoclonal, rabbit anti-mouse	9349, Cell Signaling/New England Biolabs, Frankfurt am Main, Germany
TH	WB; (BSA) 1:1000	polyclonal, rabbit anti-mouse	AB152, Merck Millipore, Billerica, MA, USA
UCP1	WB; 1:10000	serum, rabbit anti-hamster	Klingenspor 1996
2° antibody	WB; (ECL) 1:20000	IRDye800CW-conjugated goat anti-rabbit IgG (H+L)	926-32211, LI-COR Biosciences, Bad Homburg, Germany
2° antibody	WB; (ECL) 1:20000	IRDye680RD-conjugated donkey anti-mouse IgG (H+L)	925-68072, LI-COR Biosciences, Bad Homburg, Germany
2° antibody	IHC-P; 1:1000	rabbit anti-rat IgG	312-005-045, Jackson ImmunoResearch, West Grove, PA, USA
2° antibody	IHC-P; 1:1000	rabbit anti-Syrian Hamster IgG	NB120-6699, Novus Biologicals, Littleton, CO, USA

9.3 Consumables

Item	Company
96-well plate	Nunc / Thermo-Fisher Scientific, Langensfeld, Germany
Bedding and nesting material	Abedd® LAB & VET Service GmbH, Wien, Germany
Biosphere® filter tips (10, 100, 1000 µl)	Sarstedt AG & Co. KG, Nümbrecht, Germany
Bone scissors	Fine Science Tools GmbH, Heidelberg, Germany
Buckets for homogenisation	Retsch GmbH, Haan, Germany
Cage, type I (200 cm ²)	Ehret GmbH & Co. KG, Emmendingen, Germany
Cage, type III (825 cm ²)	Ehret GmbH & Co. KG, Emmendingen, Germany
Clingfilm	Sylvana, Penny-Markt GmbH, Köln, Germany
Cool rack 96-wells	Eppendorf AG, Hamburg, Germany
Corning® Costar® "stripette", disposable pipettes 2; 5; 10; 25; 50 ml	Corning® Inc., Sigma-Aldrich Chemie GmbH, München, Germany
Corning® Costar® reagent reservoirs	Corning® Inc., Sigma-Aldrich Chemie GmbH, München, Germany

Item	Company
Cotton gloves, Softline	Zefa-Laborservice GmbH, Harthausen, Germany
Cover slips 24 x 60 mm	Menzel GmbH & Co. KG, Braunschweig, Germany
Dewar flask	KGW-Isotherm, Karlsruhe, Germany
Dissection scissors	Fine Science Tools GmbH, Heidelberg, Germany
Eppendorf Combitips plus	Eppendorf AG, Hamburg, Germany
Eppendorf Multipipette® plus	Eppendorf AG, Hamburg, Germany
Eppendorf Xplorer®, multi-channel, 50 – 1200 µL, grün	Eppendorf AG, Hamburg, Germany
Forceps	Fine Science Tools GmbH, Heidelberg, Germany
Gel chamber, sled, comb	UniEquip GmbH, Planegg, Germany
Glass plates, clips, rubber, chambers, combs	Biometra GmbH, Göttingen, Germany
Glassware (beakers, cylinders, funnels)	Diagonal GmbH & Co KG, Münster, Germany
Heat sealing film	Eppendorf AG, Hamburg, Germany
Histosettes	Simport Scientific, Beloeil, Canada
Ignition thread	Parr Instrument Co., Moline, USA
Lab coat	CWS-boco GmbH, Dreieich, Germany
Laboratory aluminum foil	Carl Roth GmbH & Co. KG, Karlsruhe, Germany
Latex gloves, size "M"	Rösner-Mautby Meditrade GmbH, Kiefersfelden, Germany
Low Profile Blades SEC35™	Richard Allan Scientific/Microm/Thermo Scientific, Walldorf, Germany
Masterclear Cap Stripes and real-time PCR Tube Stripes	Eppendorf AG, Hamburg, Germany
Microtube boxes	Zefa Laborservice, Harthausen, Germany
Microtube PP, 1.5 ml	Paul Böttger OHG, Bodenmais, Germany
Microtube PP, 2 ml	Diagonal GmbH & Co. KG, Münster, Germany
Microtube tough-spots®	Diversified Biotech, Boston, USA
Microvette®, Li-Heparin, 0.5 ml	Sarstedt AG & Co. KG, Nümbrecht, Germany
Minisart syringe filter, 0.22 µm	Sartorius AG, Göttingen, Germany
Mortar	Morgan Technical Ceramics - Haldenwanger, Waldkraiburg, Germany
Multi-channel pipette 30-300 µl	Brand GmbH & Co. KG, Wertheim, Germany
Myjector® U-100 insulin syringe, 0.5 ml	Terumo® Europe N.V., Leuven, Belgium
Nitrile gloves	Kimberly-Clark Deutschland GmbH, Mainz, Germany
Pap pen	Kisker Biotech GmbH & Co. KG, Steinfurt, Germany
Paper towels	Anton Schlecker, Ehingen, Germany
Parafilm®	Pechiney Plastic Packaging, Chicago, USA
Pasteur pipettes, glass	Zefa-Laborservice GmbH, Harthausen, Germany
Pestle	Morgan Technical Ceramics - Haldenwanger, Waldkraiburg, Germany
Pipettes 10; 200, 1000 µl	Gilson Intl. B.V., Limburg, Germany
Pipettes 2,5; 10; 100, 1000 µl	Eppendorf AG, Hamburg, Germany
Pipetting aid	Gilson Intl. B.V., Limburg, Germany
Plastic ware (beakers, cylinders, funnels)	Diagonal GmbH & Co KG, Münster, Germany
Purple nitrile exam gloves, size "M"	Kimberley-Clark Health Care, Zaventem, Belgium
Pressurizer for tablets	IKA®-Werke GmbH & Co. KG, Staufen, Germany
Protran BA 83 Whatman™ (0.2 µm)	GE Healthcare Life Sciences, Freiburg, Germany

Item	Company
Reaction tubes, 0.2 ml	Zefa-Laborservice GmbH, Harthausen, Germany
Reaction tubes, 0.5 ml	Brand GmbH & Co. KG, Wertheim, Germany
Reaction tubes, 2 ml (safe-lock)	Eppendorf AG, Hamburg, Germany
Restrainer	Bruker BioSpin GmbH, Rheinstetten, Germany
Safety goggles	UVEX Winter Holding, Fürth, Germany
Scalpel	B. Braun Melsungen, Melsungen, Germany
Spatula	Carl Roth GmbH & Co. KG, Karlsruhe, Germany
Stainless steel beads	Qiagen GmbH, Hilden, Germany
SuperFrost® Plus & Polysine® slides	Menzel GmbH & Co. KG, Braunschweig, Germany
Tips, blue 1000 µl	Brand GmbH & Co. KG, Wertheim, Germany
Tips, white, 10 µl	Brand GmbH & Co. KG, Wertheim, Germany
Tips, yellow, 100 µl	Brand GmbH & Co. KG, Wertheim, Germany
Transferpette® Multi-channel, 30-300 µl	Brand GmbH & Co. KG, Wertheim, Germany
Tissue-Tek cryomolds, intermediate	Sakura Finetek Europe B.V., Alphen aan den Rijn, Netherlands
Tube racks	Brand GmbH & Co. KG, Wertheim, Germany
Tubes, 15 ml	Greiner Bio-One GmbH, Frickenhausen, Germany
Tubes, 50 ml	Greiner Bio-One GmbH, Frickenhausen, Germany
Twin.tec real-time PCR plates 96	Eppendorf AG, Hamburg, Germany
Waste bags	PAA Laboratories GmbH, Pasching, Austria
Water bottle	Vitlab®, Großostheim, Germany
Weighing dish, blue	Carl Roth GmbH & Co. KG, Karlsruhe, Germany
Western Blot Incubation Boxes	LI-COR Biosciences GmbH, Bad Homburg, Germany
Whatman paper	Carl Roth GmbH & Co. KG, Karlsruhe, Germany

9.4 Chemicals

Item	Company
1 kb DNA ladder	New England Biolabs GmbH, Frankfurt am Main, Germany
Acetic acid (100 %; C ₂ H ₄ O ₂)	Merck KGaA, Darmstadt, Germany
Acrylamide/ Bisacrylamide "Roti-Gelektrophorese" Gel 30	Carl Roth GmbH & Co. KG, Karlsruhe, Germany
Agarose, pegGOLD universal	Peqlab biotechnology GmbH, Erlangen, Germany
Ammoniumpersulphate (APS; (NH ₄) ₂ S ₂ O ₈)	Bio-Rad Laboratories GmbH, München, Germany
Aquatex® aqueous mounting medium	Merck KGaA, Darmstadt, Germany
Boric acid (H ₃ BO ₃)	Merck KGaA, Darmstadt, Germany
Bovine serum albumine, Albumin Fraction V, pH 5.2, > 97 %	Carl Roth GmbH & Co. KG, Karlsruhe, Germany
Bromophenolblue	Merck KGaA, Darmstadt, Germany
Carbogen gas (CO ₂ & O ₂)	Linde Gas, Unterschleißheim, Germany
Carbon dioxide (CO ₂ solid; "dry ice")	TKD GmbH, Fraunberg-Tittenkofen, Germany
Chloroform (CHCl ₃)	Carl Roth GmbH & Co. KG, Karlsruhe, Germany

Item	Company
Coomassie Brilliant Blue G 250	SERVA Electrophoresis GmbH, Heidelberg, Germany
Dithiotreitol (DTT; C ₄ H ₁₀ O ₂ S ₂)	AppliChem GmbH, Darmstadt, Germany
DNA-Oligonucleotides (PCR primer)	Metabion, Martinsried, Germany
ECL Advance™ blocking agent	GE Healthcare Life Sciences, Freiburg, Germany
Eosine	Medite Medizintechnik AG, Nunningen, Switzerland
EPAX 1050-TG	Goerlich Pharma International, Erding, Germany
Ethanol (C ₂ H ₆ O)	J.T. Baker; Mallinckrodt, Deventer, Netherlands
Ethanol, denaturated (C ₂ H ₆ O)	CLN GmbH, Niederhummel, Germany
Ethidium bromide (C ₂₁ H ₂₀ BrN ₃)	Carl Roth GmbH & Co. KG, Karlsruhe, Germany
Food	Ssniff Spezialdiäten GmbH, Soest, Germany
GeneRuler™, 50 bp DNA Ladder	Fermentas GmbH, St. Leon-Rot, Germany
Glycerol (C ₃ H ₈ O ₃)	Carl Roth GmbH & Co. KG, Karlsruhe, Germany
Glycerol standard solution (C ₃ H ₈ O ₃)	Sigma-Aldrich Chemie GmbH, Taufkirchen, Germany
Glycine (C ₂ H ₅ NO ₂)	Merck KGaA, Darmstadt, Germany
Hämalaun (Emallume)	WALDECK GmbH & Co. KG, Münster, Germany
Hematoxylin (Gill)	Carl Roth GmbH & Co. KG, Karlsruhe, Germany
Hydrochloric acid (HCl)	Carl Roth GmbH & Co. KG, Karlsruhe, Germany
Isopropanol (C ₃ H ₈ O)	J.T. Baker; Mallinckrodt, Deventer, Netherlands
Methanol (CH ₄ O)	Merck KGaA, Darmstadt, Germany
Nitrogen, liquid (N ₂)	Linde Gas, Unterschleißheim, Germany
Nonidet P-40 (C ₁₄ H ₂₂ O(C ₂ H ₄ O) _n n=9-10)	Sigma-Aldrich Chemie GmbH, Taufkirchen, Germany
Orange G	Sigma-Aldrich Chemie GmbH, Taufkirchen, Germany
Oxygen (O ₂)	Linde Gas, Unterschleißheim, Germany
PageBlue™ Protein staining solution	Fermentas GmbH, St. Leon-Rot, Germany
Pageruler, prestained	Fermentas GmbH, St. Leon-Rot, Germany
Paraformaldehyde	Sigma-Aldrich Chemie GmbH, Taufkirchen, Germany
Paraplast® (paraffin)	Carl Roth GmbH & Co. KG, Karlsruhe, Germany
Phosphatase inhibitor	Sigma-Aldrich Chemie GmbH, Taufkirchen, Germany
Phosphate-buffered saline (PBS) in tablets	Sigma-Aldrich Chemie GmbH, Taufkirchen, Germany
PhosSTOP phosphatase inhibitor cocktail	Roche Diagnostics GmbH, Mannheim, Germany
Polyoxyethylen (10) tridecyl ether	Sigma-Aldrich Chemie GmbH, Taufkirchen, Germany
Ponceau S	Sigma-Aldrich Chemie GmbH, Taufkirchen, Germany
Protease inhibitor	Sigma-Aldrich Chemie GmbH, Taufkirchen, Germany
QIAzol® Lysis Reagent	Qiagen GmbH, Hilden, Germany
Rnase-Zap®	Sigma-Aldrich Chemie GmbH, Taufkirchen, Germany
Roti®-HistoKitt	Carl Roth GmbH & Co. KG, Karlsruhe, Germany
Roti®-Safe GelStain	Carl Roth GmbH & Co. KG, Karlsruhe, Germany
Sodium azide (NaN ₃)	Merck KGaA, Darmstadt, Germany
Sodium chloride (NaCl)	Merck KGaA, Darmstadt, Germany
Sodium dihydrogen phosphate (NaH ₂ PO ₄)	Merck KGaA, Darmstadt, Germany
Sodium dodecyl-sulphate (SDS; NaC ₁₂ H ₂₅ SO ₄)	Carl Roth GmbH & Co. KG, Karlsruhe, Germany
Sodium hydroxide (NaOH)	Merck KGaA, Darmstadt, Germany
Sodium-deoxycholate (C ₂₄ H ₃₉ NaO ₄)	Sigma-Aldrich Chemie GmbH, Taufkirchen, Germany
Sulfuric acid (H ₂ SO ₄)	Carl Roth GmbH & Co. KG, Karlsruhe, Germany

Item	Company
Tetramethylethylenediamine (TEMED; C ₆ H ₁₆ N ₂)	Merck KGaA, Darmstadt, Germany
TissueTEK O.C.T.	Sakura Finetek Germany GmbH, Staufen
Titriplex® Ethylenediaminetetraacetic acid (EDTA; C ₁₀ H ₁₆ N ₂ O ₈)	Merck KGaA, Darmstadt, Germany
Tris base (Tris-aminomethan; C ₄ H ₁₁ NO ₃)	AppliChem GmbH, Darmstadt, Germany
Tween® 20	Sigma-Aldrich Chemie GmbH, Taufkirchen, Germany
VectaMount™ permanent mounting medium	Vector Laboratories/Biozol Diagnostica Vertrieb GmbH, Eching, Germany
Water, nuclease-free (H ₂ O)	Sigma-Aldrich Chemie GmbH, Taufkirchen, Germany
Water, purified (H ₂ O)	SG Water USA LLC, Nashua, USA
Xylene (C ₈ H ₁₀)	Carl Roth GmbH & Co. KG, Karlsruhe, Germany

9.5 Kits

Item	Company
Absolute IDQ™ Kit p180	Biocrates Life Sciences AG, Innsbruck, Austria
Agilent RNA 6000 Nano Kit	Agilent Technologies, Waldbronn, Germany
BCA Protein Assay Kit	Pierce / Thermo Fisher Scientific, Bonn, Germany
Bond Polymer Refine Detection Kit	Leica Microsystems GmbH, Wetzlar, Germany
Bond Polymer Refine Red Detection Kit	Leica Microsystems GmbH, Wetzlar, Germany
ELISA Starter Accessory Kit	Bethyl Laboratories Inc, Montgomery, USA
miRNeasy® Mini Kit	Qiagen GmbH, Hilden, Germany
Mouse Albumin ELISA Quantitation Set	Bethyl Laboratories Inc, Montgomery, USA
Mouse MCP-1 ELISA Ready-SET-Go! Set	eBiosciences Inc, Frankfurt am Main, Germany
QuantiTect® SYBR® Green RT-PCR Kit	Qiagen GmbH, Hilden, Germany
RNase-free DNase Set	Qiagen GmbH, Hilden, Germany
Serum Triglyceride Determination Kit	Sigma-Aldrich Chemie GmbH, Taufkirchen, Germany

9.6 Machines

Item	Company
Agilent 2100 Bioanalyzer	Agilent Technologies GmbH, Böblingen, Germany
CaloSys process control (994620 series ultramat/oxymat 6)	Siemens / TSE Systems GmbH, Bad Homburg, Germany
Centrifuge 5415 R	Eppendorf AG, Hamburg, Germany
Centrifuge 5424	Eppendorf AG, Hamburg, Germany
Centrifuge 5430	Eppendorf AG, Hamburg, Germany
Climate simulation station	Feutron Klimasimulation GmbH, Langenwetzendorf, Germany
DNA/RNA UV-Cleaner UVC/T-M-AR	UniEquip GmbH, Planegg, Germany

Item	Company
Electrophoresis power supply CONSORT E861	Consort, Turnhout, Belgium
Freezer -20 °C Liebherr premium	Liebherr GmbH, Biberach, Germany
Freezer "ThermoForma" -80°C	Thermo Fisher Scientific, Schwerte, Germany
Freezer "ThermoScientific HeraFreeze" -80°C	Thermo Fisher Scientific, Schwerte, Germany
Fridge 4 °C Liebherr	Liebherr GmbH, Biberach, Germany
Heat sealer	Eppendorf AG, Hamburg, Germany
Heraeus Megafuge 1.0 R	Heraeus / Thermo Scientific, Waltham, USA
Homogeniser ("Dispergierwerkzeug")	Micra (ART Labortechnik), Mühlheim, Germany
Ice machine AF 100	Scotsman ice systems, Milan, Italy
Incubator HeraCell 150	Thermo Fisher Scientific, Schwerte, Germany
Leica Bond-Max	Leica Microsystems GmbH, Wetzlar, Germany
Leica ST 5020	Leica Microsystems GmbH, Wetzlar, Germany
Microscope DMI 4000B with Leica CTR 4000 and Leica UV source	Leica Microsystems GmbH, Wetzlar, Germany
Microtome HM 355 S	Microm / Thermo Fisher Scientific, Walldorf, Germany
Microwave	MDA
Mikrom AP280-1/2/3	Microm / Thermo Fisher Scientific, Walldorf, Germany
Mikrom SB 80 water bath	Microm / Thermo Fisher Scientific, Walldorf, Germany
Mikrotom-Kryostat Cryo-Star HM 560 MV	Microm / Thermo Fisher Scientific, Walldorf, Germany
Mini Centrifuge GMC-060	LMS Group, Tokyo, Japan
Mini scale EW3000-2M	Kern GmbH, Balingen, Germany
Mini scale PE360	Mettler-Toledo, Ingolstadt, Germany
"The Minispec" mq 7.5 NMR analyser	Bruker BioSpin GmbH, Rheinstetten, Germany
ND-1000 Spectrophotometer	Peqlab biotechnology GmbH, Erlangen, Germany
Odyssey® Infrared Imaging System	LI-COR Biosciences GmbH, Bad Homburg, Germany
Parr® 6300 Calorimeter	Parr Instrument Co., Moline, USA
Power pack P25 T	Biometra GmbH, Göttingen, Germany
Printer	Intas Science Imaging Instruments GmbH, Göttingen, Germany
Realplex ⁴ Mastercycler eppgradient S	Eppendorf AG, Hamburg, Germany
S20-K SevenEasy™ pH meter	Mettler-Toledo, Ingolstadt, Germany
Scale, max 820 g	Sartorius AG, Göttingen, Germany
Spectrophotometer infinite M2000	Tecan Austria GmbH, Gröding, Germany
Thermomixer comfort	Eppendorf AG, Hamburg, Germany
Timer	Oregon Scientific GmbH, Neu-Isenburg, Germany
TissueLyser II	Qiagen GmbH / Retsch GmbH, Hilden, Germany
Tissue Processor Leica TP1020	Leica Microsystems GmbH, Wetzlar, Germany
Titramax 100 with Inkubator 1000	Heidolph Instruments GmbH & Co. KG, Schwabach, Germany
TSE Systems Calorimetry, Modul „CaloSys“	TSE Systems GmbH, Bad Homburg, Germany
TSE Systems Drinking & Feeding Monitor, Modul „ActiMot“	TSE Systems GmbH, Bad Homburg, Germany
UV-VIS gel electrophoresis detection system	Intas Science Imaging Instruments GmbH, Göttingen, Germany
Vacuum centrifuge (SpeedVac SPDIIIV)	Savant / Thermo Fisher Scientific, Marietta, USA
VARIOSCAN	Electron / Thermo Fisher Scientific, Marietta, USA

Item	Company
Vortexer "Vortex Genie 2"	Bender-Hobein, Gera, Germany
Vortexer 2x ³	Velp Scientifica, Usmate, Italy
WiseMix RK 2D digital rocker	Witeg GmbH, Wertheim, Germany

9.7 Software

Item	Company
2100 Expert Software vB.02.06.SI418	Agilent Technologies Sales & Services GmbH & Co. KG, Waldbronn, Germany
Bruker Minispec plus + OPUS v5.5	Bruker BioSpin GmbH, Rheinstetten, Germany
ChemDraw Ultra v12.0.3.1216	CambridgeSoft, Cambridge, USA
Image-Pro Plus v7.0	Media Cybernetics Inc., Bethesda, USA
ImageJ	Open Source (Wayne Rasband (NIH)), Bethesda, USA
Intas GDS	Intas Science Imaging Instruments GmbH, Göttingen, Germany
Leica Application Suite v3.7	Leica Mikrosysteme Vertrieb GmbH, Wetzlar, Germany
Microsoft Office	Microsoft Deutschland GmbH, Unterschleißheim, Germany
NanoDrop ND-1000 v3.7.1	PEQLAB Biotechnologie GmbH (Thermo Scientific), Erlangen, Germany
Odyssey application software v3.0	LI-COR Biosciences GmbH, Bad Homburg, Germany
OPUS v6.5	Bruker BioSpin GmbH, Rheinstetten, Germany
Photoshop CS	Adobe Systems GmbH, München, Germany
Prism v5.0	GraphPad Software Inc., La Jolla, USA
Realplex v2.0	Eppendorf AG, Hamburg, Germany
Tecan i-control v1.7.1.12	Tecan Austria GmbH, Gröding, Germany
TSE Labmaster v2.1.5	TSE Systems GmbH, Bad Homburg, Germany

10 List of figures

Figure 1. Selected adipose tissue depots in the mouse.....	14
Figure 2. Lipid mediators generated from long-chain polyunsaturated fatty acids (LCPUFA).....	15
Figure 3. The vessel system.....	19
Figure 4. Lipid homeostasis in BAT.....	23
Figure 5. Study design of feeding trial analysing the impact of n-3 LCPUFA and/or n-6/n-3 PUFA ratio on DIO	30
Figure 6. Study design of feeding trial analysing the impact of methyl-donor supplementation on DIO.....	31
Figure 7. Differential mRNA expression of genes encoding T lymphocyte and co-stimulatory markers, and immunohistochemical detection and quantification of T cells and B cells as well as proliferation and apoptosis markers in VATs.....	45
Figure 8. Differential mRNA expression of genes encoding M1 and M2 macrophage markers and their immunohistochemical detection and quantification in crown-like structures (CLS) or as solitary cells in VATs.....	48
Figure 9. Immunohistochemical analysis of macrophage-associated M1 and M2 marker expression in crown-like structures (CLS) of VATs.....	50
Figure 10. Subdivision of crown-like structures (CLS) of VATs according to their appearance.....	52
Figure 11. Gene expression of pro-inflammatory cytokines in VATs.....	53
Figure 12. Expression analysis of genes involved in endothelial cell activation and growth or in the regulation of angiogenesis in VATs	54
Figure 13. Differential mRNA expression of cytokines and genes encoding immune cell markers, such as M1 and M2 macrophage markers, and their immunohistochemical detection and quantification in crown-like structures (CLS) or as solitary cells in iBAT.....	56
Figure 14. Immunohistochemical analysis of macrophage-associated M1 and M2 marker expression in crown-like structures (CLS) of iBAT.....	57
Figure 15. Gene expression analysis of immune cell markers, the immunohistochemical detection and quantification of T cells in spleen and MCP1 measurement in plasma.....	60
Figure 16. Gene expression of immune cell markers and cytokines in upper (USI) and lower small intestine (LSI).....	62
Figure 17. mRNA and protein expression of genes that play a role in the regulation of nitric oxide bioavailability in small intestine.....	67
Figure 18. Gene expression of endothelial cell markers, junctional and plasmalemma vesicle-associated proteins in upper (USI) and lower small intestine (LSI).....	70
Figure 19. Albumin measurement in plasma and gene expression of albumin in liver.....	71

Figure 20. Expression of genes involved in lipid metabolism in upper (USI) and lower small intestine (LSI).....	73
Figure 21. Gene and protein expression of enzymes involved in lipid metabolism in liver.....	75
Figure 22. Gene and protein expression of enzymes involved in <i>de novo</i> lipogenesis in livers from mice fed soybean oil / beef tallow-based HFDs	78
Figure 23. Light microscopy of lipid droplets and expression of genes involved in lipid and glucose metabolism in iBAT.....	83
Figure 24. Gene and protein expression of markers involved in lipolysis in iBAT.....	85
Figure 25. Protein expression of uncoupling protein 1 (UCP1) and citrate synthase (CS) and expression levels of genes involved in energy metabolism and mitochondrial biogenesis in iBAT	87
Figure 26. Gene expression of proteins that are associated with thermogenic activation and whitening of iBAT.....	90

11 List of tables

Table 1. Composition of the soybean / palm oil-based diets.....	32
Table 2. Fatty acid pattern of the soybean / palm oil-based diets.....	33
Table 3. Composition of the soybean oil / beef tallow-based diets.....	34
Table 4. Fatty acid pattern of the soybean oil / beef tallow-based diets.....	34
Table 5. Amino acid, vitamin and trace element pattern of soybean oil / beef tallow-based diets....	35
Table 6. Correlation analysis data on macrophage phenotypes in iBAT.....	58
Table 7. Correlation analysis of the cytokine TGF β 1 and immune cell markers in LSI.....	63
Table 8. Summary of inflammatory changes in MAT and EAT.....	64
Table 9. Summary of inflammatory changes in iBAT, spleen, liver, plasma, USI and LSI.....	65
Table 10. Correlation analysis data on the regulation of nitric oxide bioavailability in USI.....	68
Table 11. Correlation analysis data on genes involved in the regulation of the transcellular pathway in USI.....	69
Table 12. Correlation analysis data on the regulation of acetyl-CoA carboxylase in liver.....	76
Table 13. Data on the regulation of hepatic metabolism by HFDs that differ in fat quantity, fat quality and substitution / supplementation.....	79
Table 14. iBAT mass, triacylglycerol and protein content.....	81
Table 15. Correlation analysis data on genes and proteins involved in the regulation of triacylglycerol synthesis and hydrolysis and their interplay in iBAT.....	86
Table 16. Correlation analysis of signalling pathway molecules and UCP1 expression or immune cell marker proteins in iBAT	92
Table 17. Correlation analysis data on the metabolic regulation in adipocytes with enlarged lipid droplets in iBAT	93
Table 18. Summary of expression data of genes and proteins involved in energy metabolism and its regulation in small intestine, liver and iBAT.....	95
Table 19. Correlation analysis data on genes involved in energy metabolism in iBAT.....	96
Table 20. Correlation analysis data on the identification of associations between food / fat intake or fat quality (n-6/n-3 PUFA and SFA/PUFA ratios) and obesity or inflammatory status in iBAT, EAT and USI	99
Table 21. Changes in gene expression upon soybean / palm oil-based HFDs in iBAT.....	122
Table 22. Changes in gene expression upon soybean / palm oil-based HFDs in EAT.....	123
Table 23. Changes in gene expression upon soybean / palm oil-based HFDs in liver.....	124
Table 24. Changes in gene expression upon soybean / palm oil-based HFDs in LSI.....	125
Table 25. Changes in gene expression upon soybean / palm oil-based HFDs in MAT.....	126
Table 26. Changes in gene expression upon soybean / palm oil-based HFDs in spleen.....	127

Table 27. Changes in gene expression upon soybean / palm oil-based HFDs in USI..... 127

Table 28. Changes in gene expression upon soybean oil / beef tallow-based HFDs in liver..... 128

12 Acknowledgements

There are a lot of people who supported me in conducting this thesis in many different ways and I want to express my deepest gratitude to all of them.

First of all, I want to thank my dissertation supervisor, **Prof. Dr. Hans Hauner**, who has given me the opportunity and freedom to study and to work in this fascinating scientific field, and my second supervisor, **Prof. Dr. Hannelore Daniel**. I am very grateful for their trust and valuable support.

I owe particular thanks to my supervisor **Dr. Bernhard L. Bader** for his scientific advice, accuracy and patience. He was always accessible for all issues and questions. I am very grateful for his valuable feedback and constructive discussions that particularly contributed to the success of this thesis.

I also want to thank **Prof. Dr. Martin Klingenspor** for taking the dissertation committee chair and for his helpful information about the topic brown adipose tissue.

I address my special thanks to **Prof. Dr. Mathias Heikenwälder** and his team for performing the immunohistochemical stainings using an automated IHC stainer, to ensure best possible quality.

I am deeply grateful to **Dr. Tobias Ludwig** for his elaborate introduction to the topic and to certain methods, and especially for entrusting the remaining material from his mouse feeding trial and previous result to me, in order to continue the project. I appreciated his helpful attitude and his support and I could benefit a lot from his structured work approach.

I would like to thank **Dr. Christoph Dahlhoff**, **Caroline Kless**, **Dr. Veronika Hillreiner**, **Valentina Schüppel** and **Dr. Jarlei Fiamoncini** for providing part of the material from their mouse feeding studies for comparative analyses or preliminary studies and/or sharing their expertise.

Many other people supported my work by introducing methods, discussing results, sharing their expertise, trouble-shooting, providing equipment and materials or other assistance.

Many thanks go to my colleagues at the Chair of Nutritional Medicine, especially **Dr. Kirsten Uebel** and **Manuela Hubersberger**, but also **Dr. Eva Sedlmeier**, **Dr. Thomas Skurk**, **Dr. Helmut Laumen**, **Britta Wessels**, **Viktoria Glunk**, **Carola Herrmann**, **Elisabeth Hofmair**, **Dr. Tina Brennauer**, **Dr. Simone Matthä**, **Dr. Julia Clavel** and **Sylvia Heinrich**.

I also want to thank **Dr. Tobias Fromme**, **Dr. Monja Willershäuser**, **Dr. David Lasar**, **Dr. Theresa Schöttl**, **Dr. Nadine Rink**, **Dr. Kerstin Lohr**, **Dr. Stefanie Maurer**, **Dr. Florian Bolze**, **Sabine Mocek** and **Raphaela Kübeck** (Chair for Molecular Nutritional Medicine); **Nico Gebhardt**, **Dr. Gabriele Hörmannspurger**, **Dr. Emanuel Berger**, **Dr. Lisa Richter** and **Dr. Sarah Just** (Chair of Nutrition and

Immunology); **Dr. Dominika Kolodziejczak, Dr. Ramona Pais, Irmgard Sperrer, Katrin Lasch, Elmar Jocham and Liese Baller** (Chair of Nutrition Physiology); **Inge Celler, Anna Bhandari and Aline Lukacs.**

I further had the support and encouragement of **Dorothea Wörner, Tamara Stelzl, Julia Vörös, Dr. Karolin Ebert,** and all the other fellows of the GRK 1482: **Dr. Sören Ocvirk, Kristina Hüttinger, Sarah-Madeleine Gabler, Dr. Elena Ferrari, Dr. Lena Staib, Sebastian Dreyer, Dr. Lena Bruder, Dr. Anamarija Markota, Dr. Natasha Stephens and Annemarie Schmidt.**

Finally, from my heart I thank my parents **Rosemarie und Rudolf Worsch.** Thank you for your unlimited support, love and belief in me. I dedicate this thesis to you. I also want to thank my whole family and all my friends for their interest and motivation.

Funding

German Research Foundation (Deutsche Forschungsgemeinschaft - DFG), Graduiertenkolleg GRK 1482 - "interface functions of the intestine between luminal factors and host signals"



13 Curriculum Vitae

Persönliche Daten

Name **Stefanie Worsch**
 Geburtsdatum/-ort 20.01.1986 in Eichstätt

Beruflicher Werdegang

07/2016 - 11/2016 **„Life Science Management“**, ATV GmbH, München
 Zertifizierte und praxisbezogene Weiterbildung u.a. in den Bereichen

- **Regulatory Affairs** und **Pharmakovigilanz**
- **Projekt- und Qualitätsmanagement**
- **Klinische Studien, BWL, Marketing** und **Vertrieb**

09/2011 - 11/2014 **Wissenschaftlicher Mitarbeiter** im Rahmen der Promotion
 Lehrstuhl für Ernährungsmedizin, TU München, Freising/Weihenstephan
 Mitglied des Graduiertenzentrums GRK 1482 (Stipendium) und der TUM-GS

Akademische Ausbildung

09/2011 - heute **Promotion** (Dr. rer. nat.)
 Lehrstuhl für Ernährungsmedizin, TU München, Freising/Weihenstephan
 Prof. Dr. J. J. Hauner, Dr. B. L. Bader
 Titel der **Doktorarbeit**:
 „Inflammatory, metabolic, and vascular changes upon high-fat diet feeding and n-3 LCPUFA supplementation in mice“

10/2005 - 05/2010 **Studium Molecular Science**
 FAU Erlangen-Nürnberg, Erlangen
 Abschluss: **Master of Science**

- Module: Drug Discovery, Molekulare Biologie und Virologie
- **Masterarbeit** in der Mikrobiologie (AG Burkovski)

Abschluss: **Bachelor of Science**

- Vorlesungen in Chemie, Biologie und Pharmazie
- **Bachelorarbeit** in der Pharmazeutischen Biologie (AG Kreis)

09/1996 - 06/2005 **Schulausbildung**
 Willibald Gymnasium, Eichstätt
 Abschluss: **Abitur**

Publications

- **Worsch S**, Hauner H, Bader BL. High fat diets with balanced or unbalanced n-6/n-3 PUFA ratios effect murine intestinal, hepatic and brown adipose tissue metabolism differently. 2017 (in preparation)
- Fiamoncini J, Lima TM, Hirabara SM, Ecker J, Gorjão R, Romanatto T, ELolimy A, **Worsch S**, Laumen H, Bader B, Daniel H, Curi R. Medium-chain dicarboxylic acylcarnitines as markers of n-3 PUFA-induced peroxisomal oxidation of fatty acids. *Mol Nutr Food Res* 59(8):1573-1583, 2015
- Dahlhoff C, **Worsch S**, Sailer M, Hummel BA, Fiamoncini J, Uebel K, Obeid R, Scherling C, Geisel J, Bader BL, Daniel H. Methyl-donor supplementation in obese mice prevents the progression of NAFLD, activates AMPK and decreases acyl-carnitine levels. *Mol Metab* 3(5):565-580, 2014
- Ludwig T, **Worsch S**, Heikenwalder M, Daniel H, Hauner H, Bader BL. Metabolic and immunomodulatory effects of n-3 fatty acids are different in mesenteric and epididymal adipose tissue of diet-induced obese mice. *Am J Physiol Endocrinol Metab* 304(11):E1140-1156, 2013
- Hasselt K, Rankl S, **Worsch S**, Burkovski A. Adaptation of AmtR-controlled gene expression by modulation of AmtR binding activity in *Corynebacterium glutamicum*. *J Biotechnol* 154(2-3):156-162, 2011

Konferenz

10th NuGOweek 2013 Nutrigenomics & More, Freising-Weihenstephan, Germany

Posterpräsentation

S. Worsch, T. Ludwig, M. Heikenwalder, H. Daniel, H. Hauner and B.L. Bader. Impact of dietary n-3 LCPUFA supplementation on adipose tissues, intestine and spleen in mice.